AN INVESTIGATION INTO HEAVY VEHICLE DRUM BRAKE SQUEAL

by

ALLAN MICHAEL LANG

A Doctoral Thesis

Submitted in partial fulfilment of the requirements

for the award of

Doctor of Philosophy of the Loughborough University of Technology

May 1994

An Investigation into Heavy Vehicle Drum Brake Squeal

Abstract

Many mechanisms have been suggested for brake squeal over many years. In order to identify the most appropriate of these mechanisms, an experimental investigation has been carried out to define in detail the vibration characteristics of a squealing heavy vehicle air operated drum brake on both a vehicle and a laboratory brake test rig. This required the development of a novel 'scanning' technique for the modal analysis of the rotating drum, which showed the presence of well-defined complex wavelike modes. From these results, the dynamic behaviour of the drum, in particular, is found to be in good qualitative agreement with the predictions of a simple 'binary flutter' mechanism of squeal. Based on the role of rotor symmetry in this mechanism, a means of decoupling flutter modes is developed involving a reduction in the rotational symmetry of the drum by means of attaching masses in a defined pattern at its periphery. It is shown theoretically that such decoupling would be expected to increase the dynamic stability of the brake, and experimental application of the technique confirms its effectiveness in reducing or eliminating squeal. Practical design aspects of reducing the rotational symmetry of the drum are considered, using finite element modelling, and it is also shown that the technique can be effective in other types of vehicle brake, such as disc brakes and hydraulic drum brakes.

The simple lumped parameter models used in the above work are inadequate as brake design tools, however, and so a novel application of finite element modelling is used to extend the principle of the binary flutter mechanism to a more detailed model of a complete brake. This is shown to be capable of predicting known features of squeal and may be used as a brake design tool for both the brake structure and the friction material.

ACKNOWLEDGEMENTS

My sincere thanks go firstly to Peter Newcomb, for his constant support and encouragement as my supervisor and friend, over more years than the call of duty requires. Peter and Audrey have provided sustenance, both spiritual and physical, when most needed.

I am indebted to my colleagues in Mintex Don Research for not only providing unstinting practical help with experimentation, but also for their forbearance when this work took precedence over my involvement in the team.

Without the foresight of Bert Smales, my manager and mentor at the commencement of the research, the physical resource and time commitment may never have come together to allow this work to succeed. Thanks Bert!

Of course, my parents, Lucy and Dick Lang, were responsible for laying the foundations on which my work has been built, and my father's pleasure, just before his death, at my embarking on this research has sustained me during the difficult periods, when I might otherwise have succumbed.

Finally, I cannot adequately express my gratitude to my wife, Chris, for her extraordinary patience and commitment to the project over many years. Without her understanding (and typing), the work could not have been completed.

CONTENTS

NOMENCLATURE

a	axial position coordinate
a	coefficient in equation of motion
b	coefficient in equation of motion
c_1	caliper damping coefficient in 'moan' model
c_2	piston/cylinder damping coefficient in 'moan' model
c_d	disc damping coefficient in pin-disc model
c_c	cantilever damping coefficient in pin-disc model
c	coefficient in equation of motion
d	coefficient in equation of motion
E	Young's modulus
$f(r)$	form of mode shape along disc radius
$f(z)$	form of mode shape across drum rubbing path
F	friction force
F_d	friction force on drum from interface spring
F_l	friction force on lining from interface spring
h	distance from drum or disc neutral axis to friction surface
i	complex operator = $(-1)^{½}$
j	integer
I	moment of inertia of drum or disc segment in binary flutter model
k	integer
k	identification number of masses added to drum
k	stiffness
k_d	transverse stiffness of drum or disc segment in binary flutter model
k_i	stiffness of interface element between friction material and drum

k_p	stiffness of friction material normal to friction surface
K	generalised stiffness of drum mode
K	stiffness of caliper in μ-velocity instability model
K	'convergence factor' in flutter model
K_c	cantilever stiffness in cantilever/disc model
K_d	disc stiffness in cantilever/disc model
l	semi-length of friction material in contact with drum segment in flutter model
l_1, l_2	dimensions defining caliper node in 'moan' model
m	mass addition to drum
m_{eq}	equivalent point mass producing same frequency 'split' as extended mass
M	generalised mass of drum mode
M	mass of caliper in μ-velocity instability model
M_c	cantilever mass in cantilever/disc model
M_d	disc mass in cantilever/disc model
n	number of pairs of axial nodal lines around drum or disc
N	normal force between lining and drum
N_d	normal force between interface spring and drum
N_l	normal force between interface spring and lining
p	real part of complex eigenvalue
q	imaginary part of complex eigenvalue
r	radius
R	reaction force between cantilever and disc
s	number of nodal circles around drum rubbing path
S	frequency 'split' due to a reduction in drum symmetry
S_d	rotational stiffness to earth of segment of drum or disc in flutter model

t	time coordinate
T	kinetic energy
u	cantilever displacement in cantilever/disc model
u	combination of coefficients in equation of motion (=-(a+d))
v	disc displacement in cantilever/disc model
v	combination of coefficients in equation of motion (= $(a+d)^2$ - 4(ad-bc))
V	linear velocity of rotor surface
x	tangential displacement of drum or lining surface
x_d	tangential displacement of drum surface
x_l	tangential displacement of lining surface
y	radial displacement of drum or lining surface
y_d	radial displacement of drum surface
y_l	radial displacement of lining surface
y_0	eigenvector amplitude
z	symmetry group order
z	number of equispaced masses added to drum
α	gradient of μ-velocity characteristic
α	semi-length of distributed mass on drum
α_k	$2nk\pi/z$ in kinetic energy evaluation of added mass
β	angular position of centre of added mass on drum
β	$4n\pi/z$ in kinetic energy evaluation of added mass
γ	strut or cantilever sprag angle
Γ	sprag angle parameter in cantilever/disc model
θ	angular position
θ	angular displacement of rotor segment in flutter model
λ	eigenvalue
ϱ	density

$\Delta\phi$	elemental length of distributed added mass
ΔT	kinetic energy of element of distributed added mass
μ	coefficient of friction between friction material and rotor
μ_0	coefficient of static friction between friction material and rotor
ν	Poisson's ratio
ϕ	angular position
ϕ	spatial phase shift between drum mode components
ϕ	phase component of transfer function
ω	angular frequency
ω_{sr}	rotational natural frequency of drum/lining system in flutter model
ω_{st}	transverse natural frequency of drum/lining system in flutter model
ω_R	rotational natural frequency of drum section in flutter model
ω_T	transverse natural frequency of drum section in flutter model
$\Delta\omega$	difference in natural frequency between a pair of similar drum modes
$\bar{\omega}$	mean natural frequency of a pair of similar drum modes

CHAPTER 1

INTRODUCTION

1.1 The Background to the Problem

The primary requirement of a vehicle brake, that of producing a controlled and predictable deceleration of the vehicle, has been the subject of continuous development and this has resulted in friction brakes which are at least adequate in performance, matching other developments in vehicle technology. The introduction of disc brakes, together with improvements in actuation systems and friction materials have not only kept pace with increased vehicle power and speed but have made reliable and consistent brake performance the accepted norm for the majority of drivers.

Along with these braking improvements, there has, of course, been a continued improvement to the whole vehicle, particular attention having been paid to 'refinement' or comfort. A major factor in such 'refinement' has been a reduction in noise and vibration perceived by the occupants, mainly achieved through reduced engine noise, improved suspension and chassis design and better aerodynamics. These improvements have, however, given brake noise and vibration, which has always been a feature of braking, a much higher profile, to the extent that amongst passenger car users, noise and judder are often the only perceived braking problems, resulting in very significant warranty costs to the vehicle manufacturers.

The need for refinement in heavy vehicles has lagged behind that for passenger cars and consequently the noise and vibration performance of their (predominantly drum)

brakes has received little attention. This situation is, however, now changing, a major motivator being the environmental impact of the loud brake squeal associated with heavy vehicles, and particularly with public service vehicles which have more occupants and regular stopping places.

Brake squeal has been recognised as a problem and been the subject of investigation for over half a century. Approaches to the problem have been to some extent polarised into theoretical and empirical investigations. Theoretical work aimed at an understanding of the fundamental mechanism involved in squeal has been predominantly the preserve of academic institutions and has received wide publication, whereas the large amount of empirical work carried out mainly by brake and friction material manufacturers aimed at practical 'fixes' has remained largely unpublished.

It is now becoming clear to the braking industry that empirical approaches are extremely inefficient and also that the simplified models used to investigate fundamental mechanisms are of very limited application in the practical reduction of brake noise. The major problem is the fugitive nature of squeal - a brake may be noisy during one application but not in another, under apparently similar operating conditions - and in the absence of a knowledge of the mechanism involved, a structured approach to a solution is therefore difficult. A better understanding of the dynamics of the squealing brake, together with much more realistic modelling of the brake structure and its dynamic stability, are now thought to be the key to a general solution to the problem.

The work described here has been aimed at producing a more complete description of the dynamic process occurring in a squealing brake and hence identifying the fundamental mechanism by which it occurs. Such a physical understanding will be

shown to lead to potential solutions to existing brake squeal problems, and will provide a sound basis for more detailed, predictive models enabling the design of 'quiet' brakes.

The remainder of this chapter is devoted to a review of developments in the whole field of vehicle brake squeal - both drum and disc brakes, as the fundamental mechanisms may be related. Discussion of the strengths and weaknesses of this previous work will indicate the need for the investigation described here.

1.2 Literature Survey

1.2.1 Early work and variable friction mechanisms

The earliest published work on brake squeal was, naturally, concerned with drum brakes and was of an essentially empirical nature. In 1935, Lamarque (1) brought together the experience of brake and vehicle manufacturers and operators on squeal prevention and found much conflicting evidence on palliatives and conditions of occurrence of noise. Although some palliatives appeared to be more generally applicable - such as increasing shoe flexibility, reducing lining friction and fitting steel bands or springs around the drum periphery, - all suffered from practical problems. It was felt that the latter method, of damping the drum, merely reduced the emission of sound without affecting the source of vibration, which was unknown.

Williams (2), in follow up work to the above, gave a qualitative description of self-sustaining oscillations due to the variation of friction with rubbing speed. He measured this characteristic of friction pairs and found that the static/dynamic friction ratio was increased by a film of moisture and by bedding in, but was reduced as brake

temperature increased - trends which reflected some aspects of service noise experience and hence lent credence to the mechanism that vibrations were frictionally induced.

The effect on squeal of varying a range of parameters was first studied in a systematic way by Mills (3) using both a complete brake assembly rig and a simplified rig using a small sample of friction material supported by a cantilever parallel to the axis of the drum, on which the material rubbed. He found that noise decreased with temperature, rubbing speed and shoe mass, but increased with load, whilst the basic squeal frequency was independent of rubbing speed or load, but in the simplified rig was a function of the mass and stiffness of the cantilever. The effect of contact geometry was indicated by rotating the cantilever to give a positive or negative servo effect (analogous to a leading or trailing shoe), when low frequency cantilever vibrations were produced only in the former position. This effect appeared to correlate with real brakes where most noise was thought to be produced by the leading shoe. The wide difference in noise produced by linings having similar static/dynamic friction characteristics led him conclude that squeal was affected more by contact geometry than by frictional characteristics.

Further experimental work on rig mounted two leading shoe brakes was carried out by Fosberry and Holubecki (4,5,6). They found distinct types of noise spanning the whole of the audible frequency spectrum, but they concentrated on the 'normal' squeal frequency range from 3kHz to 15kHz. Their observations were consistent with the friction-velocity characteristic theory producing tangential relaxation oscillations of the shoes which excited radial vibrations of the drum similar to those of a bell. Investigation of these drum modes showed that with very short linings (½in long), modes were stationary in space, similar to an externally excited drum, with a node at

the lining position. With full linings , however, the drum showed no true stationary nodes and a continuous variation of phase around the drum. This was explained by a rotation of the modal pattern around the drum at a speed related to the mode frequency.

Sinclair (7) produced a model to show how frictional vibrations could be produced by a discrete difference between static and dynamic friction. These vibrations would quickly decay in the presence of damping, however, and he concluded that an inverse friction-velocity relationship would be required to negate the damping effect. This was supported experimentally by the effect of water on the lining material, which, although reducing the overall friction, gave the required friction-velocity relationship and produced unstable vibrations. Lubrication of the lining with soap and glycerine produced the opposite effect on the μ - velocity characteristic, but could not be successfully applied to real brakes.

The mechanism of unstable vibration due to a falling friction - velocity characteristic was modelled by Basford and Twiss (8) who idealised their experimental observations of this variable (9) by the linear relationship

$$\mu = \mu_0 + \alpha(V - \dot{x}) \qquad (1.1)$$

where μ_0 is the coefficient of friction at zero rubbing speed and α is the gradient of the μ - velocity characteristic as illustrated in fig 1.1.

This friction - velocity mechanism can be illustrated by the model in fig 1.1, for which the equation of motion is

$$M\ddot{x} + c\dot{x} + Kx = N(\mu_0 + \alpha(V - \dot{x})) \qquad (1\text{-}2)$$

or

$$M\ddot{x} + (c + \alpha N)\dot{x} + Kx = N(\mu_0 + \alpha V) \qquad (1\text{-}3)$$

so that if α is negative, as is common in friction materials, and $\alpha N > c$, the system damping will be negative, and unstable oscillation will result. They suggested that if this tangential oscillation is coupled with a drum mode, the rate of amplitude build up would be increased, and based upon this and the value of α , formulated a noise probability factor which agreed with limited experimental observations. The Basford and Twiss model had no external damping but Wagenfuhrer (10) took this theoretical approach to the friction - velocity instability further by including damping in a single degree of freedom model, and assuming a more realistic hyperbolic function for the variation of friction with velocity. By a graphical solution to his equation of motion he was thus able to show vibration amplitude growth up to, and beyond, the point at which velocity matching between friction material and drum occur. The model suggests that instability is more likely to occur under heavy load conditions (as did that of Basford and Twiss) and at low rubbing speeds. Again, Wagenfuhrer considered drum vibrations to be secondary vibrations which served to radiate the noise and suggested that even though unstable vibrations occurred, the subjective noise could be decreased by control of those secondary systems.

Chikamori (11) used a similar model to Wagenfuhrer but included a discrete difference between zero speed static and dynamic friction although reverting to a linear friction-velocity characteristic. He analysed the model using an analogue computer and predicted a limit cycle instability which occurred more readily when damping was low and when the negative μ-velocity slope and the difference between static and dynamic friction was high.

Although more recent work suggests that these variable μ mechanisms are not responsible for 'mainstream' squeal, they are involved in lower frequency vibrations, often known as 'groan'. This has become particularly notable in installations where the usual elliptical, multiple leaf suspension springs have been replaced by one piece springs, almost eliminating the torsional damping applied to the brake, and hence making the value of c in equation 1.3 very small. In addition, the true 'stick-slip' mechanism has been suggested by Rinsdorf and Schiffner (48) for the mechanism of disc brake noises involving shear deformations of the friction material of the brake pad.

1.2.2 Constant friction mechanisms

The first attempt to give a mechanism by means of which frictional vibrations could be produced independently of a variation of coefficient of friction with speed, was due to Spurr (12). He described qualitatively how two noises, squeal and judder, which he had observed in a rotating bell, could be produced by a stationary 'exciter' held against the bell mouth. Observation of water waves inside the bell indicated a stationary flexural mode shape with a node at the exciter. He hypothesised that the rotational motion of the bell wall at the node associated with such a flexural mode produced variations in friction force which acted to maintain the tangential component of vibration at the node also associated with this flexural mode. It is not stated how the necessary phasing between the two motions (tangential and rotational) arises.

He considered judder of the bell to be due to what has since been termed a 'sprag - slip' action. Considering the double cantilever PO'O" in fig 1.2, with P in contact with the moving surface of the bell, and a normal load N applied at P; if O' is fixed, the friction force can be shown to be $F = \mu N/(1-\mu\tan\gamma)$ which becomes very large

as μ approaches cotγ and so spragging occurs. P now moves with the bell, forcing the cantilever O'O" to deflect, and the system PO'O" is now equivalent to a strut PO" at a smaller angle than γ to the moving surface. This reduction in the effective value of γ reduces F and the spragging action ceases, allowing P to slip back, when a further cycle commences.

He confirmed the condition μ = cotγ for squeal experimentally in a railway brake block and a modified disc brake, and considered that similar spragging conditions could be achieved by toe and heel contact in the leading shoe of a drum brake. In a later paper (13), Spurr also showed how the pad of a disc brake could wear in such a way that the real area of contact between pad and disc was localised and in the critical sprag condition. This non-uniform wear of the friction material could be due to thermal or mechanical distortion of the pad during braking or taper wear, which, under some circumstances produce a convex surface leading to localised contact. He suggested that similar wear effects in drum brakes induce 'toe and heel' contact which exacerbates squeal.

This type of mechanism was further investigated by Jarvis and Mills (14) who again considered an inclined strut, but with the rigid moving surface modelled by Spurr replaced by a flexible rotating disc. Both components were assumed to incorporate damping, and the disc to deform in a flexural mode shape having nodal diameters. The first model included a velocity dependent coefficient of friction, but analysis showed that the μ-velocity gradient required for instability was unreasonably high, and a second model, with constant friction was thus considered. In the latter model, the disc was assumed to hold two flexural modes of the same order but displaced spatially relative to each other, such that the cantilever was located at an antinode of the first mode and a node of the second. In the analysis, the role of the second mode is not

clear and it is stated that it is not a prerequisite for instability, but the solution for the first mode shows unstable conditions which depend upon the strut angle, coefficient of friction, radius at which the cantilever contacts the disc, and damping in the two components. It is significant that the damping in the cantilever has a destabilising effect as opposed to that in the disc which is stabilising. They suggested that limit cycling is the result of loss of contact between the components, and hence that the amplitude of squeal was not related to the instability mechanism. The theory was tested experimentally by measuring the minimum disc contact radius which resulted in instability for several values of cantilever angle. The departures from the predicted results, shown by these experiments, were reduced by Hales (15) in a modification to the theory which considered the radius profile of the cantilever tip.

Crisp (16) produced a simplified model of this type of instability which considered the cantilever point as a mass M_c constrained to move at the cantilever angle (γ) against a spring, and the disc as a mass M_d, constrained to move in the disc axis direction against a spring, with friction forces applied as though the masses were in relative sliding motion (fig 1.3).

The equations of motion of the cantilever and disc are, respectively,

$$\begin{aligned} M_c\ddot{u} + c_c\dot{u} + K_c u &= R(\sin\gamma - \mu\cos\gamma) \\ M_d\ddot{v} + c_d\dot{v} + K_d v &= -R \end{aligned} \qquad (1\text{-}4)$$

(where γ is here the angle of the strut to the normal to the disc surface)

Assuming contact is maintained, the kinematic constraint $v = u \sin\gamma$ applies and the equations reduce to the single degree of freedom equation in the form

$$(1 - \Gamma)\ddot{u} + \left(\frac{c_c}{M_c} - \Gamma\frac{c_d}{M_d}\right)\dot{u} + \left(\omega_c^2 - \Gamma\omega_d^2\right) = 0 \qquad (1\text{-}5)$$

where

$$\Gamma = \left(\frac{M_d}{2M_c}\right)(\mu - \tan\gamma)\sin 2\gamma \qquad (1\text{-}6)$$

The system becomes unstable when the damping term is negative, ie when

$$\frac{1}{2}\sin 2\gamma(\mu - \tan\gamma) > \frac{c_c}{c_d} \qquad (1\text{-}7)$$

Hence stability depends upon damping, cantilever angle and coefficient of friction, and damping may in this case be destabilising.

The mechanism of these 'kinematic constraint' instabilities (described as such by Crisp) was further investigated by Earles and Soar (17). They again used a cantilever - disc system but with a short cantilever, described as a pin, and assumed rigid, but mounted on a flexible beam, as shown in fig 1.4. The disc was assumed to have one, axial, degree of freedom and the pin two, one translational and one rotational, although these latter were considered independently, and were modelled as in fig 1.5. The case of the translational pin mode is identical with that due to Crisp (16) but was rejected as the cause of squeal as, experimentally, it gave only low frequency, low amplitude oscillations and theoretically required unrealistically high damping, stiffness or mass ratios between the components to produce instability. Experimentally, squeal was associated with the torsional mode of the support beam and occurred at pin angles of $0 < \gamma < \tan^{-1}\mu$, (the 'digging-in' condition). In this mode, the model leads to a non-linear equation of motion, in qualitative agreement with the harmonic content of the observed stability boundary. Further, the generation of high frequency harmonics was felt to yield the energy dissipation required to stabilise the squeal amplitude.

This pin-disc system was modified by Earles and Lee (18) to give the pin system three degrees of freedom as shown in fig 1.6, but no damping. In this latter case, the analysis showed that the pin mode in the k_2 direction is uncoupled from the other two modes, which themselves lead to the same condition for instability as the previous model, ie. $\mu > -c/l > 0$ (as from fig 1.6, $c/l = \tan\gamma$).

In order to more closely represent the situation in an actual disc brake Earles and Badi (19) investigated the effect of two pins, each modelled as above, one on each side of the disc which was again given a single, axial degree of freedom, They found, both by analysis and experimentally, that the instability boundary of $\mu > \tan\gamma > 0$ no longer applied, but could be extended if both pins had a 'digging in' action, or reduced if the second pin angle was outside the above instability region.

It is worthy of note that all these 'spragging', kinematic constraint models require only single degree of freedom disc motion for instability, and this may be an important factor in determining their relationship to actual squeal characteristics.

Perhaps the simplest constant μ instability mechanism is one proposed by Lang and Smales (20) to explain a low frequency (typically 200 Hz-400 Hz) opposed piston disc brake vibration. This occurred under non-braking conditions whilst manoeuvring, when hub deflections caused one pad only to touch the disc. The single degree of freedom model, based on rigid body caliper motion and no disc vibration, is shown in fig 1.7, and the associated equation of motion is

$$M\ddot{x} + \left[c_1 + c_2\left(\frac{l_2}{l_1}\right)\left(\frac{l_2}{l_1} - \mu\right)\right]\dot{x} + kx = 0 \qquad (1\text{-}8)$$

Unstable oscillation occurs if the damping coefficient is negative, ie when

$$\mu > \frac{l_2}{l_1} + \frac{c_1 l_1}{c_2 l_2} \tag{1-9}$$

This shows that increasing friction coefficient is destabilising, but a more complete picture of the predicted effects of μ, damping and geometry on stability is given in fig 1.8. Gouya and Nishiwaki (21) analysed a similar problem, often known as disc brake 'groan' in pin-slider calipers, but under braking conditions. Two degree of freedom rigid body rotation of the caliper was considered and again a high value of μ was found to be destabilising, with pad/disc contact positions, caliper inertias and mounting stiffnesses all influencing the occurrence of 'groan'.

1.2.3 Flutter mechanisms

A different approach to the problem of disc brake noise was taken by North (22) who modelled the essential features of an actual disc brake by an eight degree of freedom lumped parameter system, as illustrated in fig 1.9. The disc, pads and caliper were each represented by elements having mass and inertia and one linear plus one rotational degree of freedom. The provision of two independent degrees of freedom for the disc is essential to this model, and is based upon the assumption, as appreciated by Jarvis and Mills, that the disc can hold two modes of the same order with different angular positions. A simplified 2-degree of freedom version of the model is given elsewhere by North (23), illustrated in fig 1.10, in which the role of this disc behaviour is stressed. The two equations of motion are

$$\begin{aligned} M\ddot{y} + (k_d + k_p)y + 2F\theta &= 0 \\ I\ddot{\theta} - 2\mu k_p y + \left(s_d + k_p \frac{l^2}{3}\right) &= 0 \end{aligned} \tag{1-10}$$

and the associated eigenvalue problem can produce complex conjugate eigenvalues with positive real parts, indicating unstable oscillation.

The condition for instability is shown to be

$$0 < k_p < \frac{16MIF\mu h}{\left(I - \frac{Ml^2}{3}\right)^2} \qquad (1\text{-}11)$$

again showing the destabilising effect of μ, but also of the disc thickness. Unlike the previous mechanisms, 2-degree of freedom disc motion is a fundamental requirement for instability here.

In the 8-degree of freedom model, parameter values for the analysis were chosen to represent the brake used for experimental work, the equivalent mass and inertia of the disc being calculated to give the same total energy as the actual disc in an appropriate mode.

Good agreement was obtained between the calculated instability frequency and the actual squeal frequency and between calculated and measured mode amplitudes but not phases. Further, the effect of an experimental parameter change, reducing the caliper stiffness, was correctly predicted. General conclusions from the model are that both the addition of damping in any area and reduction in coefficient of friction are generally stabilising, and that instability regions are generally narrow and probably rely on the non-linearity of parameters, such as friction material stiffness, in order to readily access these regions.

A similar approach to the disc brake was taken by Millner (24), in a six degree of freedom lumped parameter model (fig 1.11), again assuming two disc modes, but

including only one pad and no damping. The model did, however, allow the contact position between the pad and caliper to be defined, in the form of an offset *a* of the contact point from the centreline of the piston. Initial analysis showed that instabilities only occurred for positive *a*, that is contact in the leading half of the pad. The predicted instability conditions are qualitatively similar to those for cantilever angle ($\tan^{-1}\mu > \gamma > 0$) in the 'sprag-slip' or 'pin-disc' models. Varying other parameters, however, showed that instabilities could occur for negative *a*, and in general, low pad modulus and high caliper stiffness produced 'negative *a*' instabilities. An increase in coefficient of friction was again found to be destabilising. These predictions of the effect of pad/caliper contact explained well a long standing fix used in the industry for low frequency squeal - that of using a 'trailing offset' shim between the pad and piston.

Squeal in modern pin-slider disc brakes has been investigated by Murakami, Tsunada and Kitamura (25), who showed experimentally that low frequency squeal (2.4kHz) involved almost rigid body pad rotation modes, but in high frequency squeal (8.4 kHz), pad bending modes occurred. They also modelled the low frequency condition, where the pads can be assumed to be rigid, by a lumped parameter system (fig 1.12) where the disc, piston and caliper were allowed only one rotational freedom each but the pads two degrees of freedom each. This single degree of freedom representation of the disc was a fundamental departure from the flutter approach of North and Millner. As the outer pad loading fingers were found both by experiment and by finite element analysis, to move antiphase to each other at the squeal frequency, these were modelled by individual stiffnesses, as were the pad abutments. A linear, negative μ-velocity characteristic was also included, and although, on analysis, this increased the instability, it was not found to be a necessary condition for instability. In general, they found that the pattern of influence of parameter variation fell into two

groups, those parameters having a 'worst' or 'best' value in terms of their effect on squeal, and those which show a continuously increasing adverse effect with change, The latter included the coefficient of friction and the 'moment arm' of each component (eg. pad and disc thickness) and the former the masses, stiffnesses and finger spacing.

1.2.4 Drum brake squeal

Most of the preceding, more recent, work has been aimed specifically at the problem of squeal as it relates to disc brakes, and in particular to conditions under which the brake pad, and in some instances the brake disc over its limited area of contact with the pad, can be considered as rigid bodies. However, in drum brakes with their large areas of contact between lining and drum, these idealisations cannot be readily applied.

Millner (26,27) tackled the specific problem of the drum brake by considering both the drum and the shoe to be flexible, represented in his model by a thin cylindrical shell and thin curved elastic strip respectively. The mode shapes taken by the drum and a leading shoe are assumed to be those for free vibration and the drum motion is, like the disc in some previous models, assumed to be the superposition of two flexural modes of the same order. The radial stress in the lining was then assumed to be proportional to the difference in deflection between the shoe and drum and the resulting changes in normal and friction force used to calculate generalised forces. Substitution in the three Lagrange equations for the three modes gave equations of motion, the complex eigenvalues of which could involve positive real parts indicating instability (the magnitude of the positive real part being used as measure of 'squeal propensity').

The model allowed variations in the distribution of the contact area between lining and drum to simulate 'crown' and 'leading and trailing' contact as well as full contact. Analysis showed that under full contact conditions the squeal propensity increased uniformly with μ, but for 'crown' or 'leading-trailing' contact, a dramatic increase occurred above specific values of μ, the required value of μ for significant crown instability being substantially higher than for leading and trailing conditions.

For the major squeal mode, involving the fundamental modes of both the drum and shoe, and which showed the greatest squeal propensity, an increase in lining stiffness had a destabilising effect. In higher squeal modes, however, the opposite effect occurred, and this difference in response to parameter changes between squeal modes extended to shoe and drum density and stiffness changes. Damping changes were found to have no significant effect on the fundamental squeal mode but in higher modes shoe damping was destabilising and drum damping stabilising.

Experimental work on a two leading shoe drum brake confirmed many of the trends due to parameter changes in the theory and gave good agreement with predicted squeal frequencies. An earlier version of the model allowing only one drum mode but including a negative μ-velocity slope, also produced instabilities, although the required slopes were unrealistically high and the resulting squeal propensities generally lower than with the constant friction model.

Okamura and Nishiwaki (28) extended Millner's analysis to include both brake shoes of a small, two-leading-shoe truck drum brake, but used the increase or decrease in kinetic energy per cycle as a measure of squeal propensity. Their results suggested that, with the shoes in contact with the drum, but no frictional force, the drum can hold two modes of slightly different frequency, but positioned such that nodes of one

mode and antinodes of the other align with the shoe centre. Increasing friction introduces tangential coupling between the shoes and drum and the two real drum modes converge in both frequency and position, ultimately coinciding, when squeal is produced. The model predicted the effects of μ (destabilising), lining modulus and the positions of the shoes and the linings, suggesting that solutions to brake squeal problems may be found in all these areas, although reducing μ, modifying lining position and shoe boundary conditions were predicted to have the greatest influence on squeal. They also carried out vibration measurements on the squealing brake to correlate the drum and shoe mode orders with those predicted by the model, although the technique was limited to obtaining amplitude information only from the drum. Suzuki and Ohno (29) carried out a similar, but, more detailed modal analysis on a large commercial vehicle drum brake and showed that, at a squeal frequency of 500 Hz, both drum and shoe vibrated in their fundamental flexural modes, as suggested by Millner. They observed in addition, a large gross tangential vibration component of the shoe, but changes to the shoe anchor stiffness produced only a change in noise frequency, suggesting that this motion was of little significance. However, modifications to the flexural modes of the shoe (by casting rather than fabricating) or the drum (by modifying the mounting region) tended to decrease squeal.

1.2.5 Experimental analysis

Kusano, Ishidou, Matsumura and Washizu (30) again carried out an experimental analysis of the vibration amplitude distribution in a squealing passenger car drum brake which showed that the modes involved, the 6 node flexural drum mode and the fundamental bending shoe mode, had approximately equal nodal spacings, with nodes aligned during squeal. Normal mode frequencies of the individual components, shoe,

drum or brake backplate, did not coincide with the squeal frequency, but they suggested that under actuation pressure, both drum and shoe frequencies increased towards the squeal frequency at different rates until, at the actuation pressure at which they coincided, squeal occurred. They showed, by normal modal analysis of the drum in a stationary actuated brake, and a shoe constrained in a manner representing the actuated condition, that in general the rate of increase of drum natural frequency with pressure was greater than that for the shoe This implied that squeal could be avoided by ensuring that the drum natural frequency was greater than that of the shoes. In practice this was achieved by both reducing the shoe web stiffness and increasing the drum plate stiffness, resulting in the predicted improvements in squeal performance.

Their suggested mechanism for this squeal was one of a feedback system instability relying on a negative μ-velocity characteristic of the friction material together with a large forward loop gain caused by coincidence of shoe and drum mode frequencies.

More sophisticated modal analysis methods have been brought to bear on disc brakes in recent years. These have generally revolved around the use of laser interferometry techniques to obtain more detailed spatial information about the vibration characteristics of both individual components and squealing brake systems. Felske, Hoppe and Matthai (31) used the standard technique of time-averaged holography to examine the modal characteristics of components but, more importantly, developed the use of double pulsed holography to allow the analysis of squealing disc brakes. The very short time period required to produce a hologram by this technique eliminated the masking effect of the low frequency gross movements of the disc during actual braking. They also applied the technique to passenger car drum brakes (32), but the problem under investigation was of relatively low frequency, the noise being radiated by a strong brake backplate flexural mode. A torsional mode of the leading shoe was

identified, and a form of coupling between this and the backplate was hypothesised. Modification of the backplate mode frequency by mass addition or stiffening flanges was shown to eliminate the squeal.

Fieldhouse and Newcomb (33) extended the technique using mirrors and cutout areas in the brake pad to obtain more comprehensive views of a squealing disc brake (fig 1.13). They examined the effect of pad abutment position in the caliper, and found that changing the friction force abutment between the trailing and the leading end of the pad could dramatically influence both noise frequency and occurrence.

1.2.6 Finite element modelling

These experimental modal analysis techniques have, more recently, been complemented by the use of finite element dynamic modelling to predict the modal behaviour of brake components and, in a few cases, to attempt to produce squeal models which represent the real brake system better than the previous lumped parameter approaches.

Kusano et al (30) used finite element models of the drum, shoe and the coupled drum/shoe to back up their difficult measurements of natural frequency convergence of the components with actuation pressure increase, noted earlier. The model also indicated a reduction in their suggested 'forward loop gain' effect when shoe and drum stiffnesses were modified.

Such finite element modal analysis of brake components has now become widely used, particularly in the context of one current approach to the 'fixing' of existing squeal

problems, that of modifying component natural frequencies to avoid coincident frequencies, as suggested by Kusano et al, above. For example Nishiwaki, Harada, Okamura and Ikeuchi (34) showed by modelling that higher order ventilated disc frequencies could be significantly influenced by the number of ventilation ducts.

This approach of component modification has had limited success in practice as it often fails to recognise the often substantial difference between the dynamics of the collection of individual components and the total system under operating conditions. Modelling of the system using finite elements has, however, proved difficult due to the necessary inclusion of frictional coupling terms at the lining/rotor interface. Liles (35) has partially overcome this problem for the disc brake by using full finite element models of the components, without friction, then representing each component by its predicted modal characteristics over the frequency range of interest, thus reducing the number of degrees of freedom involved by orders of magnitude. These modal models were then interconnected and frictional forces added, assuming these to be proportional to the relative displacements between the components. The frictional forces introduced asymmetric terms into the stiffness matrix, and eigenvalue analysis predicted instability conditions. The results confirmed the destabilising effect of μ, but also showed that increasing lining length, and decreasing lining thickness and modulus are also destabilising.

More recently, Ghesquiere (36) took a similar approach, but used experimental modal analysis in addition to component dynamic modelling to obtain the modal characteristics of the components for inclusion in a stability model. He showed how pairs of stable modes could be coupled by friction forces producing a single complex unstable mode.

1.3 Summary

The literature survey shows that a wide range of approaches to the squeal problem, both theoretical and experimental, have been taken over a long time period. In part, the disparity in approach is a result of the wide range of problems which are included under the umbrella of 'brake noise' (summarised by Lang and Smales (20)), and it is certainly clear that not all brake noise problems are the result of the same dynamic mechanisms, nor do they respond to the same solutions. A common theme, however, throughout much of the literature is that of brake squeal as a resonant dynamic instability of the brake system, rather than a response to a forcing function (although such forced vibrations can occur in brakes and are often referred to as 'judder').

The instability mechanisms which have been examined can be usefully divided into three distinct classes:-

i) μ-velocity instabilities

ii) pin-disc instabilities

iii) binary flutter - like instabilities

Each of these mechanisms can clearly induce unstable frictional vibrations, but in tackling any particular brake noise problem it would be important to distinguish between these mechanisms if an effective solution is to be found. In particular, the mechanisms are likely to involve different types of motion of the brake rotor, and thus a detailed knowledge of the rotor motion during noise generation would be a significant factor in determining their applicability.

Instability mechanisms based purely on the negative friction/sliding velocity characteristic at the friction interface appear to require no transverse motion of the rotor surface and hence rotor flexural modes are unlikely to be a significant feature of such problems. It is known that this type of instability is responsible for some low frequency resonant brake vibrations involving rigid body torsional motion of the brake in the frequency range 10 Hz - 100 Hz, significantly below the fundamental flexural natural frequencies of brake rotors. Although this mechanism is unlikely to be the major cause of the more usual higher frequency brake squeals, some workers have suggested that it has an exacerbating effect (for example Millner(26)).

Pin-disc instability mechanisms do, however, involve transverse motion of the rotor surface but, due to the single discrete contact point between the friction components, such motion can be adequately supplied by normal mode flexural vibration of the rotor.

Binary flutter type mechanisms involve distributed contact between the brake lining and rotor, and in their simplest form, usually applied to low frequency disc brake squeal, a fundamental requirement for instability is that the sector of rotor in contact with the brake lining has at least two independent degrees of freedom. These cannot be supplied by a single normal flexural mode, and the predicted phasing between the freedoms in such modelled instabilities suggests that the rotor should exhibit a complex mode.

The significance of the rotor modal behaviour in identifying the likely type of instability mechanism was appreciated as long ago as 1975 by North in a review of disc brake squeal (22). He suggested that only the binary flutter type of instability

would give rise to a pair of disc modes with well defined time and spatial phase differences.

This then provided the initial motivation for carrying out the work described in this thesis. It is clear from the literature that the majority of modal analysis carried out on squealing discs or drums have been limited to the specification of the flexural mode order involved and the approximate positioning of nodes, usually due to the non-availability of phase information. The more widespread use of holographic interferometry as an accepted modal analysis tool in brake noise has, perhaps, exacerbated this situation, the basic technique being at present limited to providing information on amplitude distribution. Phase information requires multiple images to be obtained and expensive modifications to the standard equipment and, so far, such work has been restricted to the analysis of the predominently unidirectional motion of disc brakes. An inexpensive modal analysis technique which would readily supply both amplitude and phase information from the squealing drum was clearly required to add to our knowledge of squeal behaviour. It is also clear from the literature that the traditional lumped parameter models used to examine potential instability mechanisms are limited in their ability to provide useful design criteria against squeal. This limitation is a result of one of the major predictions of such models - that most brake parameters do not have a monotonic influence on squeal, so that trends from simple models cannot generally be extrapolated to real brakes (a notable exception being the effect of friction coefficient). It is generally thought, however, that the use of finite element modelling may well provide the much needed tool for the design of dynamically stable brake systems. Some inroads have been made in this area, eg Liles (35) with a hybrid finite element/small degree of freedom model, and unpublished work continues by other workers to produce a full finite element stability model of a heavy vehicle drum brake. Such models are potentially very complex and it is

considered that efficient modelling is only possible if the dynamic characteristics of the actual squeal are known, so that essential degrees of freedom and boundary conditions can be defined correctly. A secondary purpose of this work, then, was to provide the modal characteristics for the development of such models, and, if possible, to develop a predictive model for drum brake squeal.

Finally, it was anticipated that detailed investigation of the dynamic behaviour of a squealing brake, and particularly the behaviour of the drum, of which current knowledge was most limited, may provide a level of conceptual understanding of the unstable system which could lead to a more generally applicable 'fix'. Many current fixes are very specific to the particular noise and installation for which they have been developed and the discovery of common features in the drum dynamics influencing stability could lead to stabilising rotor designs which are insensitive to other system variables.

In recent times there has been an upsurge in interest in commercial vehicle refinement, and this has encouraged the current study to focus on the squeal behaviour of the most popular type of heavy vehicle brake, the air actuated, mechanically operated drum brake.

The noise characteristics of such a brake on a vehicle are defined in Chapter 2, but in depth investigation of the brake dynamics in the vehicle environment would be both difficult and costly. The industry relies heavily on dynamometer brake performance testing to reduce cost and provide more controlled operating conditions, and such a machine has been used for this investigation, after verification of the dynamic similarity of the two installations. Different mechanisms proposed in the literature for squeal involve different rotor motions, and to help distinguish the applicability of such

mechanisms detailed measurements are made of the drum squeal modes in Chapter 3, and this required the development of a novel modal analysis technique, made necessary by the drum rotation. Standard modal analysis techniques can be applied to the stationary parts of the brake, and in Chapter 4, the shoe motion is measured and integrated with that of the drum to produce a description of the complete brake motion.

The modal behaviour of the drum is shown to be consistent with the 'binary flutter' mechanism for squeal, which is a dynamic instability due to coupling of two similar flexural meridian modes of the brake rotor. Decoupling of these drum modes is investigated in Chapter 5, and reducing the rotational symmetry, by adding masses, is found to reduce or eliminate squeal.

Practical problems of introducing such symmetry reduction are considered in Chapter 6, including the effect of extended arc length masses and the use of stiffness asymmetry. The significance of the rotational asymmetry of the complete actuated brake system is investigated in Chapter 7, using a simple binary flutter model to show how the separation of pairs of static system modes can influence the occurence of squeal.

Finally, the measured dynamic behaviour of the squealing brake and the binary flutter mechanism are brought together in Chapter 8 to develop a 2-Dimensional finite element idealisation of the brake with interface friction. The predicted squeal characteristics are shown to correlate well with the measured behaviour and it is suggested that the technique may form the basis for a brake design tool against squeal.

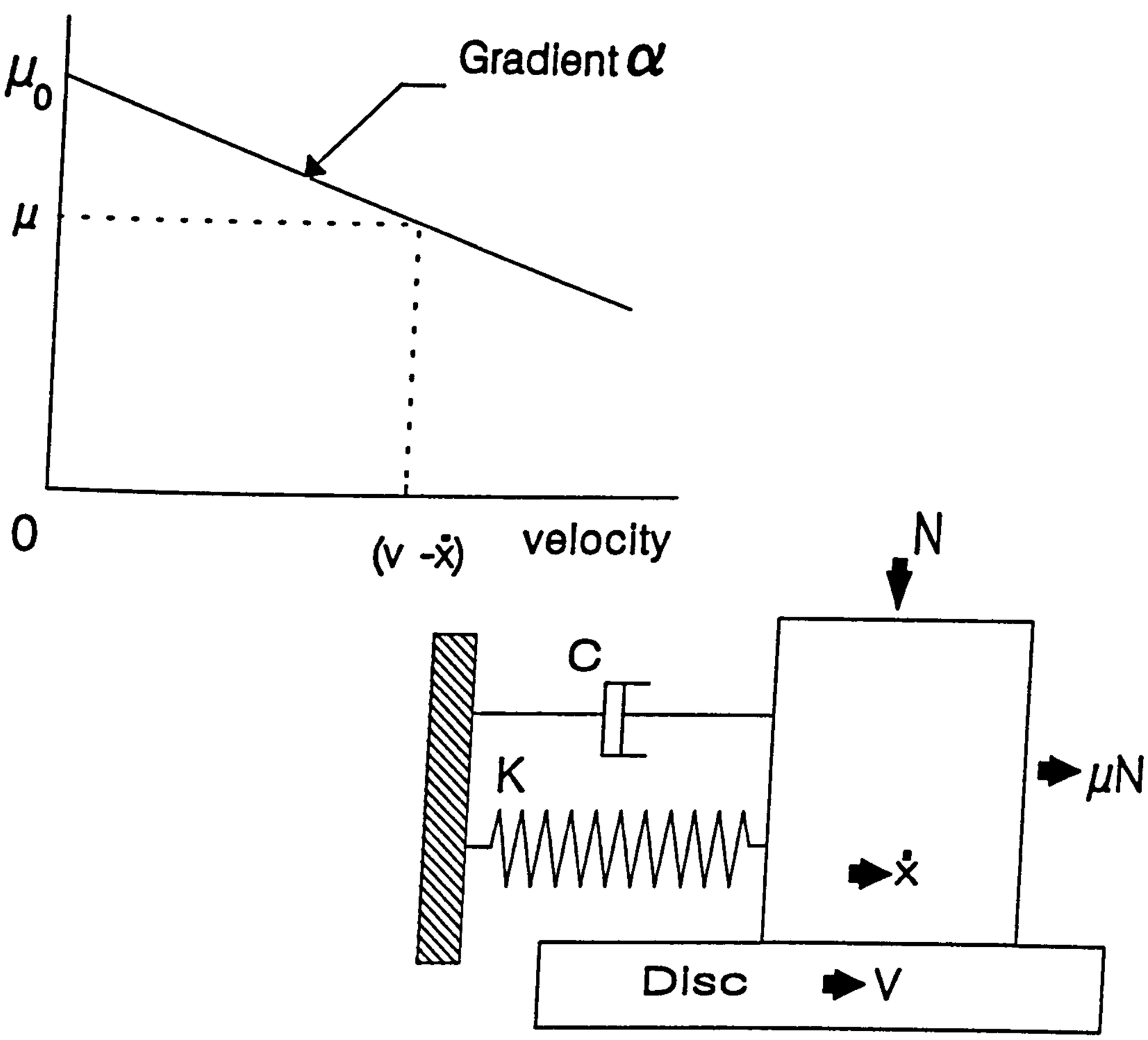

Figure 1.1 **A model for dynamic instability due to an idealised falling friction - velocity characteristic**

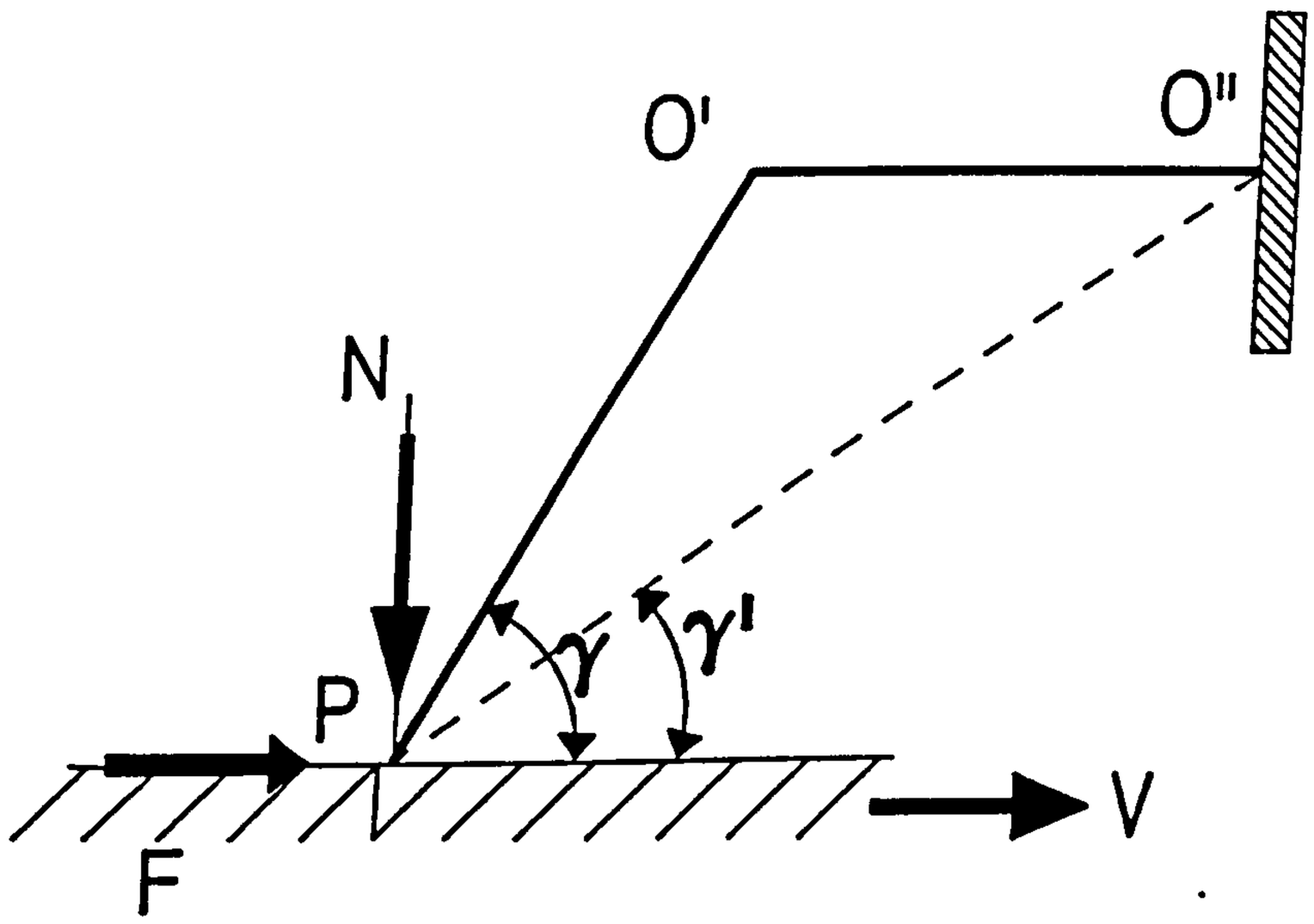

Figure 1.2 **A 'sprag-slip' mechanism for unstable vibration, due to Spurr.**

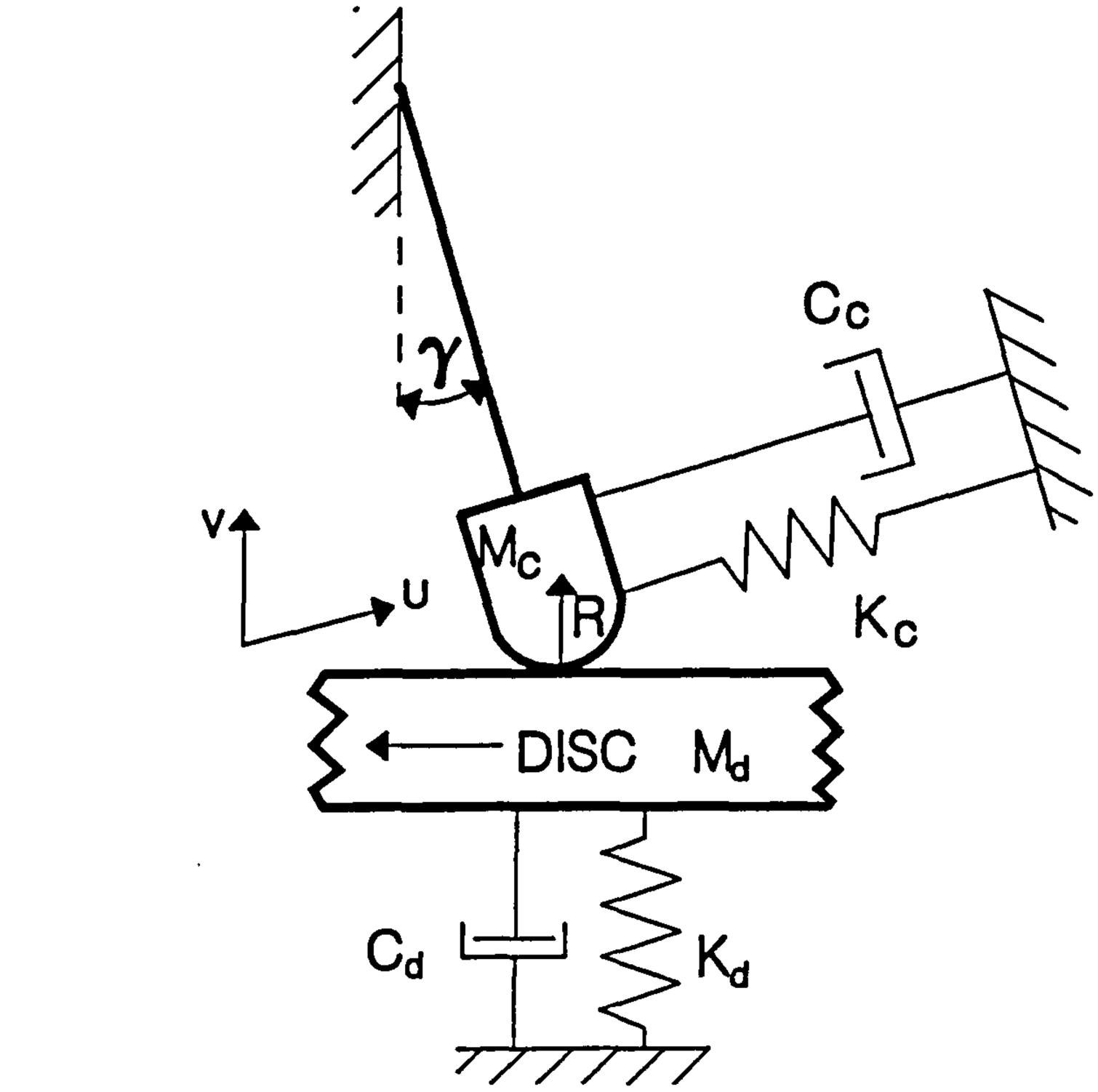

Figure 1.3 **A kinematic constraint instability mechanism due to Crisp**

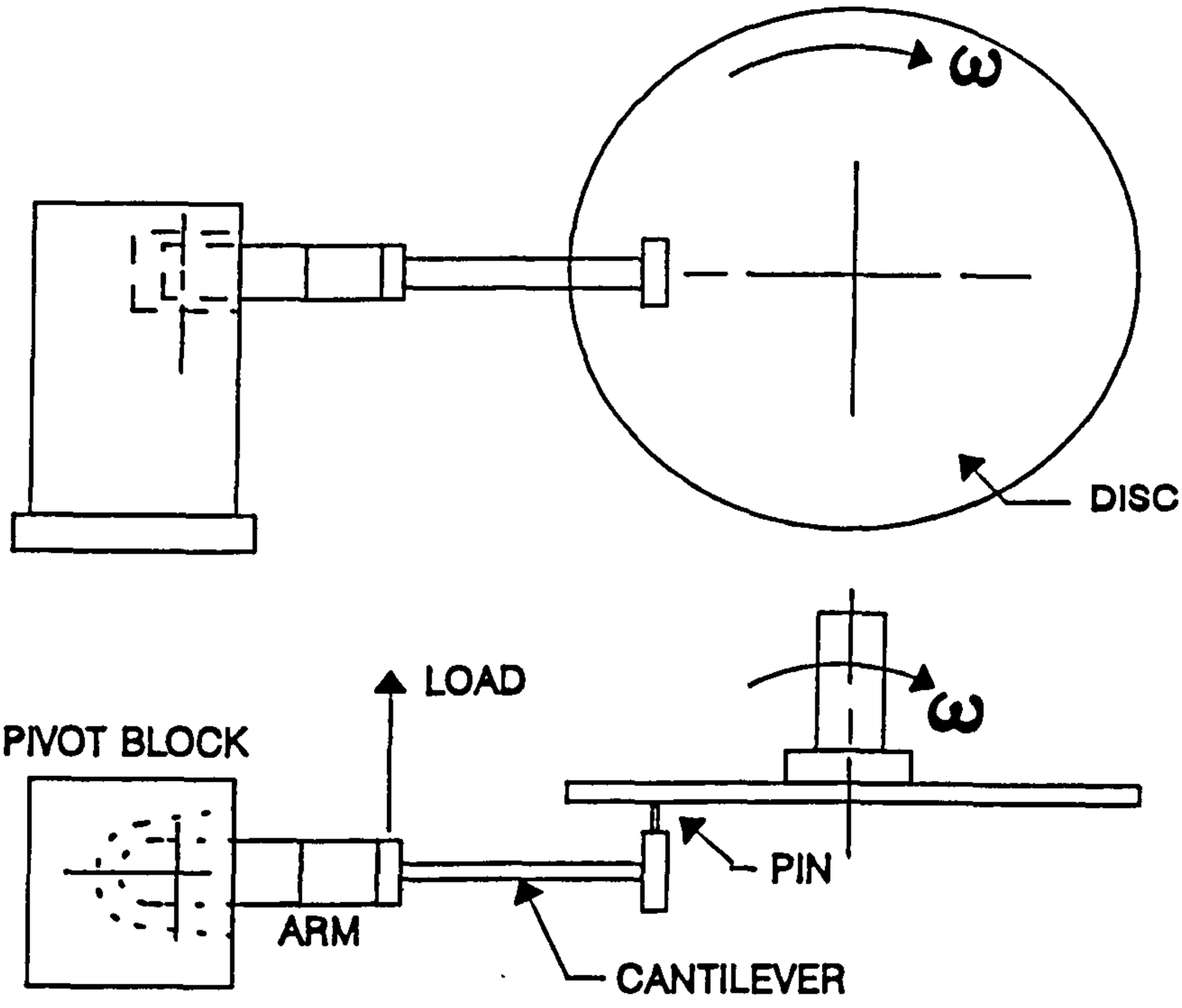

Figure 1.4 **The 'cantilever/pin/disc' arrangement used by Earls and Soar to investigate a potential squeal mechanism**

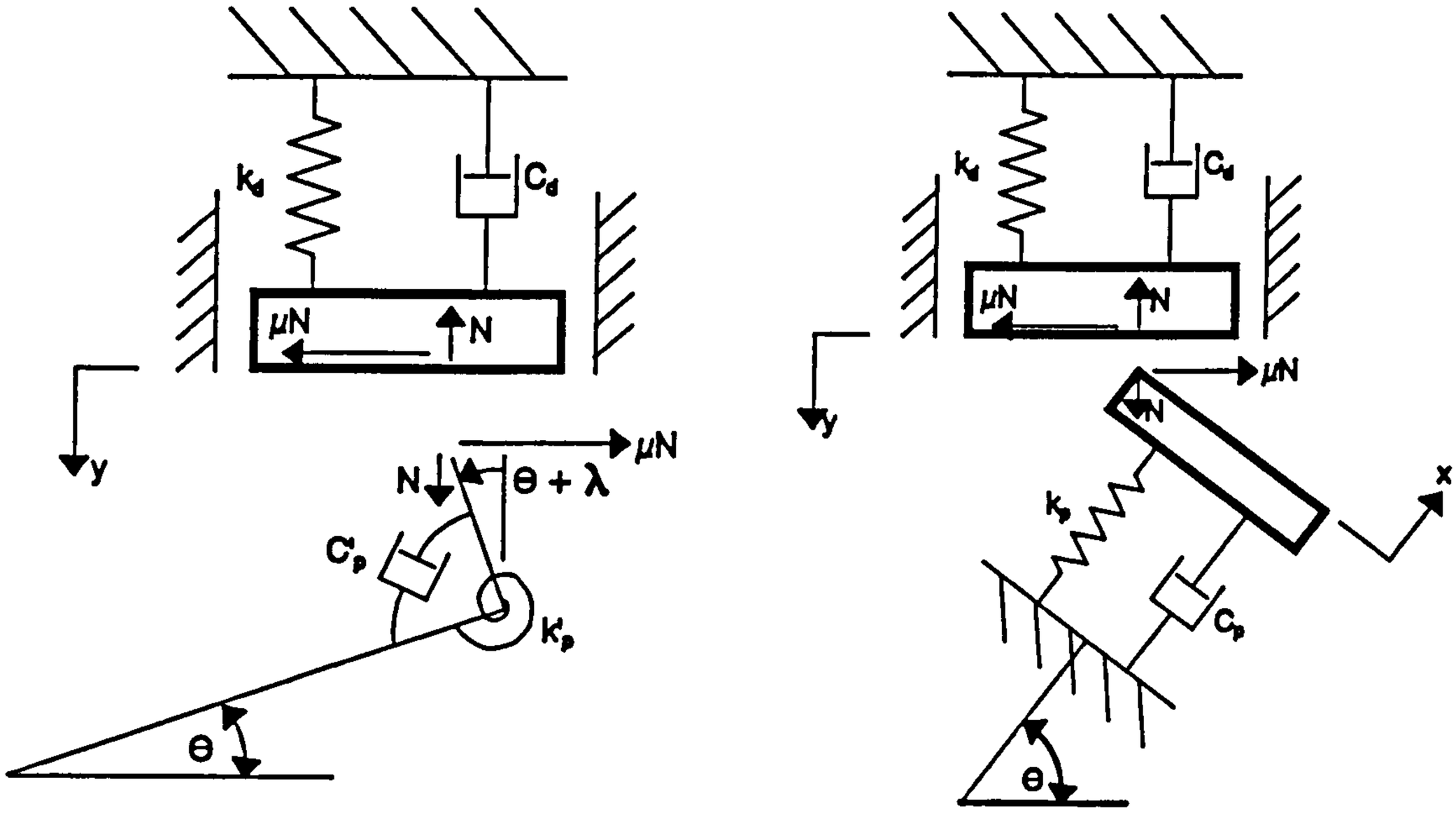

Figure 1.5 The model used by Earls and Soar for analysis of the system in fig 1.4

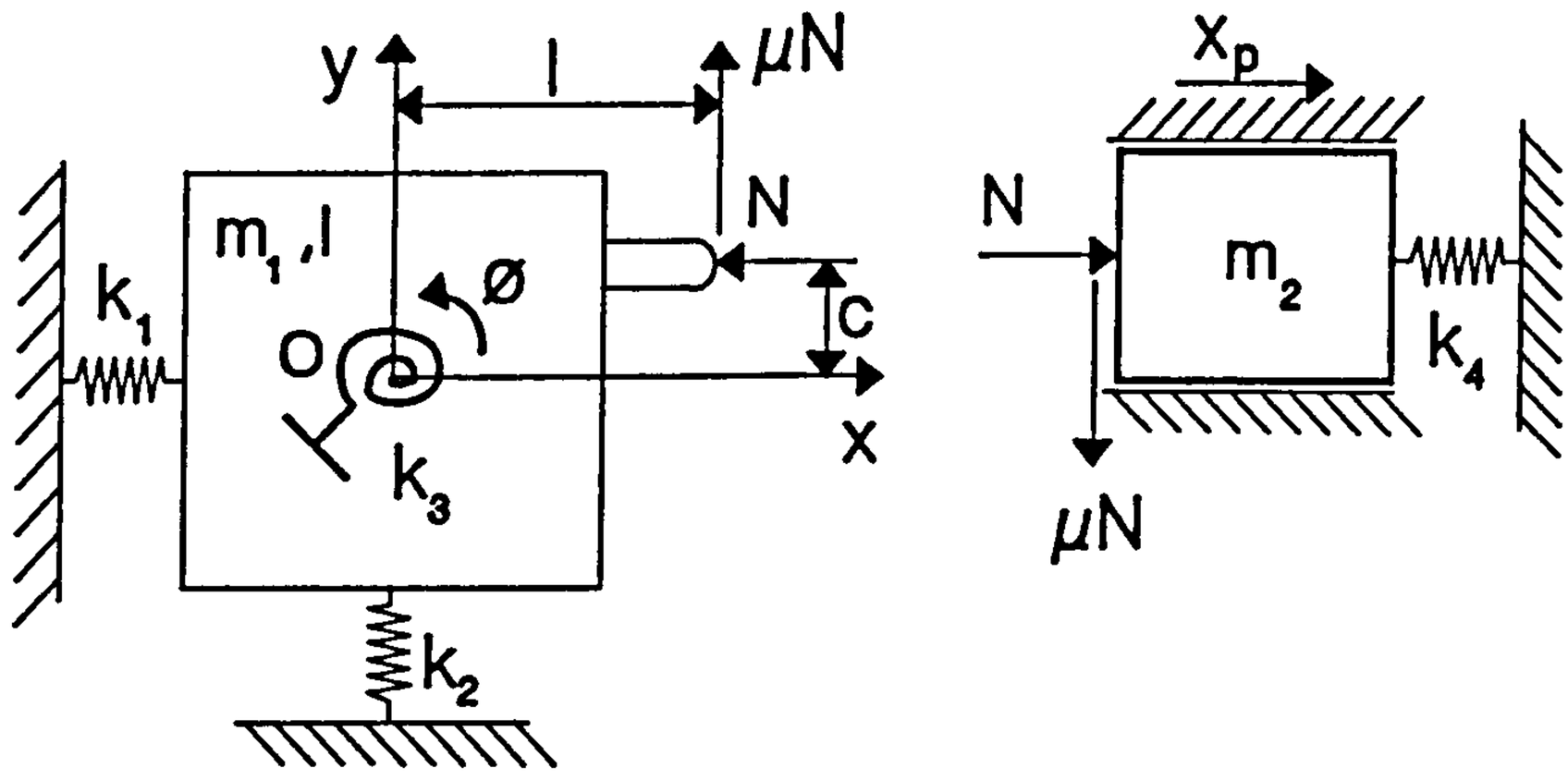

Figure 1.6 The 3-degree of freedom undamped pin model used by Earls and Lee with a single degree of freedom disc

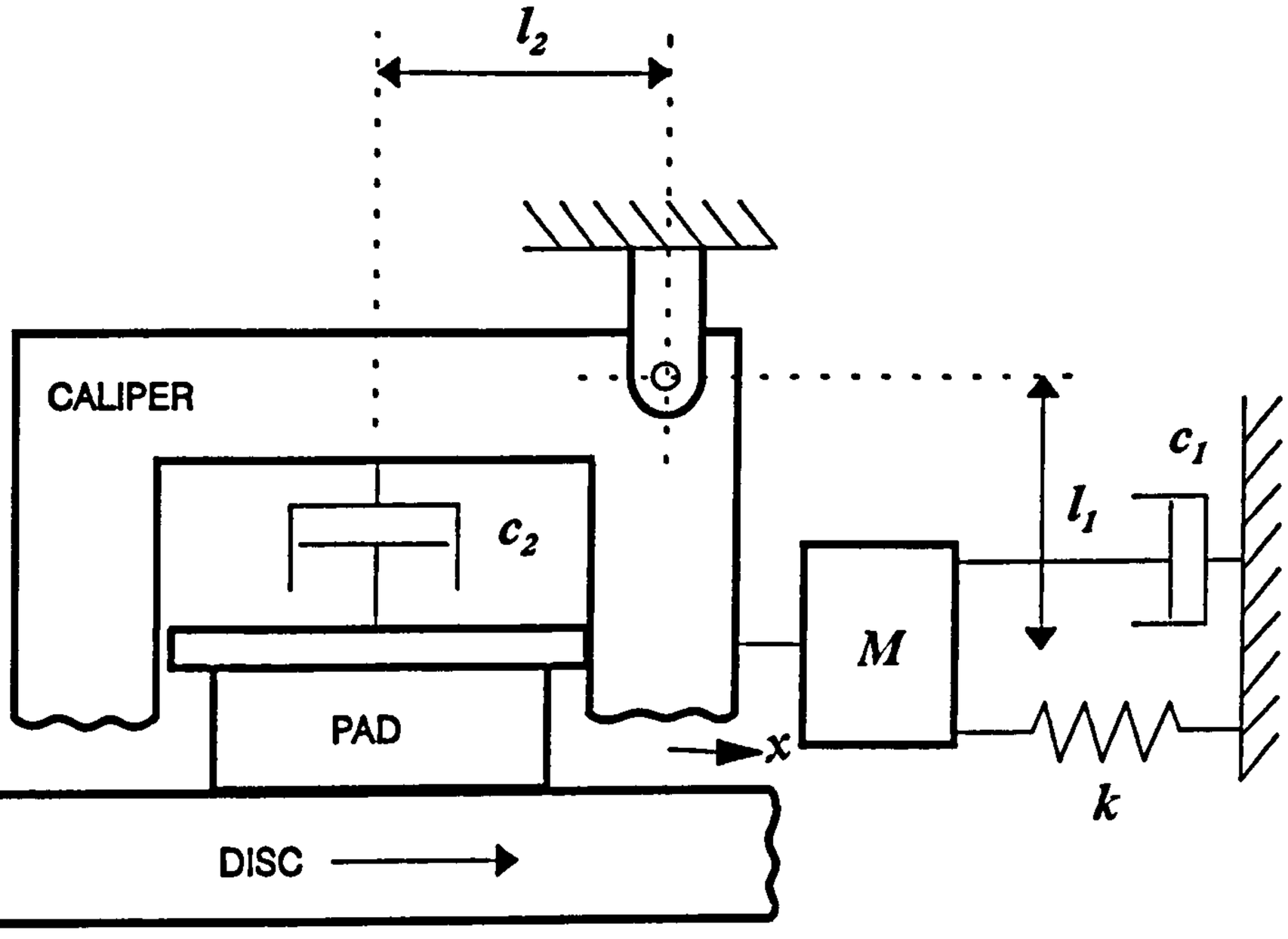

Figure 1.7 Single degree of freedom model for low frequency 'moan' noise due to Lang and Smales

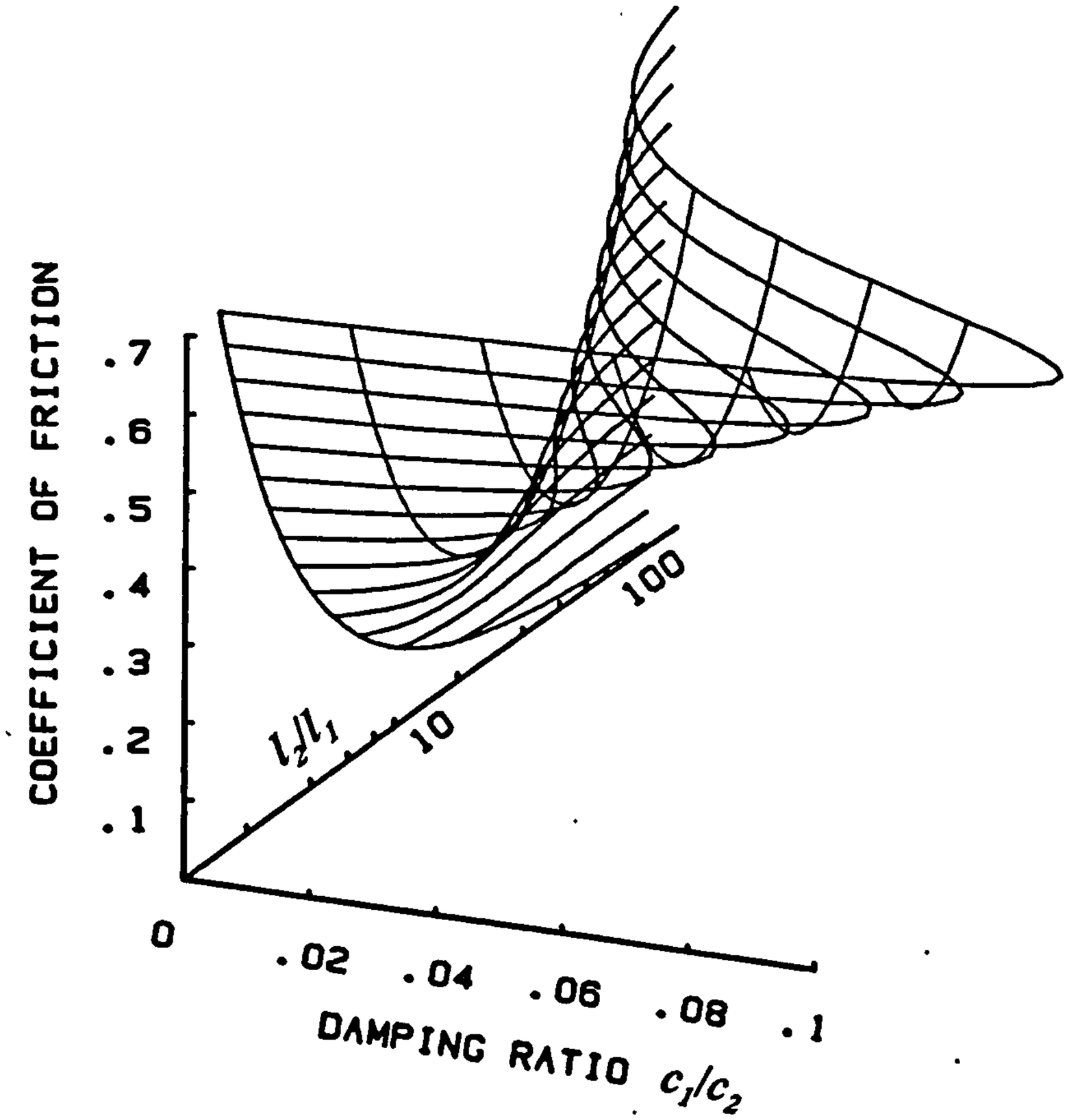

Figure 1.8 The influence of friction coefficient, damping and geometry on the stability of the model in fig 1.7

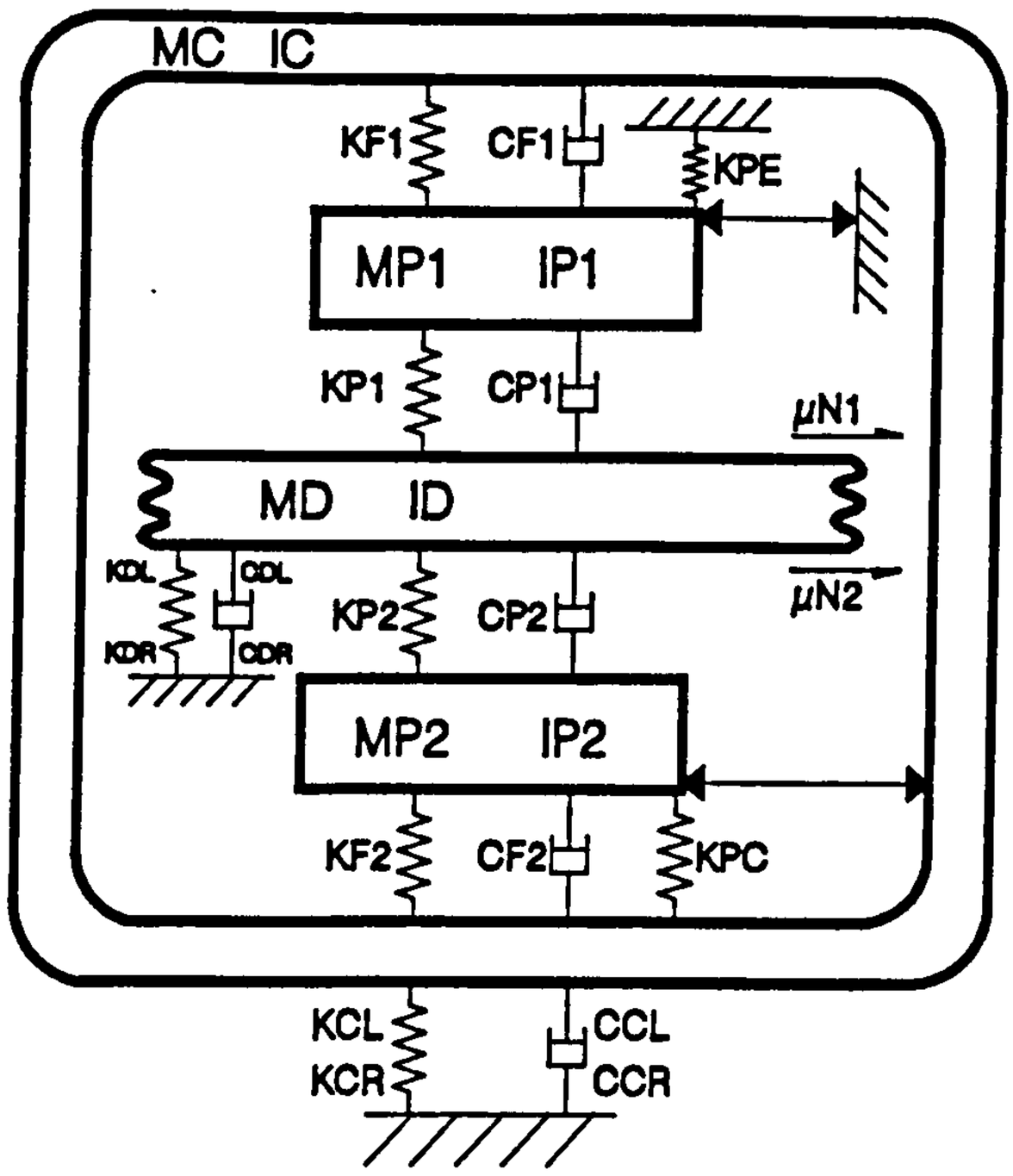

Figure 1.9 **Eight degree of freedom 'flutter' model for disc brake squeal due to North**

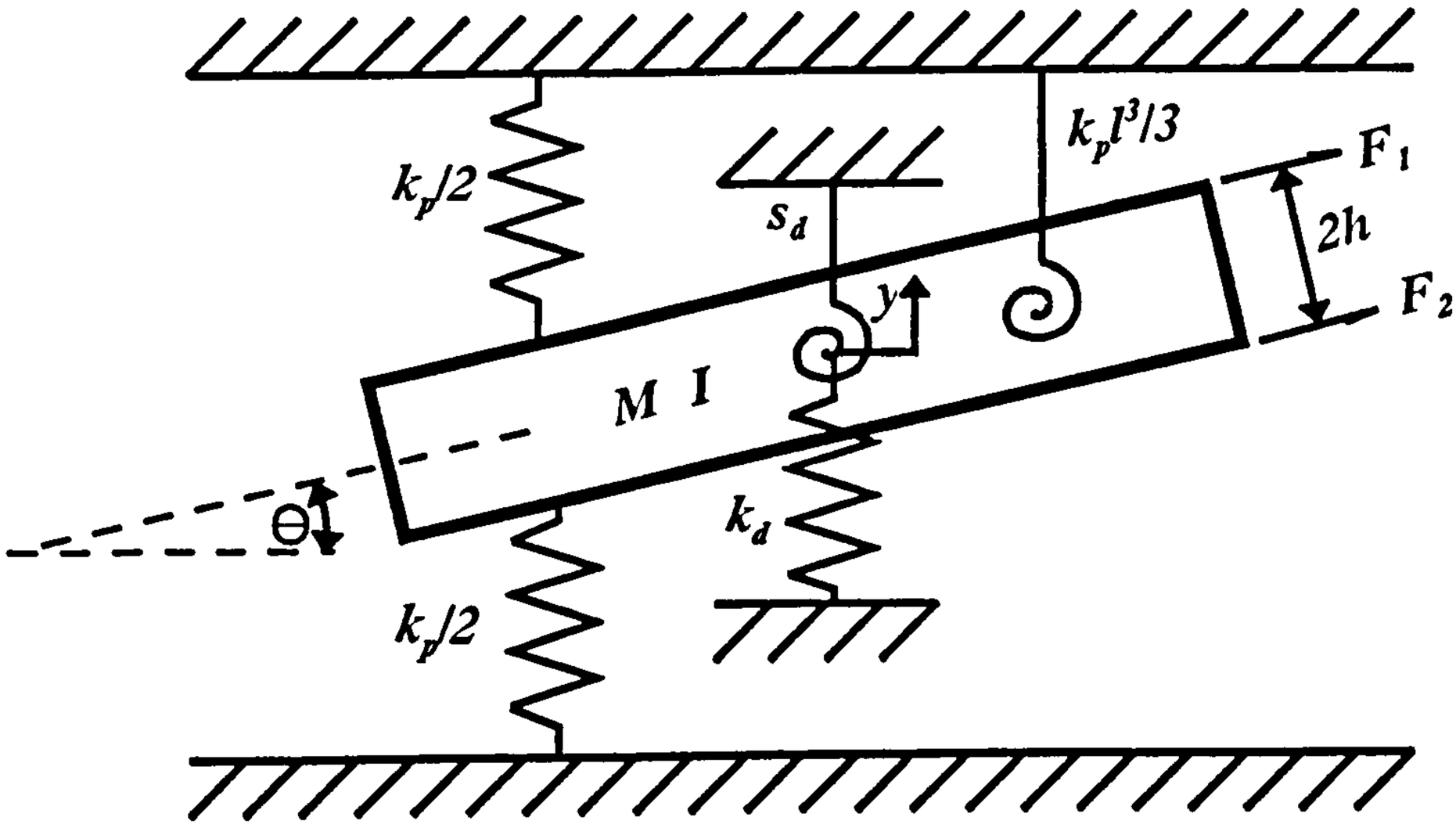

Figure 1.10 **Simplified two degree of freedom model of the binary flutter mechanism for squeal**

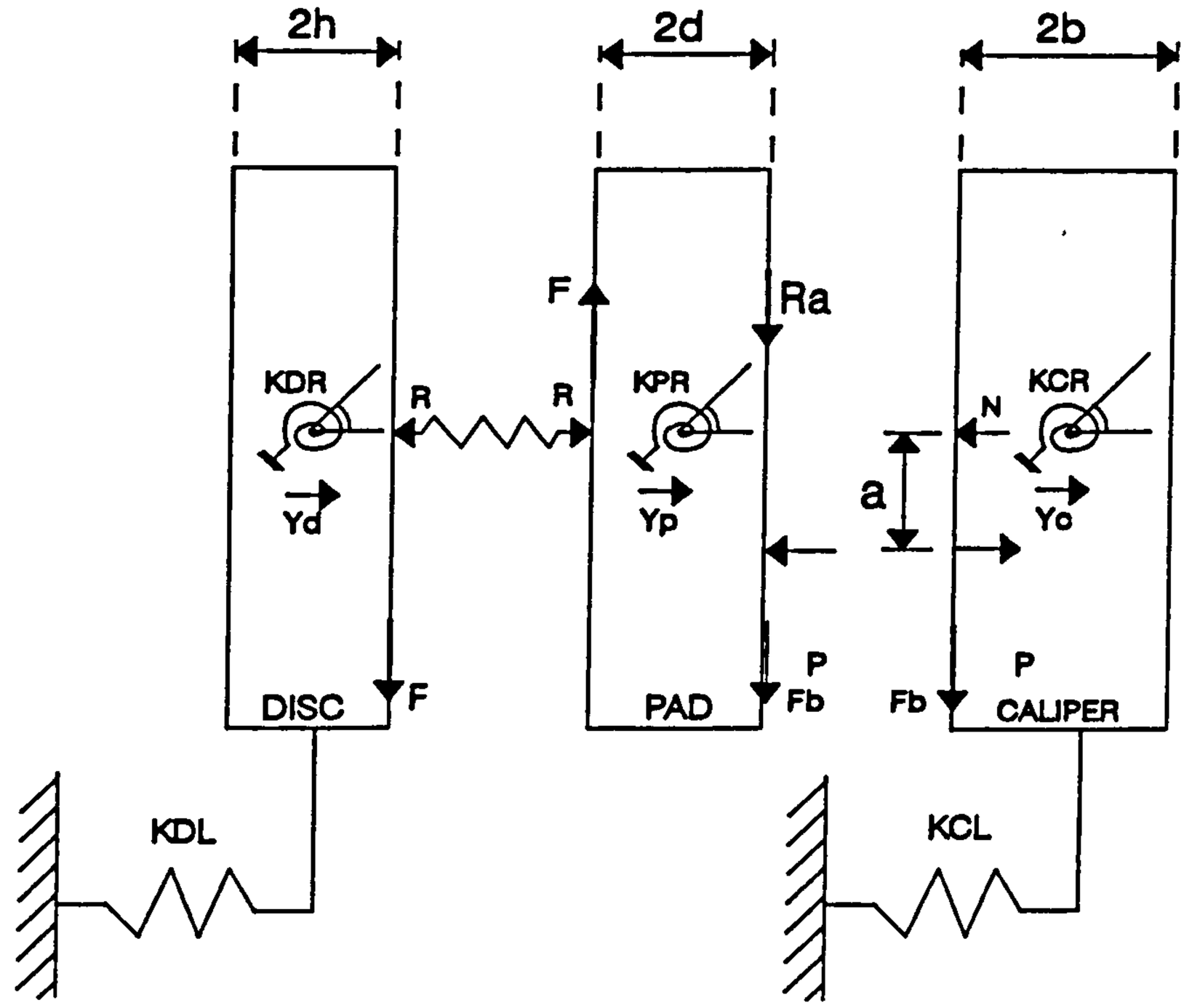

Figure 1.11 Six degree of freedom 'flutter' model for disc brake squeal due to Millner.

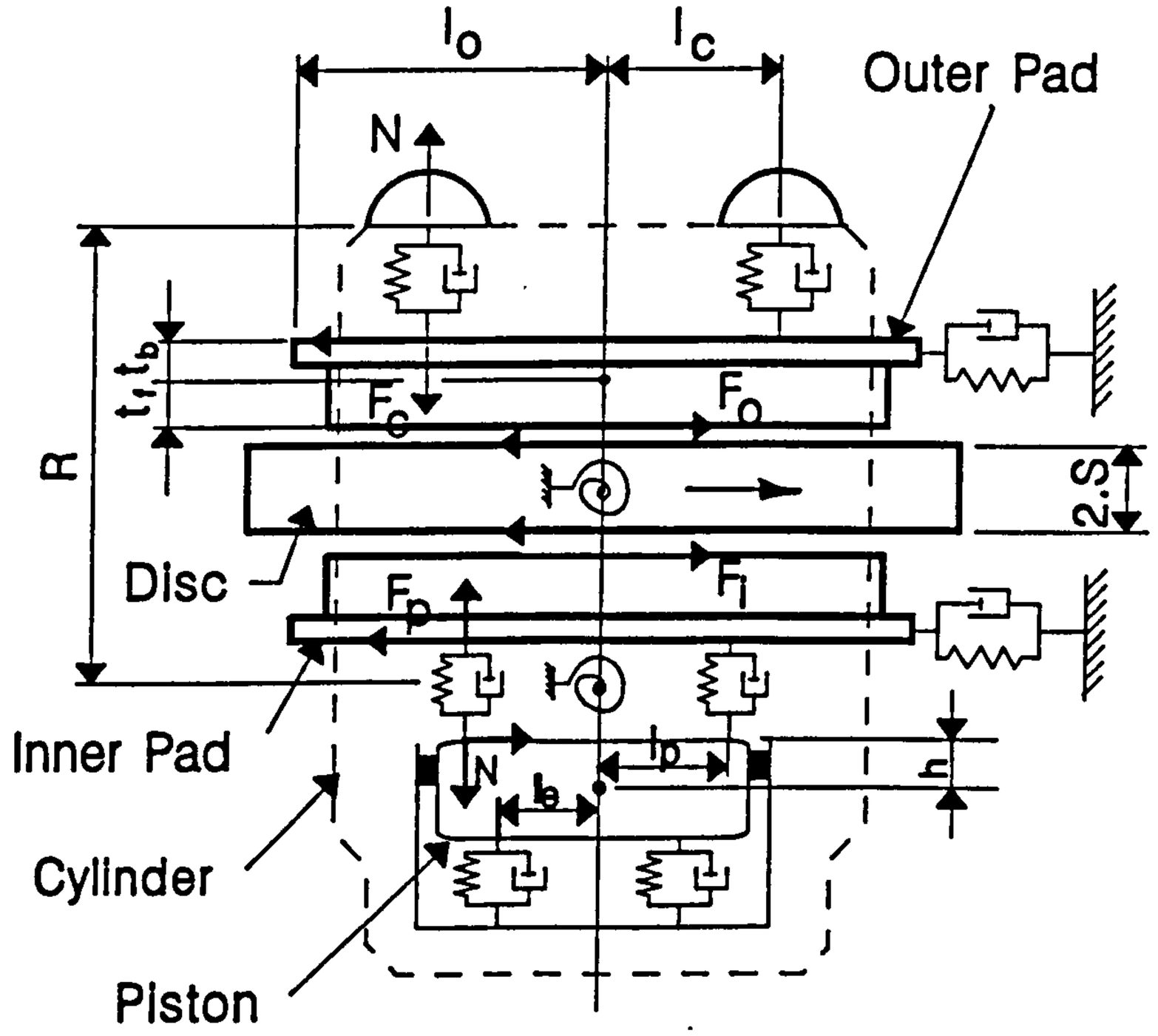

Figure 1.12 Lumped parameter model for disc brake squeal due to Murakami et al, allowing only single degree of freedom disc motion.

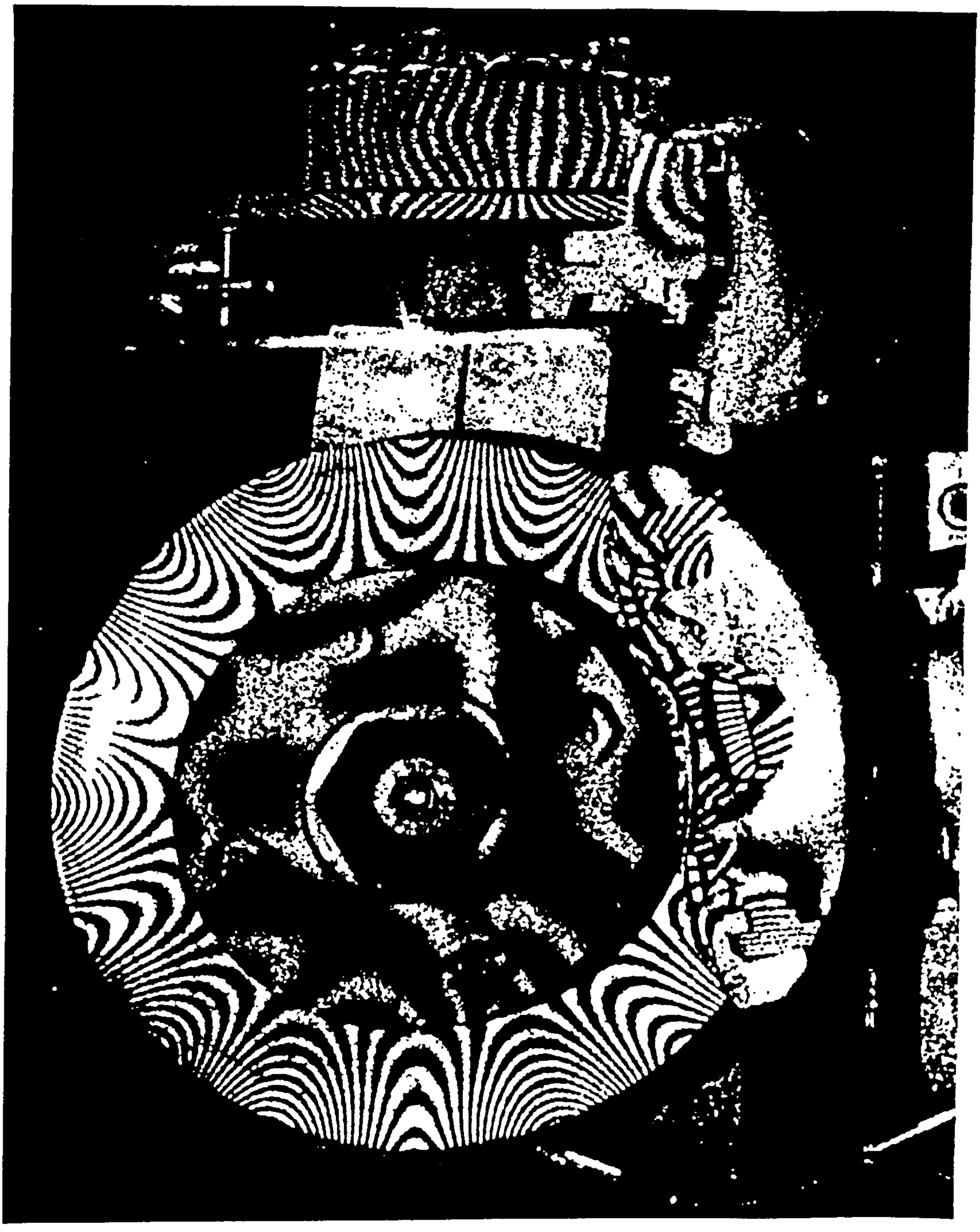

Figure 1.13 **Holographic modal analysis of disc brake squeal by Fieldhouse and Newcomb, showing a wavelike disc mode and complex flexural motion of the pad.**

CHAPTER 2

DEFINING AND REPRODUCING THE SQUEAL PROBLEM TO BE INVESTIGATED

2.1 Introduction

It is clear from the literature, and also everyday experience, that brake noise problems take many forms and occur in some form in most types of vehicle brake installation, both disc and drum. The choice of a specific squeal problem for detailed investigation, from the wide range available, is therefore not obvious, and may not, in fact, be desirable if generally applicable solutions to squeal are sought. In practice, therefore, a variety of brake installations have been used in the development of the analytical techniques, in order that common features of squeal problems, should they exist, could be identified. For continuity, however, a single brake squeal problem will form the basis of the work reported here, with reference to other brake installations and squeal problems only when significant differences or similarities are noteworthy.

The work has, however, been mainly concerned with drum brakes, in recognition of recent developments in the perceived environmental seriousness of squeal problems associated with heavy goods and public service vehicles. These vehicles currently use large air-operated drum brakes almost exclusively, and have been the subject of little recent published investigation, the literature survey indicating that more recent work has been directed predominantly at the problems of passenger car disc brakes.

2.2 Description of the Brake

The brake chosen for the majority of the investigative work reported here is the popular 412 mm x 203 mm air actuated 'S' cam brake designed and manufactured by Saab Scania in Sweden, for use on both heavy trucks and buses. The dimensions refer to the drum internal diameter and the shoe width, respectively, and the type is named after the 'S' - like shape of the actuating cam. This type of brake is very widely used on heavy goods and public service vehicles, and the brake investigated is typical except for the incorporation of unusually short brake linings (72° arc length compared with the more usual ≈120°) aimed at reduced brake judder and thermal cracking of the brake drum.

A schematic diagram of the brake is shown in fig 2.1. Both brake shoes pivot at one end on fixed 'anchor' pins attached to the axle through a 'torque plate', and are forced against the drum by rotation of an 'S' shaped cam acting on rollers fitted to the other end of the shoes. The direction of rotation of the drum differentiates between the two shoes, the drum moving from the cam end to the anchor end of the *leading shoe*, the other shoe being the *trailing shoe*. The *leading end* of either shoe is the end which any point on the drum approaches first. The cam shaft is located in rigid bearings in the brake torque plate and actuation torque is applied by an air diaphragm through an actuation lever. The direction of cam rotation is usually in the same direction as wheel rotation, and unlike a typical hydraulically operated brake, this type of actuation produces approximately equal displacements at the leading and trailing shoe ends. The shoe tip forces are therefore unequal and such that, on average, they equalise the work done by each shoe. As the leading shoe has a positive self-servo action (and hence a higher shoe factor than the trailing shoe) the greater shoe tip force will be applied to the trailing shoe. The brake shoes are lined with blocks of friction material,

attached to the shoe platform by rivets, the material chosen for most of the investigative work being designated Don D7115, manufactured by Mintex Don Ltd and having a nominal coefficient of friction of $\mu = 0.4$. Don D7115 is a modern, non-asbestos friction material, being a composite of glass fibres and phenol formaldehyde thermosetting resin, with various friction modifiers such as lubricants and abrasives designed to produce a stable friction coefficient over a wide range of operating conditions. The composite is produced from a low density mixture of the constituents in a cavity die using uniaxial pressure (with an elevated temperature), giving the material anisotropic mechanical properties.

A photograph of the brake, mounted on a brake test inertia dynamometer, is shown in fig 2.2.

This type of brake has several advantages for use in research into brake squeal :-

(i) being a drum brake, complete access is available to apply instrumentation to both the outer surface of the drum and the inner surface of the shoe platform. This is not the case with a disc brake where both sides of the disc are friction surfaces and the backs of the pads are largely obstructed by the means of actuation.

(ii) being a large brake, the dynamic behaviour of the components is less influenced by the additional mass of accelerometers than would the lightweight structure of a small, passenger car brake.

(iii) being 'S' cam actuated with a rigidly mounted camshaft, it is possible, in theory, to actuate one shoe only so that the effects of the leading and

trailing shoes can be isolated. This can be carried out in practice by removing the brake lining from the unwanted shoe, but only at low actuation pressures, higher pressures resulting in excessive distortion of the brake.

(iv) brakes of this type are known to suffer from serious low frequency squeal problems, particularly when installed on buses. Furthermore, as low frequency squeal is likely to involve low order component modes the vibrations are more amenable to analysis.

2.3 Vehicle squeal measurement

The above brake is fitted as standard to the rear axle of the Scania P93ML 17 tonne truck, which was known to suffer from brake squeal in service. Noise measurements were carried out on a vehicle instrumented for brake performance test work, which allowed manual recording of the air pressure applied to the brake actuators, the vehicle deceleration and the temperature of the inside surface of the drum (using a rubbing thermocouple). A private test track was used for squeal evaluation in order to eliminate noise from other traffic and to allow the repetition of well defined brake application conditions. Squeal was recorded using a high quality audio cassette recorder (Marantz model CP430) with a cardioid response microphone inside the cab, directed towards an open window. This position was found to suffer less from wind and road noise than when recording close to the wheel, producing a better signal to noise ratio.

By carrying out brake applications over a wide range of operating conditions, it was found that loud squeal was produced most consistently when braking from a vehicle

speed of approximately 50 kmh^{-1} with 3-4 bar air actuation pressure and a drum temperature of around 100°C. In common with many brake installations, the loudness of the squeal generally increased towards the end of the brake application.

The recordings were analysed using a fast fourier transform (FFT) spectrum analyser and a typical squeal spectrum is shown in fig 2.3(a), showing, at 3 bar actuation pressure, a fundamental squeal frequency of 585Hz with some low level (> -26dB) harmonic content. Some pressure dependency of the squeal frequency was observed and is illustrated by fig 2.3(b), showing an increase in frequency to 600Hz at a pressure of 4 bar. The spectra also show an increase, with pressure, in the relative amplitude of the first two harmonics to approximately -13dB from -27dB, indicating a more distorted waveform.

Although under some braking conditions, high frequency 'squeaks' and very low frequency vibrations could be induced, the above squeal was predominant and consistent and similar in character to many other heavy vehicle squeal problems, and, as such was chosen as the subject for detailed investigation.

2.4 The Brake Test Inertia Dynamometer

Although consistent squeal could be reproduced on the vehicle under controlled test track conditions, the basis of the proposed investigation - the detailed modal analysis of the squealing brake - would have presented significant practical difficulties on the vehicle due to the necessarily restricted access to the brake, limitations in the use of instrumentation in a mobile and hostile environment, and the problem of accurate control of braking conditions. It was felt that these difficulties could be diminished if the squeal problem could be reproduced on a type of brake test rig in general use

for highly controlled evaluation of brake performance, usually known as a brake inertia dynamometer.

Fig 2.4 illustrates the inertia dynamometer used for this investigation. It is a double ended machine with the facility for mounting two brake installations simultaneously, though only the end shown was used in these investigations. The brake drum was attached, at its normal mounting bolt positions, to a specially made adaptor plate on a rotatable shaft carrying a number of flywheels. The total inertia attached to the drum can be adjusted in steps from 20 to 3500 kgm^2 by fitting a suitable combination of various sized flywheels, and for these investigations was initially set at 1328 kgm^2, to simulate the proportion of the Scania vehicle mass effectively braked by a single rear brake. A 170 kW motor drives these flywheels at speeds up to 1000 rev min^{-1}, although braking is carried out with the motor drive disconnected so that all the braking torque is used to decelerate the flywheels. The static part of the brake, ie the torque plate, actuator and shoes, was similarly attached to a second, concentric, shaft which is mounted in bearings but restrained from rotating by a lever arm, attached, through a force cell, to the machine frame. The force cell could thus be used to measure the torque output from the brake. The whole of this non-rotating end of the machine is slidable axially relative to the driven end, to allow the brake shoes to be drawn from the drum for fitting and general access.

The normal braking procedure is to accelerate the flywheels to a predetermined speed, remove the motor torque and apply the brake, the actuation being controlled to give either a constant actuation pressure or a constant brake torque output throughout the brake application (the latter to simulate constant deceleration of the vehicle, which is often the case in practice). Alternatively, low brake torques (< 3000 Nm) can be applied at a low, constant speed, by maintaining the drive to the motor. In instances

when squeal could be generated at low actuation pressures (and hence low output torques) - ie less than 1 bar, this latter condition was advantageous in producing long periods of consistent squeal for analysis. The rig is instrumented, in its standard form, to measure brake actuation pressure, torque output, drum speed and drum surface temperature, the latter by means of a type K thermocouple, spring loaded to rub on the inside surface of the drum.

2.5 Reproducing the Squeal Problem on the Inertia Dynamometer

The friction material was first 'bedded' to the drum (ie surface conditioned and worn to develop full area contact with the drum) by carrying out an automated schedule of brake applications involving a variety of braking pressures, speeds and temperatures, typical of low duty service use. When the linings were fully bedded, evaluation over a further wide variety of application conditions showed that squeal could be most readily reproduced at 4-5 bar actuation pressure and between 80°C and 150°C drum temperature, conditions which are not dissimilar to those observed from the vehicle tests in section 2.3. Even under such optimum conditions, however, squeal was only apparent towards the very end of each brake application, typically for only the last 1 second before the drum came to rest, ie during only approximately the last 2 revolutions of the drum. In order to increase the time and the number of drum revolutions available for the modal analysis (described in chapter 3) the flywheel inertia was increased to 1917 kgm^2, which produced a corresponding increase (≈50%) in the duration of the squeal.

Spectrum analysis of audio recordings of the squeal, illustrated in fig 2.5, showed a frequency and harmonic content similar to that observed from the vehicle squeal, the dynamometer fundamental squeal frequency being typically 5% below that from the

vehicle. This frequency difference was not considered a serious drawback as it is known that differences of this order can occur between similar vehicles.

In fig 2.6, the squeal spectrum is compared with the FRF of the dynamometer mounted drum, showing that no close relationship exists between the squeal frequency and that of the drum natural frequencies. This particular squeal problem is thus one which conflicts with the popular empirical approach to such problems, noted in chapter 1, which involves the coincidence of component natural frequencies as a major factor in the mechanism, and hence in the remedy. From this limited information, the 400Hz or 900Hz drum modes might be suspected as being involved in the squeal, but clearly no informed choice could be made between them.

2.6 Summary

A specific heavy vehicle drum brake has been chosen for detailed investigation, of a type in widespread use, and which exhibits environmentally and commercially serious squeal problems. The squeal generated on the test vehicle could be reproduced on a brake test dynamometer under similar brake operating conditions and in both cases the squeal frequency was typical of that produced by many other brake installations of similar size. It is therefore considered that the choice of brake and the use of simulated vehicle braking on a test rig are justified for the detailed investigation which follows.

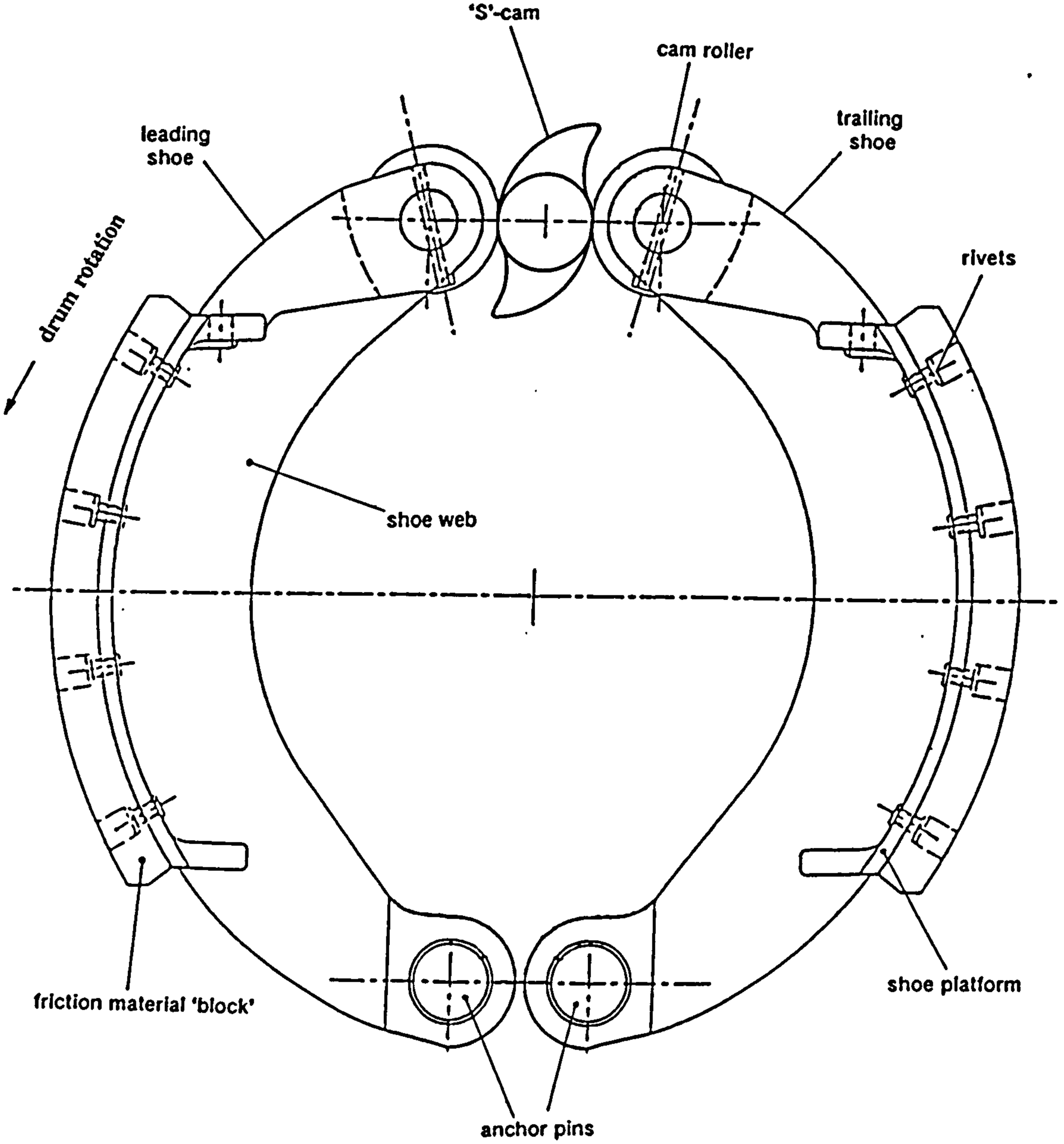

Figure 2.1 **Schematic diagram of the Scania 412mm diameter x 203mm wide 'S'- Cam brake used for the majority of the experimental work**

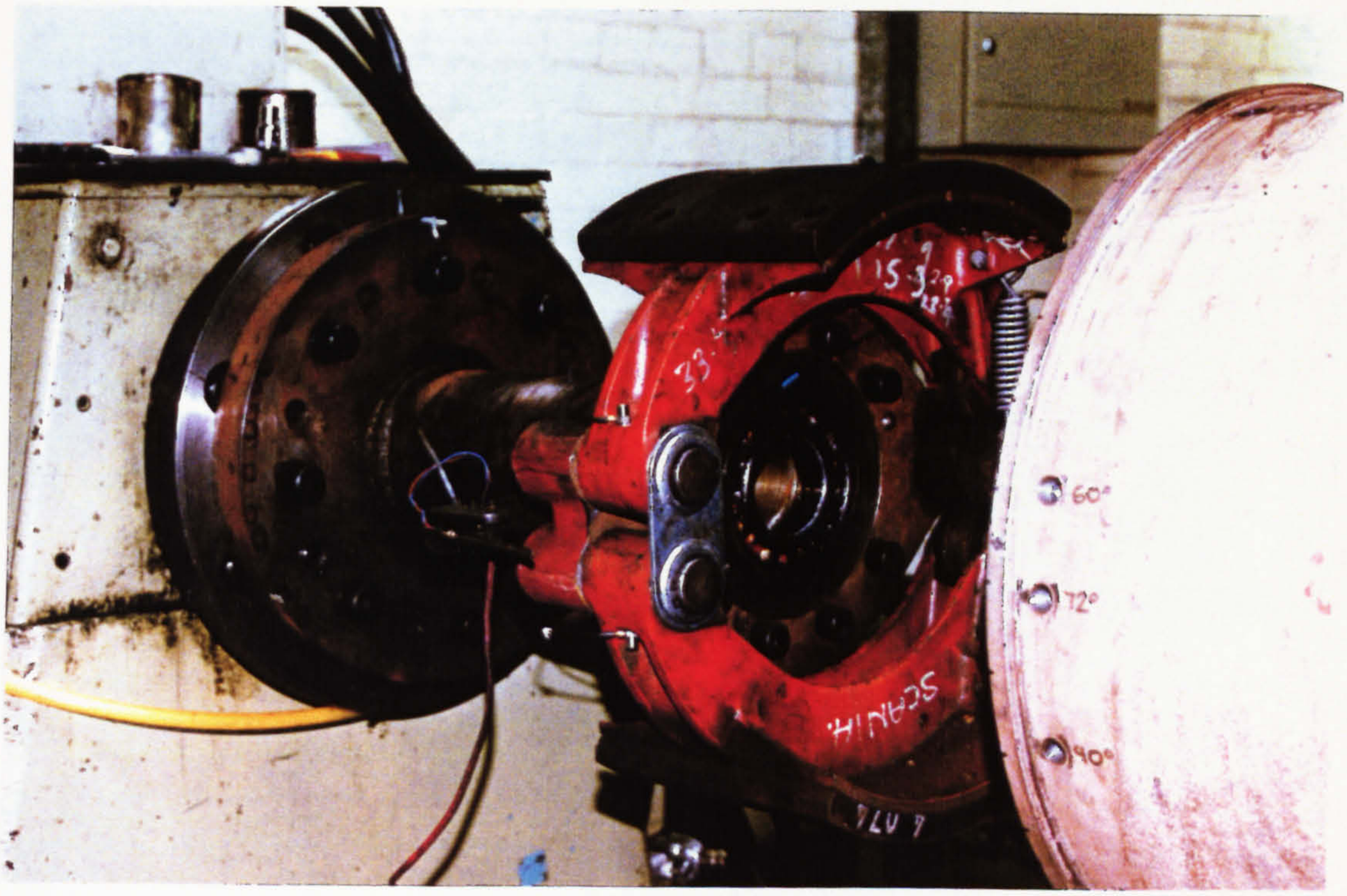

Figure 2.2 **The Scania 412mm x 203mm 'S' cam brake fitted to the brake test inertia dynamometer, showing the torque plate, actuation, and shoes withdrawn from the drum.**

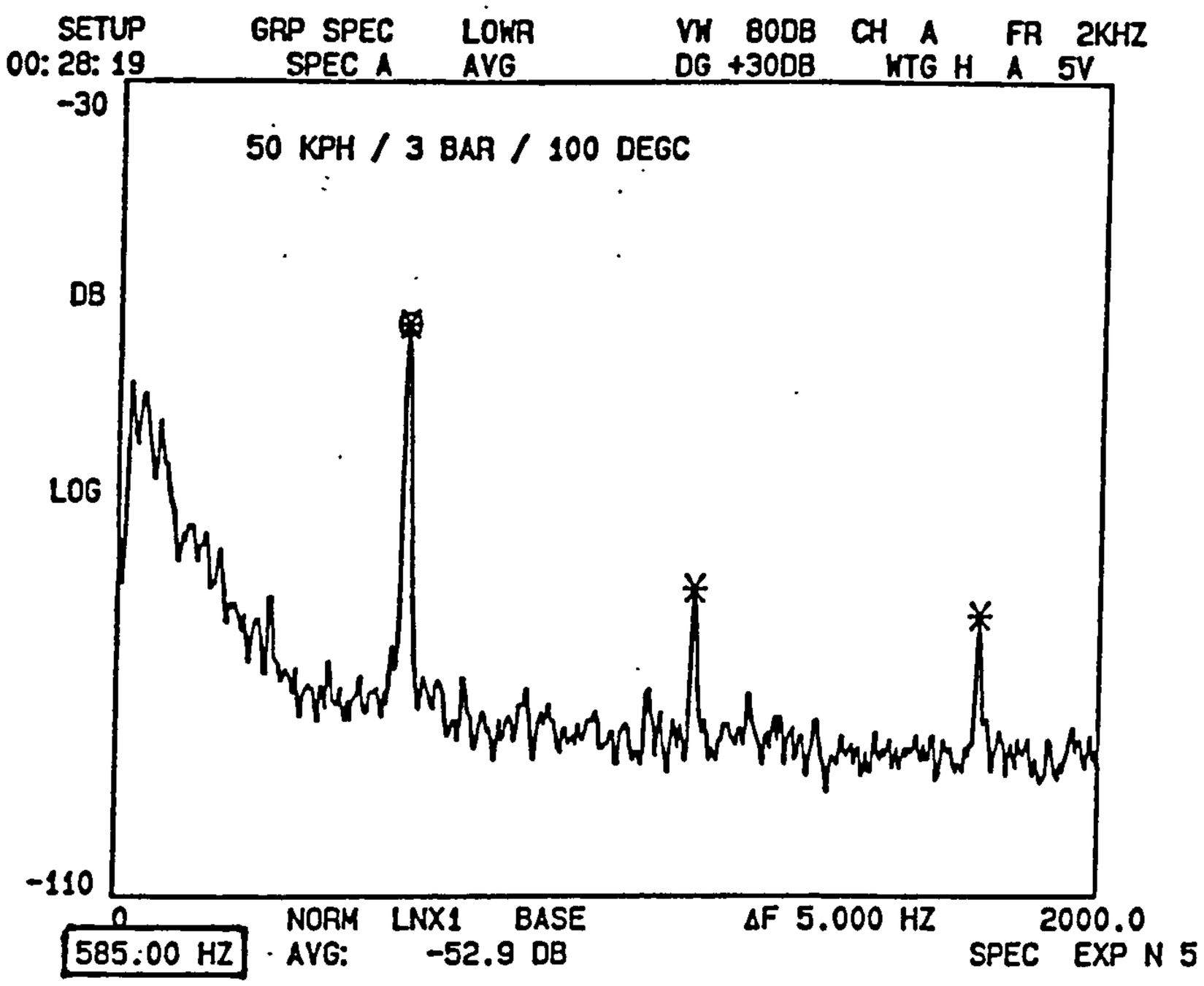

Figure 2.3(a) Spectrum of squeal from a vehicle, at 3 bar actuation pressure

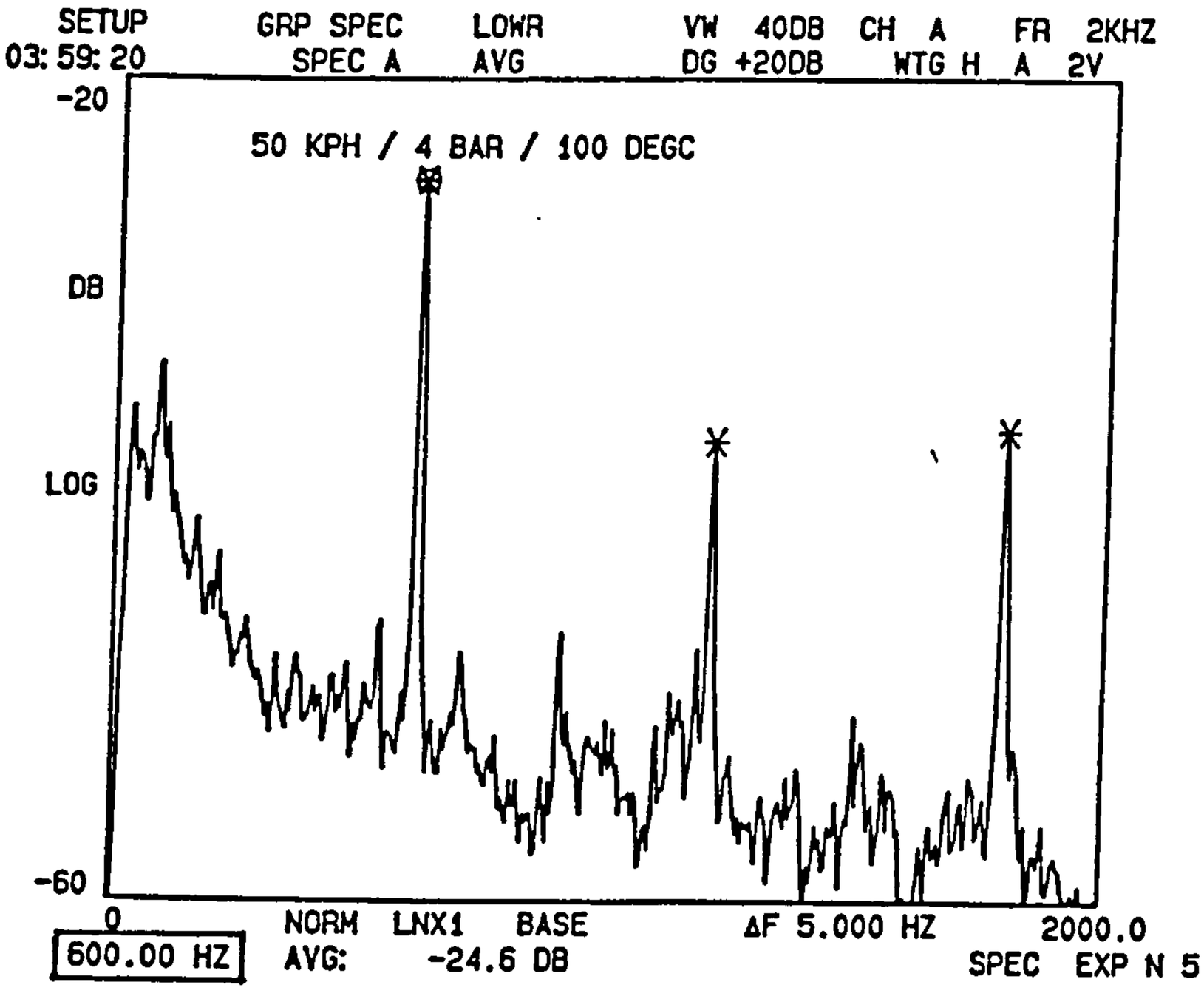

Figure 2.3(b) Spectrum of squeal from vehicle, at 4 bar actuation pressure

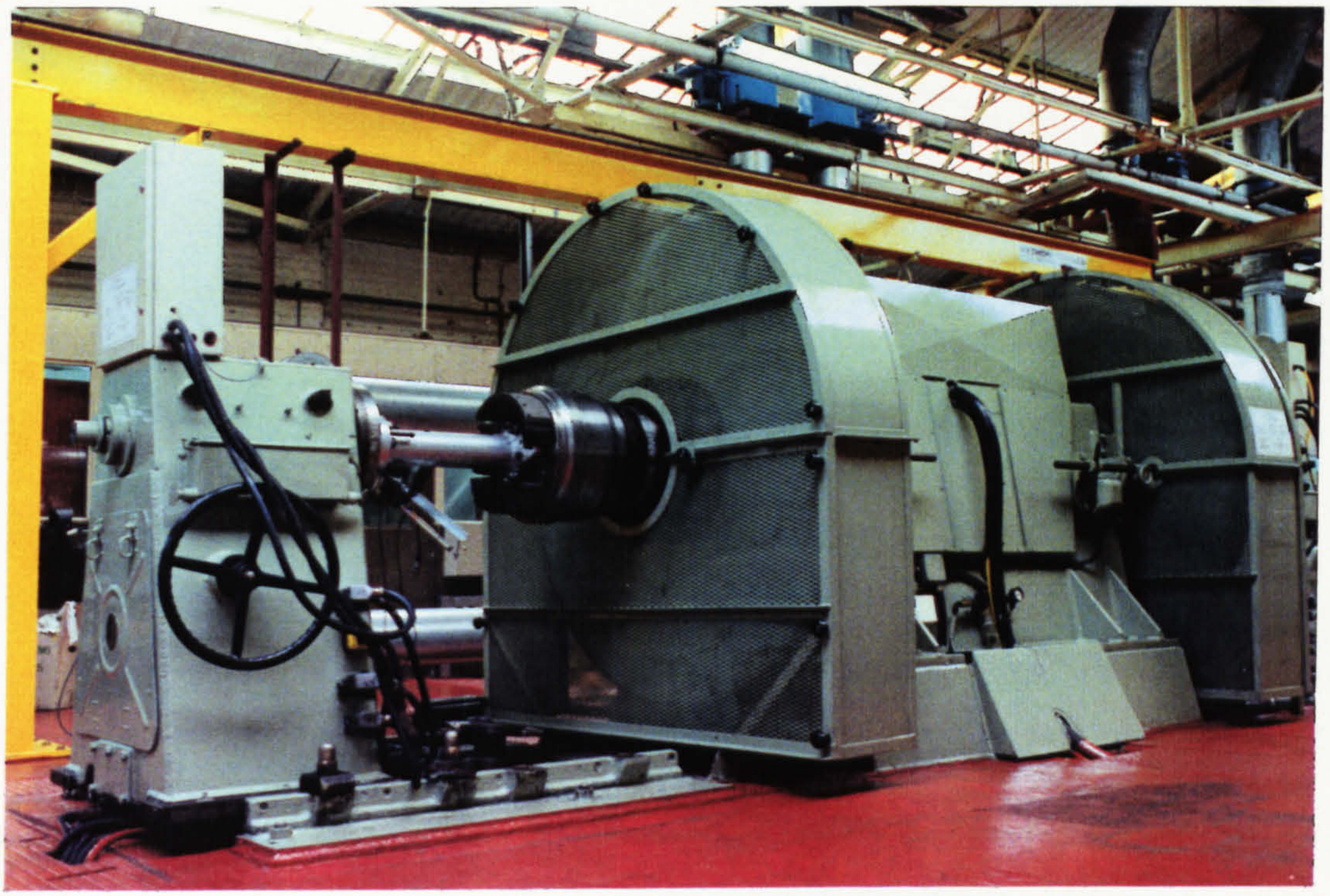

Figure 2.4 **The brake inertia dynamometer used for a major part of the experimental work. The machine is double-ended and the two sets of flywheels can be seen enclosed in safety guards. The drum is attached to the flywheel shaft, and the brake torqueplate, actuator and shoes to the tailstock on the left. The brake shoes are shown partly withdrawn from the drum, achieved by sliding the tailstock along the machine bed.**

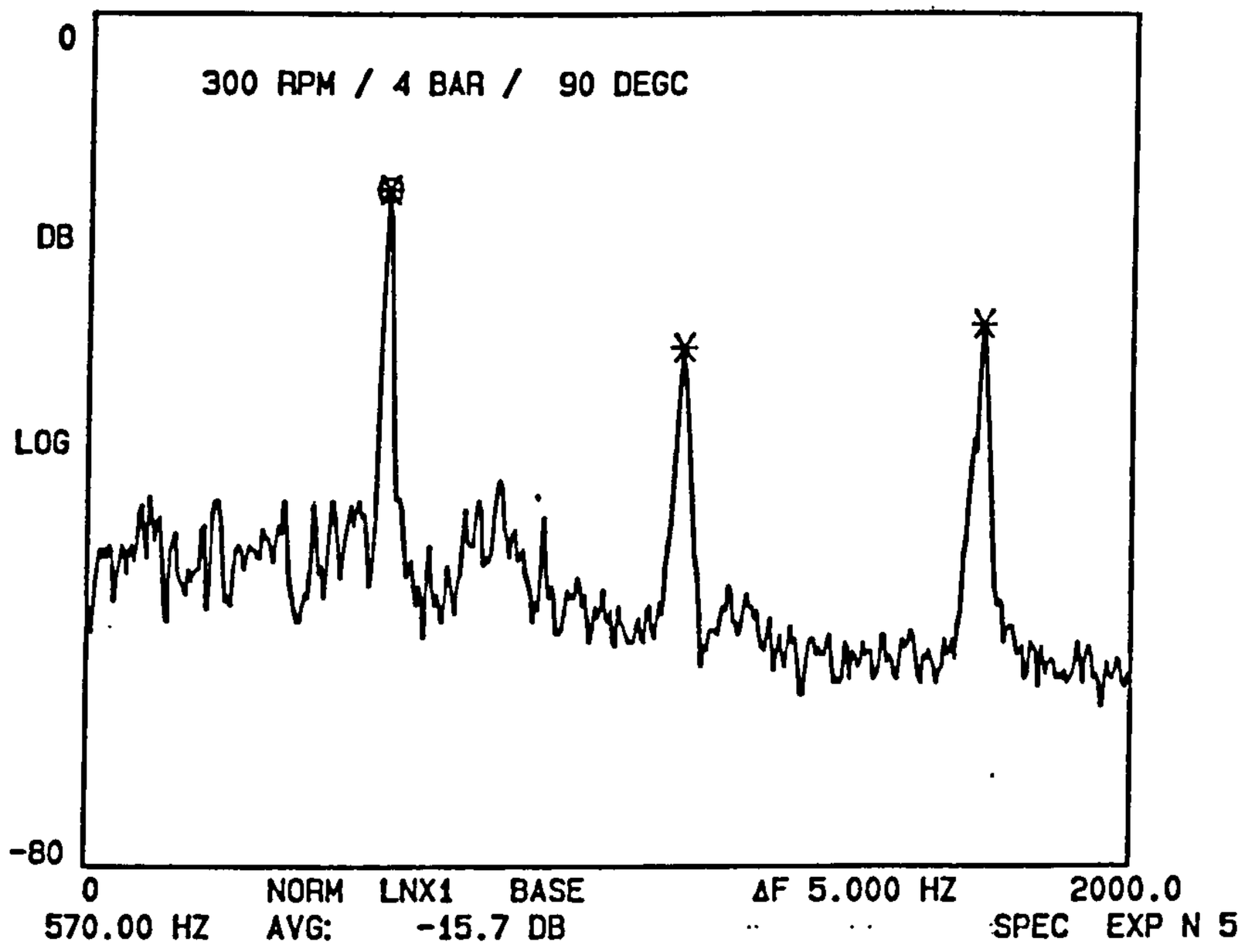

Figure 2.5 Spectrum of squeal from dynamometer mounted brake

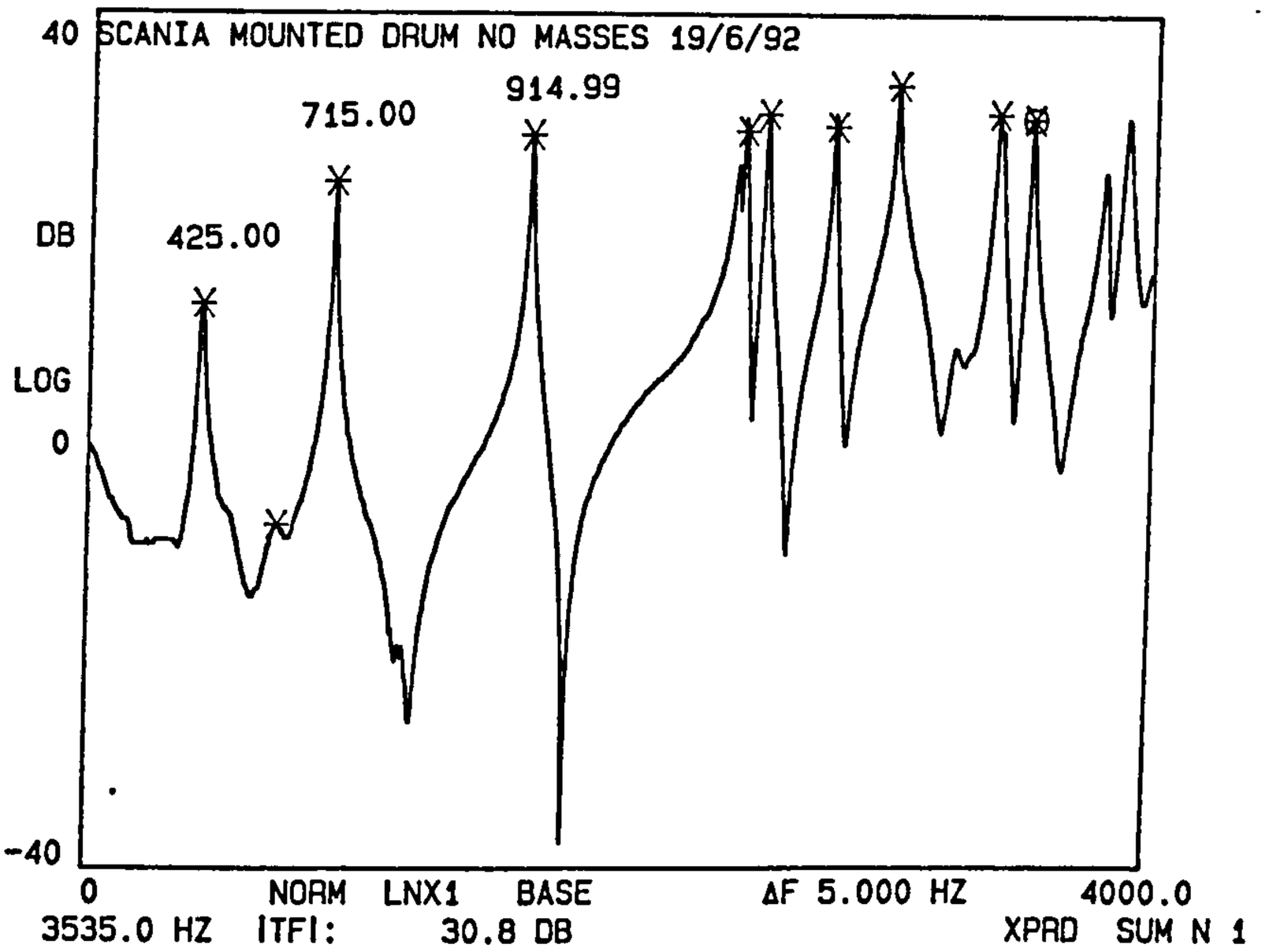

Figure 2.6 Drum frequency response function when mounted on the dynamometer for comparison with the squeal spectrum in fig 2.5

CHAPTER 3

BRAKE DRUM MODAL ANALYSIS

3.1 Introduction

It was suggested in Chapter 1 that the initial objective of this work was to provide an improved description of the dynamic characteristics of a squealing brake, and in particular to identify the complex modal behaviour predicted by some proposed instability mechanisms (for example North (22)). This would provide a basis for distinguishing between existing mechanisms and also indicate a direction for future mathematical modelling.

Standard experimental techniques are available for the complex modal analysis of stationary structures and these can be readily applied to the stationary parts of a brake. Such an application will be described in detail in chapter 4, but, briefly, the technique involves a comparison between the signals from an array of transducers (typically accelerometers), distributed around the structure, and a single amplitude and phase reference transducer. The use of a multiplicity of transducers attached to a rotating body presents formidable practical difficulties, however, particularly in extracting the large number of signals for simultaneous analysis. Although this difficulty can be partially overcome by the use of holographic interferometry (see Fieldhouse and Newcomb (33)) to examine, for example, the plane surface of a brake disc, it is more difficult both to apply, and to interpret the results generally, without extensive development of the technique. Further, the double pulsed holographic technique developed for examining rotating discs is currently inhibited in its ability to provide

phase information because of the need to produce multiple images and hence cannot easily produce a complete complex modal analysis.

In order to achieve the above objective, it was therefore necessary to develop a relatively inexpensive and convenient means of obtaining a complex modal analysis of the rotating drum whilst squealing, and a description of this development and the results obtained will form the principal part of this chapter.

Prior to this work on the squealing brake, however, the normal modes of the drum were examined to indicate the types of mode to be expected, and also to quantify the effect of mounting the drum to the dynamometer.

3.2 Brake Drum Normal Modal Analysis

Normal modal analysis was carried out on a drum under two restraint conditions :-

i) mounted on the brake inertia dynamometer using the normal drum mounting bolt positions, in the squeal test condition.

ii) unmounted, face upward, with the mounting face placed on a foam rubber block to approximate to the freely suspended or unrestrained condition.

The primary purpose of the latter condition was to provide data under well defined boundary conditions to support later finite element modelling (described in chapter 6), but in addition, a comparison between the two conditions gave an indication of the magnitude of the influence of the drum mounting on its dynamic behaviour.

The drum was excited using a force-measuring impact hammer and the response measured by a low mass (2.4g) accelerometer, attached to the outer surface of the drum mouth and directed to measure radially. The transfer function between the response and excitation force was produced by a two-channel FFT spectrum analyser.

Mode shapes were measured using a single response position at the drum mouth, and multiple equally spaced radial impact excitation points, both around the drum mouth and axially across the brake rubbing path. The resulting sets of transfer functions were assembled into waterfall diagrams (Fig 3.1 is typical for a set measured around the drum mouth) and the circumferential and axial mode shapes were then given by profiles through these diagrams at the various natural frequencies. Fig 3.2 shows typical mode components, fig 3.2(a) being the shape around the drum mouth circumference and fig 3.2(b) the shape axially across the rubbing path, and from results such as these most modes could be classified by the number of *pairs* of nodal lines in the axial direction across the brake rubbing path (n) and the number of circumferential nodal lines around the rubbing path (s). Hence the example shown is the $n = 3, s = 0$ mode. Note that because of the wavelike nature of the circumferential mode shape the axial nodes must, for continuity, occur in pairs, and will be referred to as 'meridian nodes', a term used by Perrin and Charnley (38) in their work on campanologists bells, based on the topological similarity of the nodal lines to geographical meridian lines. A more graphic illustration of the shpes of the modes was obtained by impacting over a grid of points on the outer surface of the drum and analysing the resultant transfer functions using modal analysis animation software, producing shapes typified by fig 3.3. The measured drum modes are summarised in table 3.1 overleaf.

Table 3.1 Normal Modes of the Drum

Mode	Free Natural Frequency (Hz)	Fixed Natural Frequency (Hz)
n = 2, s = 0	325	415
n = 3, s = 0	900	915
n = 4, s = 0	1637	1645
n = 3, s = 1	not found	2445
n = 4, s = 1	2462	2785
n = 5, s = 0	2512	2525

It is clear, from the comparison of free and fixed natural frequencies, that, as would be expected, mounting the drum to the dynamometer has a predominantly stiffening effect, increasing all the above natural frequencies. The fundamental, n=2,s=0 mode is particularly influenced by mounting, whilst the effect on the higher s=0 modes is small. Examination of the mode shapes across the rubbing path shows that for the higher order free modes the amplitude near the drum mounting region is small and hence will be little influenced by additional restraint. This is not the case for the n=2,s=0 and n=4,s=1 modes, where significant mounting face amplitudes are seen.

Clearly, none of the above modes is close in frequency to the measured squeal frequency of 580-600 Hz, and, although it may be suspected that the n=2,s=0 mode is likely to be involved, being closest to the squeal frequency, this is by no means certain as this would require a 42% frquency increase, whereas the n=3,s=0 mode would reqire only a 36% decrease to match the squeal frequency.

3.3 Measurement of the Modes Held by the Drum Whilst Squealing.

3.3.1 Background

The usual method employed in modal analysis of a vibrating structure is to determine the transfer function between the motion at each point of an array of points on the surface of the structure and the motion at a fixed reference point. The transfer functions can then be used to produce a vibration amplitude and phase distribution for the structure normalised to that at the reference point. This technique is, however, difficult to apply directly to a rotating drum during squealing as:-

(i) the structure being analysed is rotating, making the acquisition of a large number of simultaneous measurements, from accelerometers on its surface, difficult.

(ii) the squeal vibration is a transient phenomenon allowing little time for sequential measurements by multiplexing the signals from large number of fixed accelerometers.

To overcome these difficulties, a technique has been developed of sequential measurements, not from an array of individual transducers, but from recordings of a single transducer which effectively scans the vibration mode.

It is well known (for example Rayleigh (37)) that the normal modes of a circular disc, symmetrical about its axis, take a form which can be approximated by the equation

$$y = f(r)\sin n\theta \qquad (3\text{-}1)$$

the predominant displacement, y, being in the axial direction. $f(r)$ represents the form of the displaced shape along a radius (at $\theta = 0$) and may have zero values at certain radii corresponding to circular nodal lines.

The normal modes measured in section 3.2 also indicate that the cylindrical section of a brake drum behaves in a similar manner to that described above and the mode shapes over this cylindrical area can again be approximated by an equation of the form

$$y = f(z)\sin n\theta \tag{3-2}$$

In this case the predominant displacement, y, is radial and $f(z)$ is the displaced shape of an axial line across the drum rubbing path and again may have zero values at certain axial positions corresponding to the circular nodal lines referred to in section 3.2 (ie if $s>0$).

The initial objective of the experimental work was to detect whether such modes are present on a squealing drum and, if so, to measure their detailed form and assess their contribution to the instability. Investigation of the axial form of the mode, $f(z)$, was limited to detecting the presence or absence of circular nodal lines, the significance of which lies in classifying the squeal as essentially a 2-dimensional or 3-dimensional phenomenon. If no circular nodal lines are present, then the problem could be considered as fundamentally 2-dimensional, which may have significant repercussions in simplifying future modelling work.

The modal analysis technique developed here is based upon an initial assumption that the wavelike vibration mode of the drum will not rotate with the drum but remain fixed in space relative to the stationary brake shoes. This assumption is supported by

the observation that brake squeal is generally a continuous phenomenon with no apparent changes in characteristics related to the angular position of the drum, suggesting that the motions of the drum and shoe at the friction interface are time-invariant and hence independent of drum angular position.

If the drum mode is fixed in space and time-invariant, then accelerometers fixed to, and rotating with, the drum, can be used to 'scan' the mode at any axial (z) position, and sequential measurements of the mode can be used to determine the circumferential form during one revolution of the drum.

3.3.2 Experimental arrangement

A schematic diagram of the experimental arrangement is shown in fig 3.4, and a photograph of the brake with its local equipment in fig 3.5. Low mass accelerometers, were attached to the outer surface of the drum in the positions shown, ie two on the extreme ends of a line parallel to the drum axis running across the rubbing path, and a third at the drum mouth, displaced by 90° around the drum from the position of the first two. The accelerometers were attached using screw/adhesive adaptors with cyanoacrylate adhesive and were directed to measure radially. Low noise cables transferred the signals from these accelerometers to three battery powered charge amplifiers attached to the drum adaptor and hence rotating with the drum. Commercial, small, battery powered charge amplifiers were not available and so operational amplifier based units were designed and constructed specifically for this purpose as detailed in Appendix 1.

The voltage signals from the low impedance output of the charge amplifiers could now be transferred, through a slip ring arrangement, to three channels of a high quality frequency modulated (FM) magnetic tape recorder.

A reference accelerometer was attached to measure radially at the leading end of the leading shoe platform, as shown in fig 3.4. This signal was also transferred, via a commercial charge amplifier, to a fourth channel of the magnetic tape recorder.

The modal analysis technique, which will be described in detail in 3.3.5, requires that the angular position of the 'scanning' accelerometers on the drum are known when any measurement of the mode is taken. Measurement of the drum angular position was achieved using an optical encoder driven from the dynamometer shaft by a toothed belt. The encoder produced parallel outputs of 1 ,2, 4, 8, 16, 32, 64 and 128 pulses per revolution (ppr), of which only the 1 and 128 ppr signals were recorded on a further two channels of the magnetic tape recorder. Fig 3.6 shows the relationship between these signals. The angular position of accelerometer A on the drum was chosen such that it was passing the centre line of the brake camshaft as the leading edge of the 1ppr signal occurred. Thus, the absolute position of the accelerometers could be determined to a resolution of 1.4° (if both leading and trailing edges of the 128 ppr signals were used).

The magnetic tape recorder on which all these signals were recorded is a frequency modulated (FM) recorder with a bandwidth dependent upon the chosen tape speed. Although a speed of 4.76 cms^{-1}, giving a bandwidth of 1250 Hz, would have been adequate for the low frequency (≈600 Hz) squeal being investigated, in practice the maximum speed of 76 cms^{-1}(giving a 20kHz bandwidth) was used to allow the maximum freedom to expand time on replay, where necessary, to aid analysis.

3.3.3 System calibration

No facilities were available for the absolute calibration of the accelerometer measuring system, nor was it considered necessary that accurate absolute values of acceleration (or displacement) be obtained for modal analysis of this type, where the vibration amplitude is continually changing. The manufacturer's quoted accelerometer sensitivities, together with the known transfer functions of the charge amplifiers were used to estimate absolute amplitudes of vibration, whilst accuracy of relative values for modal analysis was assured by using accelerometers with outputs normalised to ±1% of the nominal value. The relative calibrations of the system channels were checked by 'back to back' testing of accelerometers on an electromagnetic shaker.

3.3.4 Spectrum analysis of the recorded signals

The signals from the three drum accelerometers, the reference accelerometer on the shoe and the 1 ppr and 128 ppr signals from the optical encoder were recorded on the magnetic tape recorder during squealing brake applications, under various operating conditions.

Single channel spectrum analysis of the shoe reference signal, fig 3.7, shows the frequency content of the vibration, which is similar to that obtained from the audible noise, shown in fig 2.5. The only significant differences in frequency content are in the presence of a higher level of background random noise in the sound spectrum, produced by the dynamometer drive equipment, together with some difference in the harmonic distortion of the basic squeal frequency.

The amplitude of the 580Hz squeal vibration at the shoe reference point was typically of the order of 100 ms^{-2} or 7 μm, but was not constant with time, as shown by the typical amplitude time history in fig 3.8. In addition, the overall amplitude and variability of such time histories changed with brake operating conditions. The effect of this variability in the overall amplitude of the vibration was minimised in the mode shape measurements by defining the mode shape in terms of the transfer function between the drum and shoe motion, the shoe accelerometer providing an amplitude, as well as a phase, reference. It needs to be recognised, however, that the underlying assumption of system linearity, implying that the mode shape is independent of amplitude, is unlikely to be exactly true.

3.3.5 The modal analysis technique

The procedure used to determine the drum modes during squealing can now be described as follows:-

i) the signals from a drum accelerometer and the shoe reference accelerometer, which had been recorded at a high tape speed as described in 3.3.2, were replayed, at a lower tape speed, into the two channels of the FFT spectrum analyser.

ii) the spectrum analyser was configured to calculate the magnitude of the transfer function between drum and reference signals, and to do this repeatedly on demand from an external trigger signal.

iii) the recorded 128 ppr signal from the optical encoder was used to trigger the above transfer function analyses, producing 128 transfer functions per revolution of the drum.

iv) the recorded 1 ppr signal from the optical encoder was used to form a 'window' allowing only 128 of the above pulses to trigger the analyser, thus scanning one well-defined revolution only, starting and ending at a radial line through the cam shaft centre.

v) the 128 transfer function magnitude versus frequency characteristics were assembled into a waterfall diagram by the analyser. A profile through this diagram, at the squeal frequency (corrected for reduced tape playback speed), produced the required amplitude of the mode shape of the drum.

vi) the procedure (ii) to (v) was repeated for the phase and the real and imaginary parts of the complex transfer function, as required.

Conditioning of the trigger signals from the recorder to produce the TTL level required by the analyser, and applying the one revolution window to these signals was achieved by using simple logic circuitry. The circuit allowed manual selection of the drum revolution to be analysed, with a choice of two start positions, 180° apart, on a diameter of the brake through the camshaft centre.

Even though the squeal usually occurred only at the very end of the brake application when the rotational speed was low, the time for one revolution of the drum was too short for real time transfer function analysis, together with storage to a waterfall file, to be carried out 128 times. To increase the time available for analysis the tape replay speed was reduced by a factor of 64 from the recording speed (ie from 76 cms^{-1} to 1.2 cms^{-1}), reducing the frequency of the ≈600Hz squeal to ≈9Hz. Although the associated reduction in analysis frequency range incurred an analysis time penalty, the

major benefit achieved was to reduce the frequency of the trigger pulse to less than the maximum waterfall file update rate.

A typical waterfall diagram of transfer function magnitude (|TF|) v frequency is illustrated in fig 3.9, which shows only 80 transfer functions due to a limitation of the available display, although the waterfall file stored in the analyser contains all 128. It can be seen that in the region of the (scaled down) squeal frequency, the values of |TF| show a wavelike characteristic with angular position, corresponding to the expected wavelike circumerential mode shape of the drum. At all other frequencies, except at harmonics of the squeal frequncy the values of |TF| show no pattern due to lack of coherence between the signals, which consist of low level random noise. It was usually possible, by careful choice of signal gains, to ensure higher noise levels on the reference signal and thus low levels of 'background' |TF| on the waterfall diagram, as illustrated in fig 3.9.

It is clear, from the width of the wavelike section of the diagram, that the frequency resolution used for the analysis was low. The factors affecting the choice of resolution were:-

(i) small variations in frequency are often observed during each revolution of the brake, probably due to unavoidable eccentricity and ovality in the drum, and a typical frequency variation can be seen in the high resolution spectrum analysis of fig 3.10. This frequency variability together with a high FFT frequency resolution could result in inaccuracy when attempting to produce a profile through the diagram at a single frequency.

(ii) As frequency resolution is not an important factor in mode shape determination, greater amplitude accuracy can be achieved using 'flat-top' filtering in place of the more usual 'Hanning' filtering, which is designed to achieve a compromise between frequency and amplitude accuracy.

(iii) Although 800, 400, 200, or 100 line FFT analyses were available on the analyser, using the minimum resolution of 100 lines over the analysis frequency range resulted in the highest FFT analysis speed.

FFT analysis speed was found to be an extremely important factor in obtaining accurate modal analysis results. The analysis speed obtainable depends upon the frequency range of the analysis together with the chosen number of lines of frequency resolution, as noted above. Initial results using an appropriate analysis frequency range of 0-20Hz for the ≈9Hz signals produced the expected wavelike mode shape. However, comparative analysis of the recorded signals played in the forward and reverse directions showed a significant difference in the angular positions of the modes as shown in fig 3.11, suggesting the influence of a time delay in the analysis. Increasing the analysis speed by increasing the frequency range of the analysis reduced this delay, as illustrated in fig 3.12, which shows the mode amplitude using 20Hz, 50Hz, 100Hz and 200Hz analysis ranges. This suggests that errors in the position of the mode shape will be small when using the 200Hz analysis range, and this range was therefore used for all subsequent modal analyses. It may also be noted from fig 3.12, that the error in the mode position is more marked at the beginning of the revolution than the end, and this is due to the reduction in speed of the drum during the revolution, increasing the time between encoder pulses and hence analyses, and thus making the analysis delay less significant.

3.3.6 Drum modal analysis results

A profile through the |TF| waterfall diagram of fig 3.9, at the scaled down squeal frequency of ≈10Hz, is shown in fig 3.13(a). This represents the vibration amplitude distribution circumferentially around the drum mouth (position A in fig 3.3) and the wavelike nature of the mode shape is apparent. The four 'antinodes' suggest a form similar to the n=2 normal mode measured in section 3.3, but at no point around the circumference does the measured amplitude reduce to zero, and this lack of true nodes indicates that this cannot be a normal n=2 mode. Fig 3.13(b) shows a similar amplitude distribution characteristic taken from another 'S'-Cam brake (by Steyr of Austria), although in this case the squeal mode is an n=5 type at a higher frequency of 2.5 kHz.

Repeating the procedure described in 3.3.5 for the phase(ϕ) of the transfer function produced the waterfall diagram of phase distribution shown in fig 3.14, with a profile at the squeal frequency in as illustrated in fig 3.15 (again, this particular result is taken from the Steyr 'S'-cam brake, showing an n=5 type characteristic). This shows a continuous phase change around the drum circumference (the discontinuities being merely a return to zero after a 360° shift is accumulated) unlike the discrete 180° phase changes at the nodes of a normal mode. These |TF| and ϕ results thus indicate the presence of a complex drum mode which could alternatively be described by its real and imaginary components relative to the reference signal.

Again, repeating the analysis procedure described in 3.3.5 for the Real (Re) and imaginary (Im) parts of the transfer function separately, and superimposing the waterfall diagram profiles, results in the form of the complex mode shown in fig 3.16.

The 'scanning' technique used to obtain this result is based upon assumptions that the mode is time invariant and is fixed relative to the shoes, and, as noted in section 3.3.1, data from a second accelerometer, angularly displaced from accelerometer A, is required to justify these assumptions. In fig 3.17, the complex drum mode produced using accelerometer C, which is positioned 90° around the drum mouth from A (see fig 3.3), is compared with that from A. It can be seen from the results that the mode components are identical apart from a spatial phase shift of 90°, corresponding to the 90° physical separation of the measurement points on the drum. Thus, identical modes have been measured at times separated by $\pi/2\omega$ seconds, the time taken for the drum to rotate through 90°, the separation of the accelerometers, supporting the assumtion of time-invariance of the mode.

The accelerometer in position B, fig 3.4, axially displaced across the rubbing path from A, was used to determine the presence or absence of a circumferential node around the rubbing path, as discussed in section 3.3.2. The complex modes measured using accelerometers A and B are compared in fig 3.18, from which it is clear that the circumferential mode shape at the mounted side of the rubbing path is similar to that at the drum mouth, but has a reduced amplitude. No phase shift occurred across the rubbing path, confirming that an even number of circumferential nodal circles must have been present, and, considering the low frequency of the mode, this number can be taken to be zero (particularly as the first normal mode having $s>1$ is at a frequency of $\approx$ 2.8 kHz).

3.3.7 Discussion of results

Each of the components in fig 3.16 is similar in form to a normal $n=2$ mode as measured in section 3.3 and illustrated in fig 3.19, and the complex mode can thus be

described as the superposition of two similar normal modes of the same mode order (n=2). These normal modes are time phase shifted by 90° and also spatially phase shifted relative to each other in a circumferential direction. In this case, the spatial phase shift is approximately 45°, or ¼ the wavelength of the mode shape wave, so that the nodes of one mode approximately coincide with the antinodes of the second mode.

The two components of the drum mouth mode can therefore be approximated by the equations

$$\begin{aligned} y_1 &= a_1 \sin n\theta \sin \omega t \\ y_2 &= a_2 \sin\left(n\theta + \frac{\pi}{2}\right) \cos \omega t \end{aligned} \tag{3-3}$$

If the components were of equal amplitude, a, then the sum of the components would be

$$y_1 + y_2 = a(\sin n\theta \sin n\omega t + \cos n\theta \cos \omega t) \tag{3-4}$$

$$or \quad y_1 + y_2 = a \cos(n\theta - \omega t) \tag{3-5}$$

This suggests that the complex drum mode can also be approximated by a wave of wavelength π/n radians, travelling around the drum with angular velocity ω. This is consistent with the findings of Fieldhouse and Newcomb (33), who inferred such a rotating wave from holographic analysis of a squealing disc brake. The absence of a circumferential nodal circle on the drum rubbing path indicates that the normal mode components of the complex mode are similar to the n=2,s=0 normal mode of the fixed drum measured in section 3.3.

Now the observed complex modal characteristic of the squealing drum is consistent with an essential feature of the binary flutter mechanism of squeal proposed by North (22), which requires 2-degree of freedom motion of the rotor in the region of contact

with the brake lining. North suggested that these 2 degrees of freedom could be provided by two independent flexural modes of the rotor having identical forms and frequencies, but separated angularly into 'sine' and 'cosine' modes. The relationship between the motions of the rotor segment of the flutter model and the two rotor modes is illustrated in fig 3.20, and it is clear that the spatial relationship between these modes is in close agreement with those of the drum, measured above. This complex rotor motion is not a feature of the pin-disc squeal mechanics discussed in Chapter 1 (which involve single degree of freedom drum motion), and hence the consistency of this behaviour (on a range of brakes and at a range of squeal frequencies, as will be shown in section 3.3.8), suggests that binary flutter is the more likely mechanism for the instability.

3.3.8 Comparison of drum squeal modes from other brake installations

The Scania brake used as the focus for this work produced only a single repeatable squeal frequency, the ≈580 Hz investigated in detail here. As noted ealier, a second 'S' cam brake, manufactured by Steyr of Austria, and of similar size and construction was also tested and found to produce several squeal frequencies under different operating conditions, typically 1.3 kHz at 1-2 bar, 2.5 kHz at 3 bar and 5.5 kHz at 7.3 bar. All these squeals occurred over only a small part of each revolution, however, and so proved difficult to analyse. Continuous loud squeal at 2.5 kHz was, however, obtained by applying only the leading shoe to the drum, by removing the trailing shoe lining. *It is interesting to note at this point that when the trailing shoe alone was applied to the drum, by removing the leading shoe lining, no squeal could be obtained from the brake, suggesting that, in this case, the unstable interaction is restricted to the leading shoe only.*

Drum squeal modal analysis produced the amplitude and phase distributions already shown in figs 3.14 and 3.15 and the complex mode illustrated in fig 3.21. Although a higher drum mode is involved (the n=5,s=0 mode), the spatial relationship between the real and imaginary components is clearly similar to that seen in the Scania n=2,s=0 squeal mode. In this case, the squeal frequency of 2.5 kHz is more closely related to the normal mode frequency of the mounted drum - 2275 Hz for the n=5,s=0 mode - than is the case for the Scania brake.

The similarity between the drum squeal modal characteristics of two similar heavy vehicle brakes squealing at very different frequencies and involving different drum mode orders, indicates that such complex modes may be a common feature of squeal. To further test this indication, two dissimilar squealing brakes were also analysed, a small 180mm x 30mm passenger car drum brake squealing at 3.3 kHz and a medium sized, 308mm x 89mm light truck drum brake squealing at a range of discrete frequencies between 7-10 kHz (the analysed frequency being 7.7kHz).

The measured complex drum modes, from these two different sized drum brakes, are illustrated in figs 3.22 and 3.23 respectively, and although the quality of the measurements is poor, due to discontinuous squeal, similar characteristics are seen, supporting the results obtained from the larger brakes.

3.3 Summary

By using a novel 'scanning' modal analysis technique, it has been shown that, during squeal, the drum holds a complex wavelike mode, which, when expressed in the form of real and imaginary component modes approximates to the superposition of two spatially phase shifted normal modes. The mode components are stationary in space

and similar in form to those measured on the static drum, with s=0 (ie no circumferential nodes) but the squeal frequency is significantly different from these normal mode frequencies. This modal behaviour also appears to be a common feature of a range of squeal problems on different sized brakes.

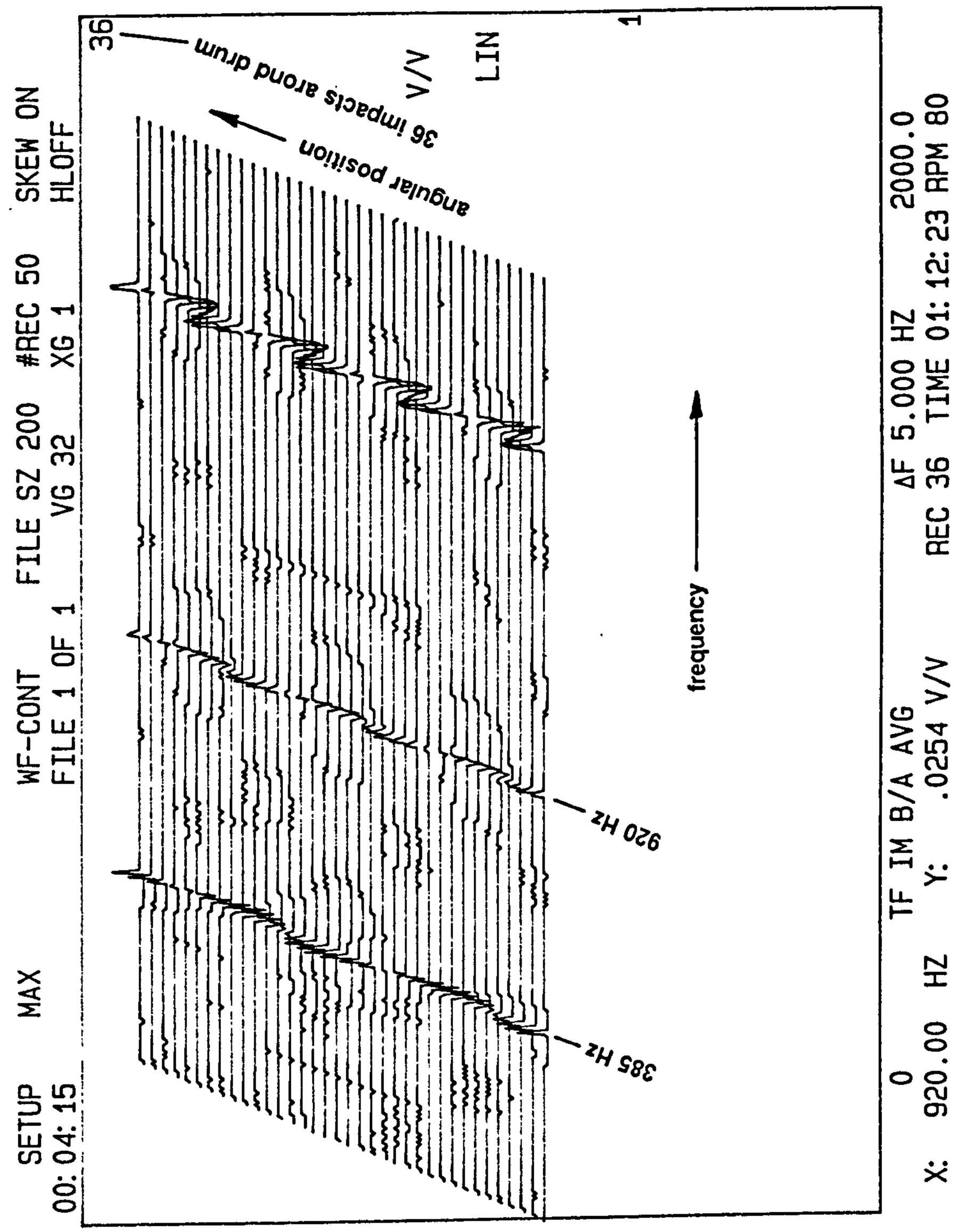

Figure 3.1 Waterfall diagram of the imaginary parts of the transfer functions, obtained from the response to impact excitation around the drum mouth

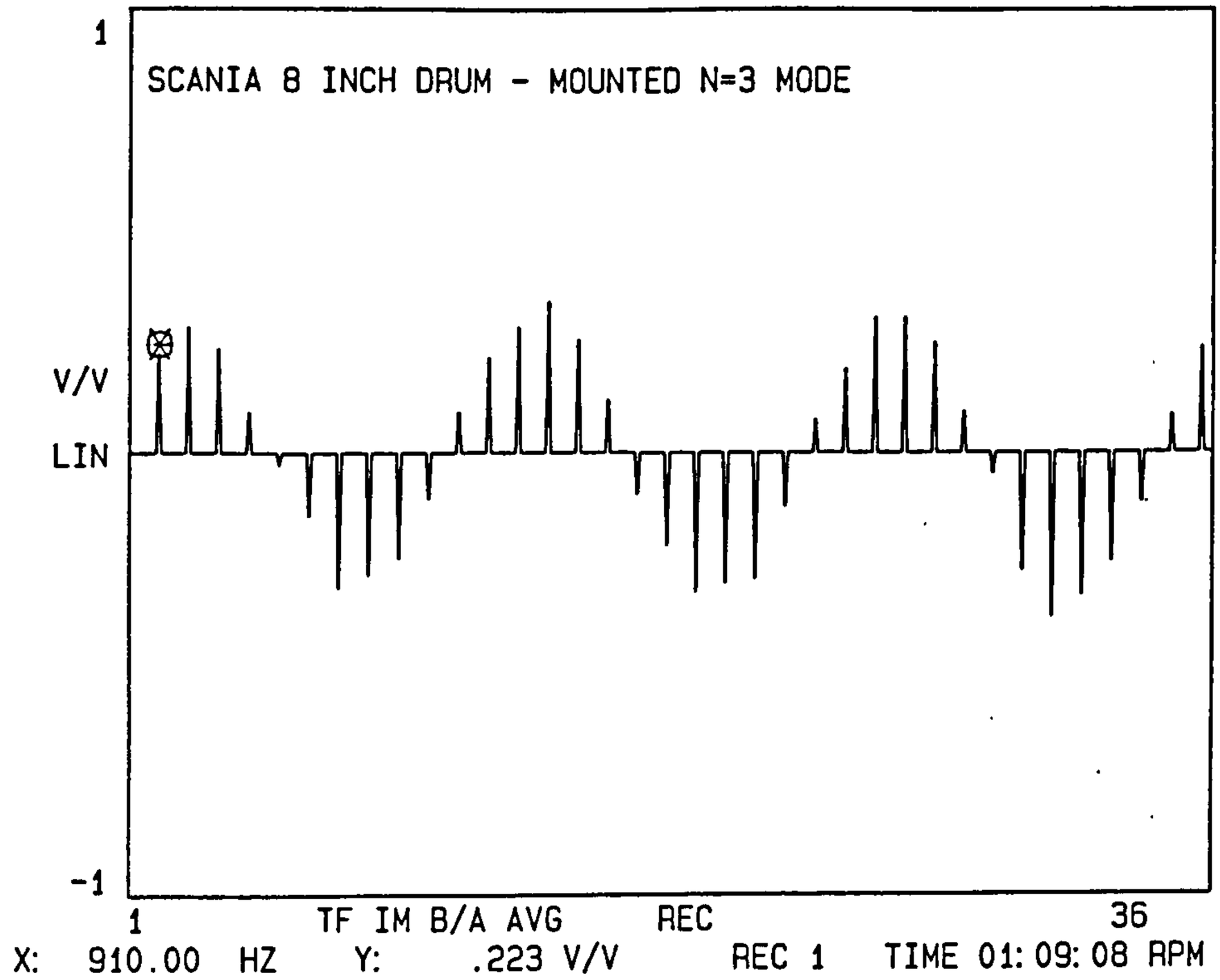

Figure 3.2(a) Typical flexural mode shape around the drum mouth, obtained from a profile taken through the waterfall diagram at a natural frequency (n=3, s=0 mode)

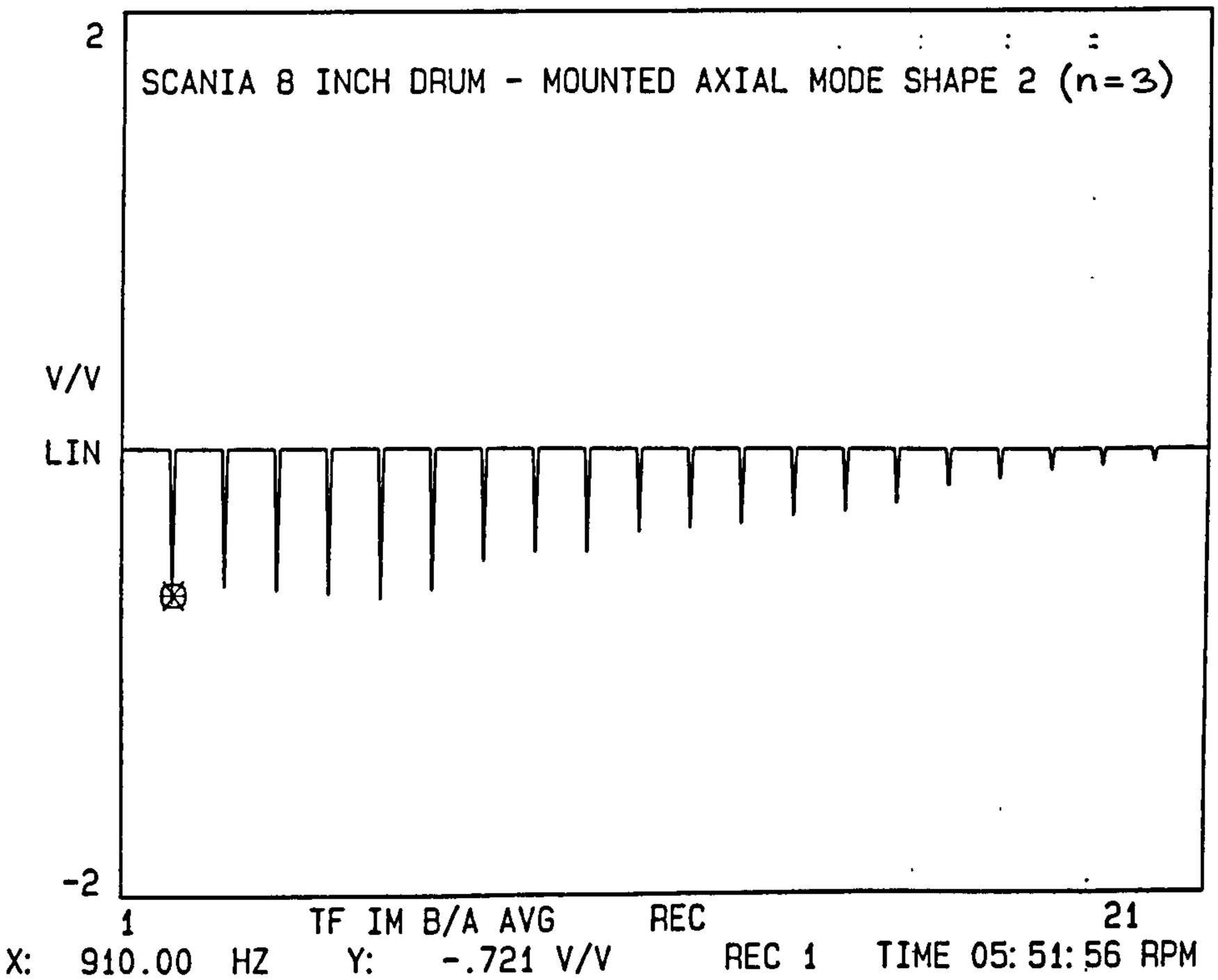

Figure 3.2(b) Typical flexural mode shape in an axial direction across the drum rubbing path obtained from profile through waterfall diagram (n=3, s=0 mode)

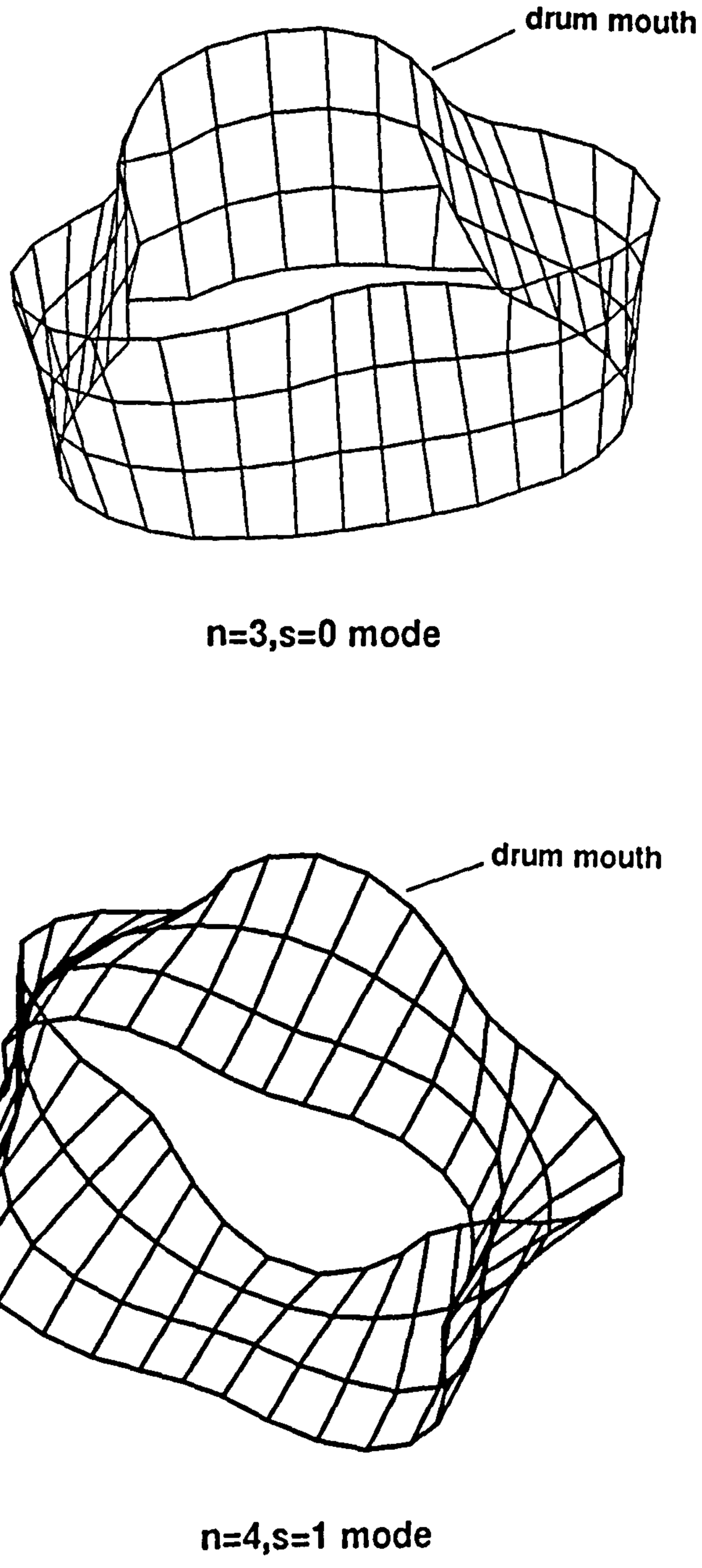

Figure 3.3 Typical drum normal mode shapes obtained using the SMS STAR modal analysis software in conjunction with the impact excitation transfer function analysis technique

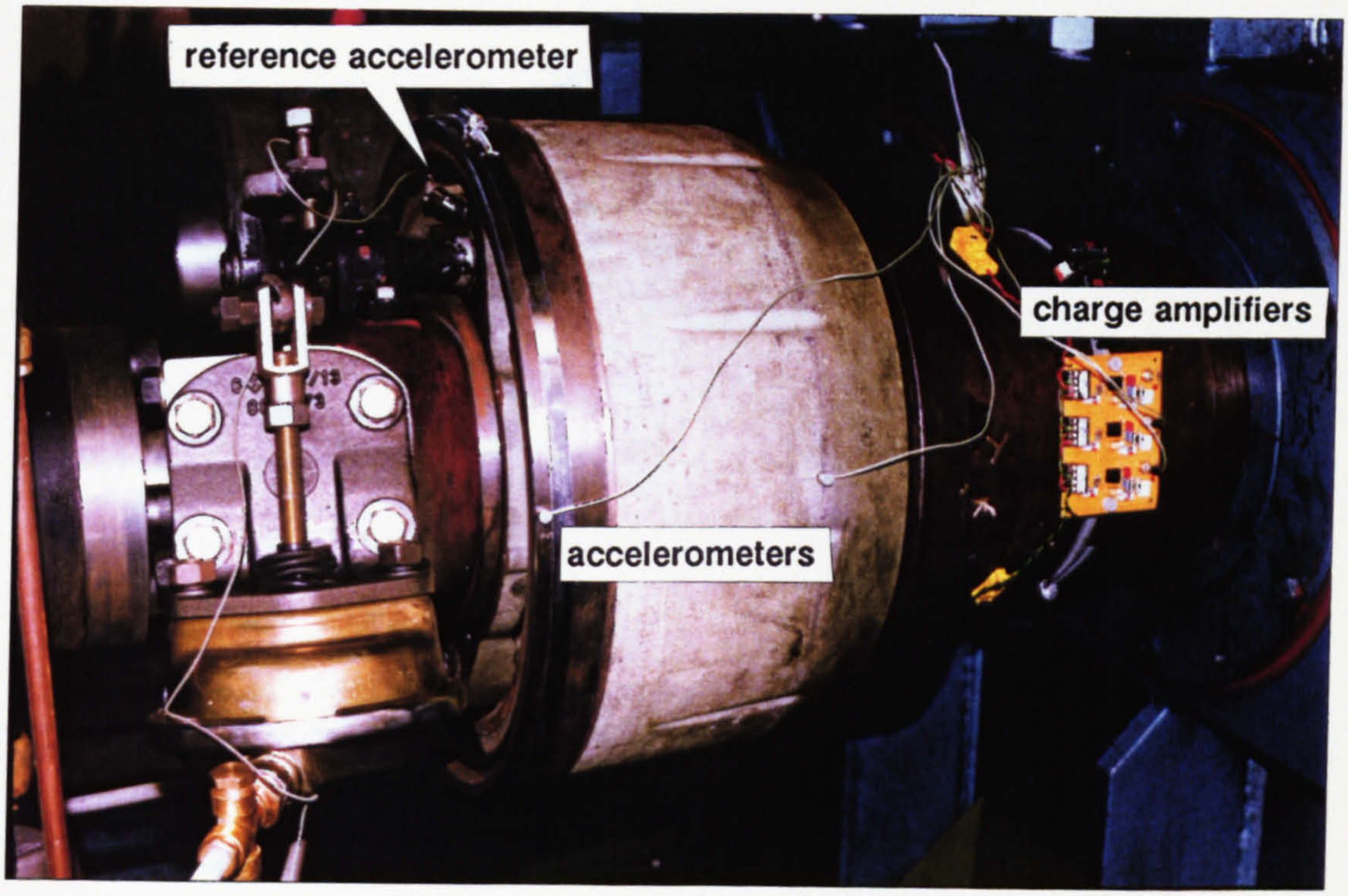

Figure 3.5 The modal analysis equipment attached to the brake

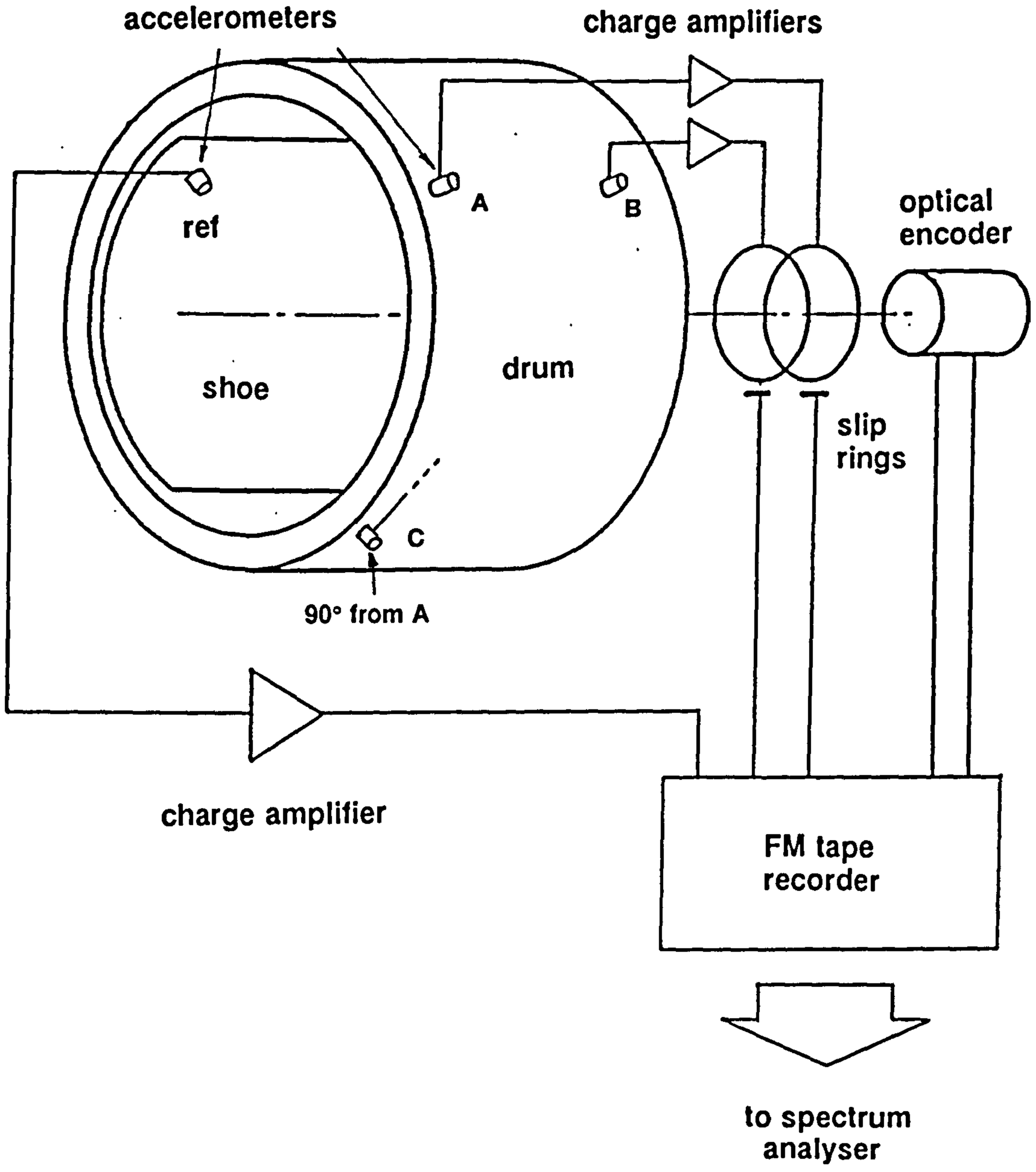

Figure 3.4 Schematic diagram of the arrangement of instrumentation for modal analysis of the drum during squealing

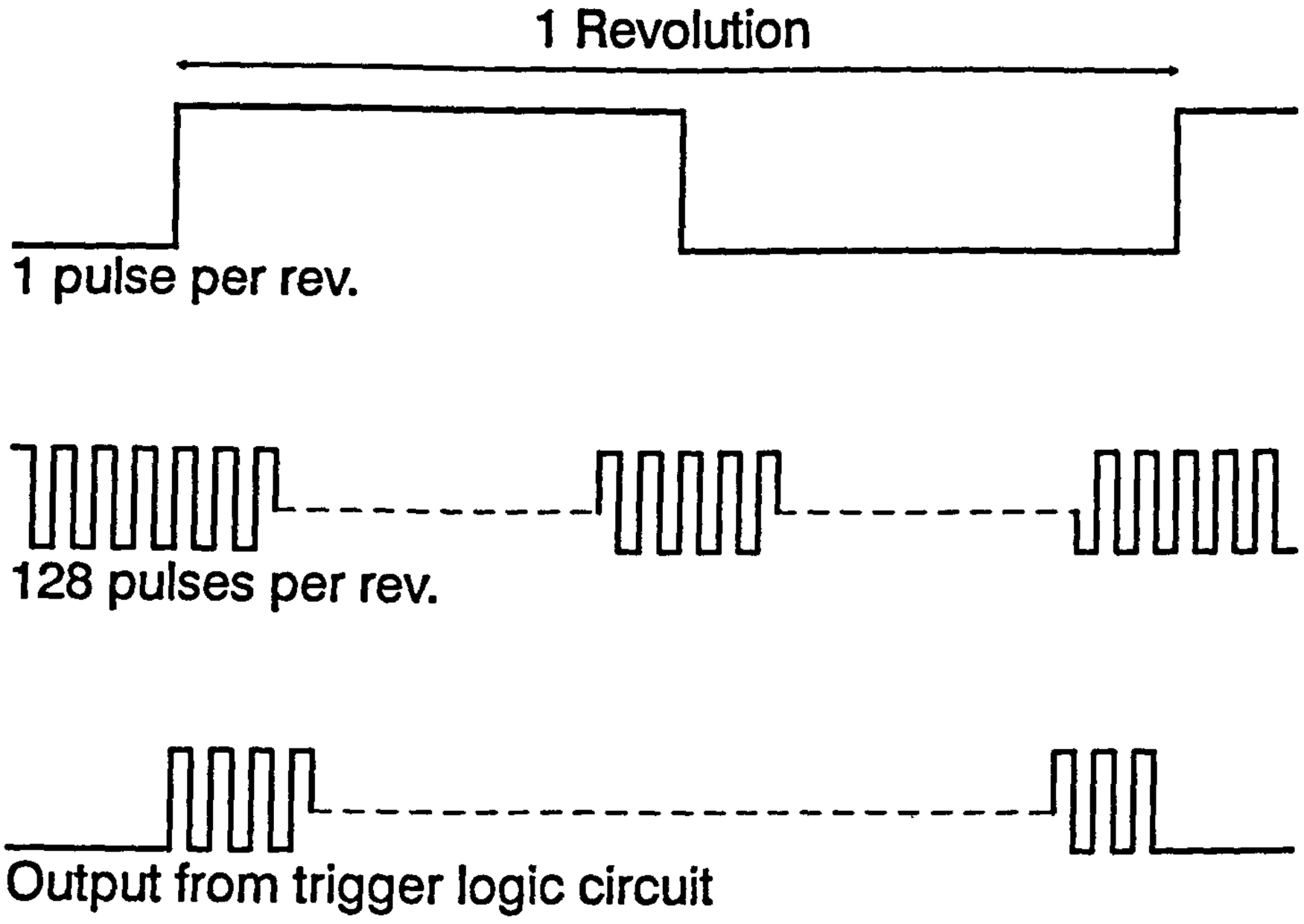

Figure 3.6 **The form of the 1ppr and 128ppr signals from the optical encoder**

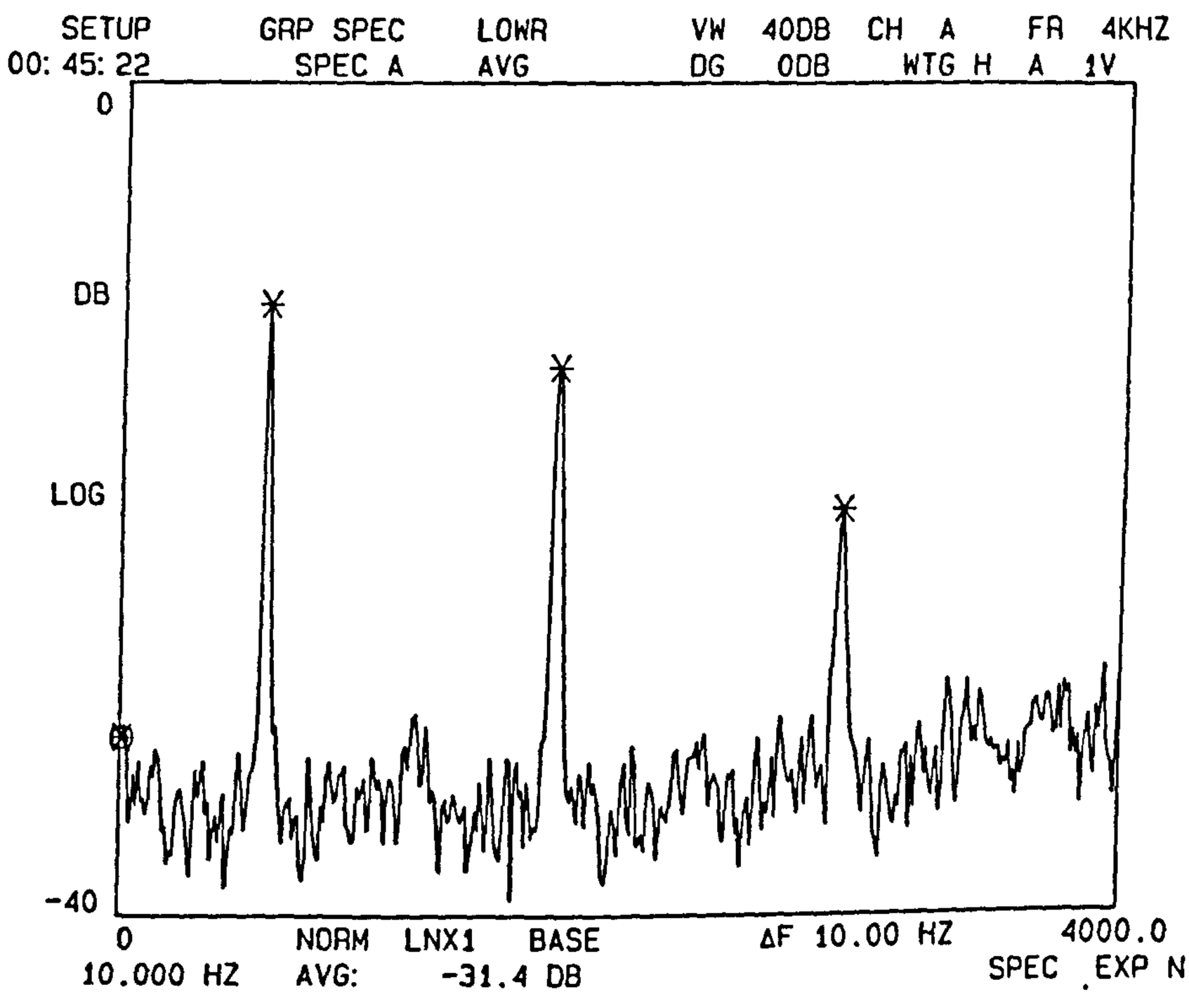

Figure 3.7 **Spectrum from reference accelerometer signal for comparison with that of audible noise shown in fig 2.5**

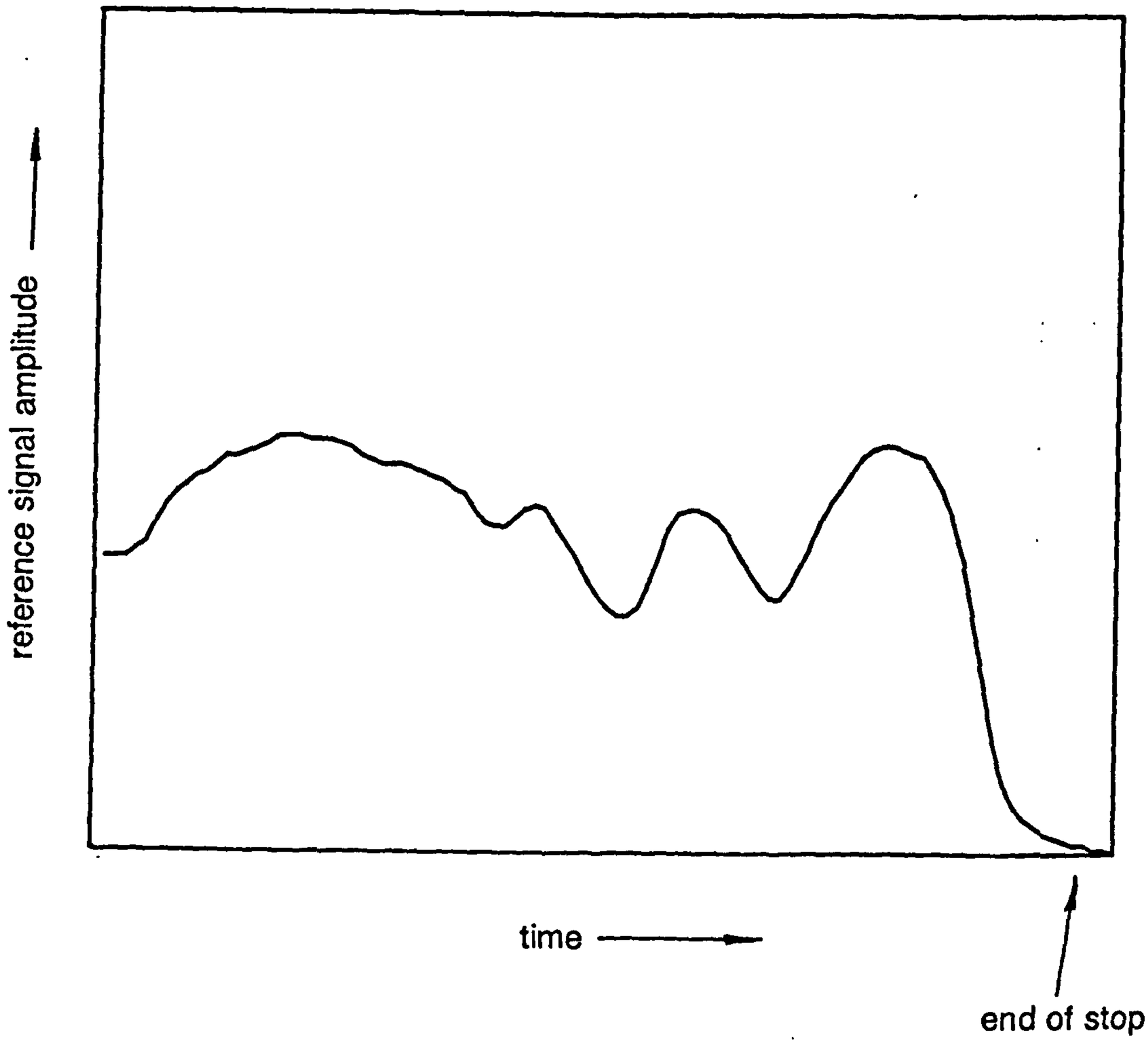

Figure 3.8 **Typical amplitude-time history produced by the reference accelerometer on the brake shoe**

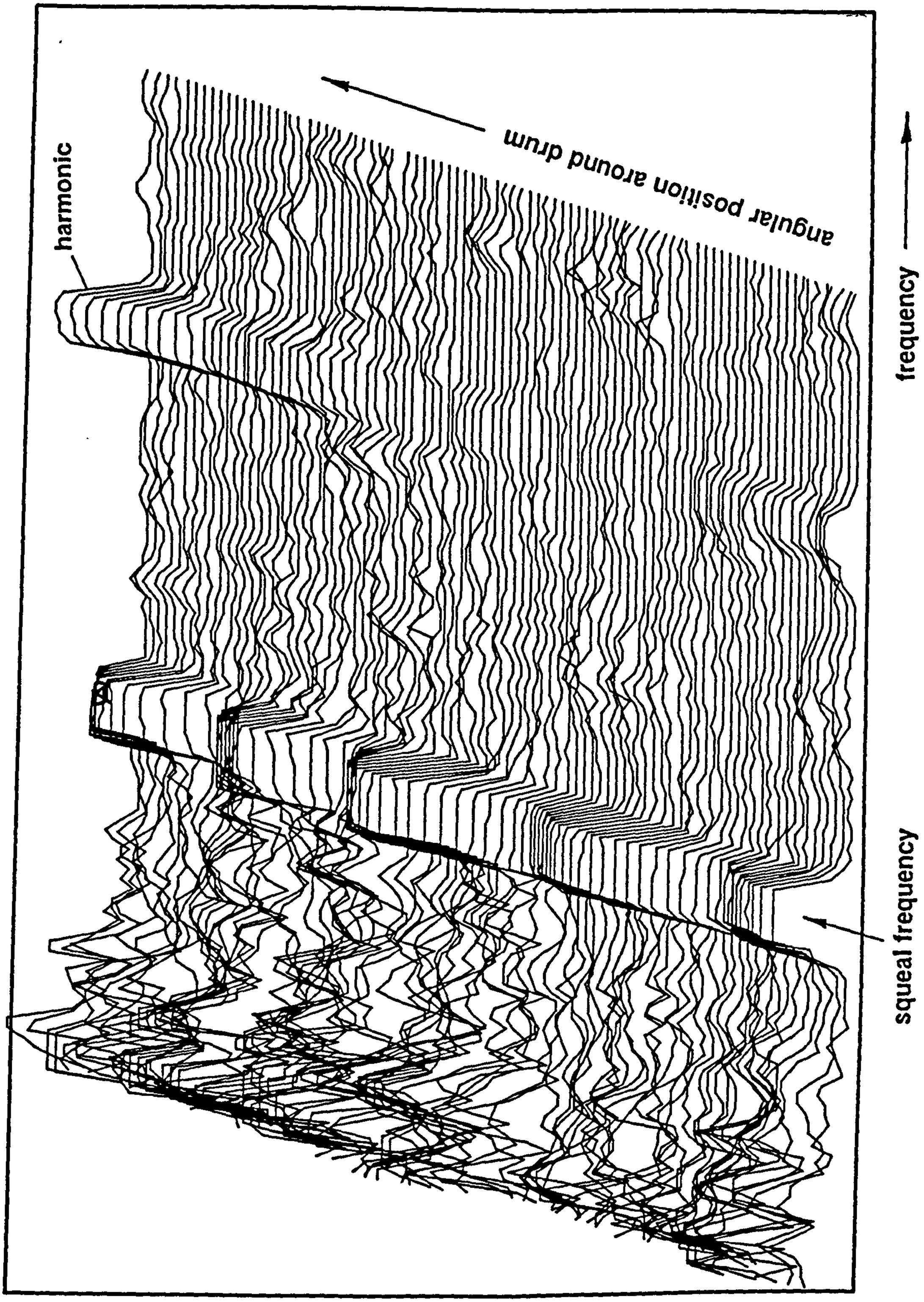

Figure 3.9 **Waterfall diagram assembled from successive transfer function magnitudes**

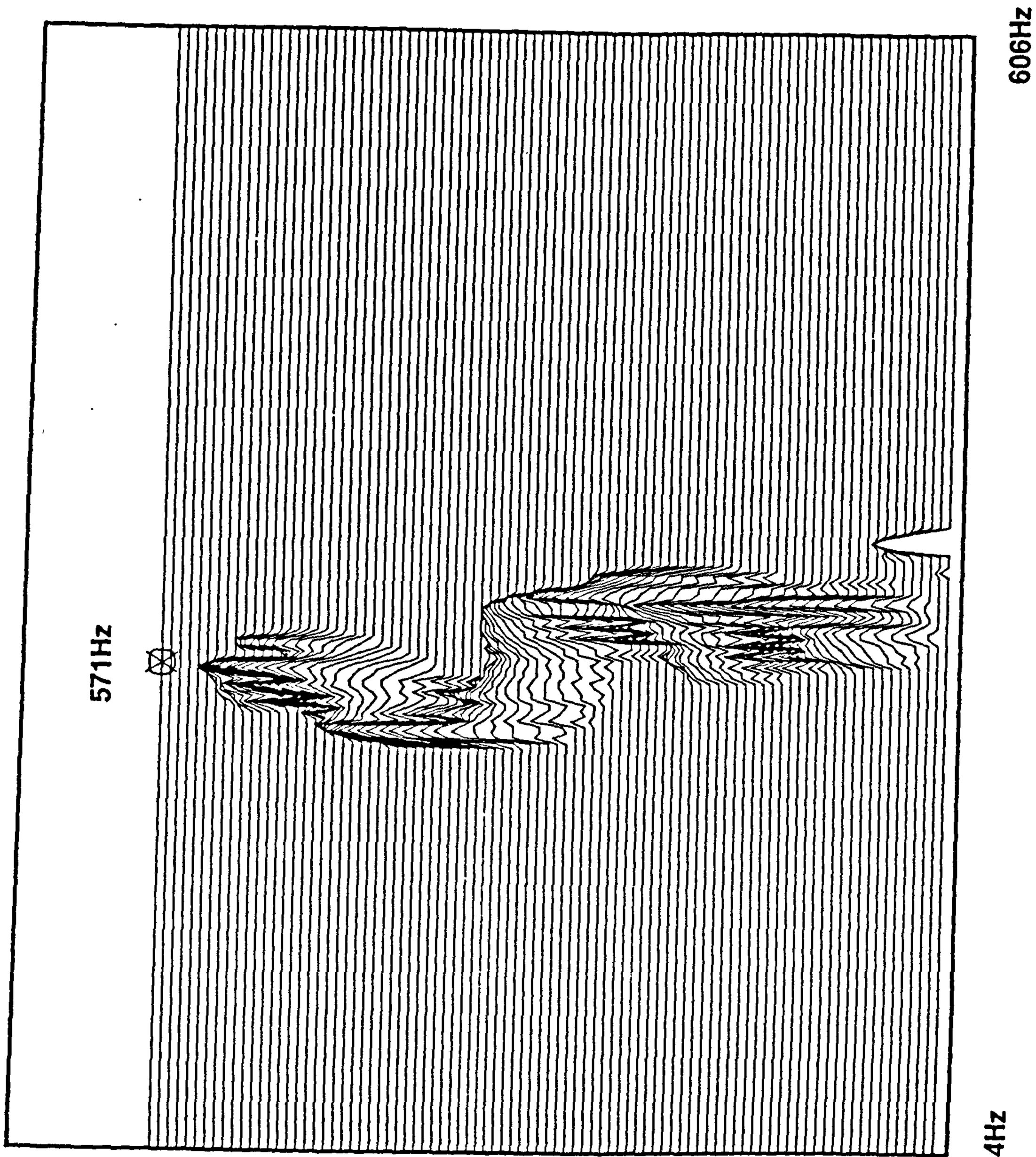

Figure 3.10 **Waterfall diagram formed from zoom spectra of the squealing brake, showing frequency variation**

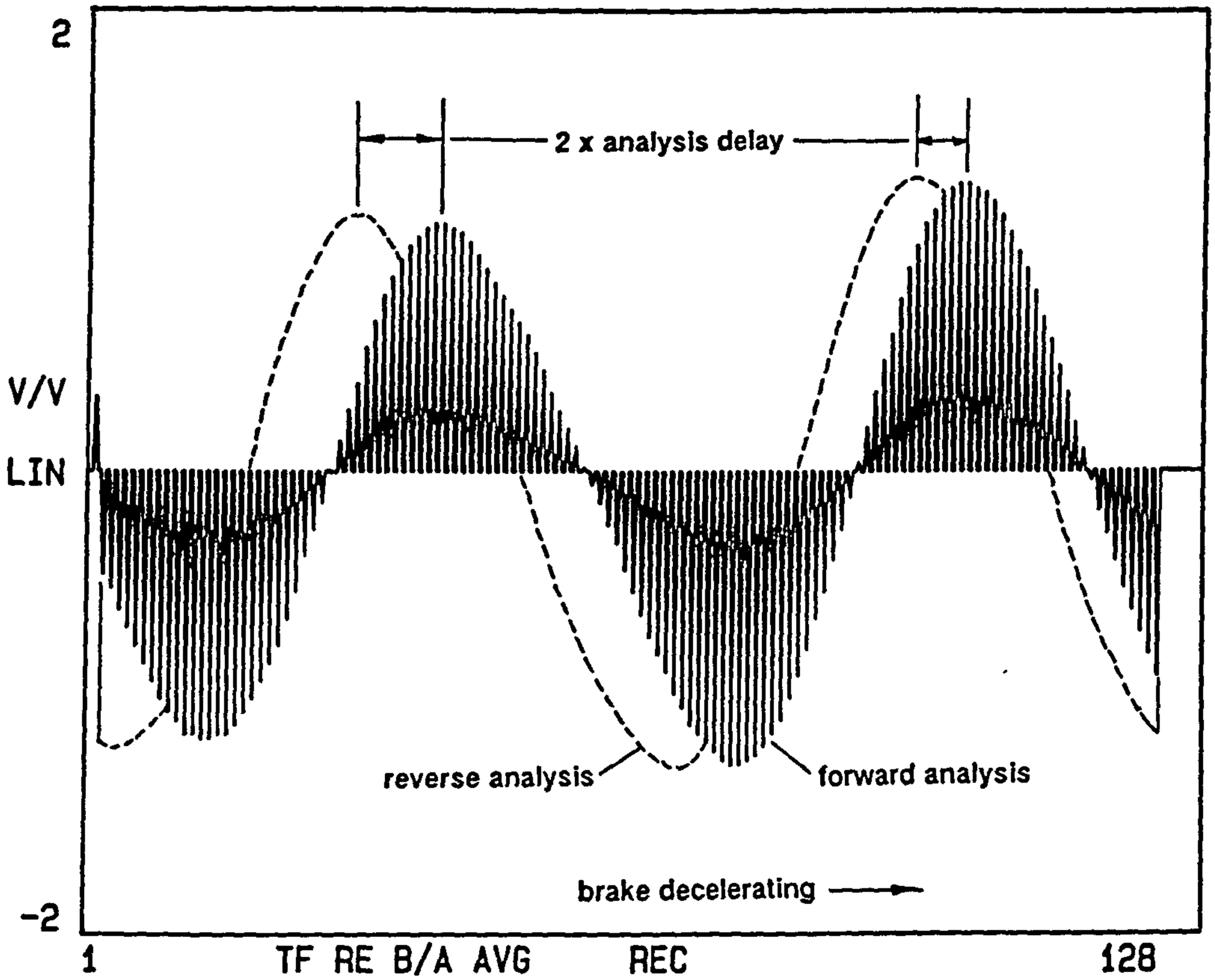

Figure 3.11 **Comparison between mode shapes analysed from forward and reverse tape playback, showing the effect of the delay in the analysis. Note that the effect of the delay reduces as the brake rotates more slowly and the time between analysis triggers is extended**

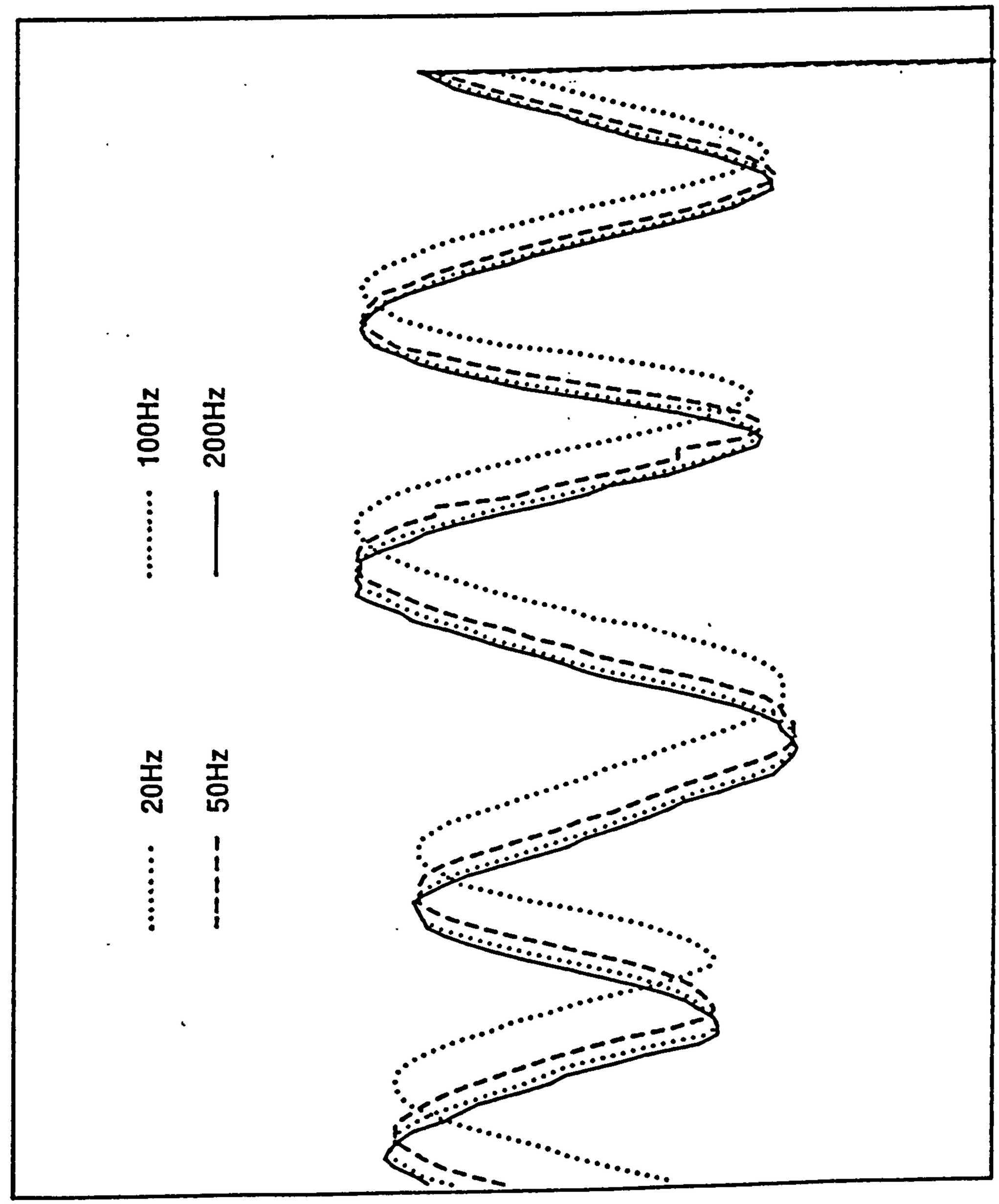

Figure 3.12 Showing the effect of the frequency range used for the transfer function analysis on the apparent angular position of the mode

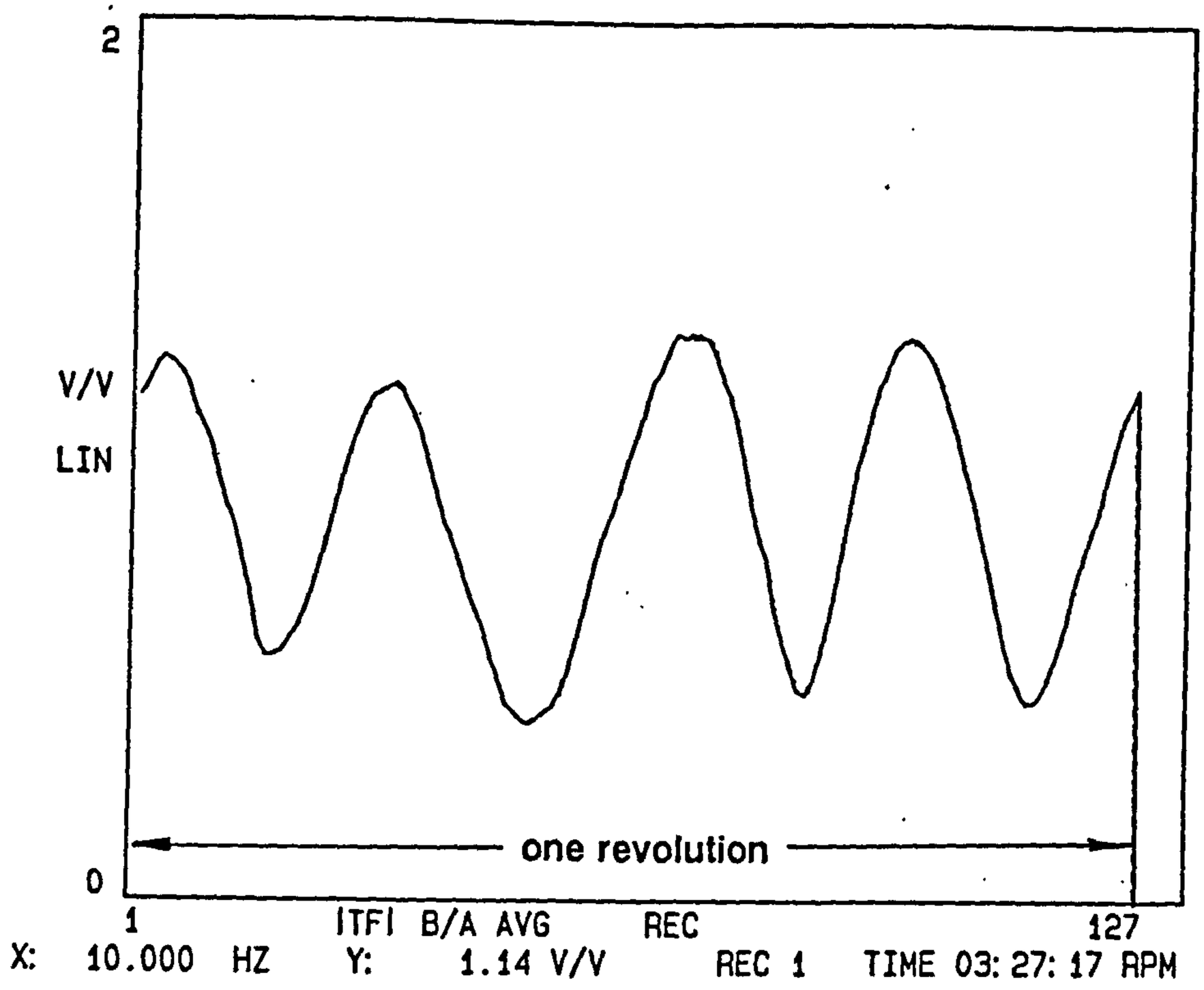

Figure 3.13(a) **Profile through the waterfall diagram of transfer function magnitude at the squeal frequency showing the amplitude distribution of the n=2 mode (Scania drum)**

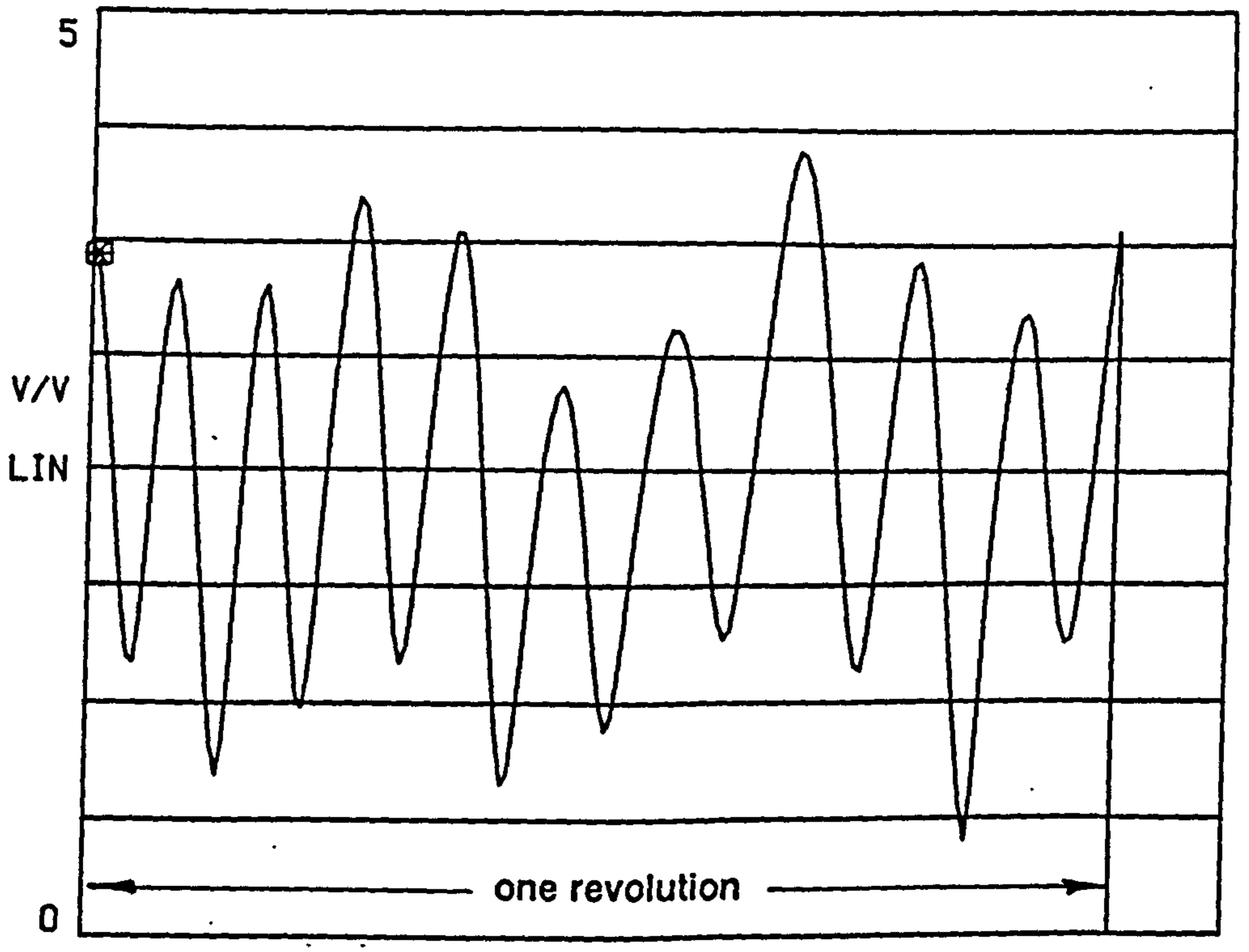

Figure 3.13(b) **Profile through the waterfall diagram of transfer function magnitude at the squeal frequency showing the amplitude distribution of the n=5 mode (Steyr drum)**

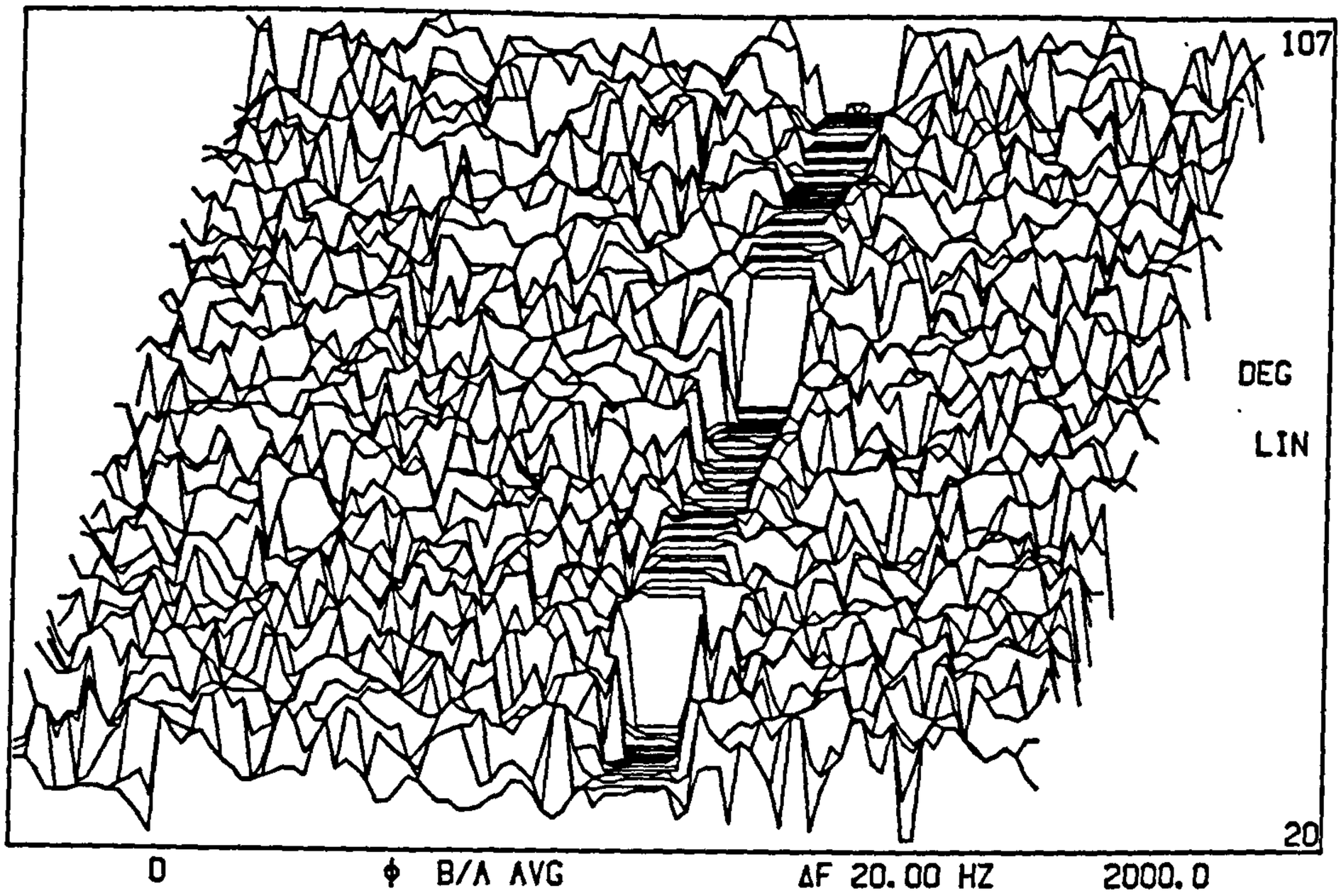

Figure 3.14 Waterfall diagram assembled from successive transfer function phases. (Note that this is obtained from a Steyr 'S' cam brake squealing at 2.5 kHz in the n=5 mode)

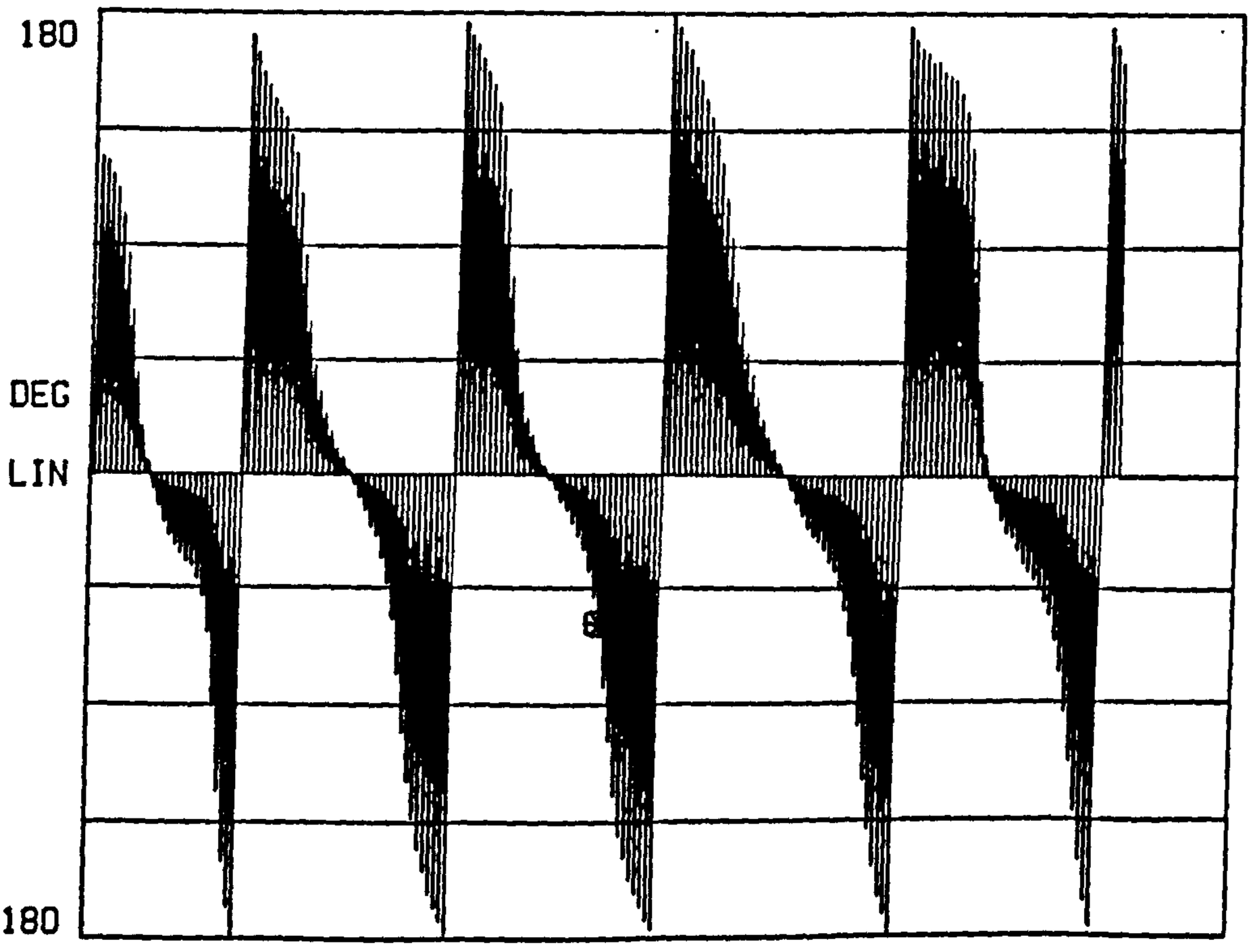

Figure 3.15 Profile through the transfer function phase waterfall diagram at the squeal frequency showing a continuously changing phase around the drum. (Note that this is obtained from a Steyr 'S' cam brake squealing at 2.5 kHz in the n=5 mode)

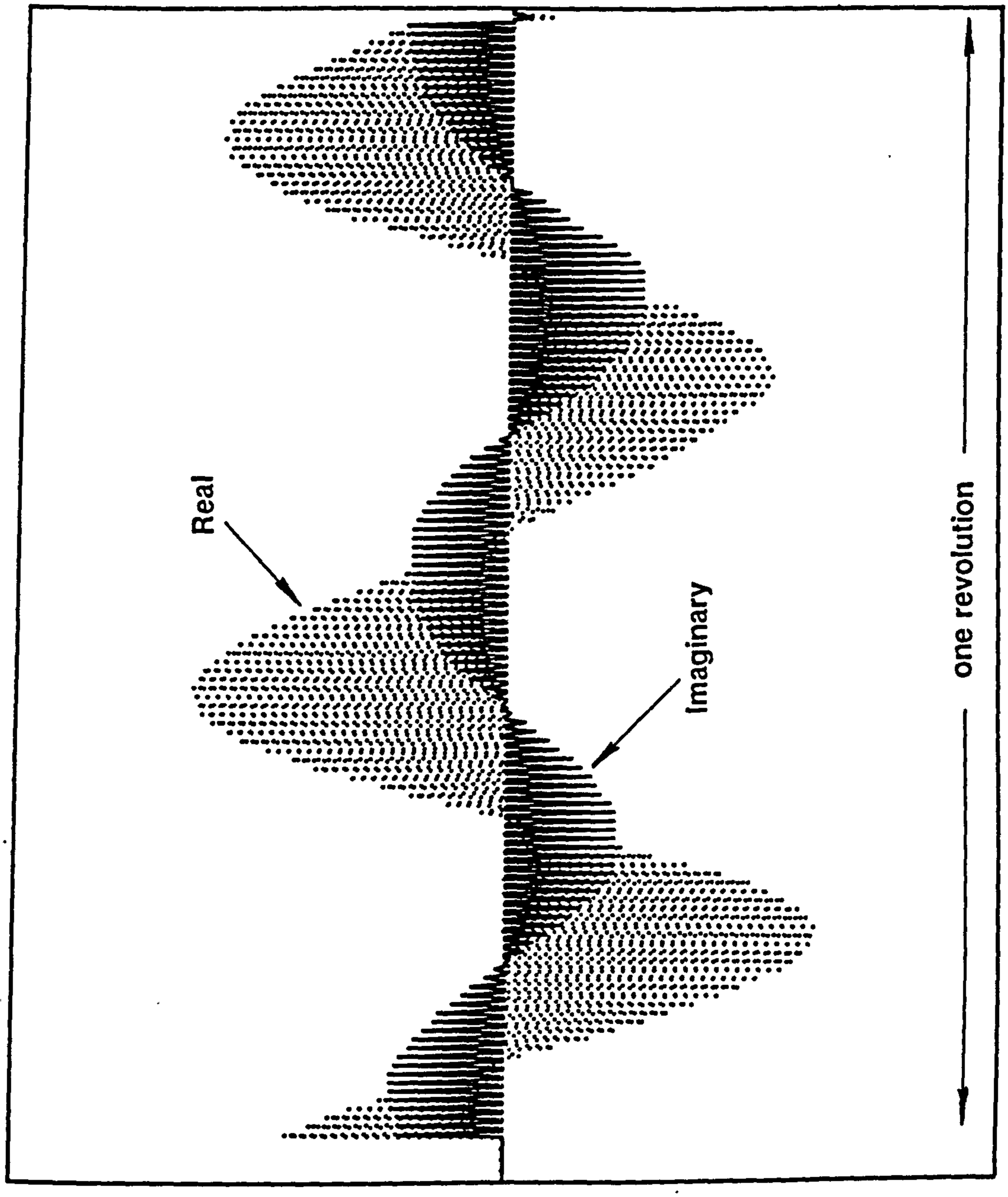

Figure 3.16 Complex squeal mode of the drum using accelerometer 'A' on the drum. This is the superposition of profiles through the waterfall diagrams of Real and Imaginary parts of the transfer functions

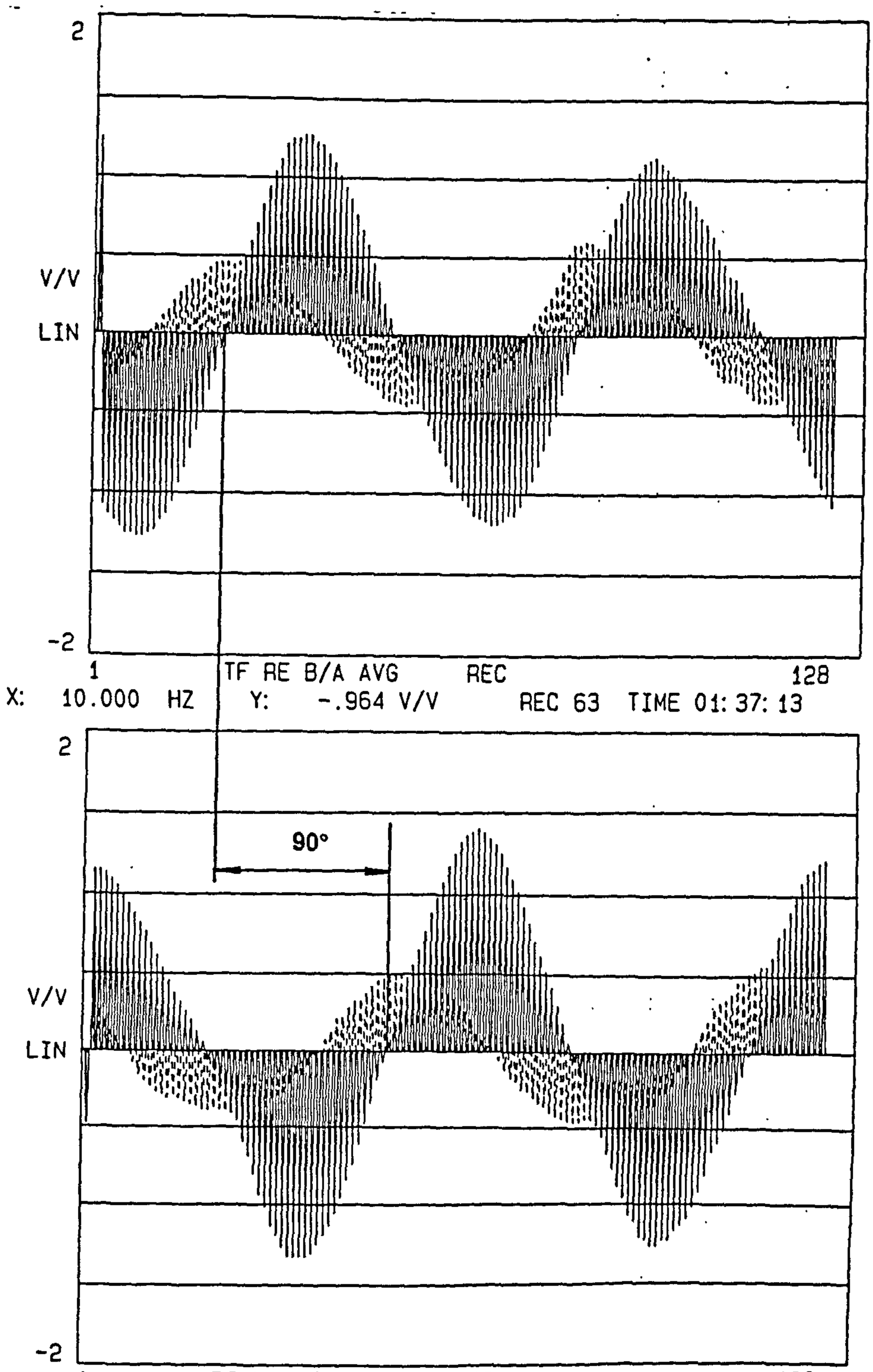

Figure 3.17 **Comparison of complex mode shapes measured using accelerometers A and C, positioned 90° apart on the drum mouth, showing 90° shift in position of mode**

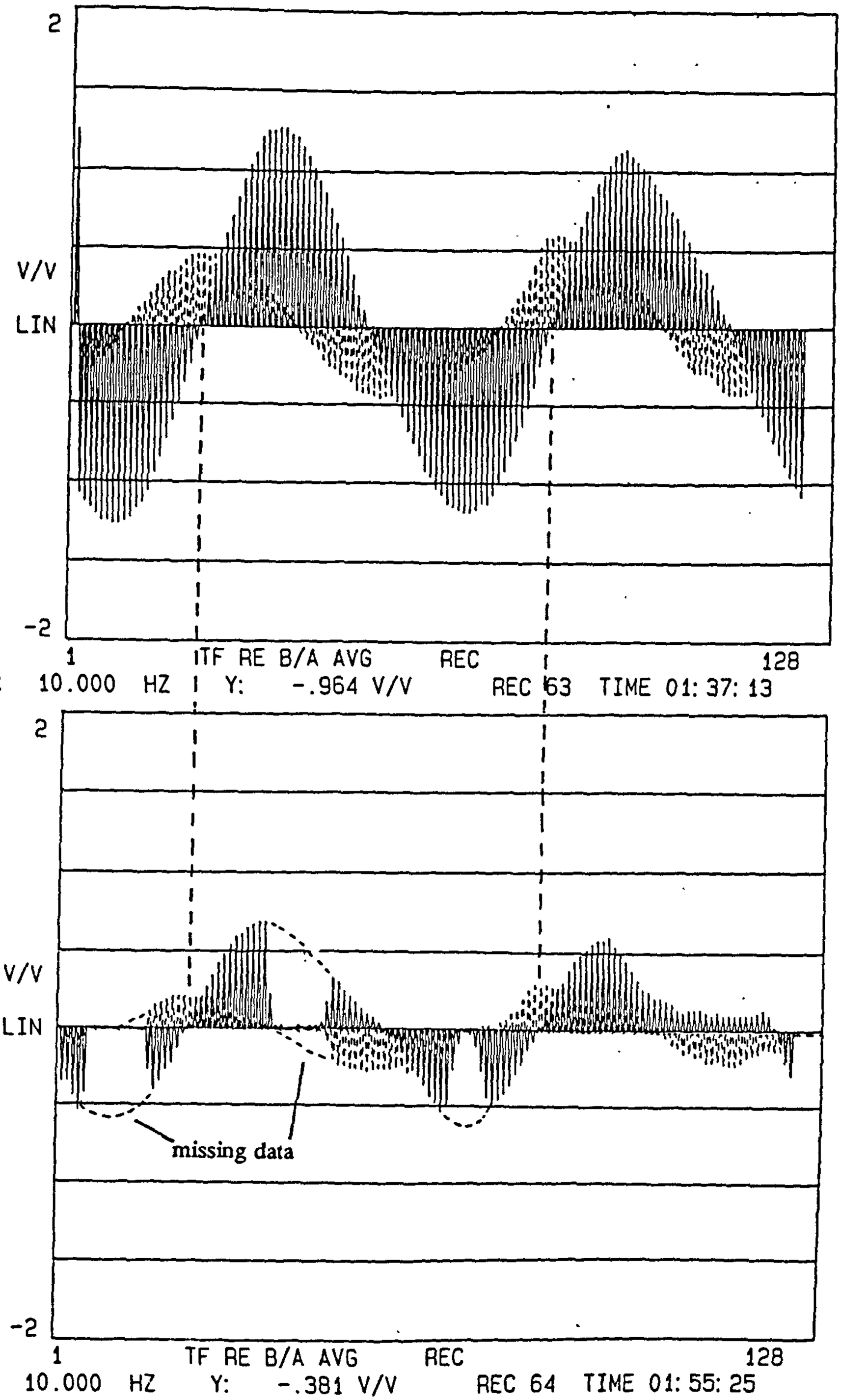

Figure 3.18 **Complex modes measured using drum accelerometers A and B, at either side of the drum rubbing path, showing an amplitude reduction but no phase shift across the rubbing path**

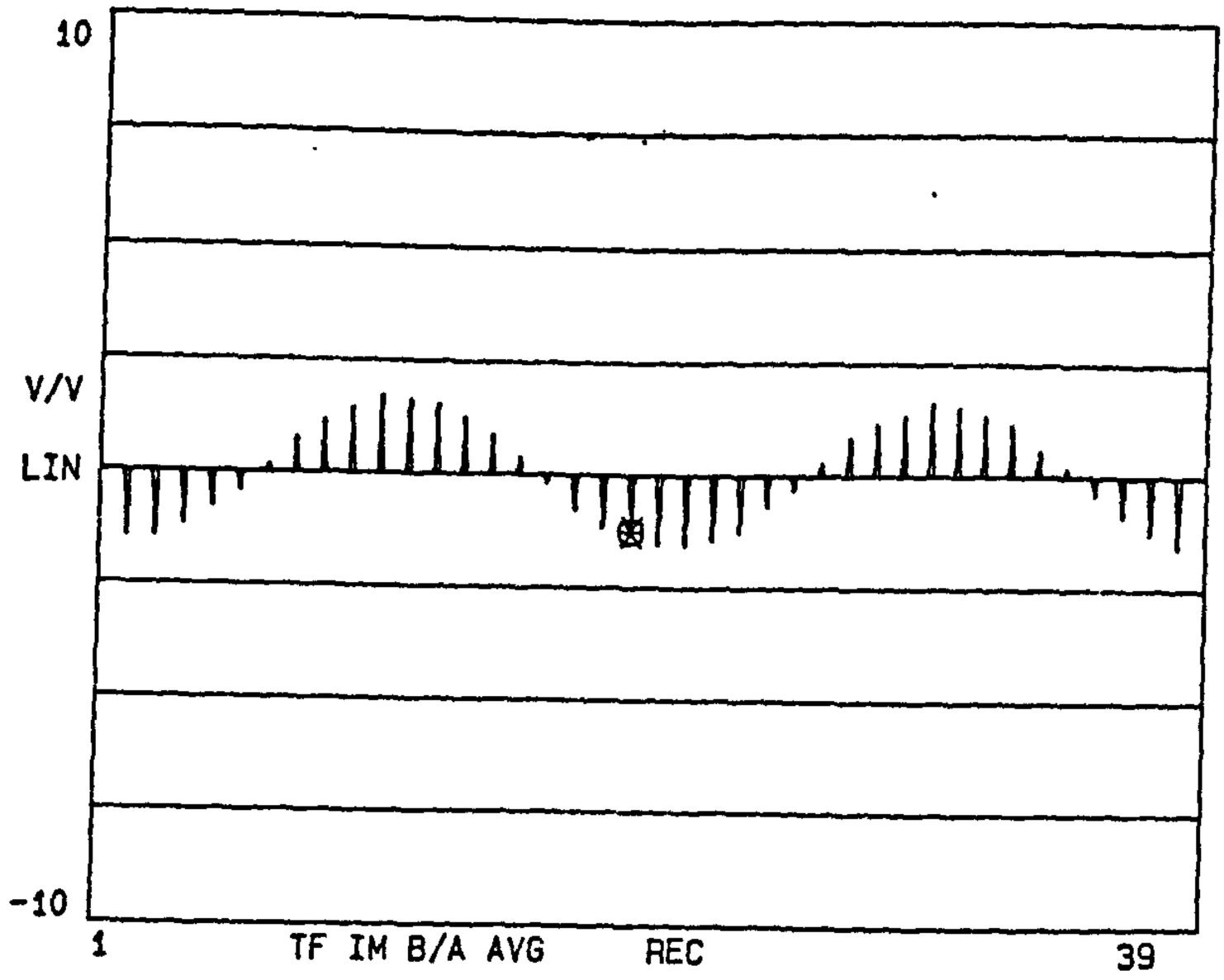

Figure 3.19 **Normal n=2 mode of the mounted drum for comparison with the complex squeal mode in fig 3.16**

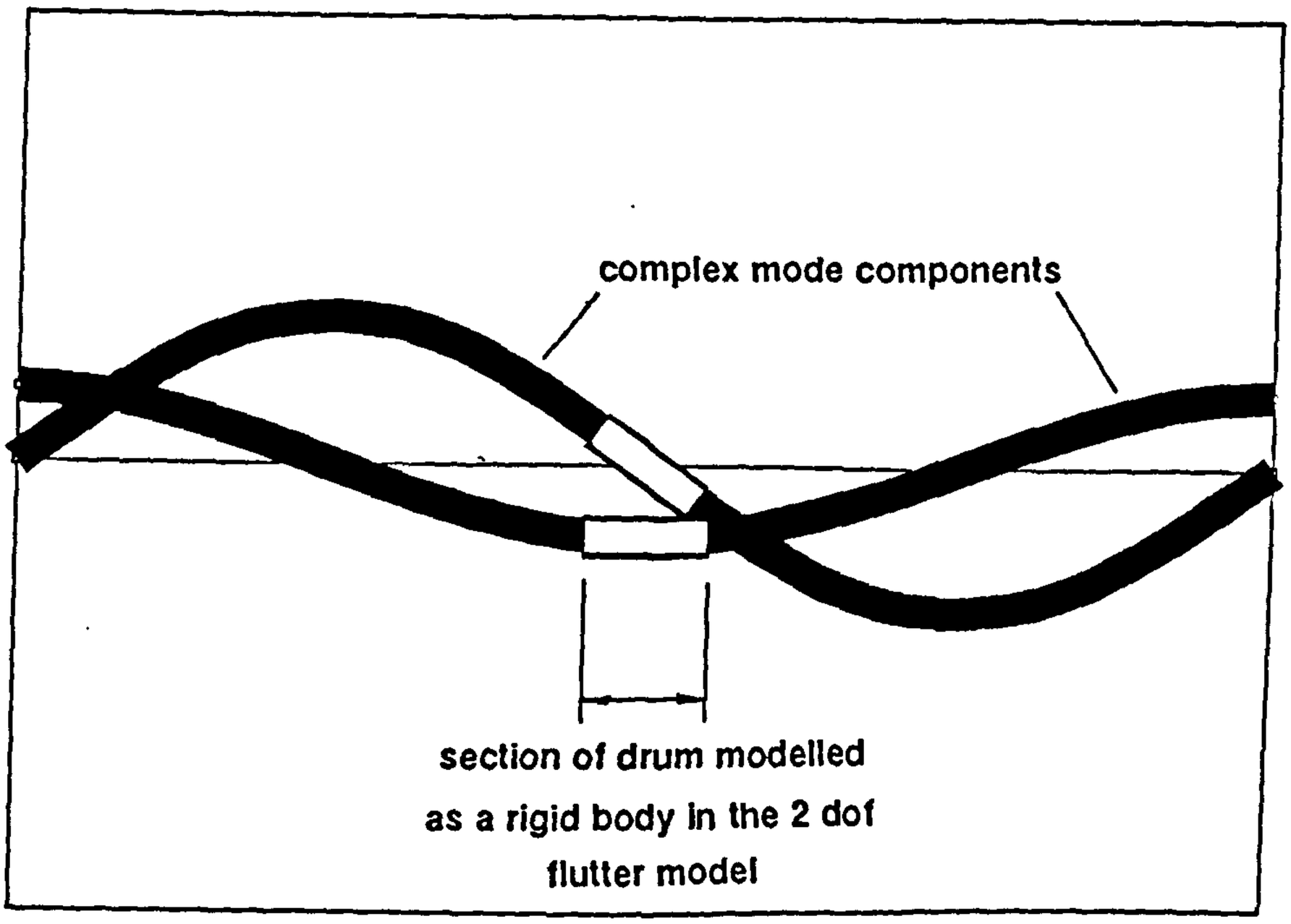

Figure 3.20 **Relation of rigid body binary flutter modes to the measured complex squeal mode**

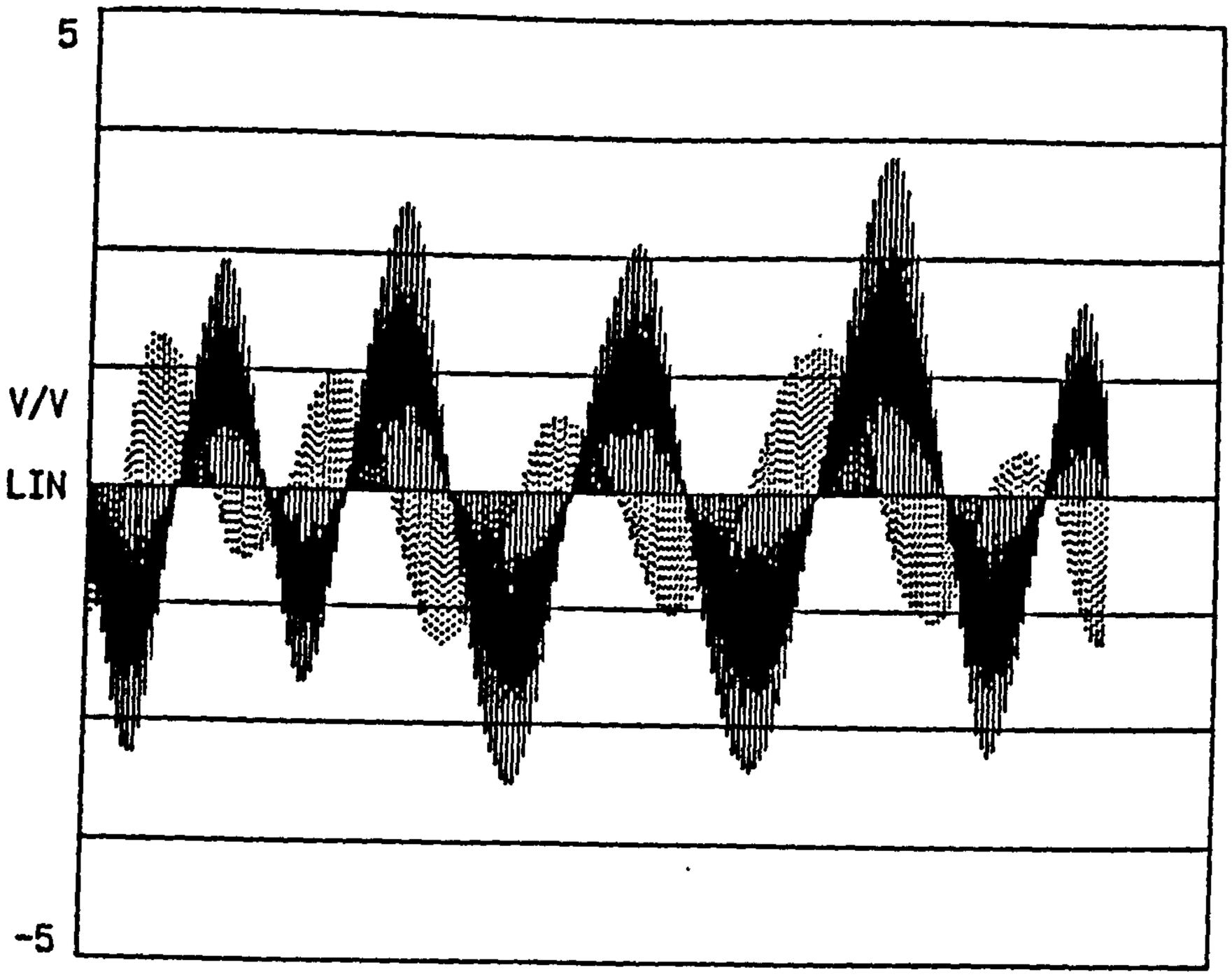

Figure 3.21 Complex drum mode measured from a Steyr 'S' cam brake squealing at 2.5 kHz, showing an n=5 squeal mode

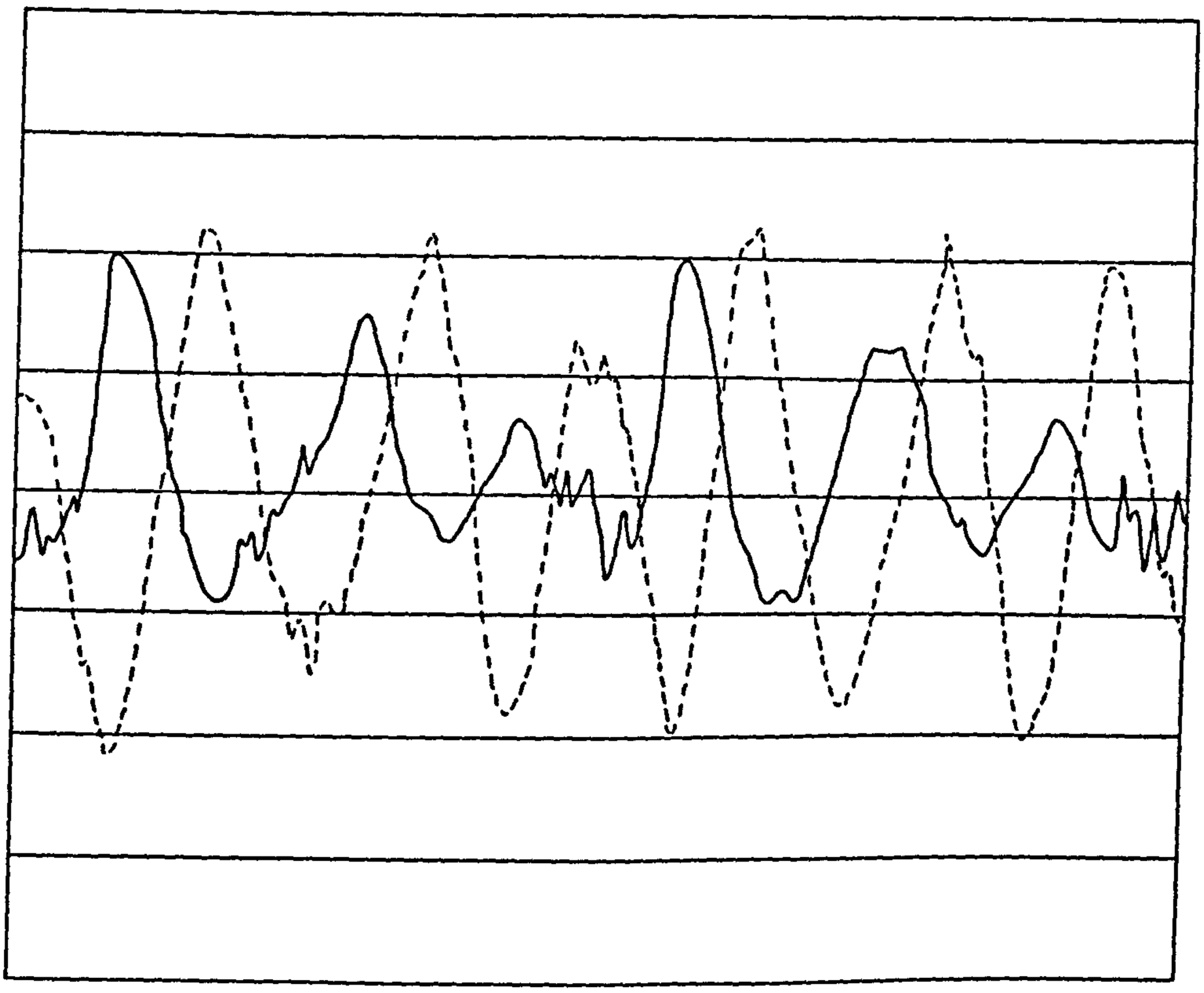

Figure 3.22 Complex drum mode measured from a 180m x 30mm Ford passenger car drum brake squealing at 3.3kHz

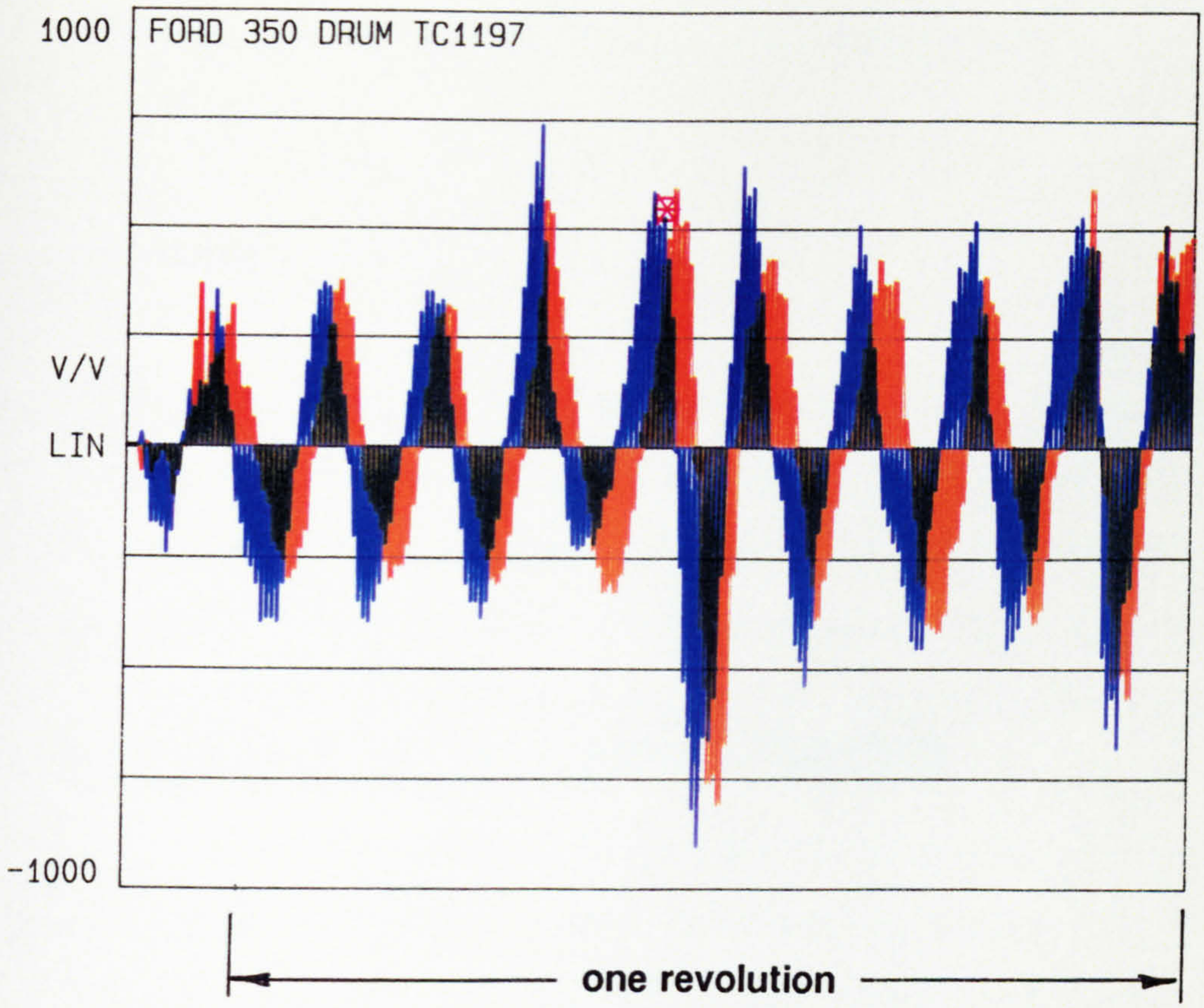

Figure 3.23 **Complex drum mode measured on Ford 308mm x 89mm light truck drum brake, squealing at 7.7kHz, showing a pair of n=9 mode components with a quarter wavelength spatial phase difference, similar to that measured on the Scania drum**

CHAPTER 4

MODAL ANALYSIS OF THE COMPLETE BRAKE

4.1 Introduction

As noted in the section 3.1, standard modal analysis techniques can be readily applied to the stationary parts of a brake, and by combining such measurements with those from the drum, a description of the motion of the complete brake, whilst squealing, could be obtained. The modal analysis technique employed on the squealing brakes, that of measuring the transfer function between discrete points on the structure and a fixed reference point, has, in practice, a limited spatial resolution, determined by the number of simultaneous measurements which can be made and/or the number of consecutive measurements which can be made under repeatable test conditions. In view of this practical limitation to the amount of modal data obtainable, the measurement resource was focused on the shoe platform, the region most closely coupled to the drum through the friction interface, together with a less detailed attempt to indicate the type of boundary conditions to which the brake shoe is subject. These latter measurements were considered to be important to the development of future stability modelling.

Prior to this squeal modal analysis, however, the normal modes of the free shoe and of the statically actuated brake system were investigated in order to :-

(i) determine if any close relationship exists between the free component natural frequencies and the squeal frequency. Such frequency

coincidences are often seen as significant in empirical squeal problem solving, motivating structural modification of components.

(ii) determine whether any close relationship exists between the modes of the static and squealing brake system.

4.2 Brake Shoe Modal Analysis

4.2.1 Introduction

The shoe used in the Scania 412 x 203 mm brake is illustrated in fig 4.1. It is of cast iron construction and consists of a 203 mm wide cylindrical platform, supported along its centre by a substantial circumferential web from which smaller axial webs support the edges of the platform. At the extremities of the central web, which is extended beyond the platform ends, are fitted a plain bearing, for location on the shoe anchor pin, and a roller, which contacts the actuating 'S' Cam (see fig 2.1 for a general arrangement of the brake). As noted in chapter 2, the arc length of the shoe platform is 72°, unusually short compared with the more typical length of 120°, and due to this short length, the friction material is manufactured and attached, by rivets, in a single block rather than the more usual two 'half-blocks'. The leading and trailing shoes are identical in construction and positioning of the friction material.

4.2.2 Shoe normal modal analysis

A normal modal analysis was first carried out on the shoe alone to determine whether any relationship exists between the free vibration of a component and its motion whilst squealing, a situation suggested by some current empirical approaches to squeal solutions (described in section 2).

The shoe was analysed, both with and without the friction material attached, in the 'freely-suspended' state on a foam rubber block, such that the rigid body frequencies were all below 20 Hz and so did not influence the flexural modes. Its response to impact excitation was measured by a single, radially directed, accelerometer attached to a corner of the shoe platform. Excitation impacts were applied radially at a range of equally spaced points around the platform periphery, and also axially (in the direction of the brake axis) along the edge of the shoe web. The imaginary part of the transfer function between response and force was used to define mode shapes. The frequency response of the shoe is shown in fig 4.2, and the modes associated with the major resonances are summarised in the table below, with the forms of the first torsion and bending modes illustrated in fig 4.3.

Table 2 Free Shoe Modes

Natural Frequency (Hz)		Mode Shape
No Lining	With Lining	
569	635	1st Torsion
1075	1220	1st Bending
1540	1755	2nd Torsion

It is already clear from Table 1 in Chapter 3 that no drum normal mode frequency coincides with the squeal frequency of 580 Hz, which is, however close to the first torsion mode frequency of the shoe, above. The empirical component modification approach to reducing squeal may well suggest, from the above observation, that changing the frequency of this shoe torsional mode by structural modification, should alleviate the squeal. It will be shown later, however, that in this case, the shoe mode

involved in the 580 Hz squeal is more akin to the first bending mode and that little torsional motion is apparent.

This lack of correlation between drum and shoe normal modes and the squeal behaviour is not, however, surprising when the close physical coupling of the components, under braking conditions, is considered. To evaluate the significance of this coupling effect, a modal analysis was carried out on the statically actuated brake on the inertia dynamometer.

4.2.3 Normal modal analysis of the actuated brake

This was carried out on the stationary brake actuated at various pressures. The response was measured from a single radially directed accelerometer, attached to the drum, to impacts at 36 positions around the drum mouth and 10 positions along an antinodal line across the drum rubbing path. A typical frequency response up to 2 kHz is shown in fig 4.4 for 7 bar actuation, and a typical collection of modes is summarised in the table below, where they are also compared with the modes of the drum alone, obtained in chapter 3.

Table 3 Normal mode frequencies of the drum and the brake actuated at 3 bar

Drum Mode Shape	Actuated Brake Natural Frequency (Hz)	Mounted Drum Natural Frequency (Hz)
n=2, s=0	528, 548, 578, 608	445
n=3, s=0	925, 970, 1045, 1070	925
n=4, s=0	1415, 1495, 1580 1647, 1710	1660

A fundamental difference between the drum mode shapes of the actuated and unactuated brakes, is that the latter is arbitrarily positioned angularly, following the excitation around the drum, whilst the former takes up preferential angular positions. This will be explored more fully in the next chapter, but it is clear from the modes shown in fig 4.5 that the actuated brake drum holds modes of similar form but with different frequencies corresponding to different angular positions of the modes on the brake.

It was observed that the above natural frequencies were sensitive to the actuation pressure, and this characteristic was measured for one of the modes involving n=2 drum motion, near the squeal frequency. Frequency response functions were measured at actuation pressures from 0.5 bar to 6 bar and the resultant frequency - pressure characteristic is shown in fig 4.6. The characteristic is extremely non-linear, probably due to non-uniform contact between the linings and drum at very low actuation pressures (0.5 bar is only just above the 'threshold' pressure of the brake - the pressure required to extend the shoe pull-off spring and close the gap between lining and drum). It is worthy of note that the frequency at 0.5 bar is less than that of the fundamental (n=2,s=0) drum mode, suggesting a mass loading effect. At higher pressures, where good contact is established, the frequency is less sensitive to pressure and is above the drum fundamental, suggesting a predominant stiffening effect.

4.2.4 The significance of normal modal analysis

The above results suggest that no normal modal analysis of the brake or its components can give a reliable picture of the situation whilst squealing, and hence that modification to components based on such normal modal analysis cannot be readily used to produce a predictable influence on the occurrence of squeal.

4.3 Analysis of the Squeal Mode of the Brake Shoe

As indicated in the introduction to this chapter, the shoes, being a stationary part of the brake, can be analysed using an array of accelerometers attached at discrete points on the structure. In this case, measurements were limited to the radial direction (the same direction as the drum mode measurements in chapter 3) on the shoe platform only. Low mass accelerometers were attached, using screw/adhesive adaptors and cyanoacrylate adhesive, at the positions along the inner and outer edges of the platforms, shown in fig 4.7. A single reference position, position 1 at the drum mouth side of the leading end of the shoe, was used for all measurements, this being the same reference position used for the drum squeal modal analysis in chapter 3. This common reference position allowed later combination of the drum and shoe modes.

The amplified signals were recorded on the multichannel magnetic tape recorder together with the 1ppr and 128ppr optical encoder signals, the latter to be used to ensure simultaneity of analysis. Due to the limitation of the number of recording channels available, not all signals could be recorded simultaneously, and several brake applications were required with groups of signals being recorded from each. Overlapping of the groups of signals (for example signals 1-9 from one application and 1,3,5,9,10,11,12,13,14 from another) allowed consistency of the modes between applications to be confirmed.

Transfer functions between each accelerometer signal and the reference signal were produced using the 2-channel spectrum analyser, and the real and imaginary components of the complex transfer function were assembled into waterfall diagrams, triggered from the optical encoder signals. Profiles through the waterfall at the squeal

frequency show the time history of the transfer function through one revolution, illustrated in fig 4.8 for one accelerometer position.

These profiles indicate the variation in transfer function during one revolution of the drum, and would be expected to be constant if the assumption of time-invariance, used in the drum modal analysis of chapter 3, were valid. Bearing in mind the small in-stop variations in squeal frequency (shown in fig 3.10), it was considered that the transfer functions indicated a sensibly constant dynamic condition and average values of the transfer function components were used to define the shoe mode.

The real and imaginary components for each accelerometer position on the leading shoe are shown in fig 4.9, and the form of the component modes on the shoe illustrated in fig 4.10. It is clear from these results that no significant torsional motion of the shoe platform is present (as may have been envisaged from the free shoe modal analysis), the mode shape and phasing being similar at both edges. The reduction in amplitude from the mouth side across the rubbing path is qualitatively similar to that seen from the drum modal analysis (the amplitude ratio being slightly greater here, $\approx$0.4 cf $\approx$0.5 for the drum). The form of the mode components in the circumferential direction is a combination of bending with rigid body rotation such that the resulting curve approximates to part of a sinusoidal function.

The wavelength of this sinusoid approximates to that of the wavelength of the n=2 drum mode measured during squeal, that is it has an angular wavelength of 180°. It also appears that the spacial phasing of the real and imaginary component waves of the shoe complex mode is similar to that of the drum complex mode components (cf fig 3.16). The measurements thus show that the overall form of both the drum and shoe modes are very closely related, both being complex wavelike modes of approximately the same wavelength and amplitude ratio across the rubbing path.

4.4 Combined Drum and Shoe Squeal Modes

The use of a common reference point for the drum and shoe squeal mode transfer function measurements enabled the modes to be combined so that the true relative motions of drum and shoes could be obtained. The position of the drum complex mode in fig 3.16, relative to the stationary parts of the brake, is defined, as the waterfall used to produce this mode was initiated when the drum accelerometer was at the position of the cam centreline, Thus, the shoe modes can be superposed on fig 3.16 at positions corresponding to the shoe platform angular positions to produce the combined mode shown in fig 4.11.

4.5 Summary

Only the shoe first torsion mode natural frequency is found to be close to the squeal frequency, and this is shown to be coincidental as the shoe exhibits bending motion while squealing. The natural frequencies of the statically actuated brake system are sensitive to the actuation pressure, and multiple modes are found involving a single drum mode form, each drum mode occupying a unique angular position on the brake.

During squealing, the shoe platforms exhibit complex bending motion of a similar form to that of the drum to which they are coupled through the friction material.

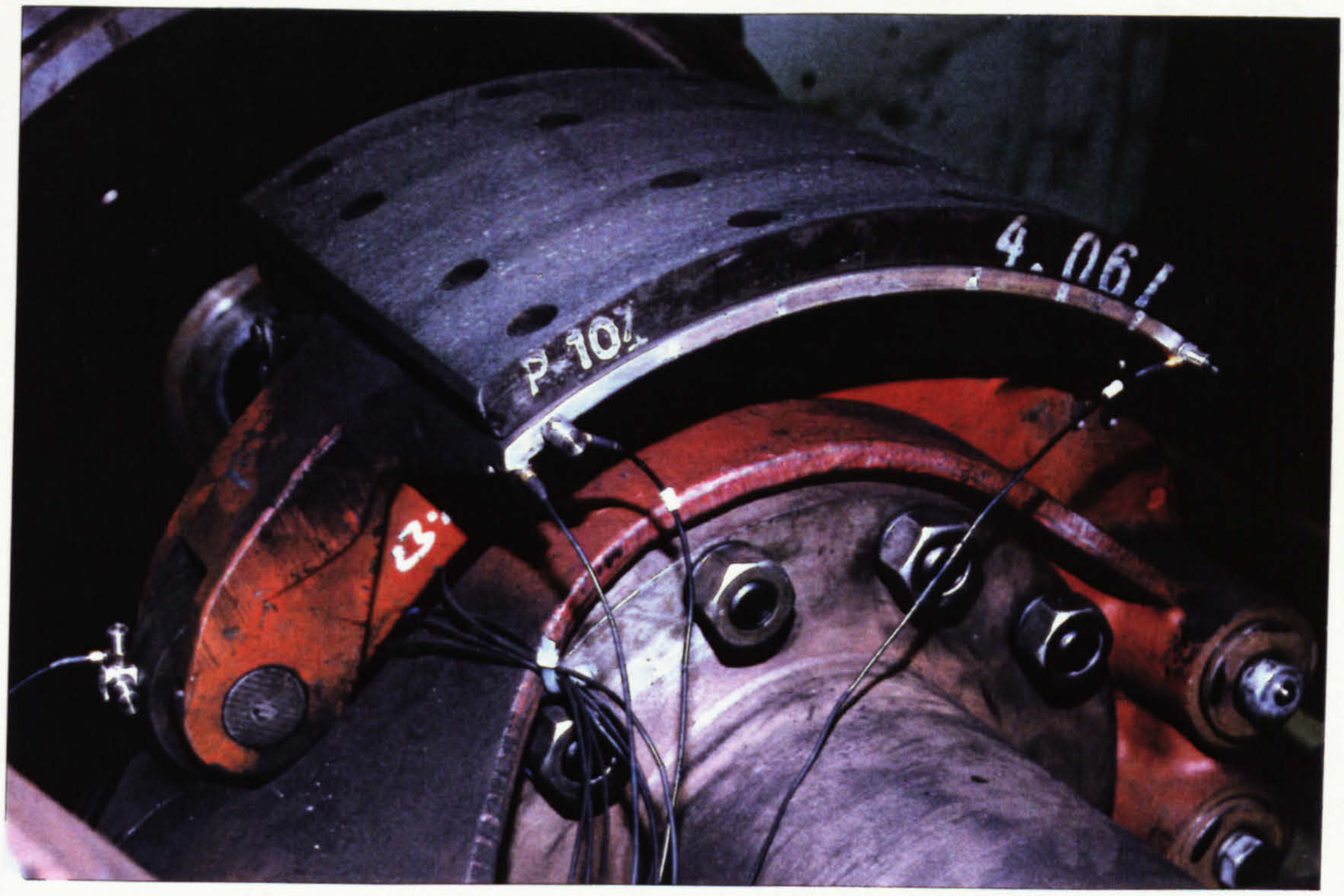

Figure 4.1 Brake shoe used on the Scania 412x203mm brake

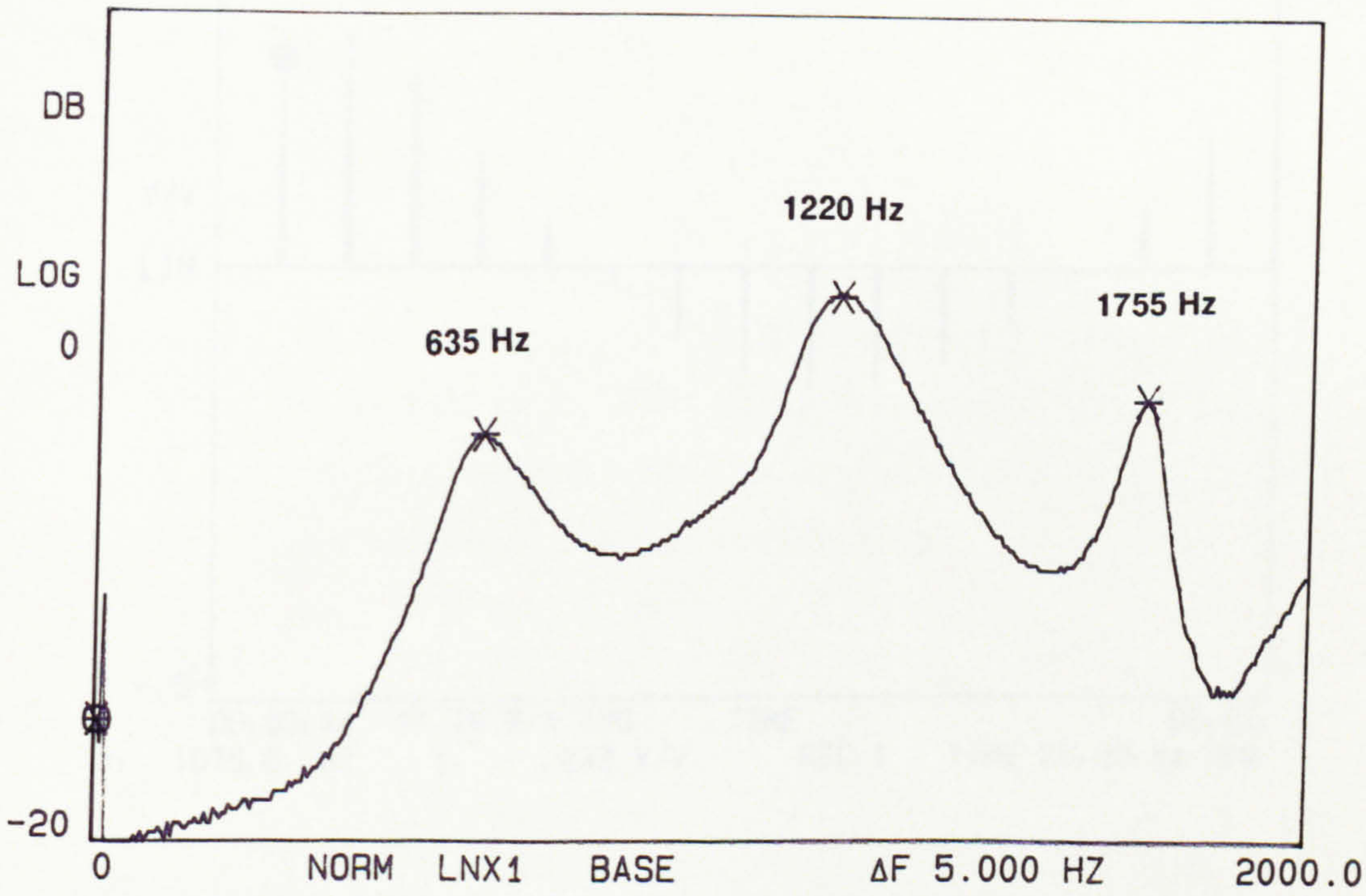

Figure 4.2 Frequency response of a freely suspended shoe

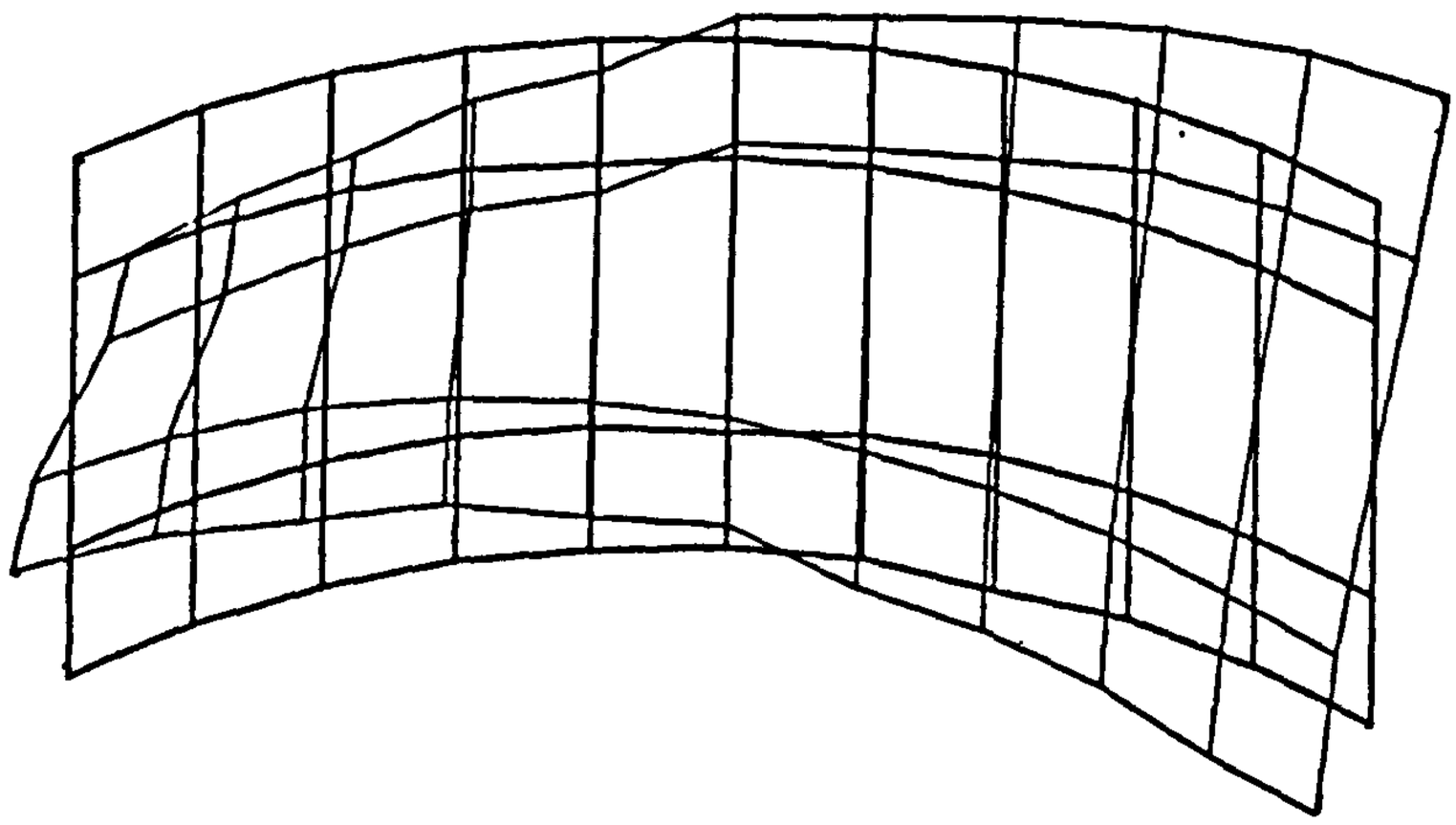

First torsional mode

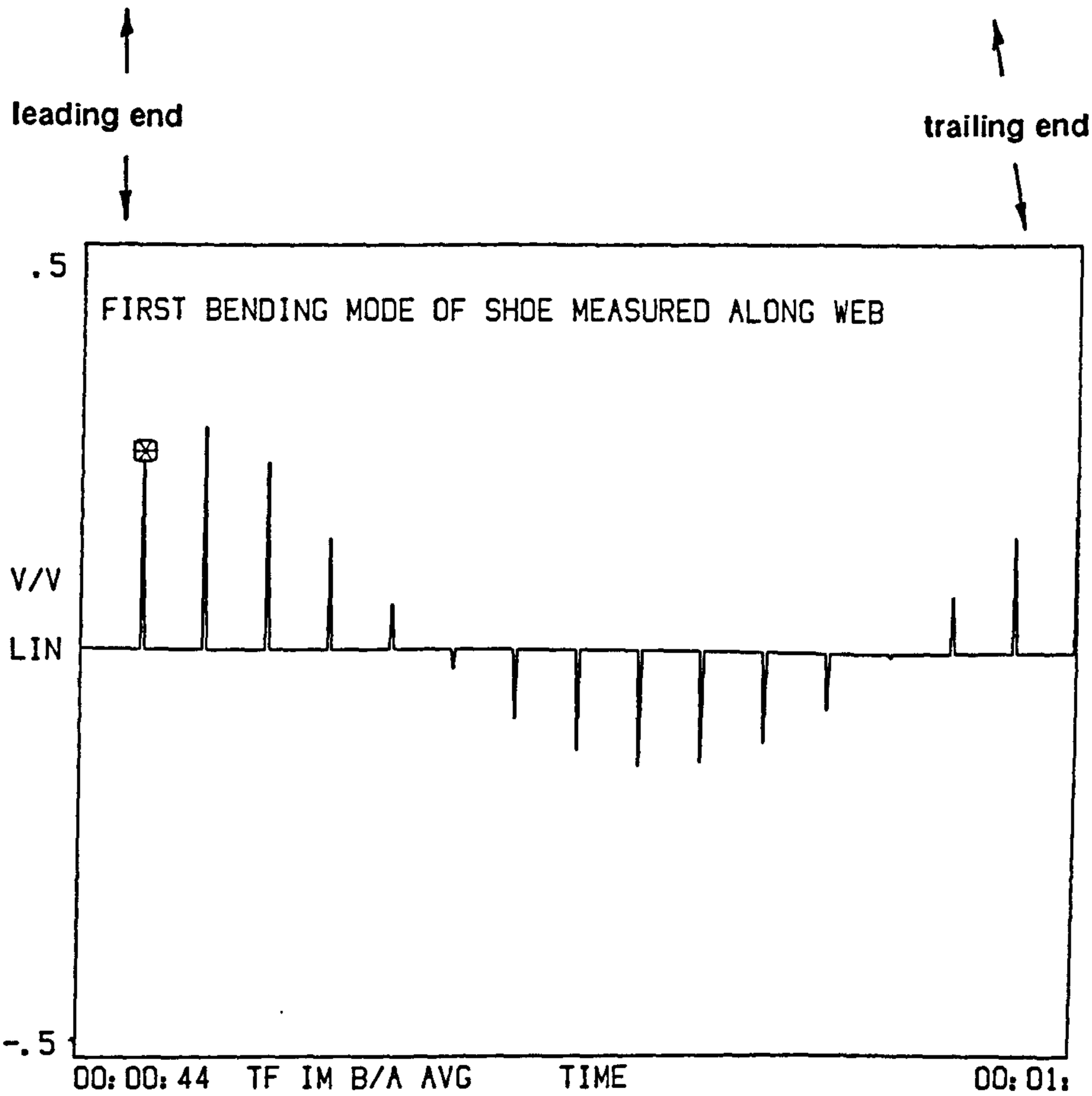

Figure 4.3 **The first torsional mode shape of the platform of a freely suspended shoe and the first bending mode of the shoe web**

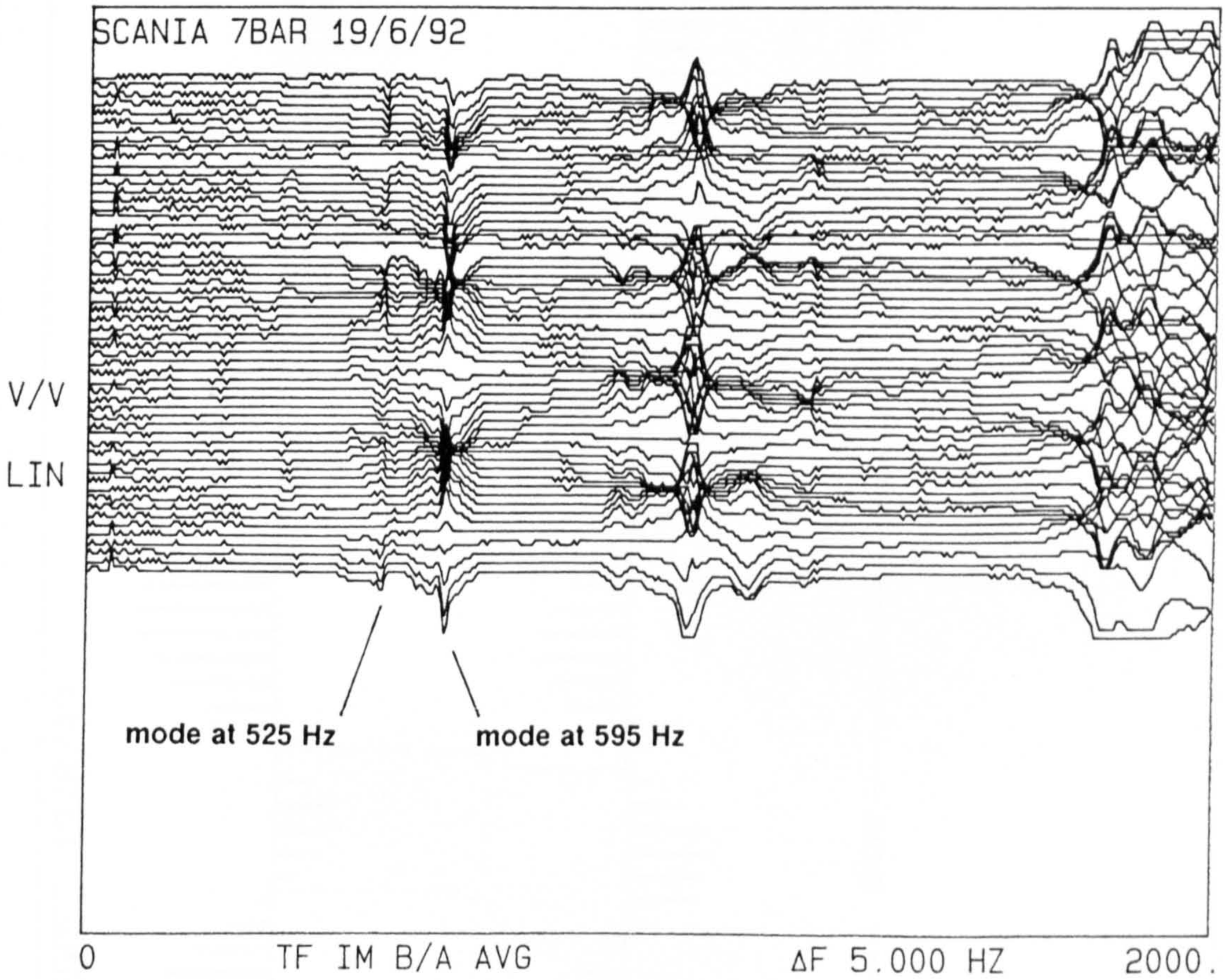

Figure 4.4 **Waterfall diagram of transfer functions taken from impacts around the drum of the statically actuated brake, showing multiple modes involving n=2 and n=3 drum motion. the two predominent n=2 modes are identified**

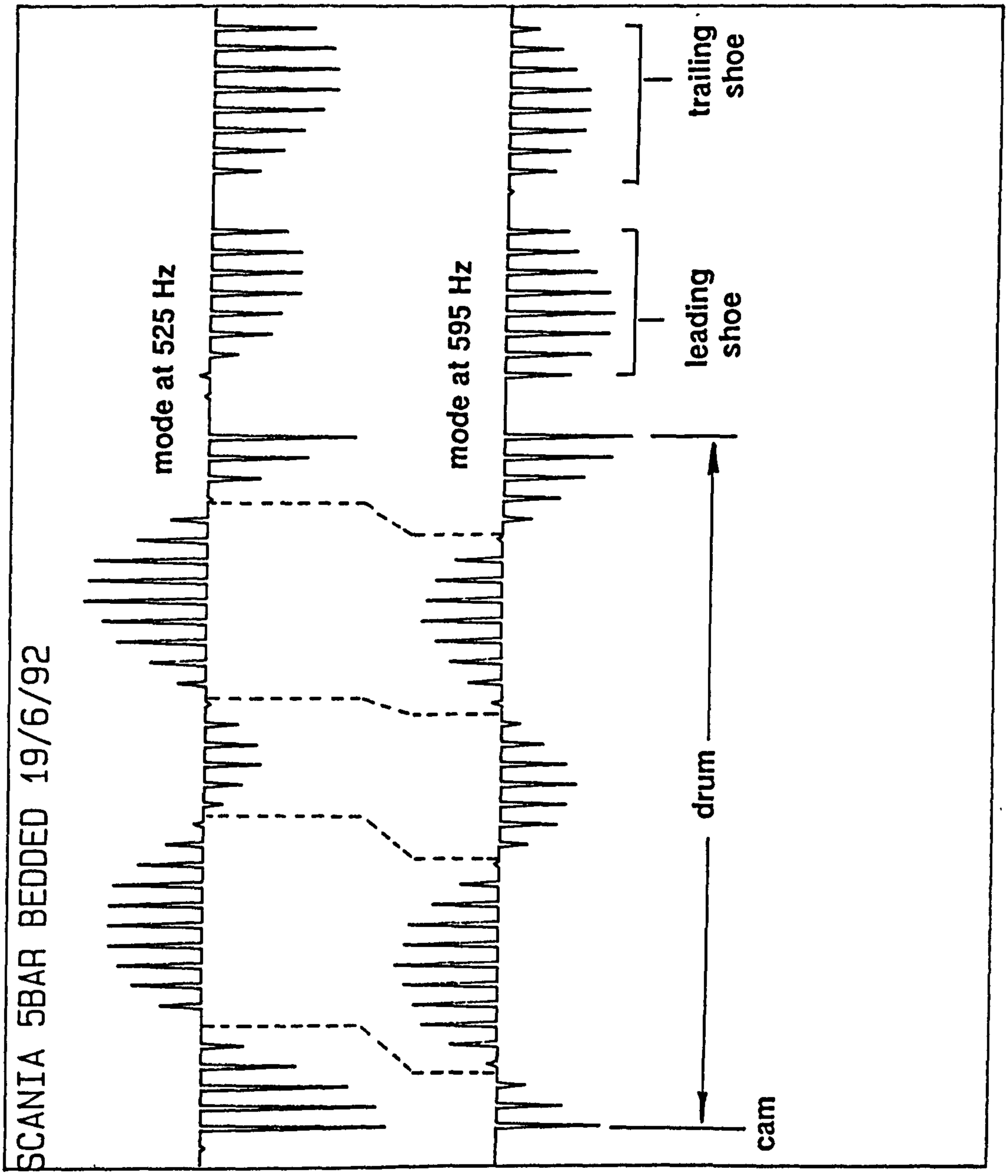

Figure 4.5 **Typical mode shapes of the drum and shoes on a brake subjected to 5 bar static actuation pressure on the dynamometer**

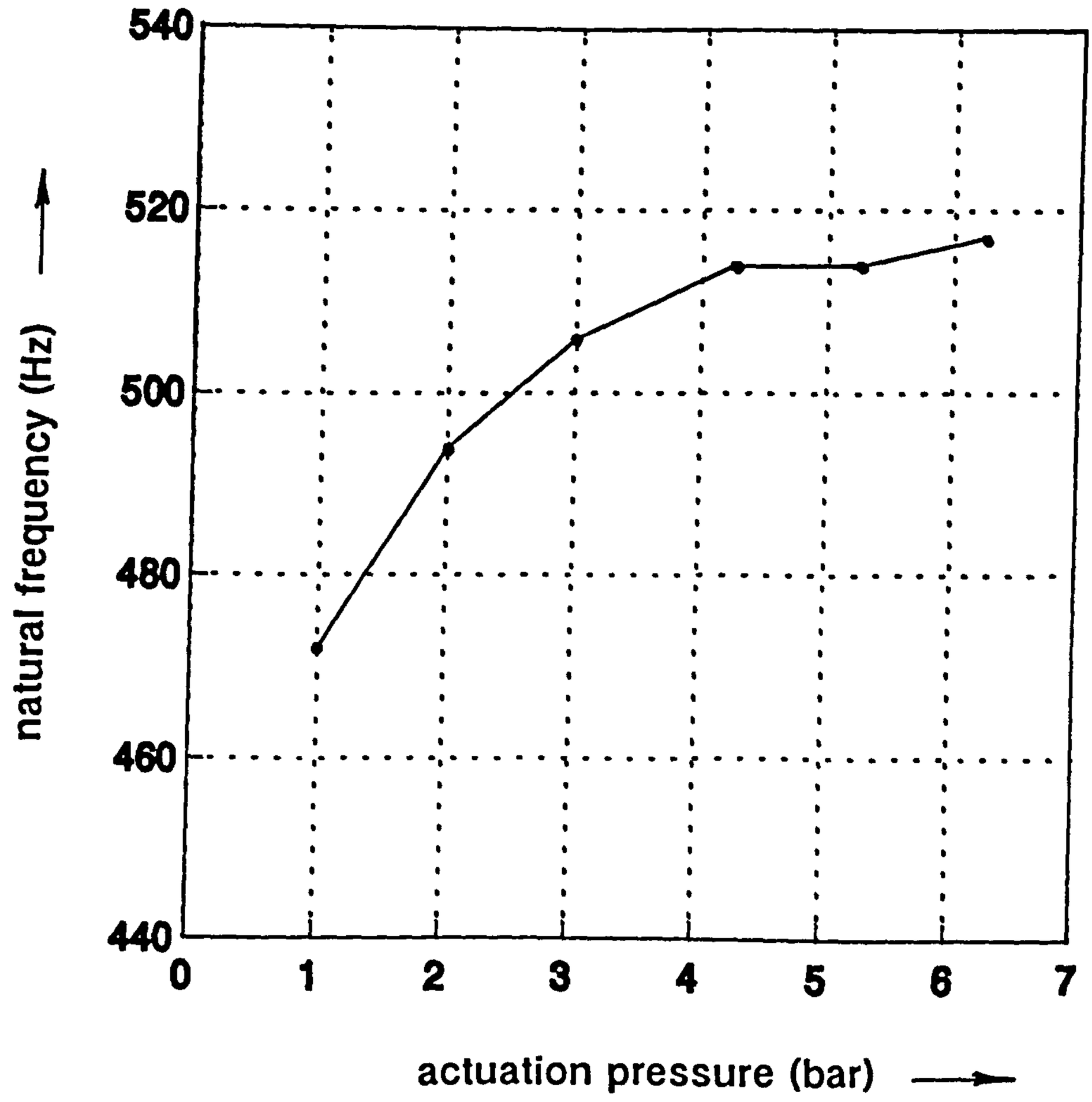

Figure 4.6 The effect of actuation pressure on a natural frequency of the actuated brake involving the n=2, s=0 drum mode

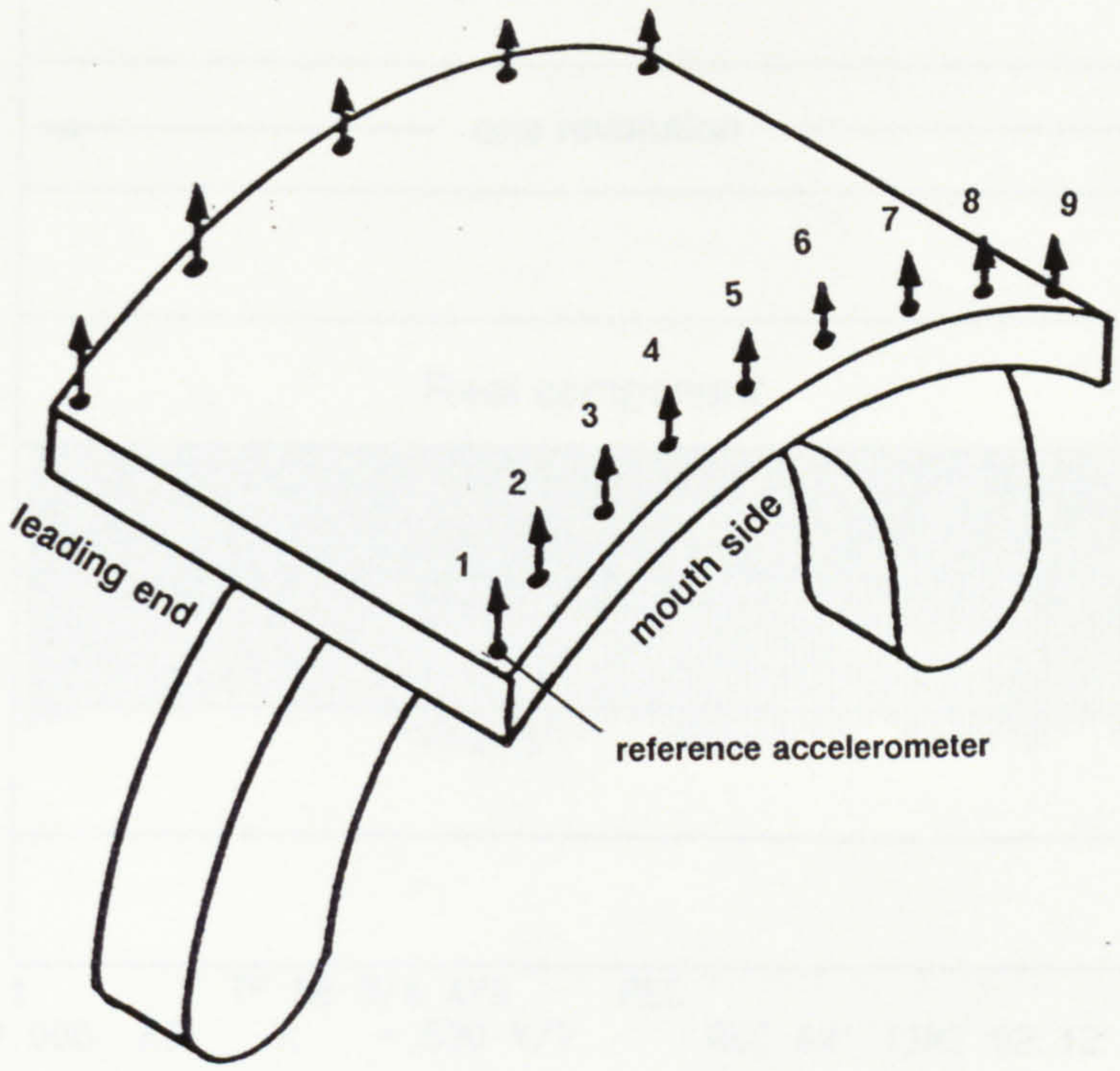

Figure 4.7(a) Positions of the accelerometers on the leading shoe, used for squeal modal analysis

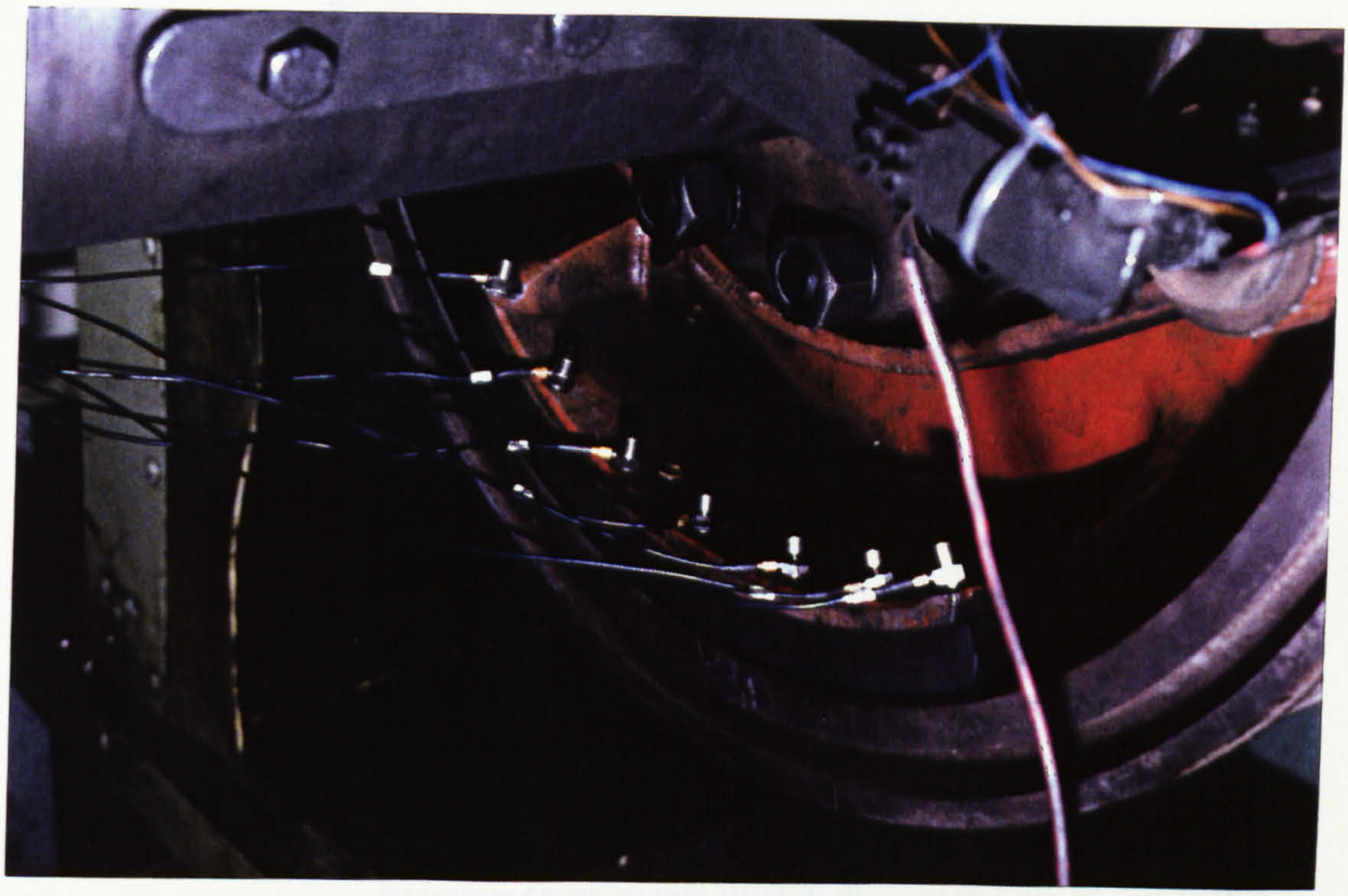

Figure 4.7(b) The accelerometers attached to the shoe platform

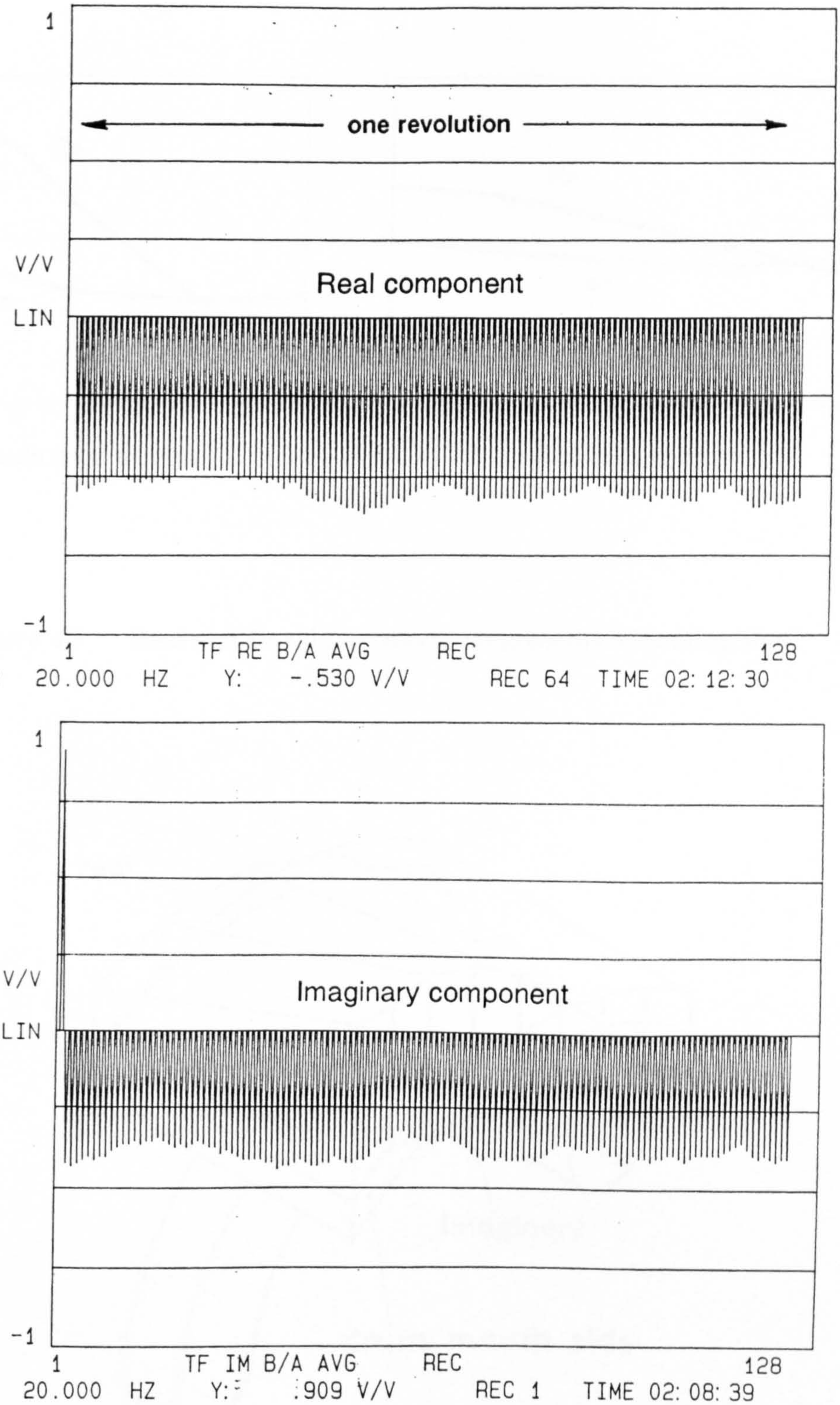

Figure 4.8 **Typical variation of the Real and Imaginary shoe transfer function components during one revolution of the drum**

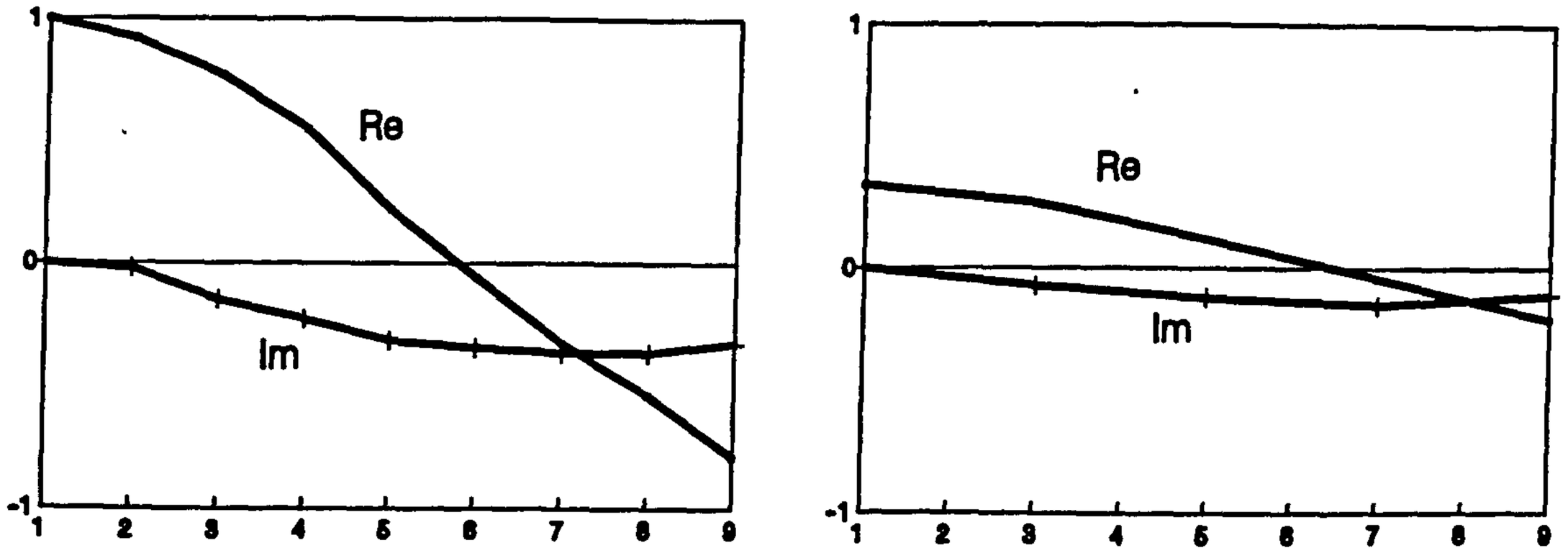

Figure 4.9 Real and Imaginary mode components of leading shoe

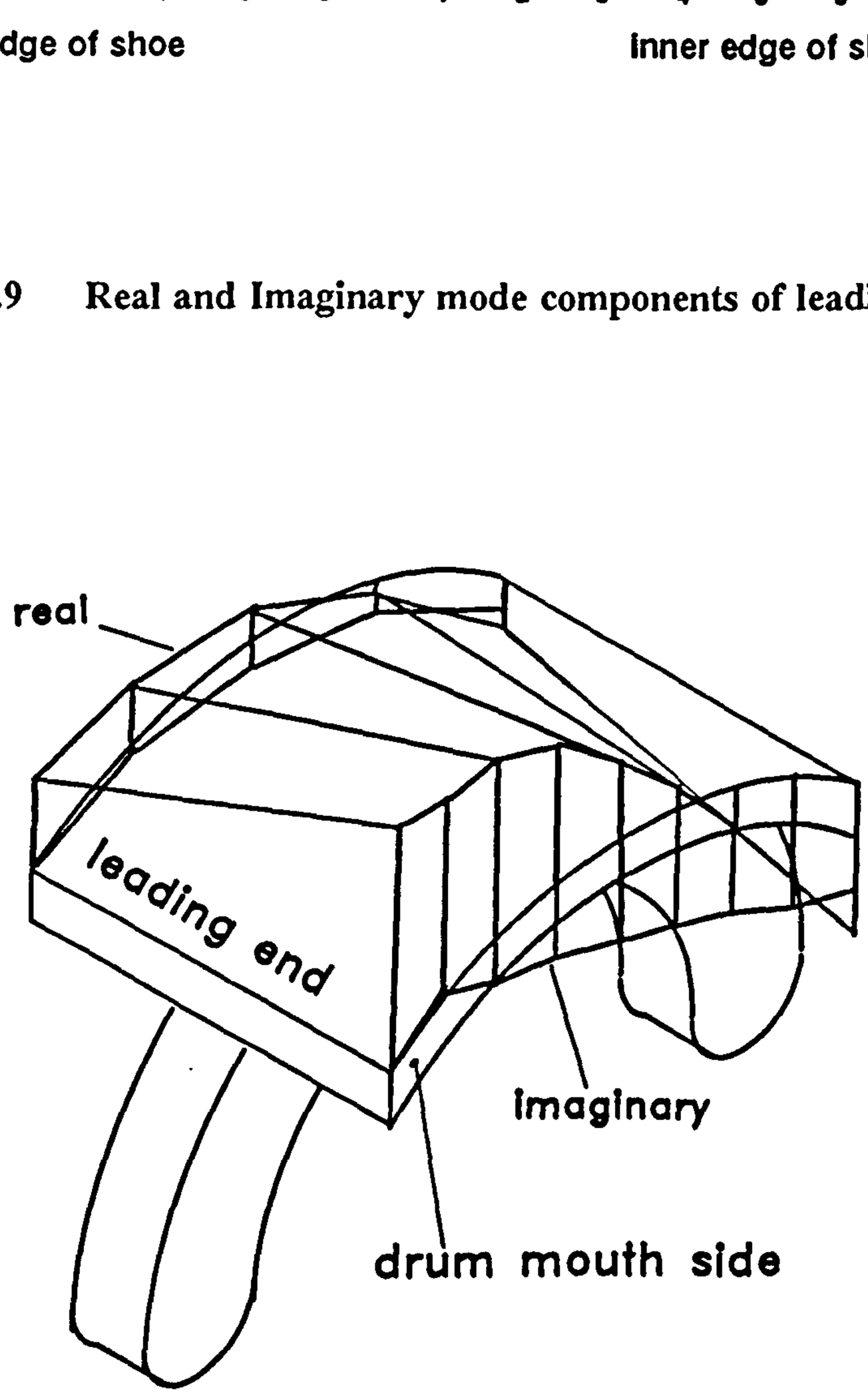

Figure 4.10 The complex squeal mode of leading shoe

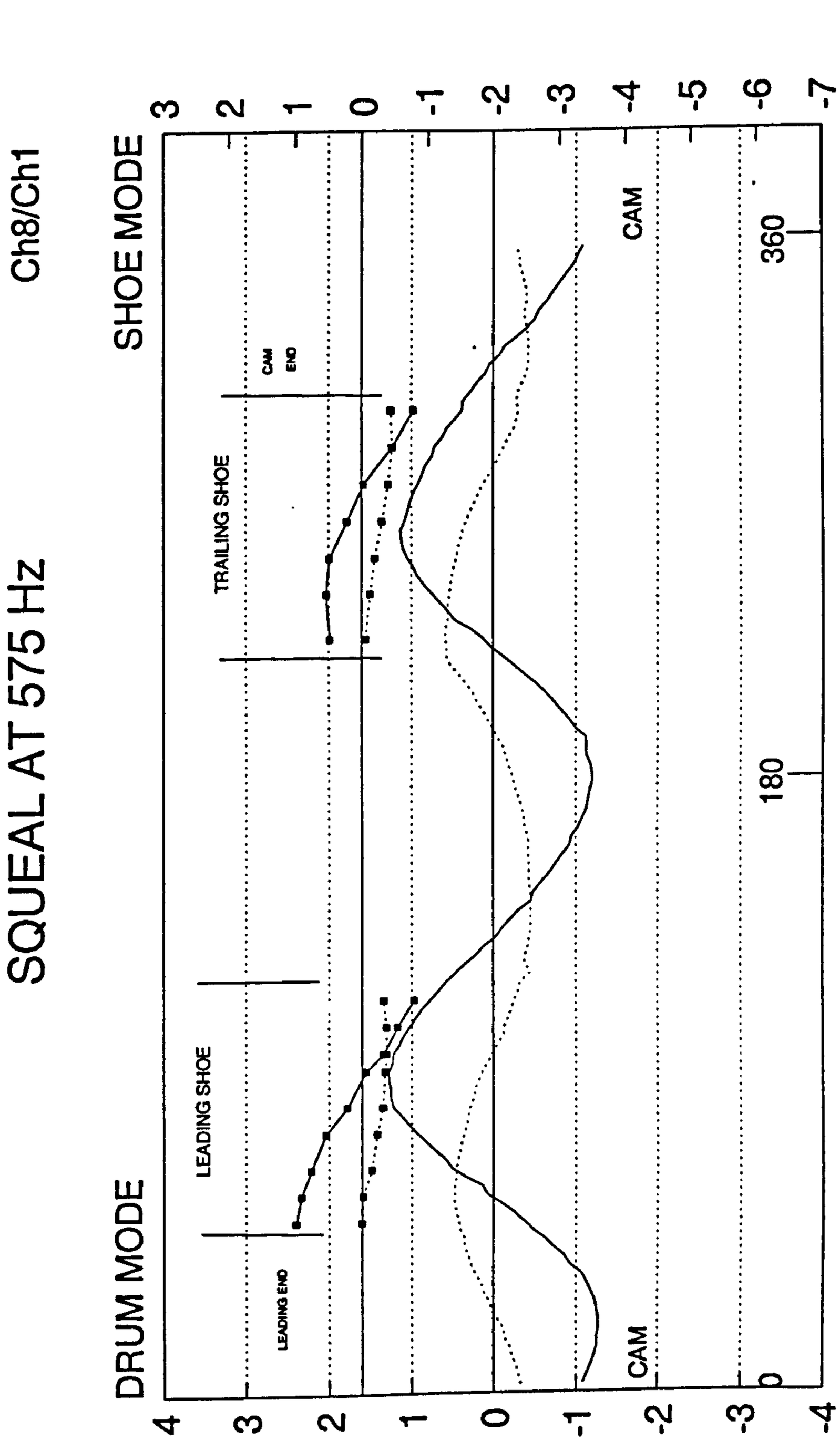

Figure 4.11 The combined drum and shoe complex modal analysis

CHAPTER 5

THE SYMMETRY OF THE BRAKE DRUM

5.1 Introduction

An important feature of the drum modal analysis, produced in chapter 3, is the stationary nature of the components of the complex mode shape relative to the brake shoes. As the drum is rotating during braking, this implies that the mode components rotate relative to the drum with variable angular velocity, whilst maintaining an approximately constant squeal frequency. Such rotation of the mode, at constant frequency, is only possible due to the inherent symmetry of the drum about its axis of rotation.

When considering the normal modal behaviour of the drum, as measured in section 3.3, it is clear that the angular position of the measured mode on the drum is arbitrary, being determined, during modal analysis, only by the position used for excitation, which becomes an antinode. This feature makes the normal modal analysis of an axisymmetric structure, such as a brake drum, fundamentally different from the analysis of more arbitrarily shaped structures.

Normal modal analysis is generally carried out by measuring the response, at one point on a structure, to an excitation at a different point on the structure and repeating for either an array of response positions with a fixed excitation point or an array of excitation points with a fixed response position. If impact excitation is used, the latter is, in practice, more readily carried out and was used for the normal modal analysis of the drum in chapter 3. For most structures, this technique is based upon the effect

that, although the response position is fixed relative to the structure's mode shape, the response amplitude is proportional to the mode amplitude at the excitation point. In particular, excitation at a nodal point of a mode produces no response in that mode. Thus, the transfer functions between the response at a fixed position and excitation at a range of positions, exactly reproduce the mode shape.

The general structure, considered above has mode shapes which are fixed in position relative to features on the structure or its boundaries, whereas on an axisymmetric structure, such as a brake drum, no such features or boundaries exist, in the circumferential direction, to locate the modes. The angular position of such modes is thus arbitrary and follows the excitation position as it is moved during the modal analysis. Hence, in this particular case, the response measurement position, although fixed to the drum, effectively 'scans' the mode shape, which is being moved around the drum by the movement of the excitation position. In this sense, the normal mode measurement technique and the squeal mode technique developed in chapter 3 are very similar, the shoe reference accelerometer signal in the latter effectively replacing the impact excitation signal in the former.

5.2 The Effect of Reducing Symmetry on the Normal Mode Behaviour of the Drum

5.2.1 Defining rotational symmetry

The arbitrary positioning of circumferential drum modes, which appears to be a necessary condition for the observed stationary complex squeal modes, is, as noted above, a direct consequence of the high degree of symmetry of the drum structure about its axis of rotation.

In considering this symmetry of the drum it is useful to employ the well defined mathematical concept of 'a symmetry' - that of an operation on a figure or structure which leaves the figure or structure unchanged. Thus, a plane equilateral triangle has three rotational symmetries:- rotation through 0°, 120° and 240°, and these symmetries form a Group of order 3. By this definition, a perfectly circular drum with constant wall thickness would have an infinite number of rotational symmetries forming a Group of order infinity. Thus any angular position of the drum is indistinguishable from any other.

The number of rotational symmetries can be reduced by identifying specific points on the drum structure. When considering the drum as a dynamic system, this could be achieved by attaching discrete masses to the drum periphery. Any random arrangement of masses is likely to reduce the symmetry group order to one - the identity element of the group, but if equal masses are attached at equispaced intervals around the drum periphery the symmetry group order will be equal to the number of masses. For example, attaching 3 equispaced masses to the drum will reduce the drum rotational symmetries from an infinite number to just 3, rotation through 0°, 120° and 240°.

Perrin and Charnley (38) have investigated the effect of rotational symmetry on campanologist's bells, which have some similarity in form to brake drums. They recognised that natural imperfections in bells were responsible for 'warbling' due to cyclic transfer of energy between the two preferentially orientated meridian modes, and their solution to this problem was to cast in a mass or rib to swamp the spurious natural 'splitting' and, by striking the bell at the mass point only one of the pair of modes would be excited. Although there is little similarity between the problems of 'warbling' in a static bell and self-excited vibration in a rotating brake, the degree of

rotational symmetry in a brake will be shown to be fundamental to its capacity to squeal.

5.2.2 Modal analysis of a drum with reduced rotational symmetry

In order to evaluate the effect of a reduction in the symmetry group order of the drum on its normal mode behaviour, steel blocks, of mass 1.38 kg, were attached to the outside surface of the drum mouth by bolts into tapped holes in the drum (as in fig 5.1). The dynamic response of the drum was measured using impact excitation and accelerometer response as for the normal modal analysis in 3.3. In this instance, however, the modes were not expected to be arbitrarily positioned and so any arbitrary impact position and response measurement point would not necessarily capture all the modes of interest. For initial response tests, the involvement of all modes of interest was ensured by impacting and measuring responses at a large number of angular positions between two masses and averaging the resultant transfer functions (automatically, using the spectrum analyzer). The resultant average frequency response is shown in fig 5.3 for the case of 2 equispaced masses attached to the drum, and this is compared with the response of the same drum, with no masses attached, in fig 5.2.

It can be seen that for each circumferential mode of the 'symmetric' drum, two natural frequencies are now present, one identical with the 'symmetric' drum natural frequency, and one below it. (*Modes corresponding to these pairs of natural frequencies will be referred to as 'split' modes*). Repeating the measurements with 3, 4 and 5 equispaced masses attached to the drum produced the frequency responses shown in fig 5.4 (a-c). Comparison of these results with the 'symmetric' drum responses indicate that, in these cases, the masses have not modified the response in

all modes to produce two natural frequencies, or split modes. The measured natural frequencies for each mass arrangement are summarised in the following table.

Table 4 Effect of discrete mass addition on normal mode frequencies

Mode	Number of equispaced 1.38 kg masses				
	0	2	3	4	5
n=2,s=0	425	385 425	395	360 415	375
n=3,s=0	915	860 915	835 920	860	855
n=4,s=0	1645	1505 1650	1535	1380 1655	1465
n=5,s=0	2530	2445 2535	2445	2435	2265 2550

The above results suggest that the addition of equispaced masses only introduce a second natural frequency if the number of masses divides exactly into the number of axial nodal lines (ie twice the number of nodal diameters). That is, a second mode is introduced only if the following condition is satisfied

$$\frac{2n}{z} = \text{integer} \qquad (5\text{-}1)$$

where z = no of equispaced masses, and hence is equal to the rotational symmetry group order.

This condition will be explored more fully in section 5.3.

The mode shapes corresponding to the natural frequencies in table 1 were measured using the same techniques described in section 3.3. The circumferential mode shapes of a typical pair of split modes (n=2,s=0), produced by the addition of 2 equispaced masses, are shown in fig 5.5. Unlike the arbitrary angular positioning of the single mode of the symmetric drum, these two modes occupy fixed positions relative to the masses, such that the masses coincide with nodes of the higher frequency mode and antinodes of the lower frequency mode. The upper mode will thus be unmodified in frequency by the mass addition (except for a small effect due to rotational inertia of the masses) as observed in fig 5.3

5.3 Analysis of the Effect of Reduced Symmetry on the Drum Modes

In order to explain the foregoing experimental observations, the effect of the addition of discrete, equispaced masses to the drum periphery will be examined by considering the kinetic energy of the masses in the drum meridian modes.

Consider a series of z equispaced, equal, point-like masses of mass m, attached to the drum periphery at a fixed axial position, a, as shown in fig 5.6.

If the masses are small it can be assumed that the mode shape of the drum rubbing path in the meridian mode of order n will be of the form

$$y = f(a)\sin n\theta \qquad (5\text{-}2)$$

(Where f(a) is the form of the mode axially across the drum rubbing path) and is identical in form to the normal mode of the symmetric drum, measured in section 3.3.

Referring to fig 5.6, the angular position of mass k is $\theta_k = 2k\pi/z - \phi$ and its amplitude, shown in fig 5.7, in the meridian mode of equation 5-2 is given by the equation

$$y_k = f(a)\sin n\left(\frac{2k\pi}{z} - \phi\right) \tag{5-3}$$

The total kinetic energy of the z masses is therefore

$$T = \sum_{k=1}^{z} \frac{m}{2}\omega^2 y_k^2 = \frac{m\omega^2}{2}\sum_{k=1}^{z} y_k^2 \tag{5.4}$$

The meridian modes of the drum will have no preferential angular position on the drum structure, relative to the masses, only if the natural frequency of the mode is independent of the angular position, ϕ, of the set of masses relative to the mode. In order that the natural frequency of the mode be independent of the angular position of the masses, the total kinetic energy of the masses in this mode of vibration must be independent of ϕ, ie

$$\frac{dT}{d\phi} = 0 \quad \textit{for all } \phi \tag{5-5}$$

From equations 5-3 and 5-4

$$T = \frac{m\omega^2}{2} f^2(a) \sum_{k=1}^{z} \sin^2\left(\frac{2nk\pi}{z} - n\phi\right) \tag{5-6}$$

putting $2nk\pi/z = \alpha_k$ and differentiating gives

$$\frac{dT}{d\phi} = \frac{nm\omega^2}{2} f^2(a) \sum_{k=1}^{z} -2n\sin(\alpha_k - n\phi)\cos(\alpha_k - n\phi) \tag{5-7}$$

$$\rightarrow \frac{dT}{d\phi} = \frac{nm\omega^2}{2} f^2(a) \sum_{k=1}^{z} \sin(2\alpha_k - 2n\phi) \tag{5-8}$$

$$\rightarrow \quad \frac{dT}{d\phi} = \frac{nm\omega^2}{2} f^2(a)\left(\sin 2n\phi \sum_{k=1}^{z} \cos 2\alpha_k - \cos 2n\phi \sum_{k=1}^{z} \sin 2\alpha_k\right) \tag{5-9}$$

In this expression, consider evaluating first the summation

$$\sum_{k=1}^{z} \sin 2\alpha_k \quad \text{ie} \quad \sum_{k=1}^{z} \sin \frac{4nk\pi}{z}$$

$$\text{Putting} \quad \frac{4n\pi}{z} = \beta \tag{5-10}$$

$$\rightarrow \quad \sum_{k=1}^{z} \sin \frac{4nk\pi}{z} = \sum_{k=1}^{z} \sin k\beta \tag{5-11}$$

$$= \sin\beta + \sin 2\beta + \ldots\ldots + \sin(4n\pi - 2\beta) + \sin(4n\pi - \beta) + \sin 4n\pi \tag{5-12}$$

$$\text{But} \quad \sin(4n\pi - k\beta) = -\sin k\beta \tag{5-13}$$

and hence, if z is even, all such terms cancel, whilst if z is odd, all such terms cancel except

$$\sin \frac{z\beta}{2} = \sin 2n\pi = 0 \tag{5-14}$$

The final term, $\sin 4n\pi$, is also zero and so

$$\sum_{k=1}^{z} \sin 2\alpha_k = 0 \quad \text{for all z} \tag{5-15}$$

Equation (5-9) now becomes

$$\frac{dT}{d\phi} = \frac{nm\omega^2}{2} f^2(a) \sin 2n\phi \sum_{k=1}^{z} \cos 2\alpha_k \tag{5-16}$$

Evaluating now the summation

$$\sum_{k=1}^{z}\cos 2\alpha_k \;=\; \sum_{k=1}^{z}\cos k\beta \;=\; \frac{1}{2}\sum_{k=1}^{z}(e^{ik\beta}+e^{-ik\beta}) \tag{5-17}$$

which is the sum of a geometric progression, and may be expressed in the form

$$\sum_{k=1}^{z}\cos k\beta \;=\; \frac{1}{2}\left(\frac{1-e^{(z+1)i\beta}}{1-e^{i\beta}} + \frac{1-e^{-(z+1)i\beta}}{1-e^{-i\beta}} - 2\right) \tag{5-18}$$

$$\rightarrow \sum_{k=1}^{z}\cos k\beta \;=\; \frac{1}{2}\left(\frac{2-2\cos\beta+2\cos z\beta-2\cos(z+1)\beta}{2\;-\;2\cos\beta}\right) \tag{5-19}$$

$$\text{But as}\quad z\beta = 4n\pi \;\rightarrow\; \begin{matrix}\cos(z\beta) = 1\\ \cos(z+1)\beta = \cos\beta\end{matrix} \tag{5-20}$$

$$\rightarrow \sum_{k=1}^{z}\cos k\beta \;=\; \frac{1}{2}\left(\frac{4\;-\;4\cos\beta}{2\;-\;2\cos\beta} - 2\right) \tag{5-21}$$

$$\rightarrow \sum_{k=1}^{z}\cos 2\alpha_k = 0 \quad,\quad \text{only if} \quad \begin{matrix}\cos\beta \neq 1\\ \text{ie}\;\; \cos\frac{4n\pi}{z} \neq 1\end{matrix} \tag{5-22}$$

Equation (5-16) now becomes

$$\frac{dT}{d\phi} \;=\; 0 \qquad \text{if} \qquad \cos\frac{4n\pi}{z} \neq 1 \tag{5-23}$$

The condition $\cos 4n\pi/z=1$ implies that $4n\pi/z$ must be an integral multiple of 2π and that $2n/z$ must be an integer. This signifies that the kinetic energy of the masses, and hence the natural frequency of the meridian mode, order n, is independent of ϕ for any number of z equally spaced masses except where z is consistent with the condition $2n/z$ = integer, mentioned earlier.

Substituting this condition in equation (5.6) for the kinetic energy of the masses gives

$$T = \frac{m\omega^2}{2} f^2(a) \sum_{k=1}^{z} \sin^2(jk\pi - n\phi) \qquad (5\text{-}24)$$

where j and k are integers.

$$\rightarrow T = \frac{m\omega^2}{2} f^2(a) \sum_{k=1}^{z} \sin^2 n\phi \qquad (5\text{-}25)$$

$$\rightarrow T = \frac{m\omega^2}{2} f^2(a) z \sin^2 n\phi \qquad (5\text{-}26)$$

and the kinetic energy of the masses is clearly a function of the angular position, ϕ, of the masses relative to the origin of the mode shape.

5.4 The Effect of Reduced Symmetry on Squeal

The experimental and theoretical analysis in sections 5.2 and 5.3 suggest that the addition of suitably placed discrete masses to the drum structure could result in modal behaviour inconsistent with that measured on a squealing drum in section 3.5. In particular, if pairs of modes which rotate relative to the drum do occur, as measured in 3.5, then their frequencies would not be always identical (as in the case when squealing) due to the 'splitting' effect of the added masses. It may thus be expected that the addition of such masses will have an effect on the squeal characteristics of the brake.

The effect on squeal propensity was examined using the same range of equispaced 1.38 kg masses attached to the drum during brake applications known to induce consistent ($\approx$ 580Hz) squeal from the unmodified brake. Subjective evaluation of the audible squeal associated with each mass arrangement is listed overleaf.

No masses	gives	- Continuous squeal
2 masses	gives	- Cyclic squeal
3 masses	gives	- Continuous squeal
4 masses	gives	- No squeal
5 masses	gives	- Continuous squeal

It was clear from these subjective assessments that the squeal propensity was modified only by the addition of 2 or 4 masses, which are the only values of z which satisfy the $2n/z$ = integer condition for n=2 (the drum mode order associated with the 580 Hz squeal). There thus appears to be a relationship between squeal propensity and the 'splitting' of drum modes.

The 'cyclic' description of the squeal produced with 2 masses attached indicates non-continuous squeal which occurs in several bursts per revolution of the drum. A measurement of the time history of this cyclic squeal was obtained from an accelerometer on the leading shoe platform. Spectra measured repeatedly during the brake application were assembled into a waterfall diagram and a profile at the squeal frequency is shown in fig 5.8. Two cyclic characteristics are apparent, corresponding to one and eight cycles per revolution of the drum. The one cycle per revolution component is the normal amplitude variation associated with drum runout or eccentricity whilst the eight cycles per revolution is due to the influence of the two masses.

Although the subjective evaluation of the squeal noise was the same with 0, 3 or 5 masses, spectrum analysis showed a decrease in squeal frequency with mass addition, and a comparison between spectra with 0 and 5 masses is shown in fig 5.9. The lack of influence of 3 and 5 masses on the amplitude of the squeal, or squeal propensity,

effectively eliminates other possible contributors to stability, such as potential additional damping from the mass attachment interfaces. It is also noted that the observed invariance of the squeal frequency with the angular position of the masses is in a agreement with the analysis of section 5.3 which shows that the total kinetic energy of the masses is independent of their angular position relative to the mode if $2n/z \neq$ integer.

5.5 A Suggested Mechanism for the Effect of Reduced Drum Symmetry on Squeal

5.5.1 Introduction

The theoretical treatment, in section 5.3, of the effect of structural asymmetry on flexural drum modes explains the normal mode behaviour of the drum observed in section 5.2. It does not, however, directly explain the effect of such reduced symmetry on the squeal propensity discussed above. The squealing drum is observed to hold a complex mode whose real and imaginary components appear similar in shape and position to the pairs of normal modes produced by a suitable reduction in symmetry. In the squealing condition, however, the mode components are, of course, of the same frequency and rotate around the drum, whilst the 'split' pairs of normal modes are not coincident in frequency and are fixed relative to the drum.

It was initially considered that the positional 'fixing' of the drum modes to the drum, by the masses, resulted in the observed elimination of squeal by forcing rotation of the complex squeal mode components and thus disturbing the observed consistent dynamic conditions at the frictional interface. This view is, however, difficult to relate to the single frequency cyclic squeal produced by small reductions in symmetry.

A mechanism more consistent with the observed behaviour is provided by consideration of the squeal as a binary flutter type of instability and the applied masses as decoupling the flutter modes.

5.5.2 Decoupling of binary flutter modes

The binary flutter mechanism for brake squeal is, as noted in the Literature Survey, most readily related to the low frequency squeal of disc brakes, where the section of disc in contact with the pads can be approximated as a rigid beam with two degrees of freedom. Such an approximation cannot be applied to a drum brake due to the greater length of friction material in contact with the drum, with the consequent significant amount of drum bending over this length even in the lower drum flexural modes. The observed complex drum mode which occurs during squeal is, however, consistent with the type of rotor motion predicted by the binary flutter mechanism. The ability of the drum to vibrate in two differently positioned modes with identical frequencies provides the two independent degrees of freedom at any point at the frictional interface, required for binary flutter, and hence a simple flutter model of a short section of the interface will now be considered.

Consider a simple model of a section of the drum/lining interface of length $2l$, as shown in fig 5.10. It is assumed that the section of drum has two independent degrees of freedom, y and θ, and is in contact with a section of friction material over its whole length. The friction material is assumed to be attached to a rigid fixed shoe, and its

total stiffness through its thickness is k_p, resulting in a rotational stiffness of $k_p l^2/3$ over this length, $2l$. The equations of motion of the system are

$$M\ddot{y} + (k_d + k_p)y + \mu(N + k_p y)\theta = 0 \quad (5\text{-}27)$$

$$I\ddot{\theta} - \mu h k_p y + (S_d + k_p \frac{l^2}{3})\theta = 0 \quad (5\text{-}28)$$

where N is the normal force applied at the interface during braking. For small displacements, y, it can be assumed that $k_p y \ll N$ and so equation 5.27 can be approximated by

$$M\ddot{y} + (k_d + k_p)y + \mu N\theta = 0 \quad (5\text{-}29)$$

Putting

$$a = \frac{k_d}{M} + \frac{k_p}{M}, \quad b = \frac{\mu N}{M}$$
$$c = -\frac{\mu h k_p}{I}, \quad d = \frac{S_d}{I} + \frac{k_p l^2}{3I} \quad (5\text{-}30)$$

equations (5.27) and (5.28) become

$$\ddot{y} + ay + b\theta = 0 \quad (5\text{-}31)$$
$$\ddot{\theta} + cy + d\theta = 0 \quad (5\text{-}32)$$

or in matrix form

$$\begin{bmatrix} \ddot{y} \\ \ddot{\theta} \end{bmatrix} + \begin{bmatrix} a & b \\ c & d \end{bmatrix} \begin{bmatrix} y \\ \theta \end{bmatrix} = 0 \quad (5\text{-}33)$$

Assuming a solution of the form

$$\begin{bmatrix} y \\ \theta \end{bmatrix} = \begin{bmatrix} y_0 \\ \theta_0 \end{bmatrix} e^{\lambda t} \quad (5\text{-}34)$$

equation (5.33) becomes

$$\lambda^2 \begin{bmatrix} y_0 \\ \theta_0 \end{bmatrix} + \begin{bmatrix} a & b \\ c & d \end{bmatrix} \begin{bmatrix} y_0 \\ \theta_0 \end{bmatrix} = 0 \qquad (5\text{-}35)$$

$$\text{ie} \quad \left[\lambda^2 \begin{bmatrix} 1 & 0 \\ 0 & 1 \end{bmatrix} + \begin{bmatrix} a & b \\ c & d \end{bmatrix} \right] \begin{bmatrix} y_0 \\ \theta_0 \end{bmatrix} = 0 \qquad (5\text{-}36)$$

The characteristic equation of this eigenvalue problem is

$$\det \begin{bmatrix} a+\lambda^2 & b \\ c & d+\lambda^2 \end{bmatrix} = 0 \qquad (5\text{-}37)$$

$$\begin{aligned} &\rightarrow (a + \lambda^2)(d + \lambda^2) - bc = 0 \\ &\rightarrow \lambda^4 + (a + d)\lambda^2 + (ad - bc) = 0 \end{aligned} \qquad (5\text{-}38)$$

This is a quadratic equation in λ^2 and so

$$\lambda^2 = \frac{1}{2}\left(-(a + d) \pm \sqrt{(a + d)^2 - 4(ad - bc)} \right) \qquad (5\text{-}39)$$

$$\rightarrow \quad \lambda = \pm \frac{1}{\sqrt{2}} \left(-(a + d) \pm \sqrt{(a + d)^2 - 4(ad - bc)} \right)^{\frac{1}{2}} \qquad (5\text{-}40)$$

The criterion for oscillatory instability is the occurrence of a pair of complex conjugate eigenvalues having positive real parts, and such eigenvalues occur when

$$4(ad - bc) > (a + d)^2 \qquad (5\text{-}41)$$

(a condition which is derived in Appendix 2)

or, simplifying, for instability,

$$-4bc > (a - d)^2 \qquad (5\text{-}42)$$

$$\rightarrow \quad \frac{4\mu^2 N h k_p}{MI} > \left(\frac{k_d}{M} + \frac{k_p}{M} - \frac{S_d}{I} - \frac{k_p l^2}{3I}\right)^2 \qquad (5\text{-}43)$$

Now for a standard brake drum, the y and θ coordinate motions of the short segment of drum wall can be considered as parts of two identical normal modes, related as shown in fig 5.11. These normal mode frequencies are identical, and so

$$\frac{k_d}{M} = \frac{S_d}{I} \qquad (5\text{-}44)$$

and the condition for instability reduces to

$$\rightarrow \quad \frac{4\mu^2 N h k_p}{MI} > k_p^2 \left(\frac{1}{M} - \frac{l^2}{3I}\right)^2 \qquad (5\text{-}45)$$

$$\rightarrow \quad 4\mu^2 N h > k_p MI \left(\frac{1}{M} - \frac{l^2}{3I}\right)^2 \qquad (5\text{-}46)$$

which is similar to the condition obtained by North from the simple disc brake flutter model (23).

Although this criterion for stability is based on an oversimplified model of the brake, some features are consistent with observed squeal behaviour. The consensus of opinion from most empirical work (for example Newcomb and Spurr (39)) is that increasing μ is destabilising, and also the current experimental work suggests an increase in noise propensity with increased applied pressure, and hence normal force, N.

If it is now assumed that the two identical normal drum modes are decoupled, by, for example, the addition of discrete masses to the drum, then the equivalent rotational

and translational modes of the section of the drum in the binary flutter model will now have different frequencies. That is

$$\frac{k_d}{M} \neq \frac{S_d}{I} \tag{5-47}$$

and by putting

$$\frac{k_d}{M} - \frac{S_d}{I} = \omega_T^2 - \omega_R^2 = S \tag{5-48}$$

then the criterion for instability, equation (5-43), becomes

$$\frac{4\mu^2 N h k_p}{MI} > \left(S + k_p\left(\frac{1}{M} - \frac{l^2}{3I}\right)\right)^2 \tag{5-49}$$

from which it can be seen that the frequency split, S,certainly influences the stability, and will have a positive stabilising effect if

$$|S| > \left|k_p\left(\frac{1}{M} - \frac{l^2}{3I}\right)\right| \tag{5-50}$$

but may be destabilising if S is small.

Note:- S is a measure of the separation or 'split' of any pair of drum modes as

$$\omega_T^2 - \omega_R^2 = (\omega_T - \omega_R)(\omega_T + \omega_R) = 2\bar{\omega}\Delta\omega \tag{5-51}$$

5.5.3 Cyclic decoupling of drum modes

The above simplified binary flutter analysis considered the effect of decoupling normal drum modes by, for example, the addition of suitably placed masses. In practice, any discrete mass attached to the drum will rotate with the drum, and hence move relative

to the stationary drum modes measured during squeal. Thus, even when the arrangement of attached masses satisfies the $2n/z$ = integer criterion, the decoupling effect on stationary nodes will depend upon the angular position of the masses relative to the modes.

The real and imaginary components of the complex squeal mode, measured in section 3.5, can be approximated at the axial position of the drum mouth by two normal modes in the form

$$\text{mode1:} \qquad y_1 = a_1 \sin n\theta \sin \omega t \tag{5-51}$$

$$\text{mode2:} \qquad y_2 = a_2 \sin n(\theta - \phi) \cos \omega t \tag{5-52}$$

where ϕ is the angular separation of the two mode components.

As the shapes of these two modes are identical, their generalised mass and stiffness will also be the same, say M and K respectively, referred to antinodal positions, and their natural frequencies will be $\omega_n = (K/M)^{1/2}$. The addition of a small mass, m, at position θ, will modify these natural frequencies. Assuming that the mode shape is unchanged by the small added mass, the total energy in mode 1 is

$$\frac{1}{2}M\dot{y}_1^2 + \frac{1}{2}m(\dot{y}_1 \sin n\theta)^2 + \frac{1}{2}K\dot{y}_1^2 = \text{constant} \tag{5-53}$$

Differentiating this equation gives

$$M\dot{y}_1\ddot{y}_1 + m\dot{y}_1\ddot{y}_1 \sin^2 n\theta + K\dot{y}_1 y_1 = 0 \tag{5-54}$$

$$\rightarrow \quad (M + m\sin^2 n\theta)\ddot{y}_1 + Ky_1 = 0 \tag{5-55}$$

and the modified natural frequency is thus

$$\omega_1 = \left(\frac{K}{M + m\sin^2 n\theta} \right)^{\frac{1}{2}} \tag{5-56}$$

Similarly, the modified natural frequency of mode 2 is

$$\omega_2 = \left(\frac{K}{M + m\sin^2 n(\theta - \phi)} \right)^{\frac{1}{2}} \tag{5-57}$$

The difference of the squares of the natural frequencies given by equations (5.56) and (5.57) results in

$$\omega_1^2 - \omega_2^2 = \frac{K}{M} \left(\frac{1}{1 + \frac{m}{M}\sin^2 n\theta} - \frac{1}{1 + \frac{m}{M}\sin^2 n(\theta - \phi)} \right) \tag{5-58}$$

and

$$\frac{\omega_1^2 - \omega_2^2}{\omega_n^2} = \frac{\frac{m}{M}(\sin^2 n(\theta - \phi) - \sin^2 n\theta)}{1 + \frac{m^2}{M^2}\sin^2 n\theta \sin^2 n(\theta - \phi) + \frac{m}{M}(\sin^2 n\theta + \sin^2 n(\theta - \phi))} \tag{5-59}$$

where $\omega_n^2 = K/M$

Now, assuming m is small, ie $m/M \ll 1$, and that $n\phi = \pi/2$, as is approximately the case for the component modes measured in section 3.5, equation 5.59 reduces to

$$\frac{\omega_1^2 - \omega_2^2}{\omega_n^2} = \frac{m}{M}(\sin^2 n(\theta - \pi/2) - \sin^2 n\theta) \tag{5-60}$$

$$or \quad \frac{\omega_1^2 - \omega_2^2}{\omega_n^2} = \frac{m}{M}\cos 2n\theta \qquad (5\text{-}61)$$

This equation describes the decoupling effect of a single mass, m, on two drum modes of similar shape and relative position as those measured during squeal. It is clear from fig 5.12 that if mass m is divided equally into z equispaced masses, m/z, such that $2n/z$ = integer, these will have an identical effect on the modes.

In section 5.5.2 it was suggested, through a simplified binary flutter ana;ysis, that 'splitting' the frequencies of the component modes could have a stabilising effect, which increases with the magnitude of the split, $|S| = |\omega_T^2 - \omega_R^2|$.

Equation (5-61), above, approximates the magnitude of the frequency split, and

$$\left|\omega_1^2 - \omega_2^2\right| = \left|\omega_n^2 \frac{m}{M}\cos 2n\theta\right| \qquad (5\text{-}62)$$

which is clearly dependent upon not only the size of the added mass, but also its angular position θ, relative to the modes. Hence, as the added mass rotates with the drum, $|\omega_1^2 - \omega_2^2|$ varies between zero and $\omega_n^2 m/M$ with $4n$ cycles per revolution.

The real and imaginary components of the measured squeal mode have n=2 (see fig 3.16) and so suitably placed added masses will produce 8 cycles of decoupling/coupling of the modes per revolution. This is consistent with the observed cyclic squeal obtained with a small total added mass illustrated in fig 5.8, which shows 8 bursts of squeal per revolution, and thus lends credence to the suggested decoupling mechanism.

5.6 Squeal and the effects of drum symmetry related to aircraft flutter

The binary flutter mechanism proposed for brake squeal is so named because of its original application to an unstable vibration phenomenon known as 'flutter', in the aerofoil surfaces of aircraft such as the wings. This vibration occurs as a result of aerodynamic coupling between a bending and a torsional mode of the wing, which is possible because twist of the wing alters its angle of attack to the airstream and hence its lift, which in turn bends the wing. These two modes of the wing are clearly related to the two degrees of freedom of the rotor segment in the simple binary flutter model for squeal, the wing twist corresponding to the rotational mode and the bending to the translational mode. As for the brake, at rest the two modes are distinct, but as airspeed increases (together with the aerodynamic forces) they can coalesce and produce a single unstable mode, potentially resulting in structural failure.

In the aircraft industry the technique used to increase stability (in terms of increased airspeed at which instability arises - the equivalent of increased friction level for squeal to occur in brakes) is to decouple the torsional and bending modes further by attaching a mass at the wing tip on the nodal line of the torsional mode, thus reducing the bending frequency only, as illustrated in fig 5.13. The mass in this case is, however, stationary relative to the wing structure, unlike the rotating masses used to decouple drum modes, and hence will be more effective. This similarity in the modal behaviour and a potential solution to the problems of brake squeal and aircraft flutter reinforces the view that the mechanism of squeal is a form of binary flutter.

5.7 Summary

The stationary nature of the complex squeal mode on the drum is only possible due to the rotational symmetry of the drum structure, such that its modes have no preferential angular position. Reducing this rotational symmetry by, say, attaching discrete masses to its periphery 'splits' some modes into pairs which are in fixed angular positions. The condition for such behaviour is that the rotational symmetry group order, z (or number of masses) should be related to the mode order, n, by $2n/z$ = integer. It is found that a suitable reduction in symmetry can reduce or eliminate the squeal and, by analysis of the symmetry effect applied to a simple binary flutter model for squeal, its mechanism is found to be consistent with the decoupling of pairs of flutter modes.

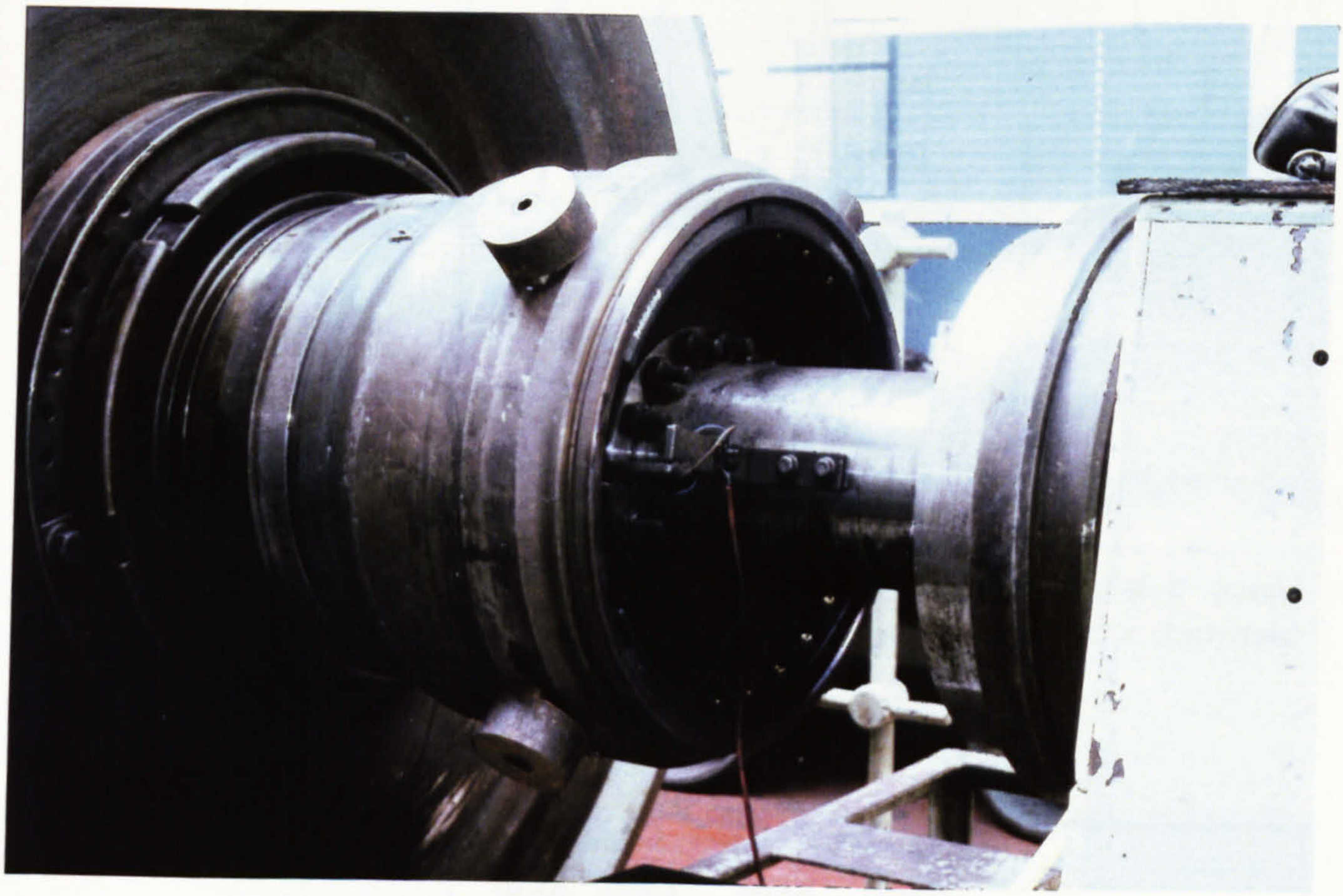

Figure 5.1 **Typical arrangement of masses attached to the drum periphery to reduce its rotational symmetry**

no mass

MARK	LIST X
0	425.00
1	715.00
2	914.99
3	1645.0
4	2450.0
5	2530.0
6	2790.0
7	3020.0
8	3405.0
9	3535.0

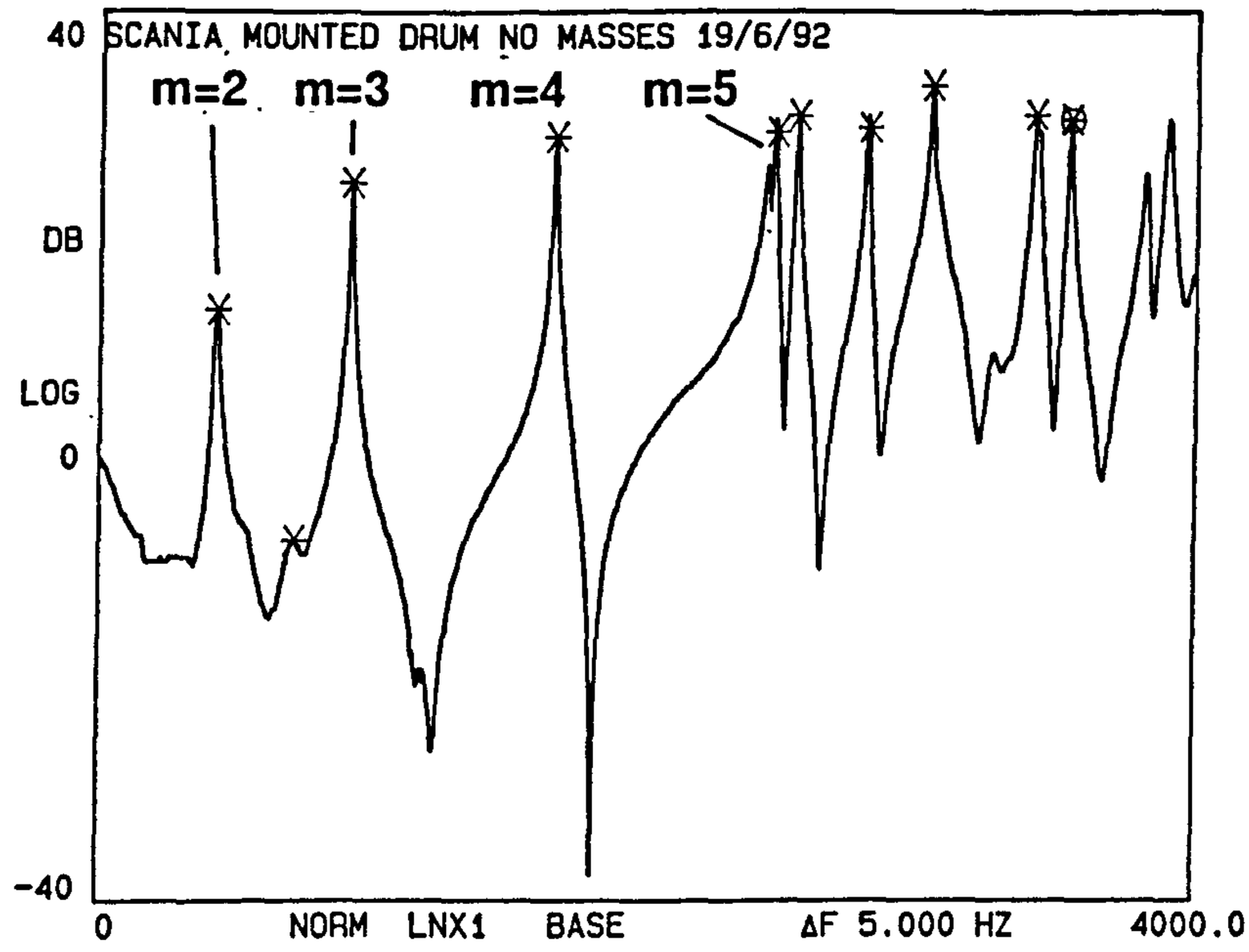

Figure 5.2 **Frequency response function of the unmodified drum mounted on the dynamometer, showing the first 4 diametral modes**

2 masses

MARK	LIST X
0	385.00
1	425.00
2	860.00
3	914.99
4	1505.0
5	1650.0
6	2305.0
7	2445.0
8	2535.0
9	2575.0

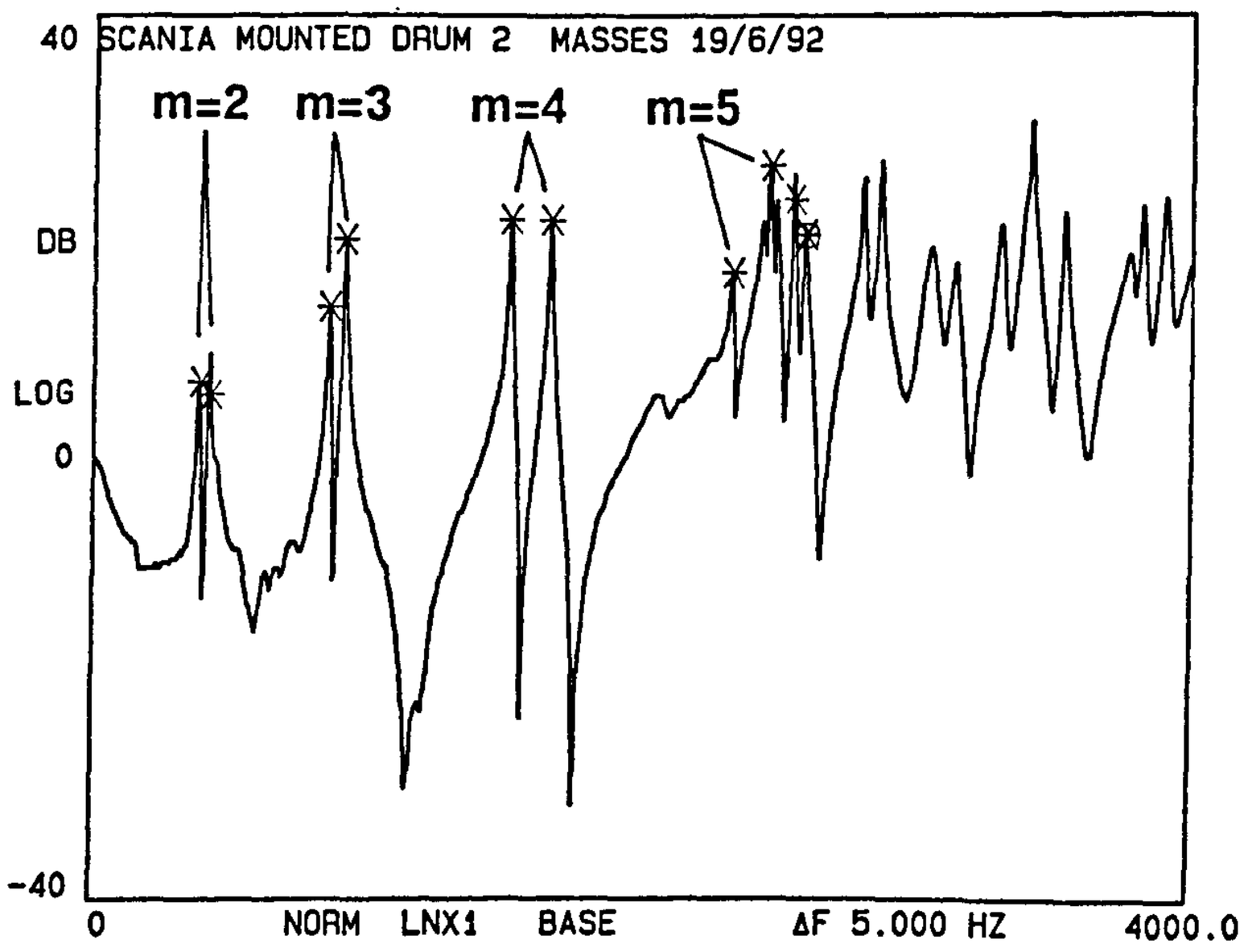

Figure 5.3 **Frequency response function of the drum with two 1.38 kg masses attached at diametrically opposite points on the drum mouth, showing that all diametral modes are 'split'**

(a)

3 masses

MARK	LIST X	Y
0	395.00	9.8
1	835.00	12.4
2	920.00	16.6
3	1535.0	26.6
4	2220.0	15.3
5	2445.0	29.3
6	2625.0	24.4
7	2710.0	20.9
8	3215.0	20.7
9	3320.0	23.9

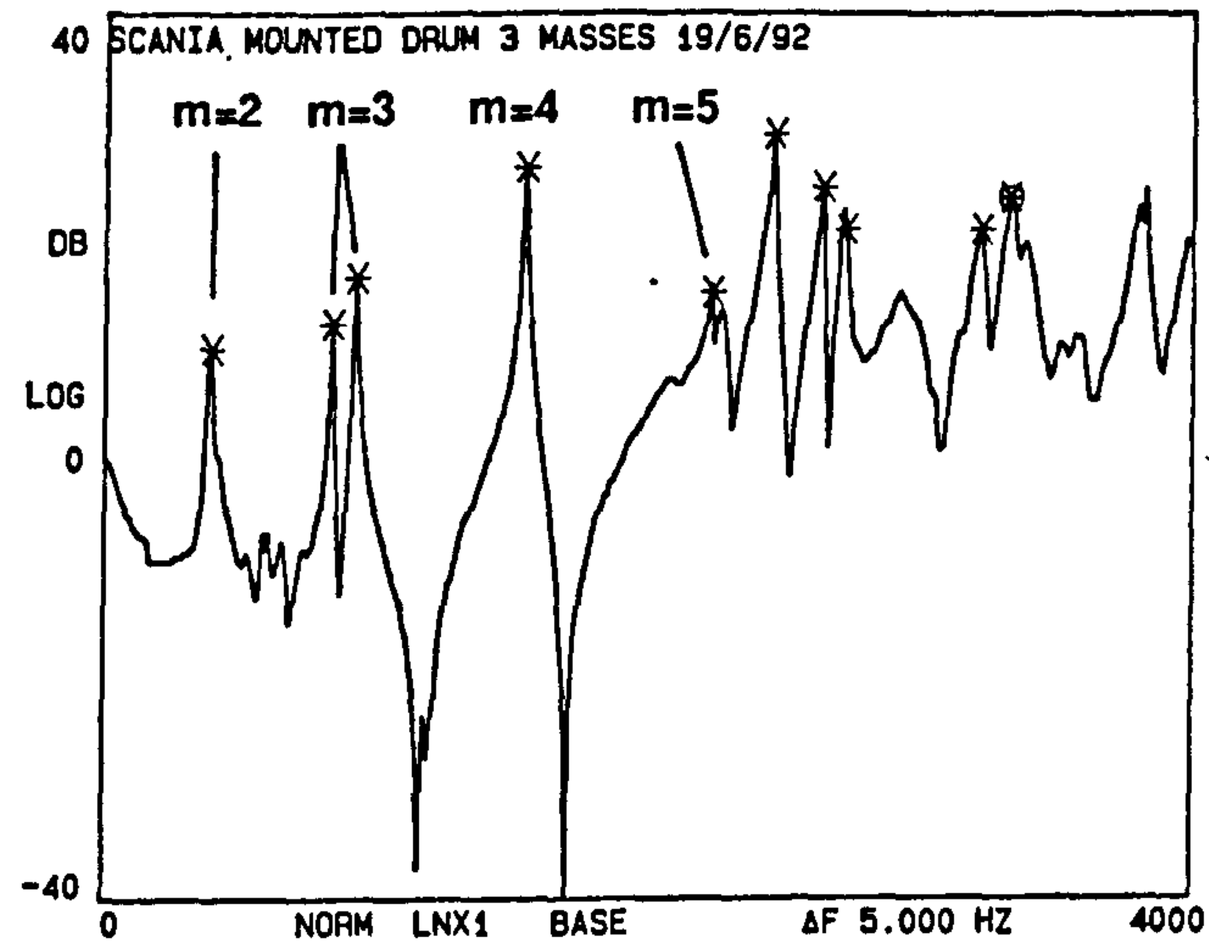

(b)

4 masses

MARK	LIST X	Y
0	360.00	5.7
1	415.00	8.0
2	860.00	19.1
3	1380.0	18.8
4	1655.0	22.6
5	2040.0	8.8
6	2435.0	24.1
7	2475.0	27.5
8	2645.0	12.7
9	2790.0	28.5

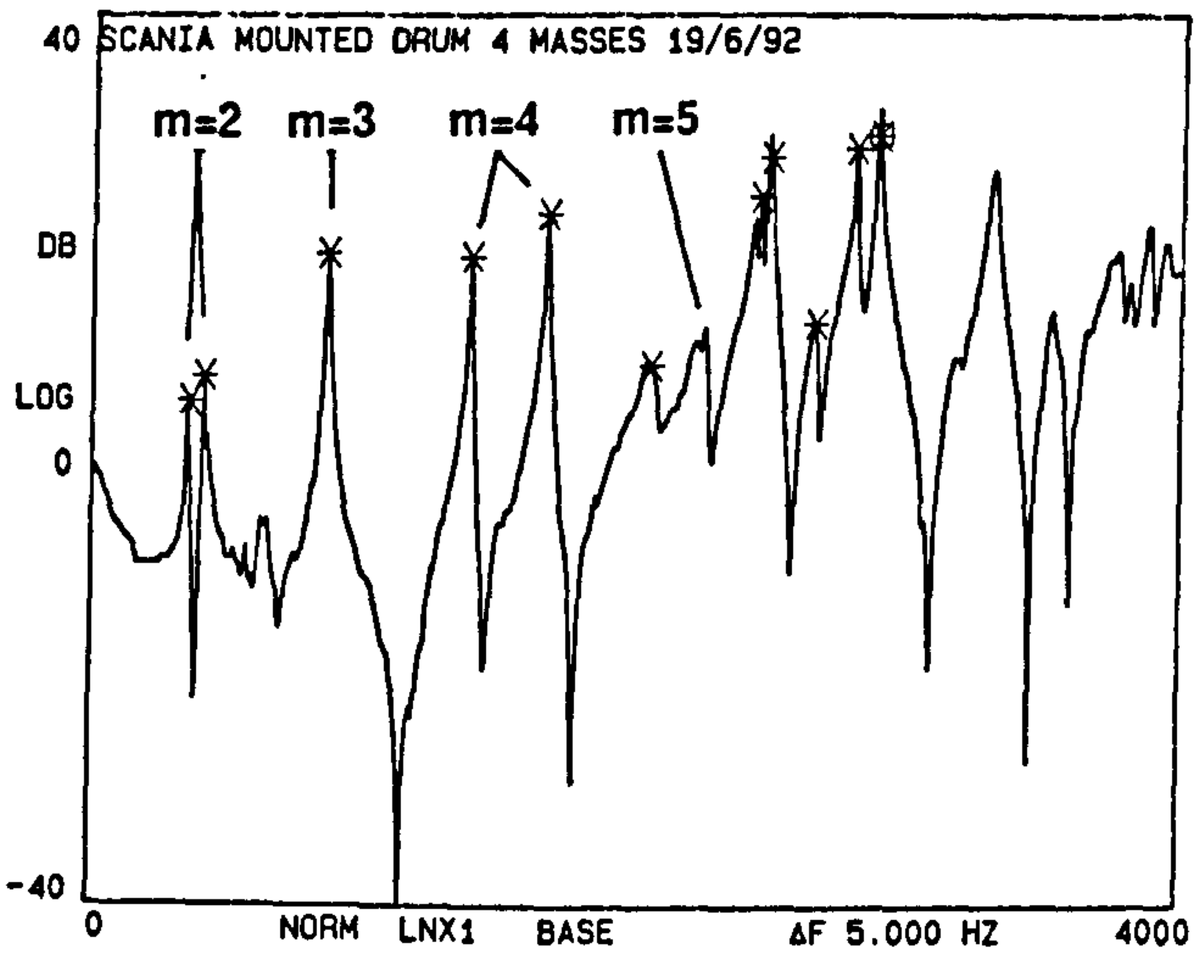

(c)

5 masses

MARK	LIST X	Y
0	375.00	9.9
1	650.00	-5.1
2	855.00	19.1
3	1465.0	18.1
4	1860.0	15.9
5	2265.0	17.1
6	2435.0	22.5
7	2475.0	15.4
8	2550.0	19.2
9	2785.0	26.2

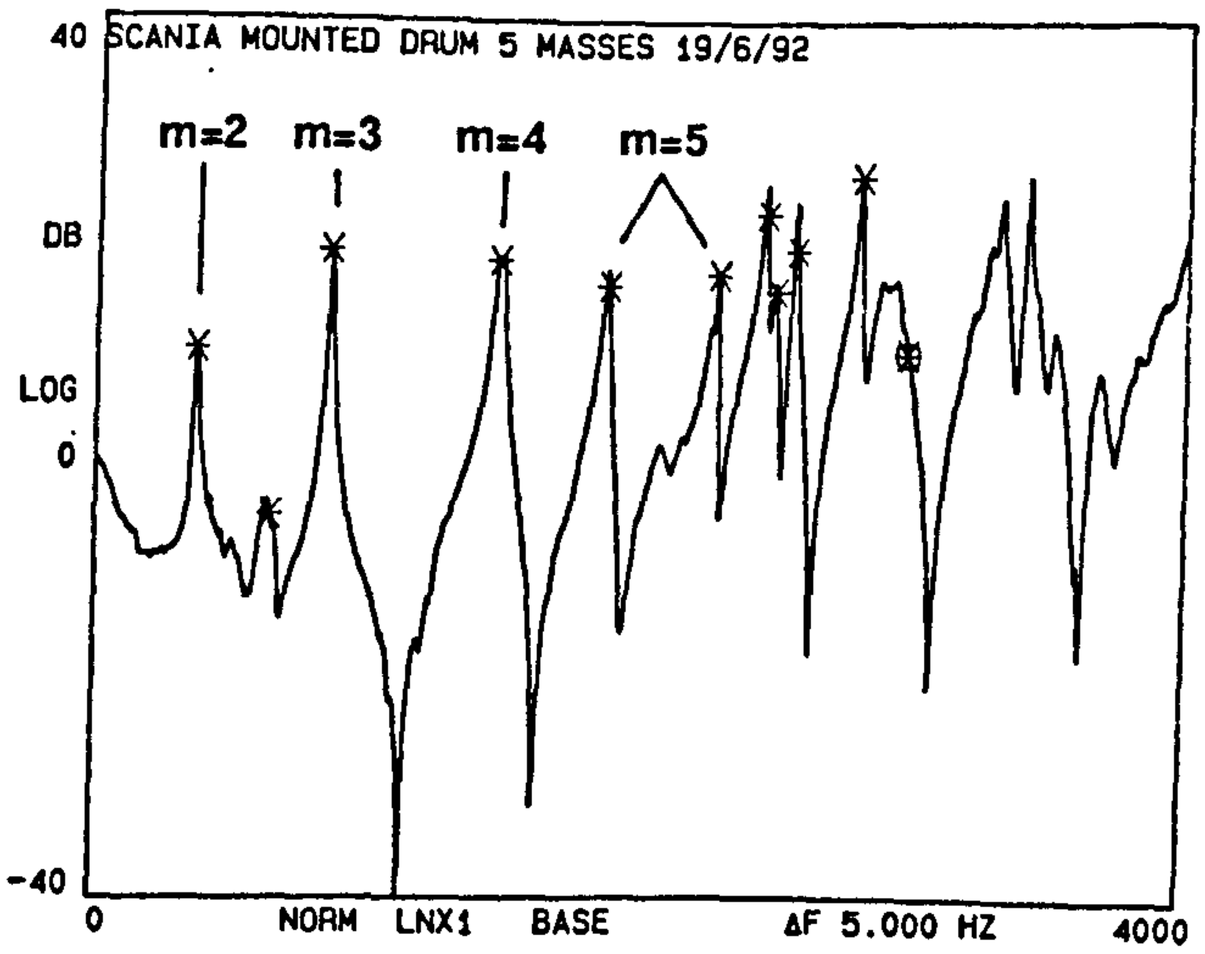

Figure 5.4 **FRF's of the drum with 3, 4 and 5 equispaced masses attached around its mouth, showing how the modes which are 'split' are consistent with the $2n/z$=integer condition, and also that the non-split modes are reduced in frequency due to the mass addition**

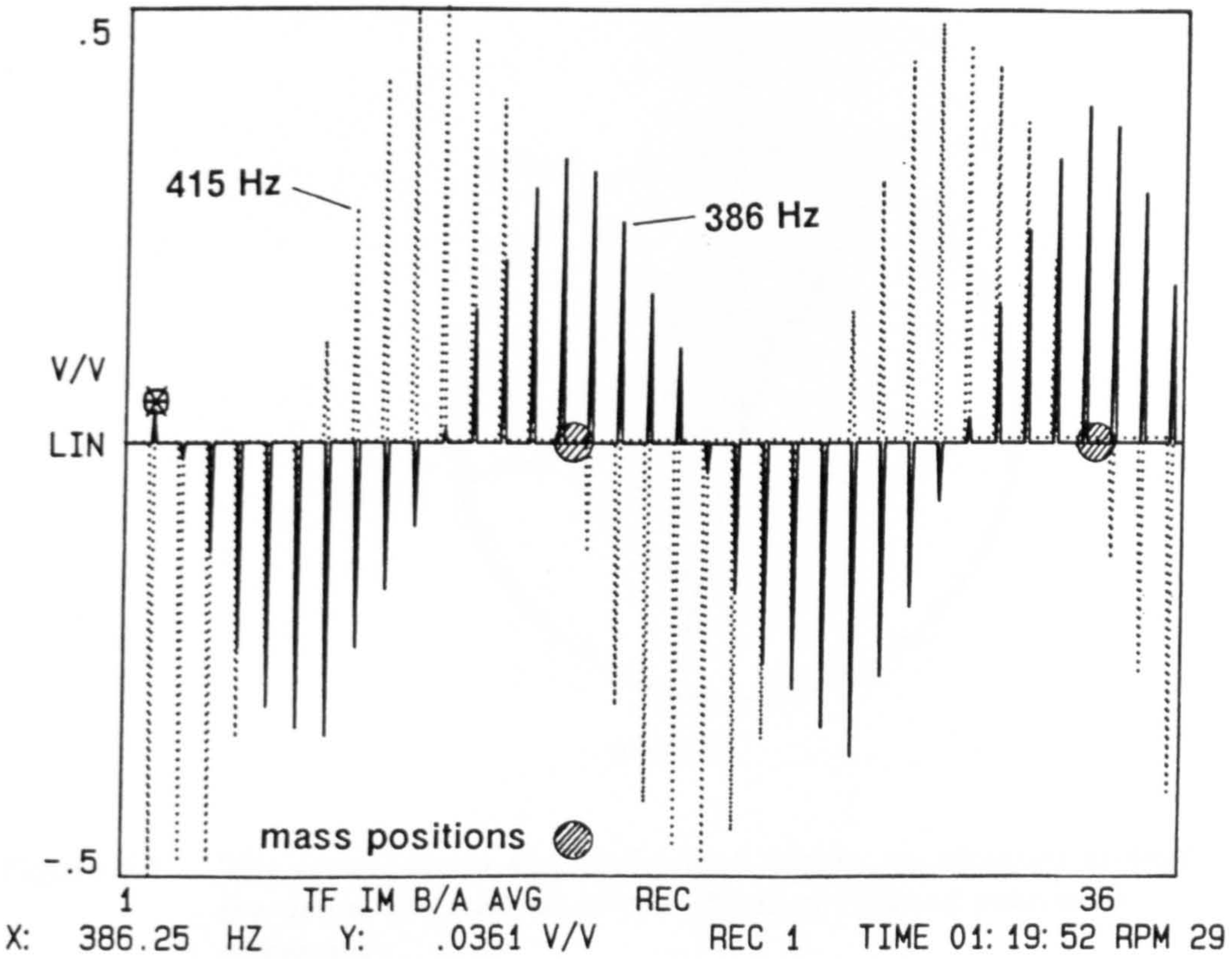

Figure 5.5 The pair of 'split' n=2,s=0 modes produced by the addition of two equispaced 1.38kg masses to the drum periphery

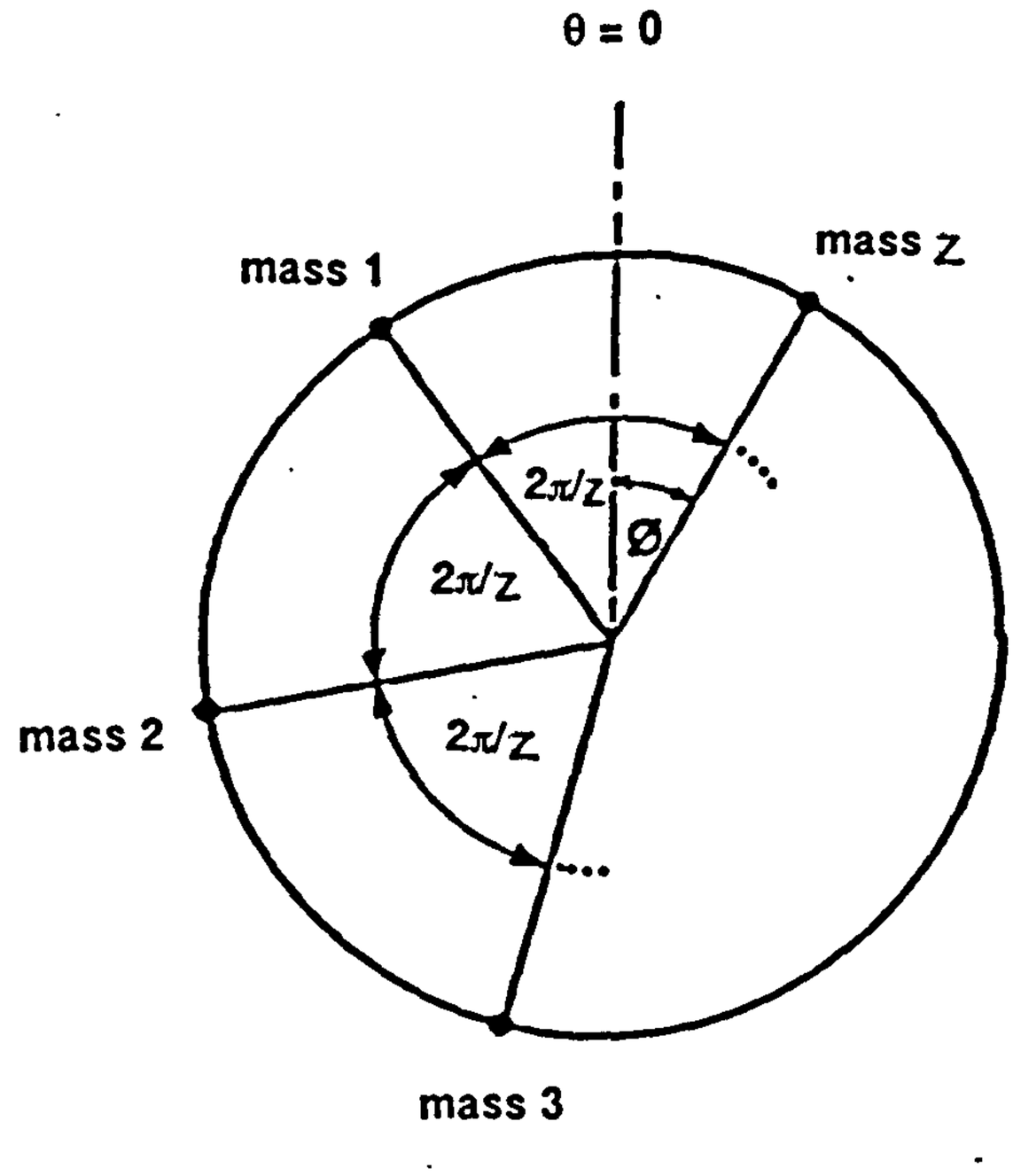

Figure 5.6 The arrangement of s equispaced masses, m, attached around the drum, for analysis of the effects of reduced rotational symmetry

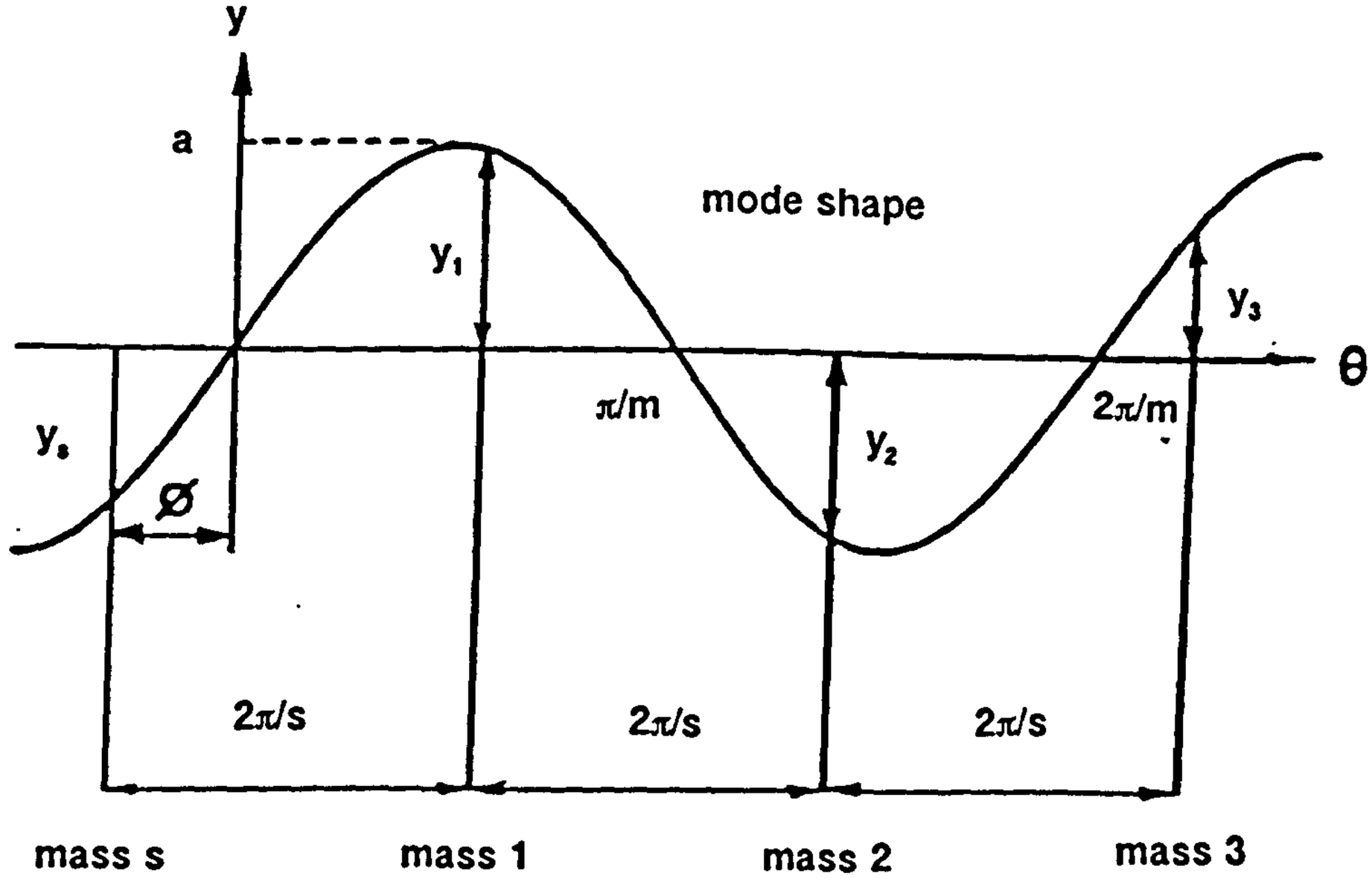

Figure 5.7 The amplitudes of the s masses in an m-diameter mode

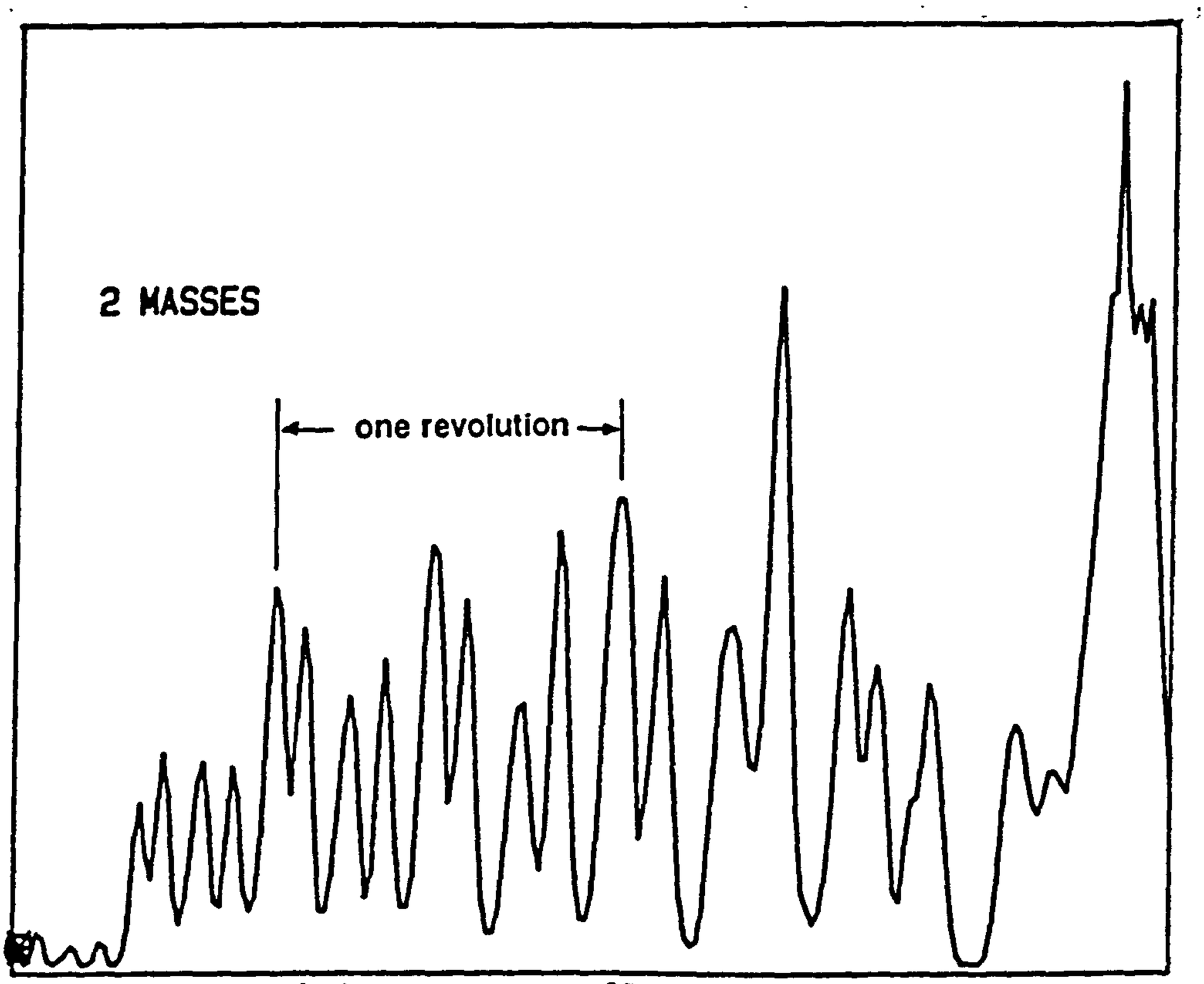

Figure 5.8 **A typical cyclic squeal vibration amplitude resulting from the cyclic decoupling effect of two masses attached to the drum periphery**

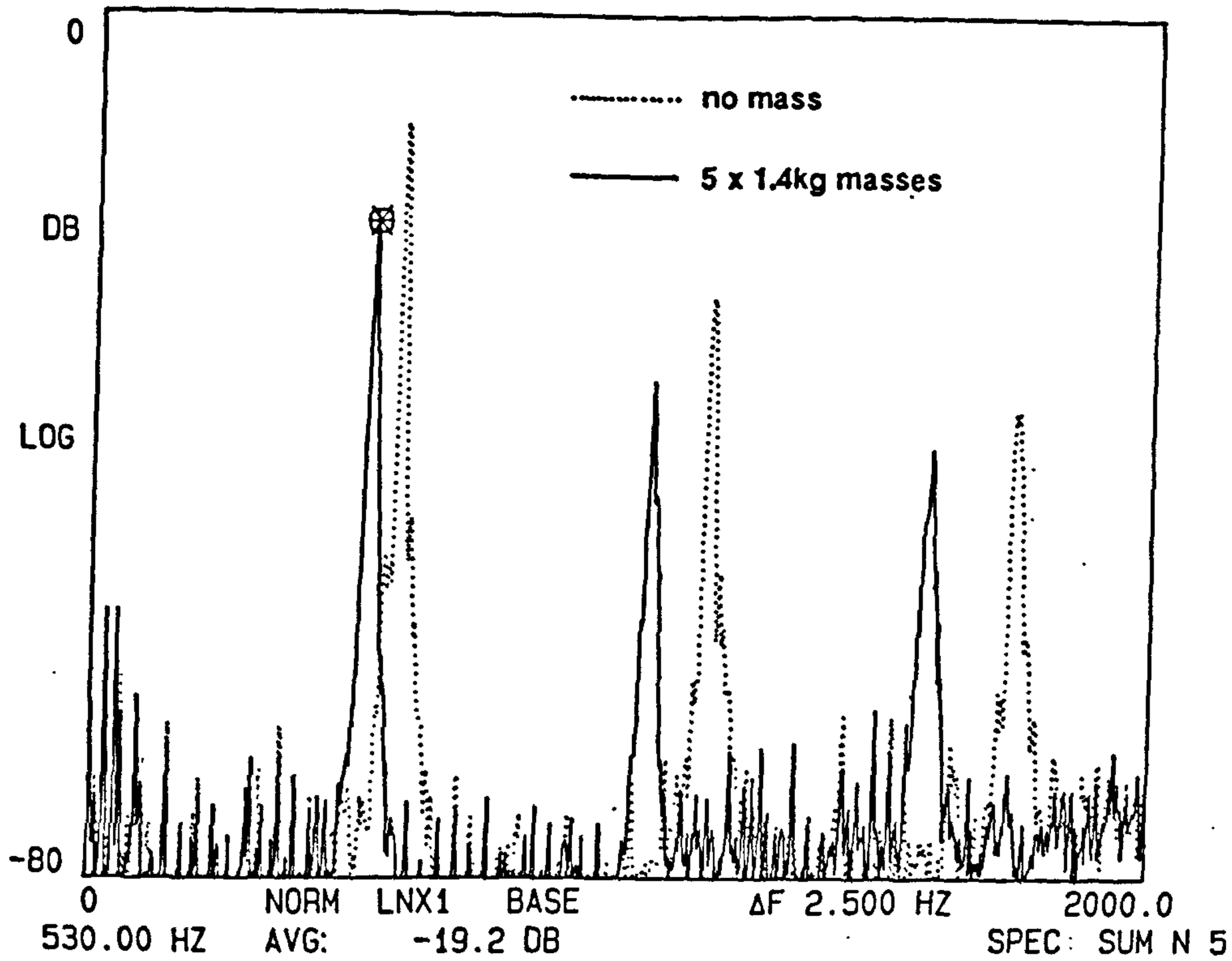

Figure 5.9 **Comparison of squeal spectra with and without 5 attached masses, showing frequency reduction due to mass addition**

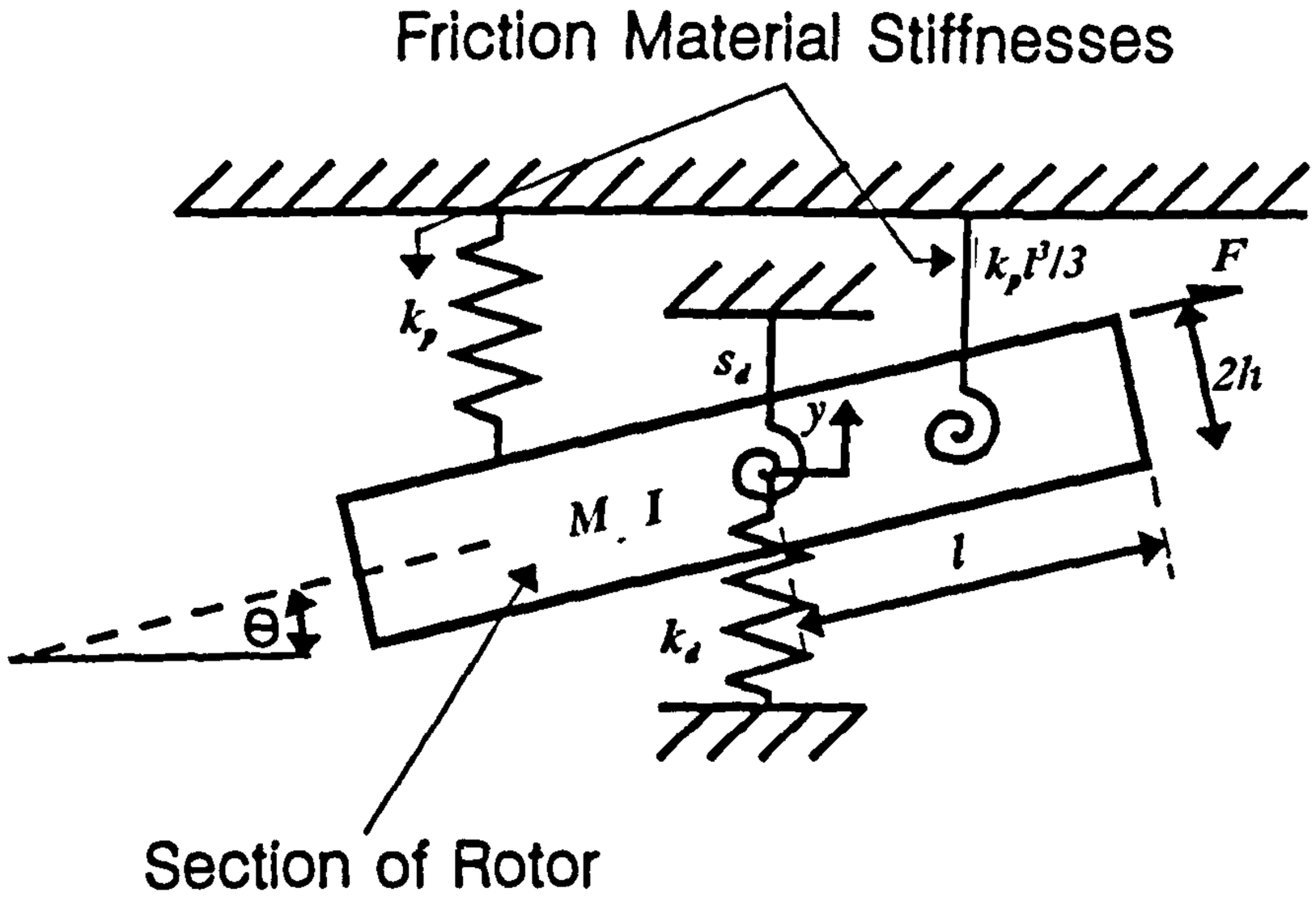

Figure 5.10 **Lumped parameter flutter model of a short section of the drum/lining interface**

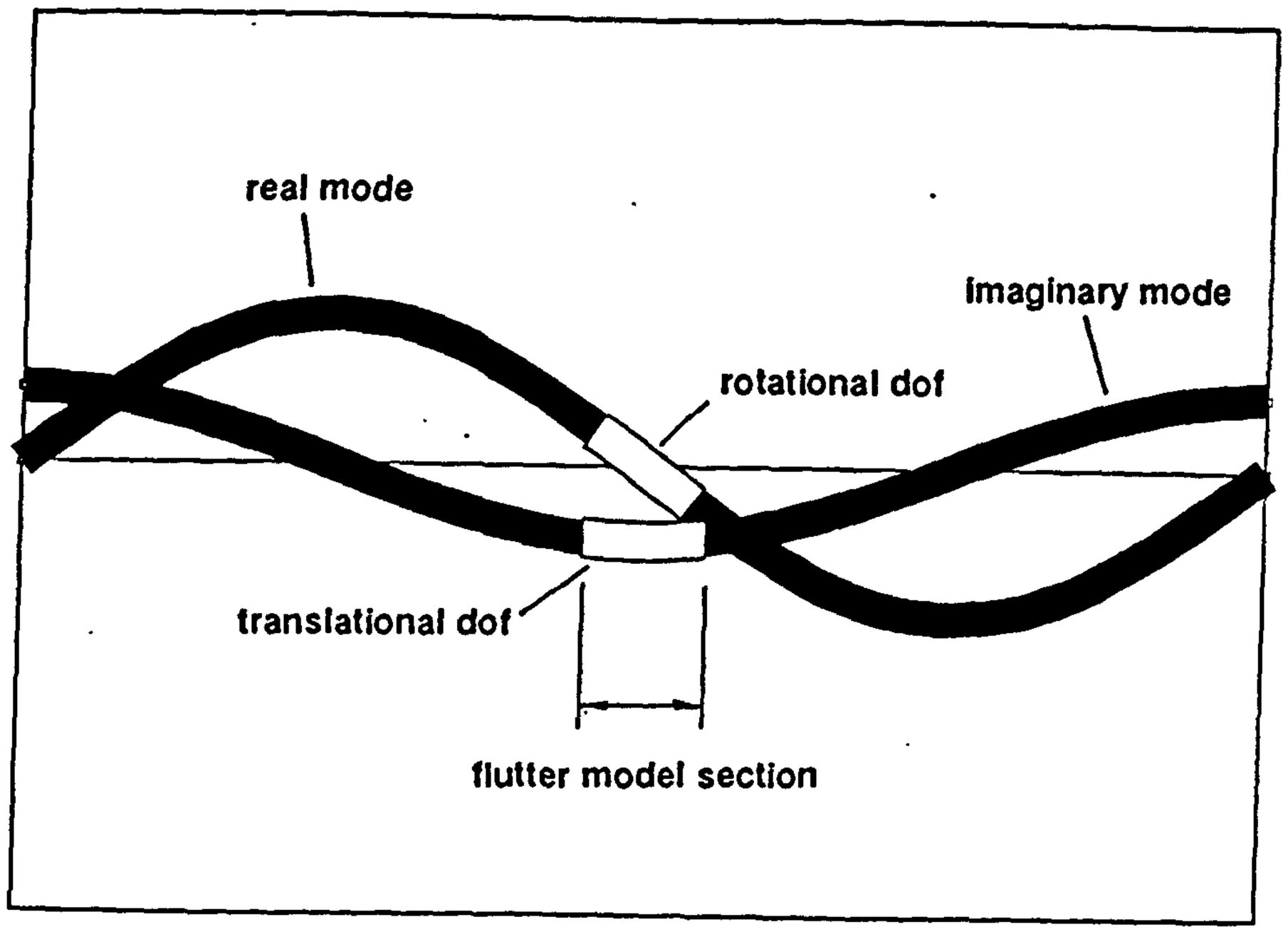

Figure 5.11 Showing how the translational and rotational degrees of freedom of the flutter model can be provided by identical, but differently positioned, flexural modes of the drum

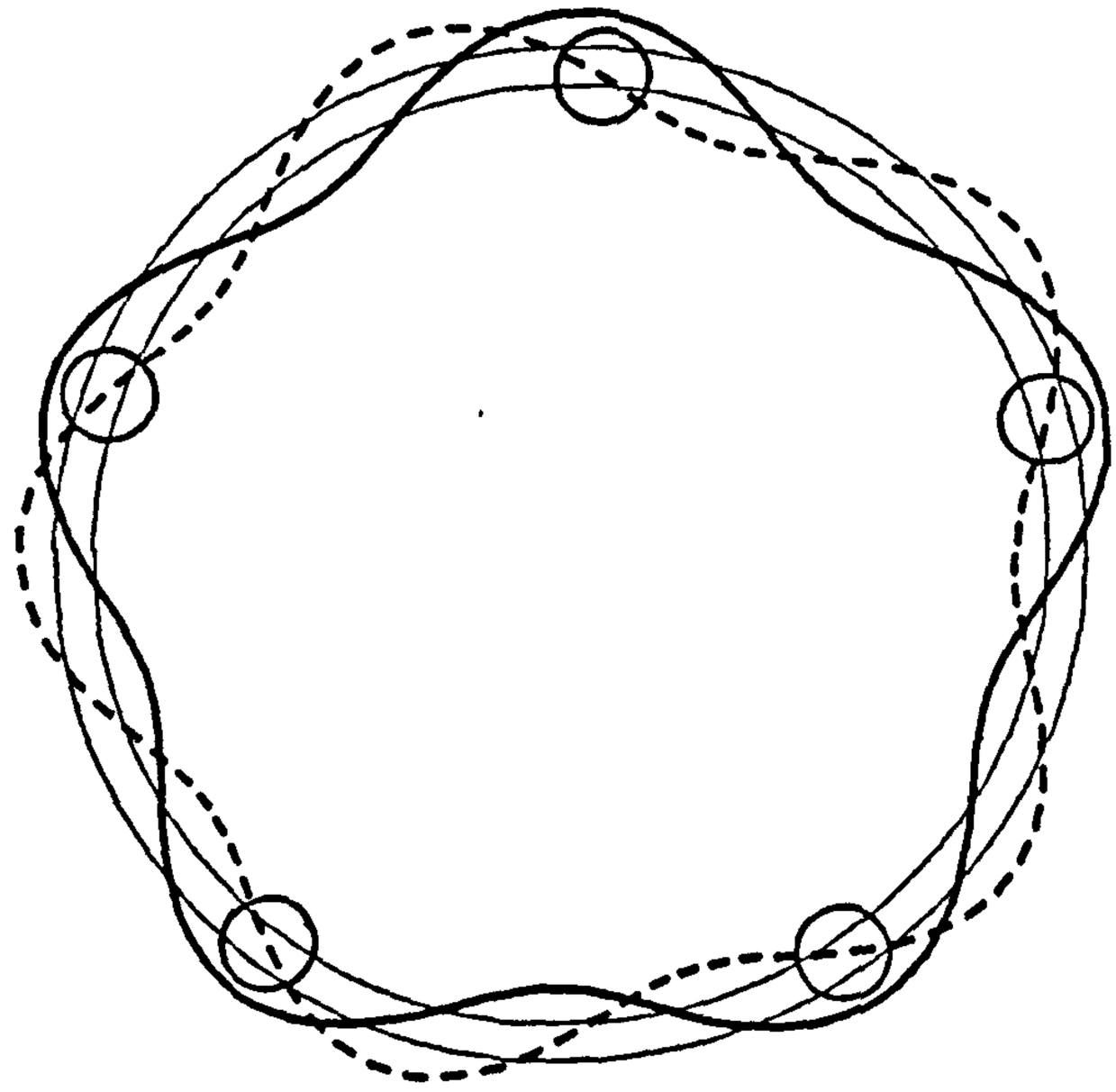

Figure 5.12 Showing how z equispaced masses, m/z, are equivalent to a single mass m, in a model where 2n/z = integer. In this case z = 5

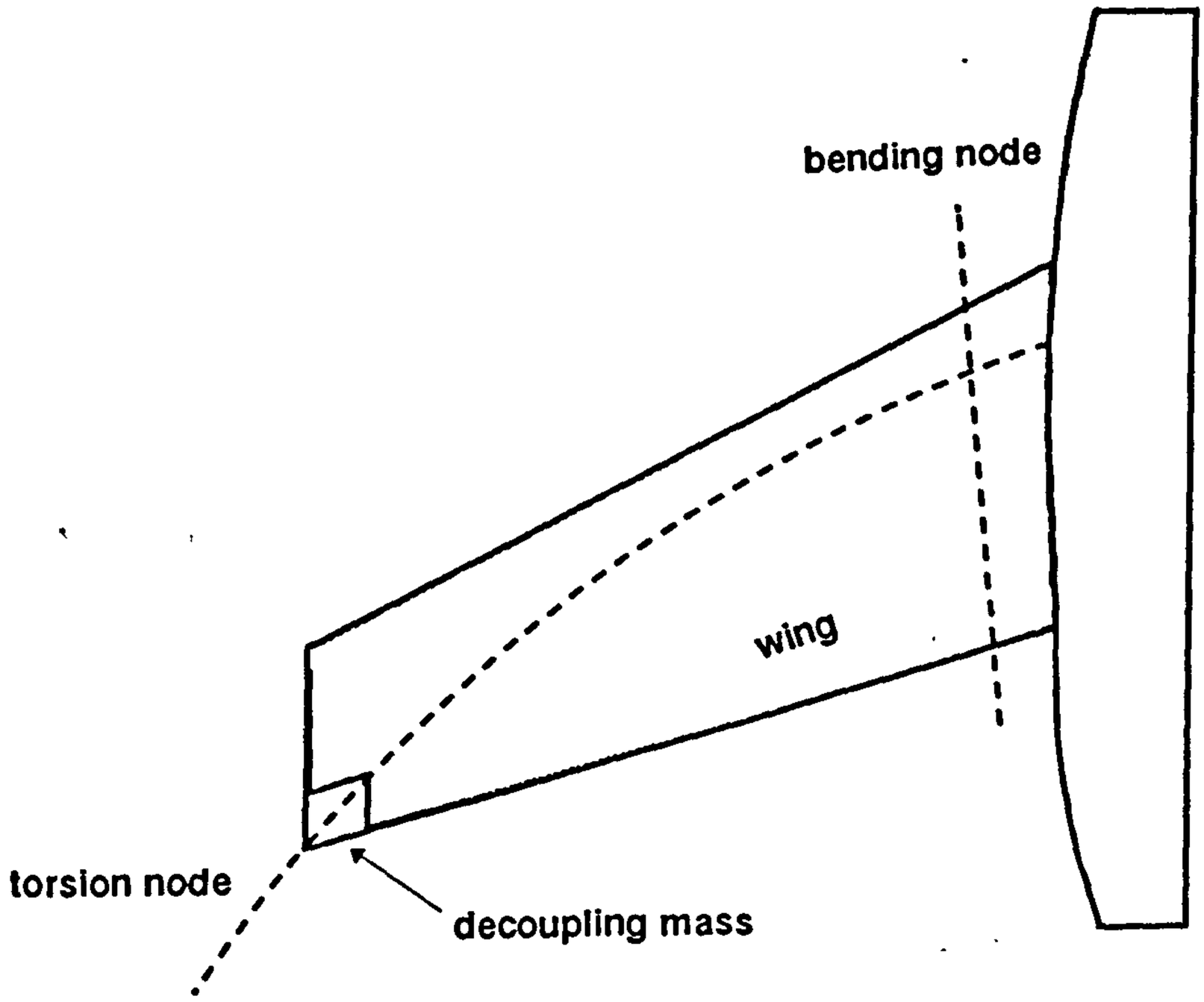

Figure 5.13 **The use of a 'mass balance weight' to decouple the bending and torsional flutter modes of an aircraft wing**

CHAPTER 6
REDUCING DRUM SYMMETRY - PRACTICAL CONSIDERATIONS

6.1 Introduction

In chapter 5 it was shown experimentally that the addition to the drum structure of suitably positioned discrete masses could reduce or eliminate the squeal, and that the likely mechanism of this effect is the decoupling of meridian modes which couple in the symmetric drum to produce squeal. This decoupling of meridian modes is a result of introducing a suitable reduced order of symmetry into the drum structure, and its implementation should not be limited to the addition of discrete masses. In practice, the attachment of substantial masses at discrete points around the drum periphery may not be practicable due to limitations of space inside the road wheel and to potential problems with the mechanical integrity of the attachments. In a commercial drum, some form of modification to the shape of the casting, such as a non-uniform drum wall thickness, would be preferable from production, space and structural integrity considerations. Simple changes in section of the drum wall would result in the distribution of the added masses over significant areas of the periphery of the drum, together with associated increases in stiffness over these areas. The effect of extended added mass will be considered first in isolation assuming that, by careful design, the variation in stiffness could be made minimal.

6.2 The Effect of Distributing Added Mass

It was observed in the modal analysis in section 5.2.2, illustrated in fig 5.5, that a single, arbitrarily positioned meridian mode could be split into two similar modes

having fixed, but different angular positions, and different natural frequencies, by a suitable arrangement of discrete added masses. The frequency difference between the two modes is due to their positioning on the drum such that the masses lie at antinodes of one mode, lowering its frequency, and nodes of the second, leaving its frequency unchanged. The observations of the effect of such added masses on the squeal propensity, in section 5.4, together with the mechanism discussed in section 5.5, suggest that it is desirable to maximise this frequency difference. Distributing the added mass away from the localised nodal and antinodal points will clearly influence the frequency difference, and this effect is examined below.

Consider the situation illustrated in fig 6.1, where an added mass, m, is distributed uniformly over a sector 2α of the drum periphery. The centre of this distributed mass is located at some angle β to the origin of a mode defined by the relationship

$$y = a \sin n\theta \sin \omega t \tag{6-1}$$

$$\text{ie} \quad y = y_a \sin n\theta \ , \ \text{where} \ \ y_a = a \sin \omega t \tag{6-2}$$

Consider also a small element of the mass, positioned at angle ϕ from the centre of the mass, having width $\Delta\phi$ and hence mass $m\Delta\phi/2\alpha$. The velocity of this element is

$$\dot{y}_\phi = \dot{y}_a \sin n(\beta - \phi) \tag{6-3}$$

and its kinetic energy is

$$\Delta T = \frac{m\Delta\phi}{4\alpha} \dot{y}_a^2 \sin^2 n(\beta - \phi) \tag{6-4}$$

The total kinetic energy of the mass, m, is thus

$$T = \frac{m}{4\alpha} \dot{y}_a^2 \int_{-\alpha}^{\alpha} \sin^2 n(\beta - \phi) d\phi \tag{6-5}$$

$$\rightarrow \quad T = \frac{m}{8n\alpha}\dot{y}_a^2\,(2n\alpha - \cos 2n\beta \sin 2n\alpha) \tag{6-6}$$

Now, if the generalised mass and stiffness of the unmodified drum mode are M and K, referred to an antinode, the total energy in the mode is

$$E = \frac{1}{2}M\dot{y}_a^2 + \frac{m}{8n\alpha}\dot{y}_a^2(2n\alpha - \cos 2n\beta \sin 2n\alpha) + \frac{1}{2}Ky_a^2 = \text{constant} \tag{6-7}$$

Differentiating E with respect to time and dividing by $\dot{y}_a$ gives the equation of motion

$$M\ddot{y}_a + \frac{m}{4n\alpha}\ddot{y}_a(2n\alpha - \cos 2n\beta \sin 2n\alpha) + Ky_a = 0 \tag{6-8}$$

and the natural frequency of the mode, ω_β , with the mass centred at position β, is given by

$$\omega_\beta^2 = \frac{K}{\left(M + \frac{m}{4n\alpha}(2n\alpha - \cos 2n\beta \sin 2n\alpha)\right)} \tag{6-9}$$

Now, if the mass is centred on a node, then $n\beta = k\pi$, where $k = 0,1,2...$,

$\Rightarrow \cos 2n\beta = 1$ and

$$\omega_1^2 = \frac{K}{\left(M + \frac{m}{4n\alpha}(2n\alpha - \sin 2n\alpha)\right)} \tag{6-10}$$

If, however the mass is centred on an antinode,

$n\beta = (2k + 1)\pi$, $k = 0,1,2,...$, $\Rightarrow \cos n\beta = -1$, and

$$\omega_2^2 = \frac{K}{\left(M + \frac{m}{4n\alpha}(2n\alpha + \sin 2n\alpha)\right)} \tag{6-11}$$

Subtracting the reciprocals of equations (6-10) and (6-11) gives

$$\frac{1}{\omega_2^2} - \frac{1}{\omega_1^2} = \frac{m}{2n\alpha K}\sin 2n\alpha \qquad (6\text{-}12)$$

If the effect of a point mass, m, is now considered, the natural frequency with m at a node will be unchanged at $\omega_3^2 = K/M$, whilst with m at an antinode, the frequency will be reduced to $\omega_4^2 = K/(M + m)$. Hence

$$\frac{1}{\omega_4^2} - \frac{1}{\omega_3^2} = \frac{m}{K} \qquad (6\text{-}13)$$

Taking $1/\omega_2^2 - 1/\omega_1^2$ and $1/\omega_4^2 - 1/\omega_3^2$ as measures of the frequency splits, S_d and S_p, produced by the distributed masses and point masses respectively (see note 1 below), equating equations (6-12) and (6-13) gives the equivalent point mass, m_{eq}, which would produce the same split as the distributed mass, m, that is

$$m_{eq} = \frac{m \sin 2n\alpha}{2n\alpha} \qquad (6\text{-}14)$$

The effect of the arc length of the distributed mass on the effectiveness of the mass in producing split frequencies (from equation (6-14)), is shown in fig 6.2. It is clear that the effectiveness of the mass addition reduces as the arc length increases, becoming zero when $2\alpha = 180°/n$ and hence that localised mass addition is desirable, especially as the mode order increases.

The physical reason for the reduced effectiveness of the distributed mass in separating the frequencies is clear from equations 6-10 and 6-11, the former indicating that, unlike a point mass at a node, which has no effect on that mode frequency, the distributed mass centred on a node must add to the modal mass and thus reduce the frequency of the higher mode. This, together with reduced depression of the frequency of the lower mode by the extended mass indicated by equation 6-11, is responsible for the reduced frequency difference.

Note 1 :- For a small frequency difference, $\omega_1 - \omega_2$,

$$\frac{1}{\omega_2^2} - \frac{1}{\omega_1^2} = \frac{(\omega_2 - \omega_1)(\omega_2 + \omega_1)}{\omega_1^2\omega_2^2} \approx 2\left(\frac{\omega_2 - \omega_1}{\omega_1^3}\right) \qquad (6\text{-}15)$$

6.3 The Effect of Non-uniform Drum Wall Thickness

As suggested in section 6.1, the symmetry of the drum could, in practice, be reduced by varying the thickness of the drum wall in a cyclic manner but this would produce a cyclic variation in the flexural stiffness of the drum wall in addition to adding the distributed mass discussed above. This cyclic variation in stiffness will modify the flexural mode frequencies of the drum and hence influence the frequency split and decoupling effect. Adding flexural stiffness to the same region of the drum as the mass addition would, intuitively, be expected to oppose the frequency depressing effect of the mass alone and hence, potentially reduce the decoupling effect.

To investigate this possibility, a simple 2-dimensional finite element model of the drum rubbing path was constructed using the ANSYS-386D educational FEM package, installed on a personal computer. The model idealises the rubbing path region of a 400mm cast iron drum as an unrestrained cylinder made up of 60, 8-noded elements each of 6° arc length and 20mm radial thickness, as illustrated in fig 6.3. The axial length of the rubbing path is not defined in this 2-dimensional model, and although this does not affect the natural frequencies, which are independent of the length of the cylinder, the rubbing path width was assumed to be 200mm, the width of the Scania drum, for the purpose of mass addition calculations (mass addition must be specified as mass/unit thickness in a truly 2-dimensional model). Initially, natural frequencies were calculated for the unmodified drum and with discrete point-like masses attached

to the mid plane of the drum section for comparison with the analytical approach taken in the previous chapter. Results for the first four flexural modes with 0, 2, 3, 4 and 5 equispaced 1kg masses are summarised in the table below, and a typical pair of split modes is shown in fig 6.4 which illustrates the angular relationship between the modes, with the nodes of one mode aligned with the antinodes of the second.

Table 4 Drum natural frequencies from the 2-D Finite Element Model

No.of Masses (z)	Natural Frequencies (Hz)				
		n=2	n=3	n=4	n=5
0	upper	222.6	625.9	1190.3	1906.6
	lower	222.6	625.9	1190.3	1906.6
	split	**0**	**0**	**0**	**0**
2	upper	220.4	622.7	1186.9	1903.5
	lower	213.8	599.1	1137.8	1824.4
	split	**6.6**	**23.6**	**48.9**	**79.1**
	2n/z	**2**	**3**	**4**	**5**
3	upper	214.3	621.3	1148.3	1844.7
	lower	214.3	585.2	1147.9	1844.1
	split	**0**	**36.1**	**0.4**	**0.6**
	2n/z	**4/3**	**2**	**8/3**	**10/3**
4	upper	218.1	595.5	1183.6	1821.7
	lower	205.9	595.5	1084.7	1821.5
	split	**12.2**	**0**	**98.8**	**0.2**
	2n/z	**1**	**3/2**	**2**	**5/2**
5	upper	209.2	590.5	1119.0	1898.9
	lower	209.2	590.5	1118.8	1689.1
	split	**0**	**0**	**0.2**	**209.8**
	2n/z	**4/5**	**6/5**	**8/5**	**2**

Several features of these results are worthy of note:-

i) the results are consistent with equation 5.1, the condition for producing pairs of flexural modes with different frequencies, ie $2n/z$ = integer, suggested by both experimental modal analysis and the theoretical analysis presented in chapter 5. The very small frequency splits predicted when this condition does not apply in the above table are likely to be the result of small inherent asymmetries in the model.

ii) even with no masses added, the model produces two modes of the same order, with identical frequencies, but angularly positioned such that the nodes of one mode coincided with the antinodes of the other.

iii) when split frequencies are produced, the magnitude of the split for any mode order is approximately proportional to the total mass addition.

iv) in the examples where equation 5-1 is satisfied, ie where a frequency split occurs, the associated mode shapes always show that the higher frequency mode is positioned with nodes at the angular positions of the masses, and as such no reduction in frequency of this mode would be expected. The above results do, however, show a small frequency reduction in the upper frequency which appears, from detailed examination of the associated mode shapes, to be due to a combination of circumferential motion at the 'nodes' (predominant in the n=2 mode) and rotation of the drum wall section at the 'nodes' about a centre radially displaced from the added mass position (predominant in the n=5 mode)

Regions of increased wall thickness were now modelled by adding elements of radial width 10mm to the outside of the drum, as illustrated in fig 6.5. The thickness was increased in two diametrically opposite arcs of equal length varying from 0 to 15 elements each (or 0° to 90° in 6° increments), and the effect on the frequencies of the pairs of n=2 to n=5 modes was investigated (the n=6 modes were calculated but were found to couple with an 'expansion' mode of the drum and so were not valid for this purpose).

The resulting natural frequencies are plotted in fig 6.6(a) - 6.6(d), as functions of the arc length of the thickened regions. It is immediately clear that the effect is fundamentally different from that of pure mass addition, which depresses the lower frequency of the pair, leaving the upper frequency sensibly constant. In fig 6.6, the opposite effect is found at low values of stiffening arc length, the lower frequency remaining sensibly constant whilst the upper frequency of the pair increases with arc length. These results imply that, of the mass and stiffness additions incorporated by the increased drum wall thickness, the effect of stiffness is dominant.

Fig 6.7 shows the difference between these upper and lower natural frequencies (the frequency 'split') as a percentage of the natural frequency of the unmodified drum. The frequency differences are shown as a function of the arc length of the increased thickness region, for each of the n=2 to n=5 modes, and in each case the split reaches a maximum at an arc length of ≈45% of the mode wavelength, and then decreases to zero at typically 70% - 75% of the mode wavelength.

As the arc length of the stiffened region of drum is increased, the mass added to the drum is also increased proportionally, and fig 6.8 compares the actual frequency split with that which would have been achieved if all this added mass had been localised

at diametrically opposite discrete points. Comparing this result with fig 6.2 (which can also be interpreted as comparing the extended mass frequency split with that produced by the same localised mass), some important differences are seen. Fig 6.2 had suggested that the addition of mass in practice, by casting thicker sections on the drum, would be most effective if such sections were restricted to a very short angular length, and initial trials were made on this basis. Fig 6.8 indicates, however, that such short thickened sections of, say, 5°-15°(or 17mm-52mm for the Scania drum) would be relatively ineffective for low order modes, and that 25°-50° arc lengths (87mm-175mm) would most effectively use the extra mass, depending on the mode involved. In the case of the n=2 and n=3 modes the effectiveness of the mass added by drum wall thickening is seen to be potentially greater than that from the same localised mass addition.

The choice of the optimum number of discrete masses demands a foreknowledge of the drum mode order involved in the squeal problem, except in the case of two diametrically opposite masses, which are predicted by equation 5-1 to be effective in all modes. The motivation for adding more than two masses would therefore be to reduce the individual sizes of the relatively large masses for practical installation. This limitation would be, to a large extent, overcome by distributing the mass over a significant arc length of increased drum wall thickness, making a more generally applicable reduced symmetry fix a possibility. Although fig 6.8 shows that, for maximum effectiveness, even two diametrically opposed thickened regions require arc lengths matched to the mode order, it is clear that an arc length of, say, 30° (or 105mm) will have a significant splitting effect on all of the first 4 modes considered here.

6.4 Practical Experience With Reduced Symmetry Drums

The technique developed here for reducing drum symmetry, in an attempt to reduce or eliminate brake squeal, has been evaluated in various forms on different types and sizes of drum brakes, and this experience is summarised below.

6.4.1 Heavy vehicle pivoted shoe 'S' cam brake

This brake, a 420mm diameter x 165mm wide brake manufactured by Steyr Daimler Puch, although of a similar type and size to the Scania brake used for the majority of the work described here, squealed at a much higher frequency. As noted in section 3.3.8, the brake could be made to squeal most effectively by removing the trailing shoe brake lining and thus using the leading shoe only, when exceptionally loud and continuous 2.5kHz squeal was obtained. Drum modal analysis during squeal showed a complex n=5,s=0 mode (illustrated in fig 3.21), corresponding to a mounted drum natural frequency of 2280Hz. Attaching 5 equispaced 900g masses near the drum mouth produced a frequency 'split' of 370Hz, or 16% of ω_n, and almost completely eliminated the squeal, which was only present as a short 'peep' at the very end of a stop.

It is interesting to note that this drum had 10 shallow axial grooves cast into its periphery, as shown in fig 6.9, which themselves introduced a small split in the n=5,s=0 mode, although of insufficient magnitude to influence the squeal. Lang and Newcomb (50) show more detail of this effect.

6.4.2 Heavy vehicle sliding shoe 'Z' cam brake

This again is a brake of similar size, 400mm x 200mm, to the Scania brake, manufactured by Lucas Heavy Duty Braking Systems to operate with a Volvo drum, but with some significant design differences :-

i) the shoes are not pivoted on anchor pins, but slide against fixed abutment faces. This difference influences the shoe self servo effect and hence both torque output and lining wear pattern.

ii) the shoes are actuated indirectly by the rotating cam, through sliding tappets, and this influences the direction of the shoe tip forces.

iii) the shoes are fabricated from steel plate rather than by casting.

Despite these differences, the brake squeals at a similar frequency to the Scania brake, 580Hz, but in addition an 1100Hz squeal is often apparent. Modal analysis showed that these squeals involve the n=2,s=0 and n=3,s=0 modes of the drum respectively and hence the $2n/z$ = integer condition limits the number of equispaced added masses to 2, if both modes are to be influenced. Based on this analysis, Volvo produced the experimental cast drums shown in fig 6.10, with 2 masses, each slotted to reduce additional stiffness. These produced splits of only 2% and 4% in the frequencies of the n=2 and n=3 modes, and although trials on a vehicle showed some small improvement, it was clear that in this case larger masses would be needed to completely eliminate the noise. Larger frequency splits were expected from this configuration, and it is thought that the inherent asymmetry of the drum casting

through eccentricity or variable wall thickness, may have partially offset the effect of the additional masses.

6.4.3 Light truck hydraulic drum brake

This is a medium sized, 308mm diameter x 89mm wide, hydraulically operated sliding abutment drum brake used on the Ford (US) 350 light truck, which squeals at a range of discrete frequencies between 7kHz and 10kHz. Drum modal analysis (of which fig 3.23 is typical, showed the involvement of n=9,s=0, n=10,s=0, and n=11,s=0 drum modes, again limiting the number of added masses to two if all squeal nodes are to be decoupled.

Experiments with 2 x 400g masses on a dynamometer mounted brake, shown in fig 6.11, produced a typical split of 8% of the unmodified natural frequency, and almost eliminated the squeal. In this case, due to severe space restrictions within the wheel, a 3-dimensional dynamic finite element model of the drum, produced by Dr D.R. Schafer of Mintex Don Limited (40), and illustrated in fig 6.12, was used to aid in the design of a modified drum, which significantly reduced the service noise problem.

6.4.4 Passenger car hydraulic drum brake

This is a typical small passenger car rear drum brake, 180mm diameter x 30mm wide, manufactured by Bendix, for use with a drum designed and manufactured by Ford Motor Company. A modal analysis of the drum, squealing at 3.3kHz on a dynamometer, and using the arrangement shown in fig 6.13, produced the n=3,s=0 complex mode illustrated in fig 6.14. Six equispaced 60g masses, attached using

adhesive as in fig 6.15, produced an 18% frequency separation and eliminated the squeal, again with the exception of a light 'peep' at the very end of some brake applications.

6.5 Summary

If reduced drum rotational symmetry is to be used in a commercial environment to reduce brake squeal then a means of incorporation into the drum structure without fitting additional components must be found. The analysis carried out here shows that the 'ideal' configuration would be the addition of two compact masses attached at discrete points 180° apart, but this would be difficult to achieve in practice. Employing the localised stiffening effect of a change in drum wall thickness can, however, be as effective for a limited range of modes, but could potentially produce other detrimental effects on braking refinement due to cyclic non-uniform deformation under braking loads and non-uniform thermal stresses.

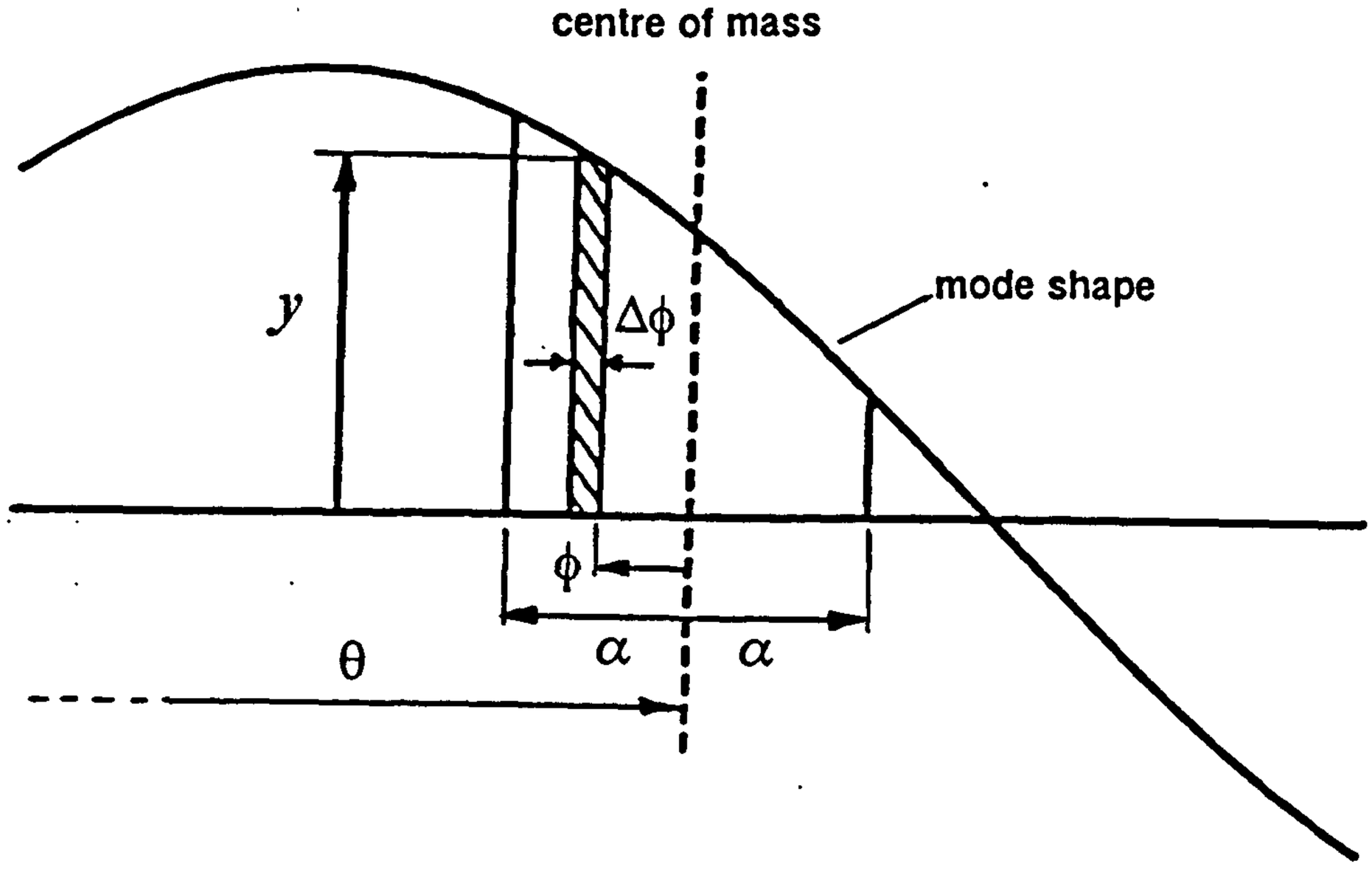

Figure 6.1 Position of extended mass, of length 2α, relative to a drum normal mode.

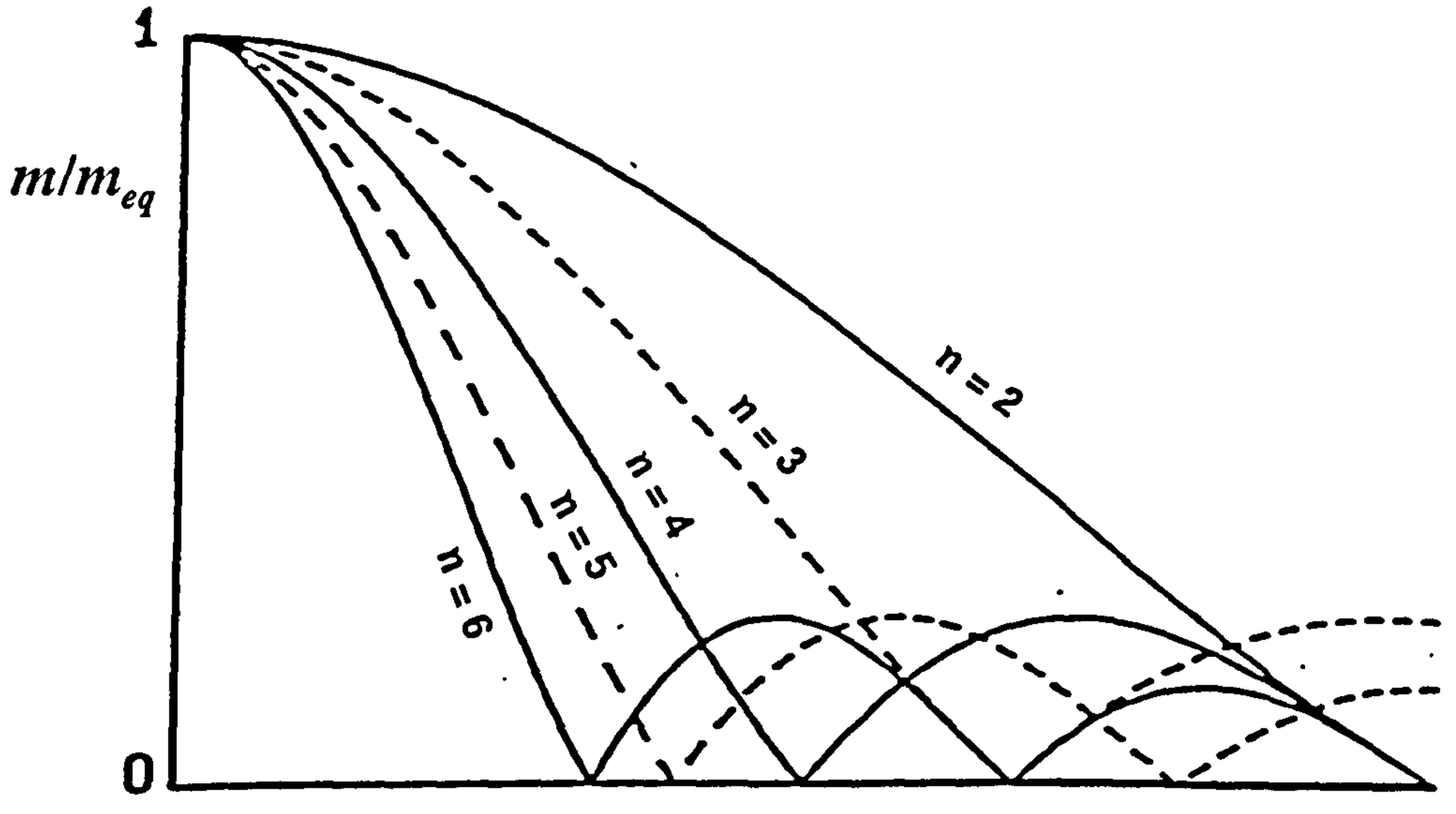

Figure 6.2 The discrete mass equivalent, m, of an extended mass, m_{eq}, distributed over an arc length 2α.

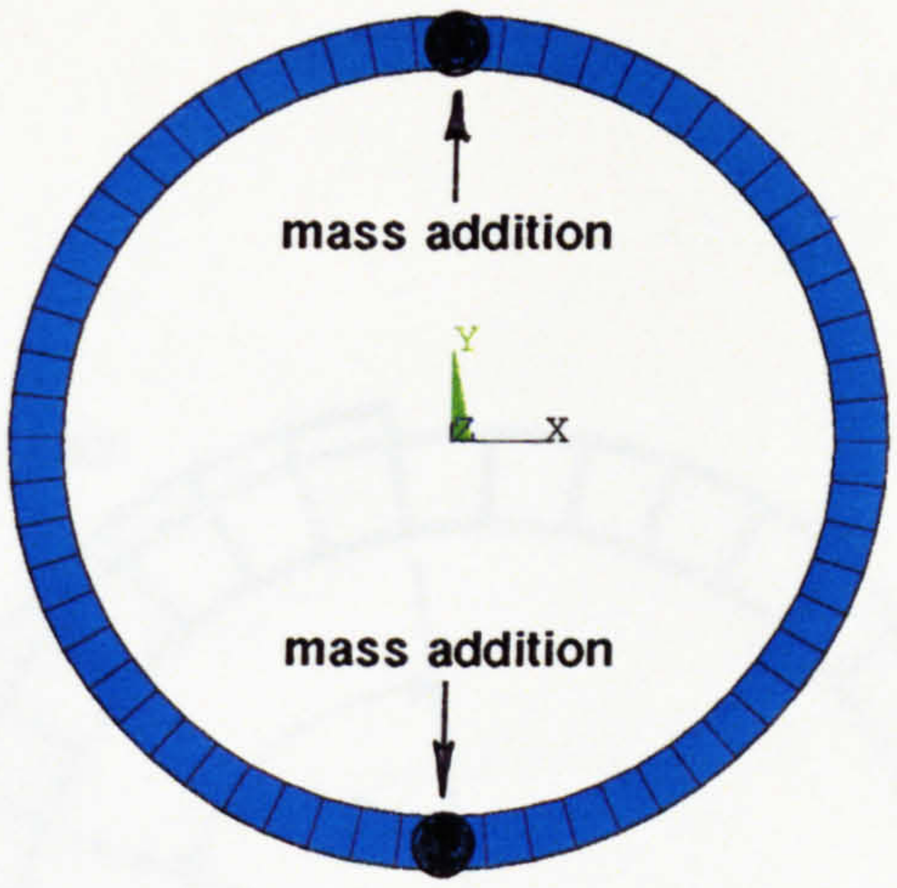

Figure 6.3 2-dimensional drum model used to investigate the effect of reduced rotational symmetry

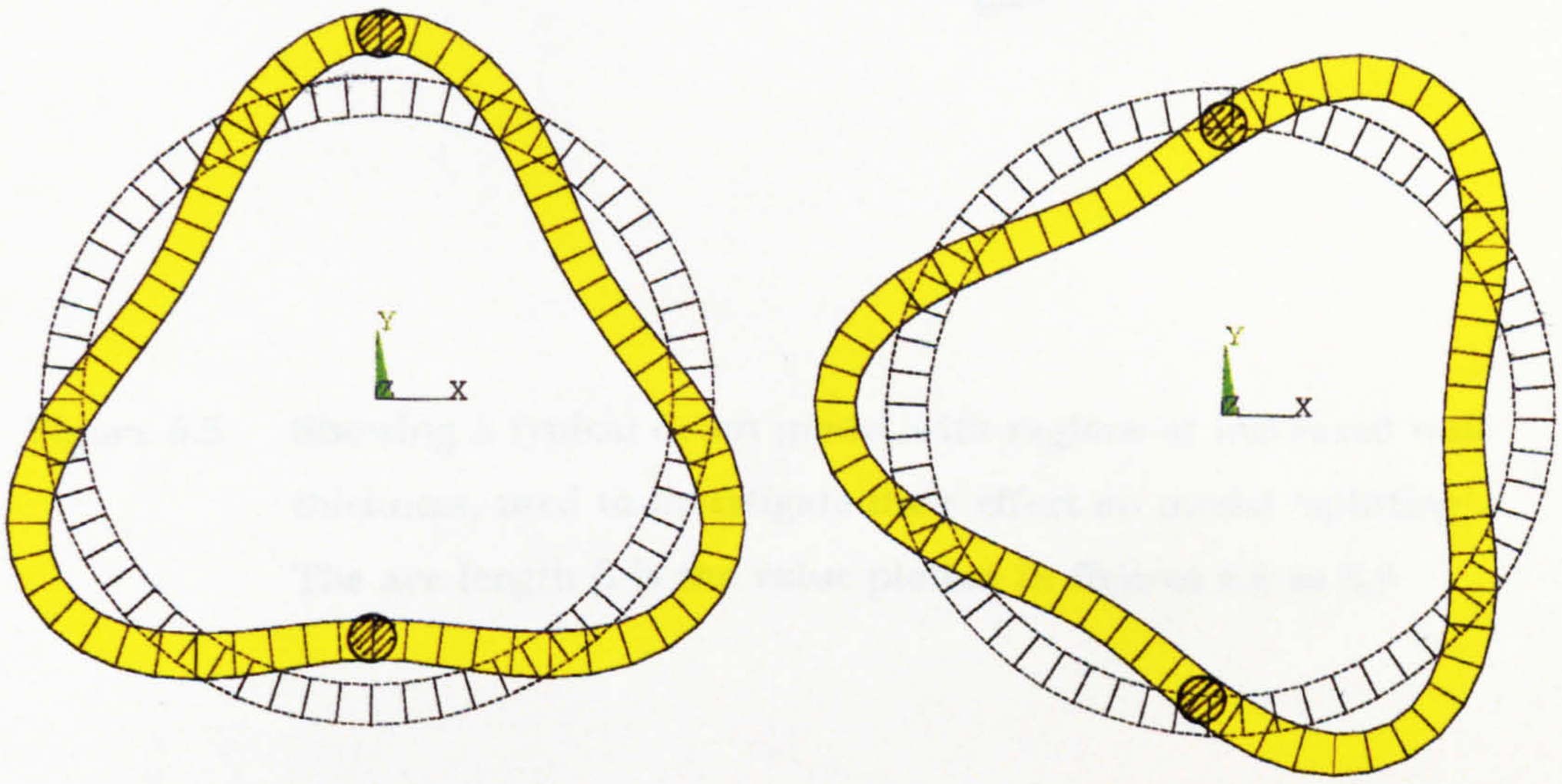

Figure 6.4 Typical pair of modes of the same order, but different frequencies, showing their fixed positions relative to added masses.

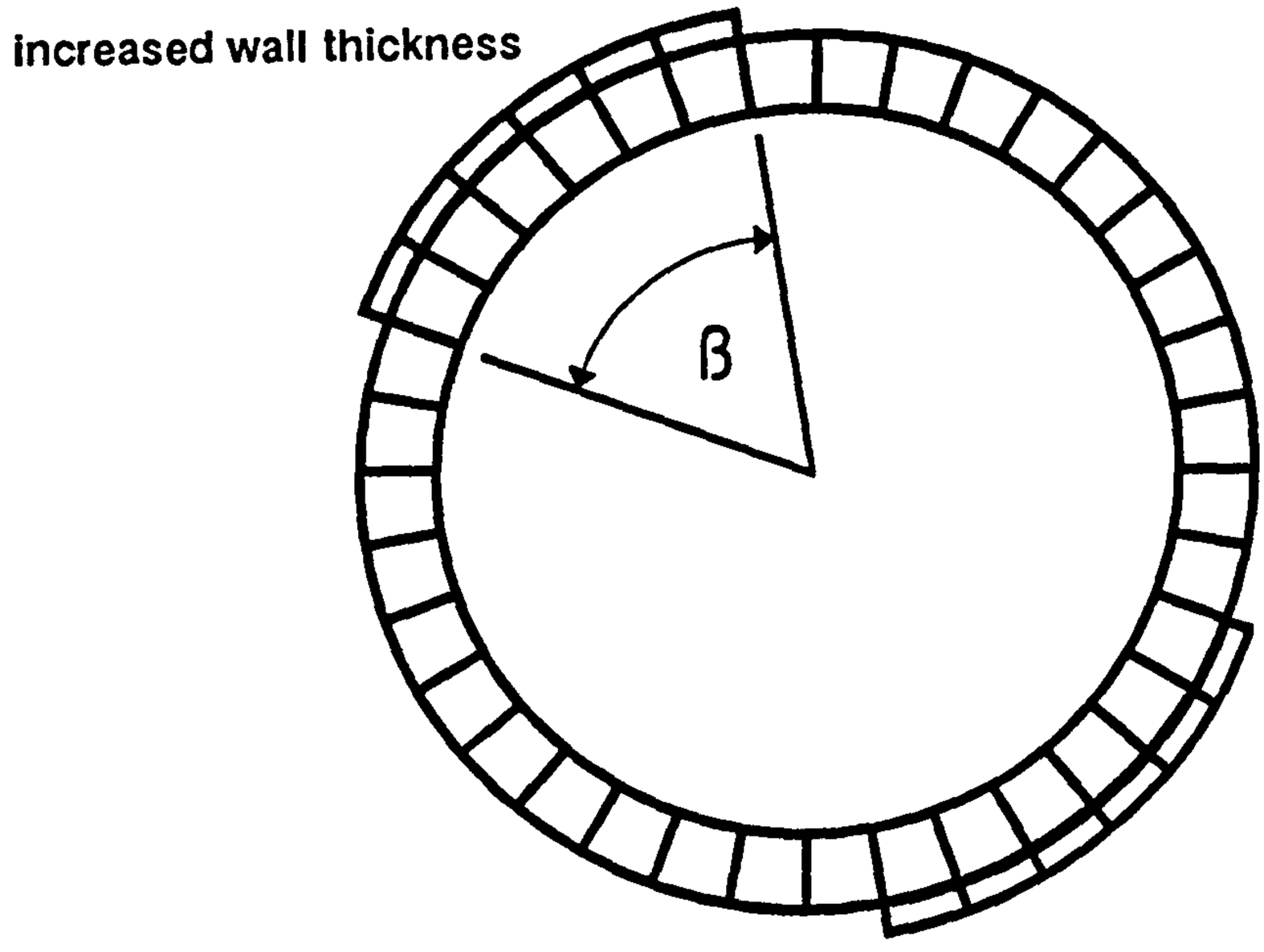

Figure 6.5 Showing a typical drum model with regions of increased wall thickness, used to investigate their effect on modal 'splitting'. The arc length β is the value plotted in figures 6.6 to 6.8

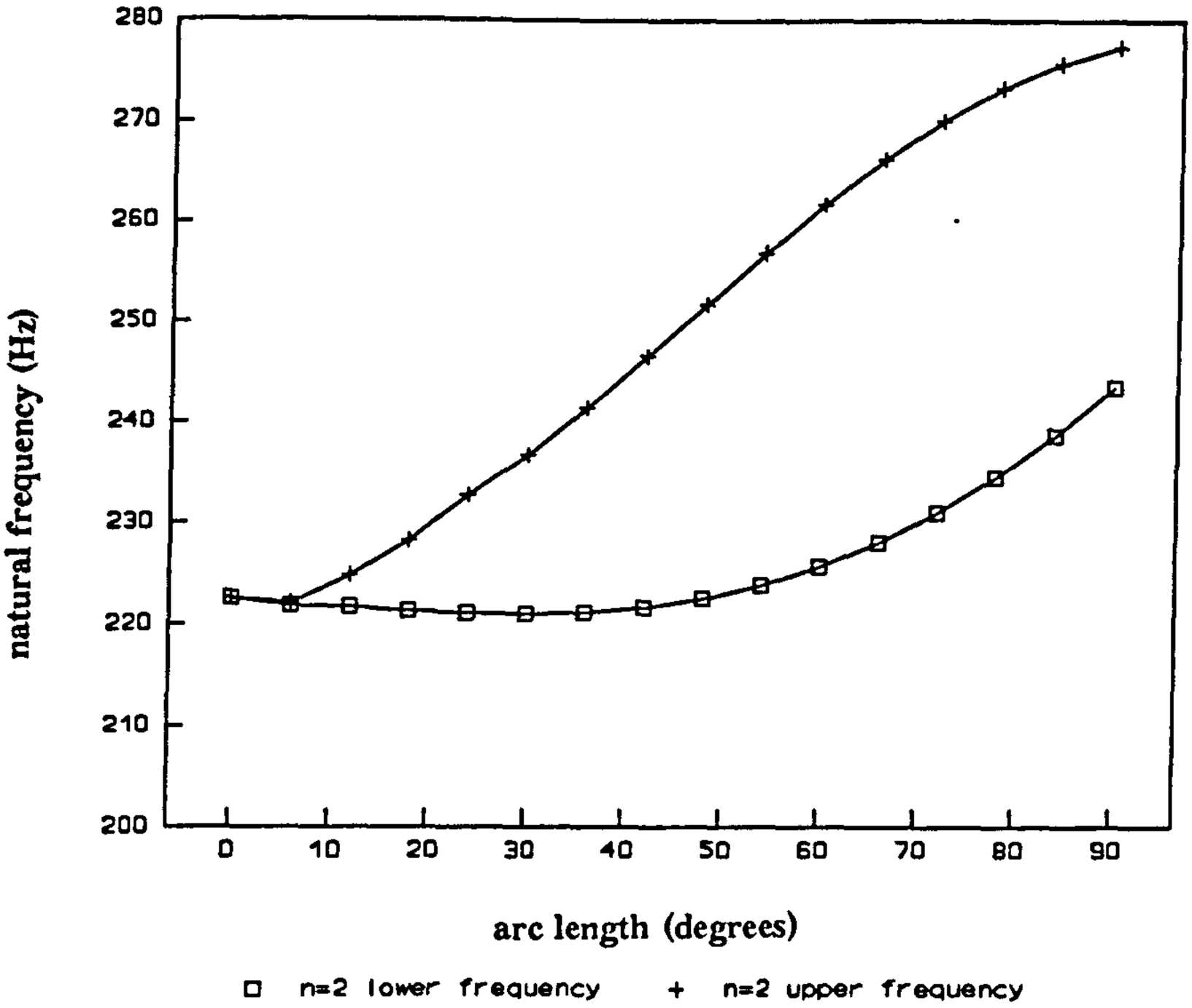

Figure 6.6(a) The influence of the arc length of the region of increased drum wall thickness on the n=2 mode

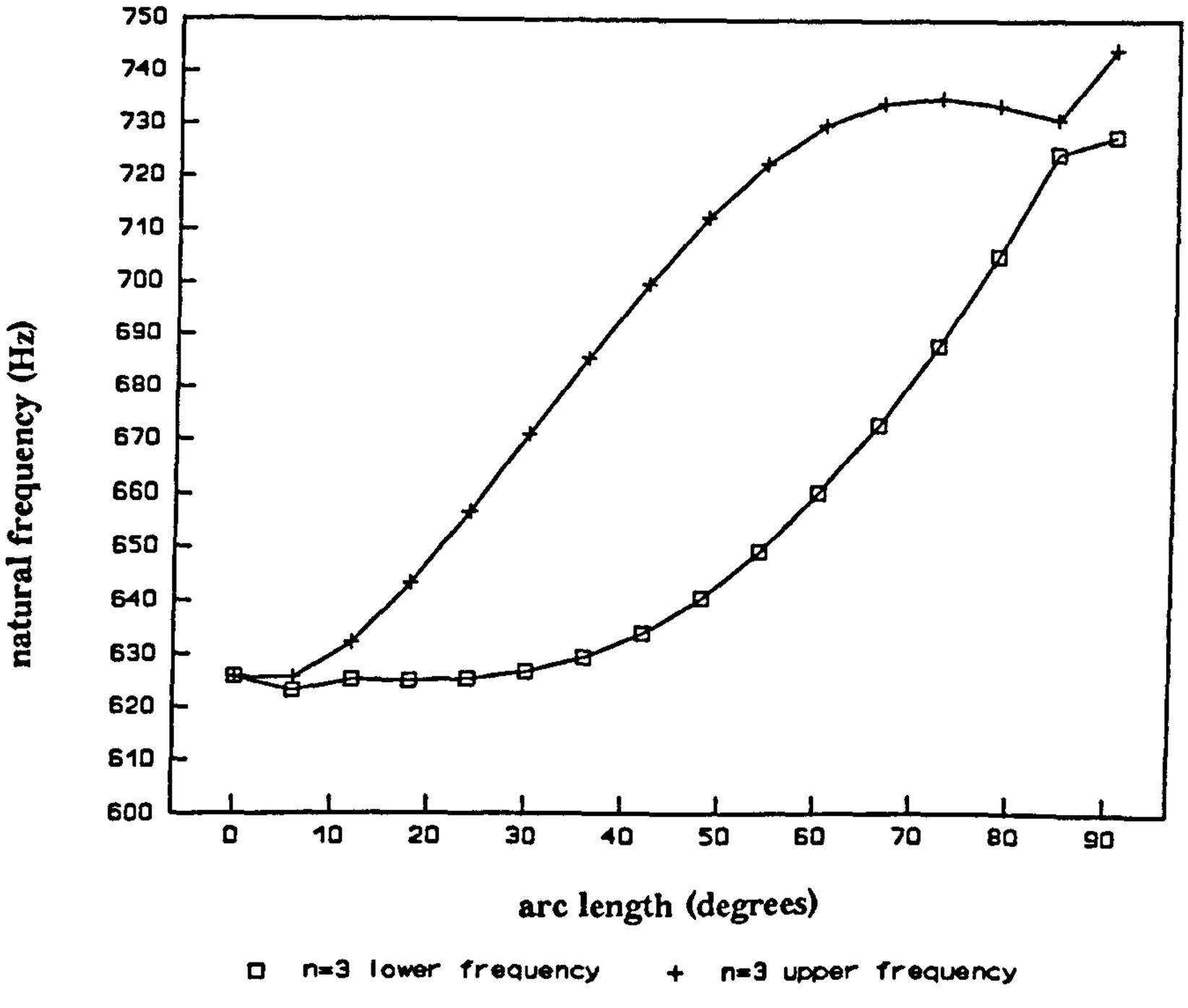

Figure 6.6(b) The influence of the arc length of the region of increased drum wall thickness on the n=3 mode

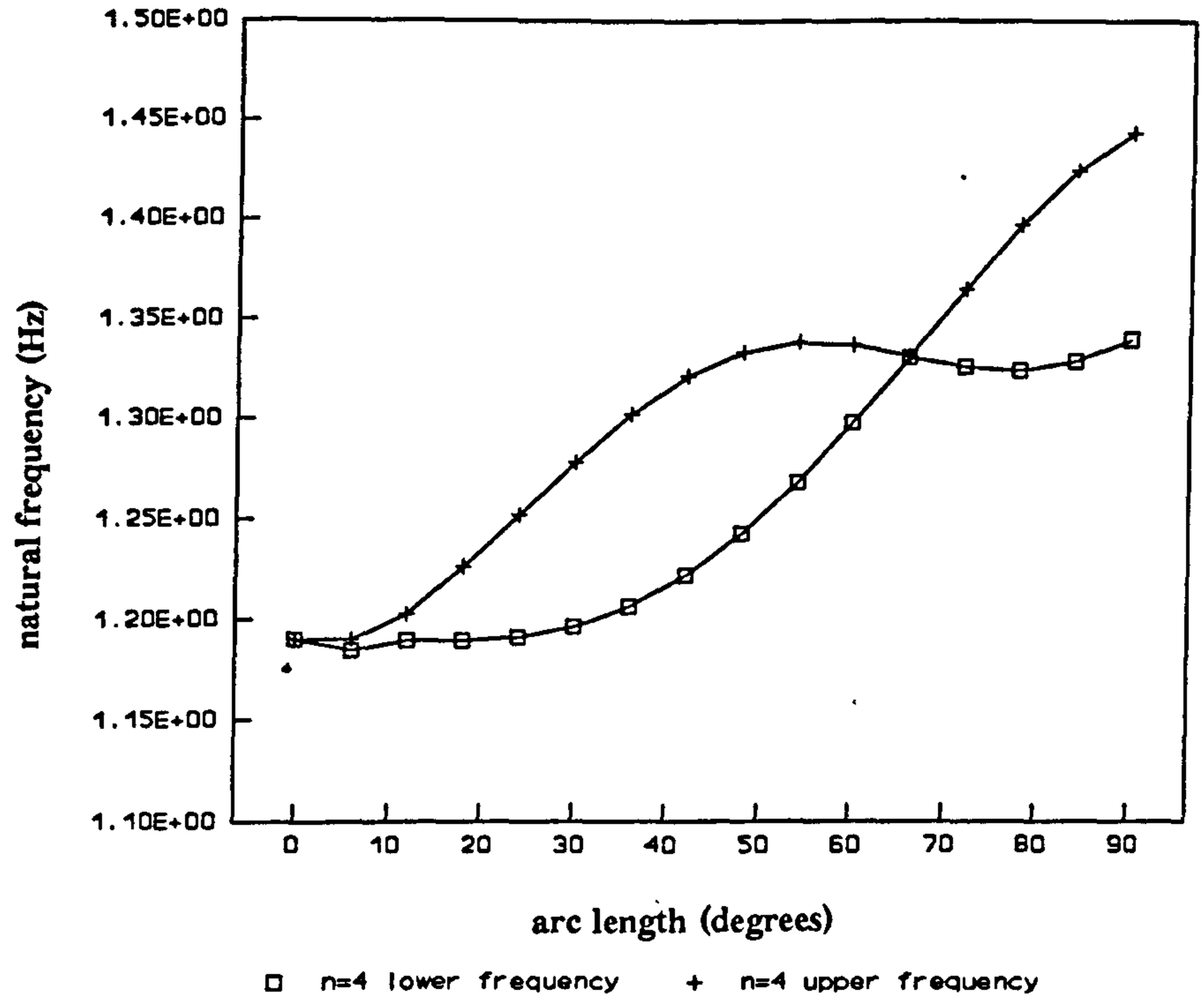

Figure 6.6(c) The influence of the arc length of the region of increased drum wall thickness on the n=4 mode.

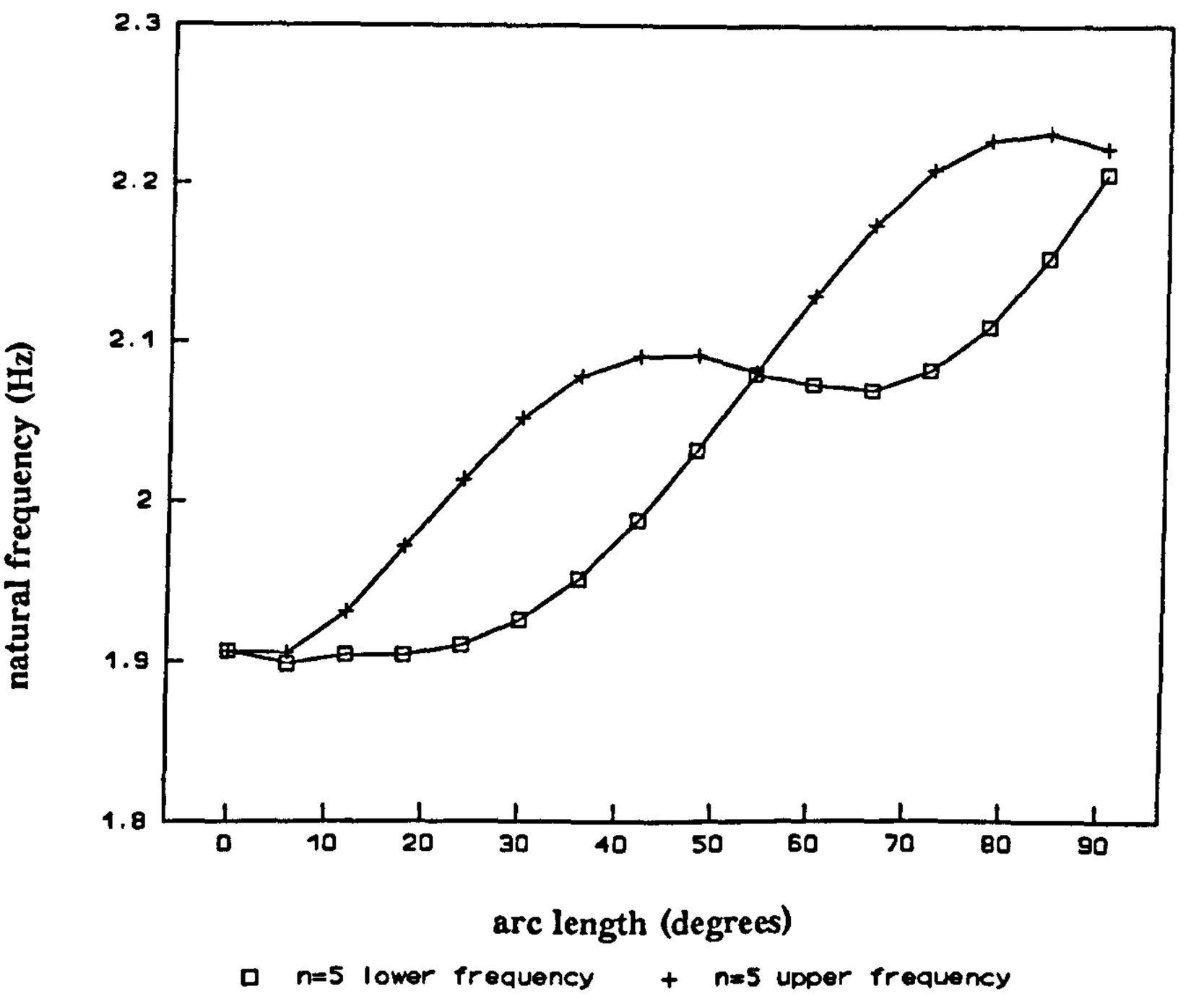

Figure 6.6(d) The influence of the arc length of the region of increased drum wall thickness on the n=5 mode

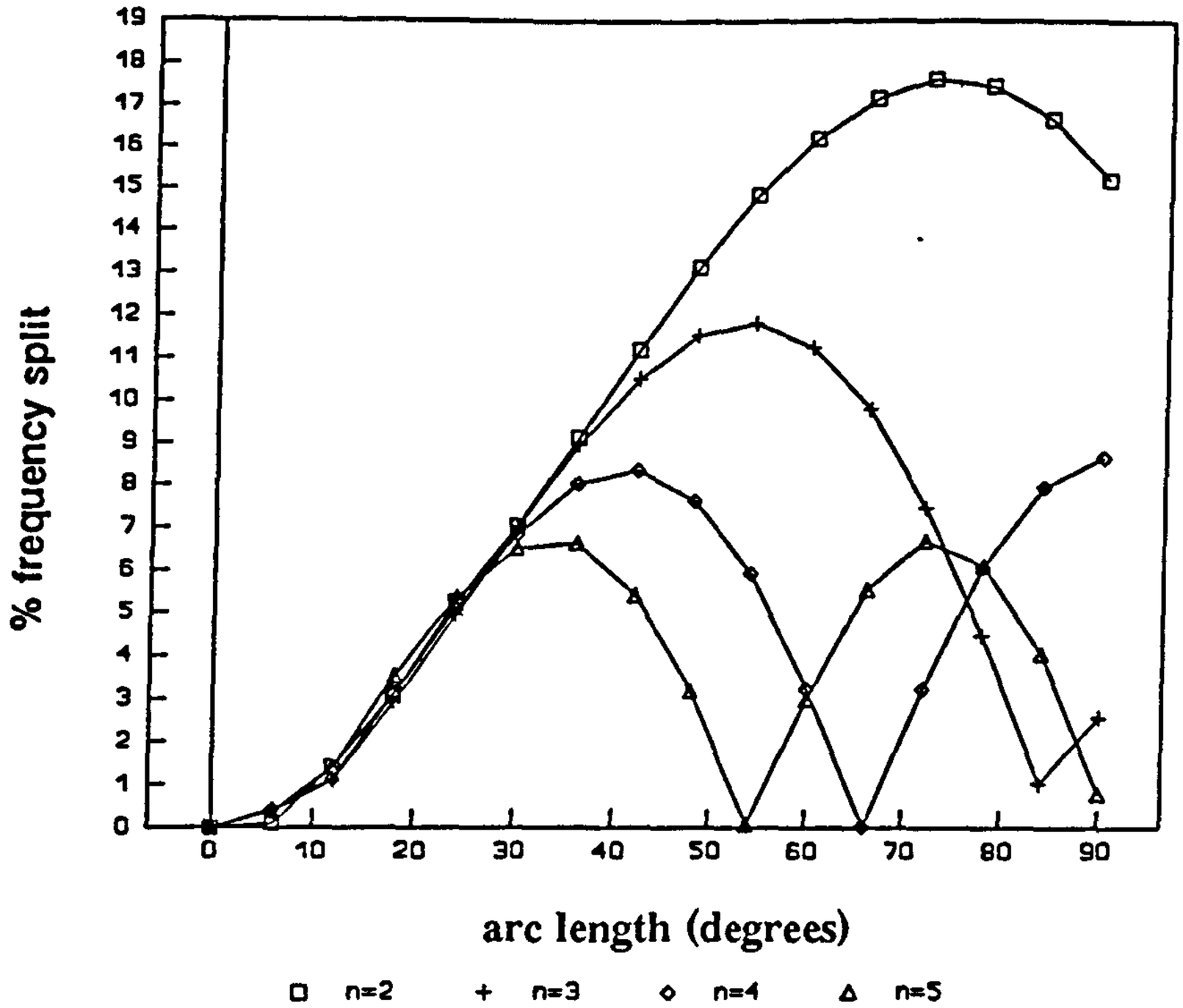

Figure 6.7 The frequency 'split' as a percentage of the natural frequency of the unmodified drum modes

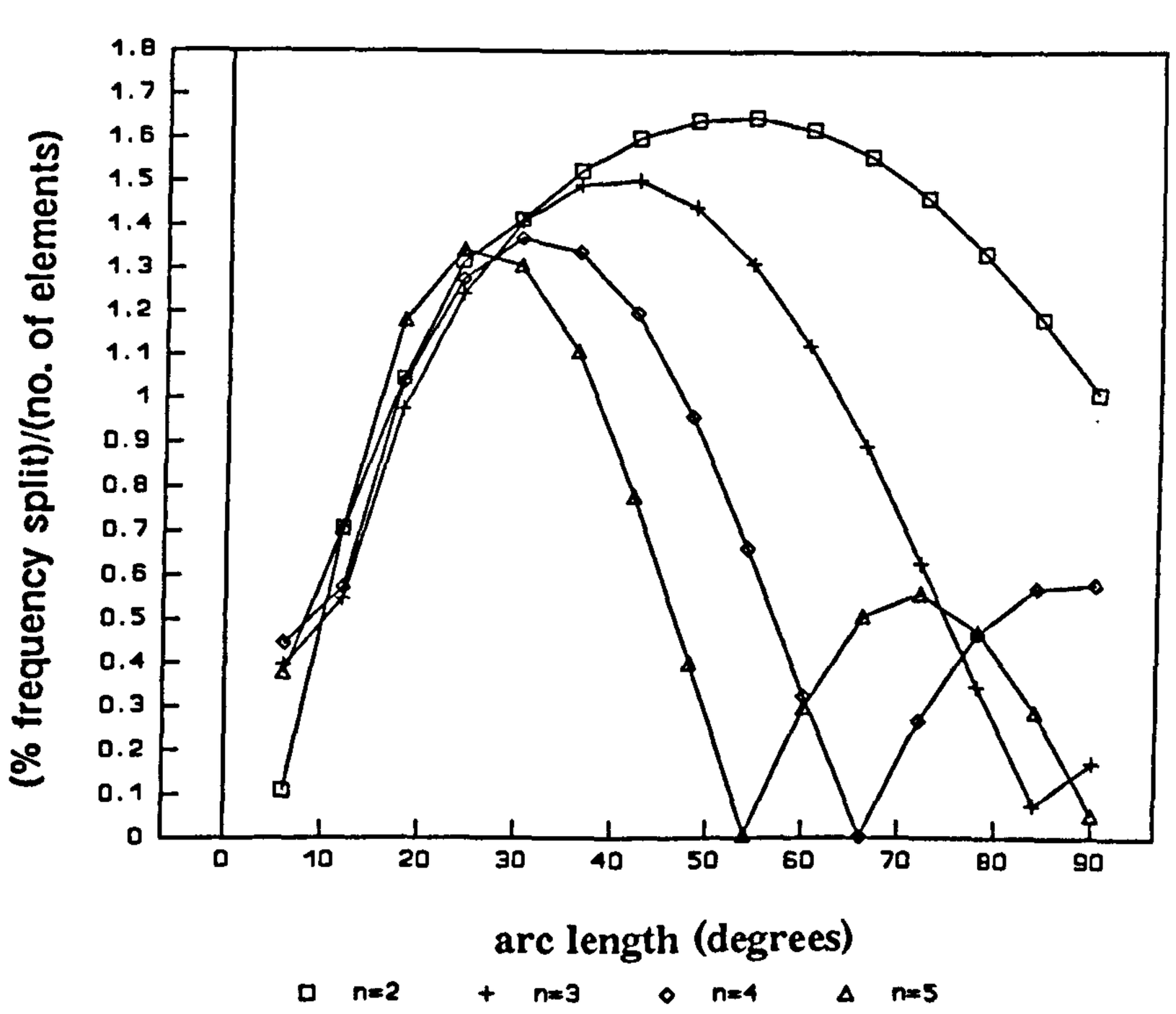

Figure 6.8 The percentage frequency'split' per element of additional wall thickness, indicating the effectiveness of the added mass in reducing symmetry

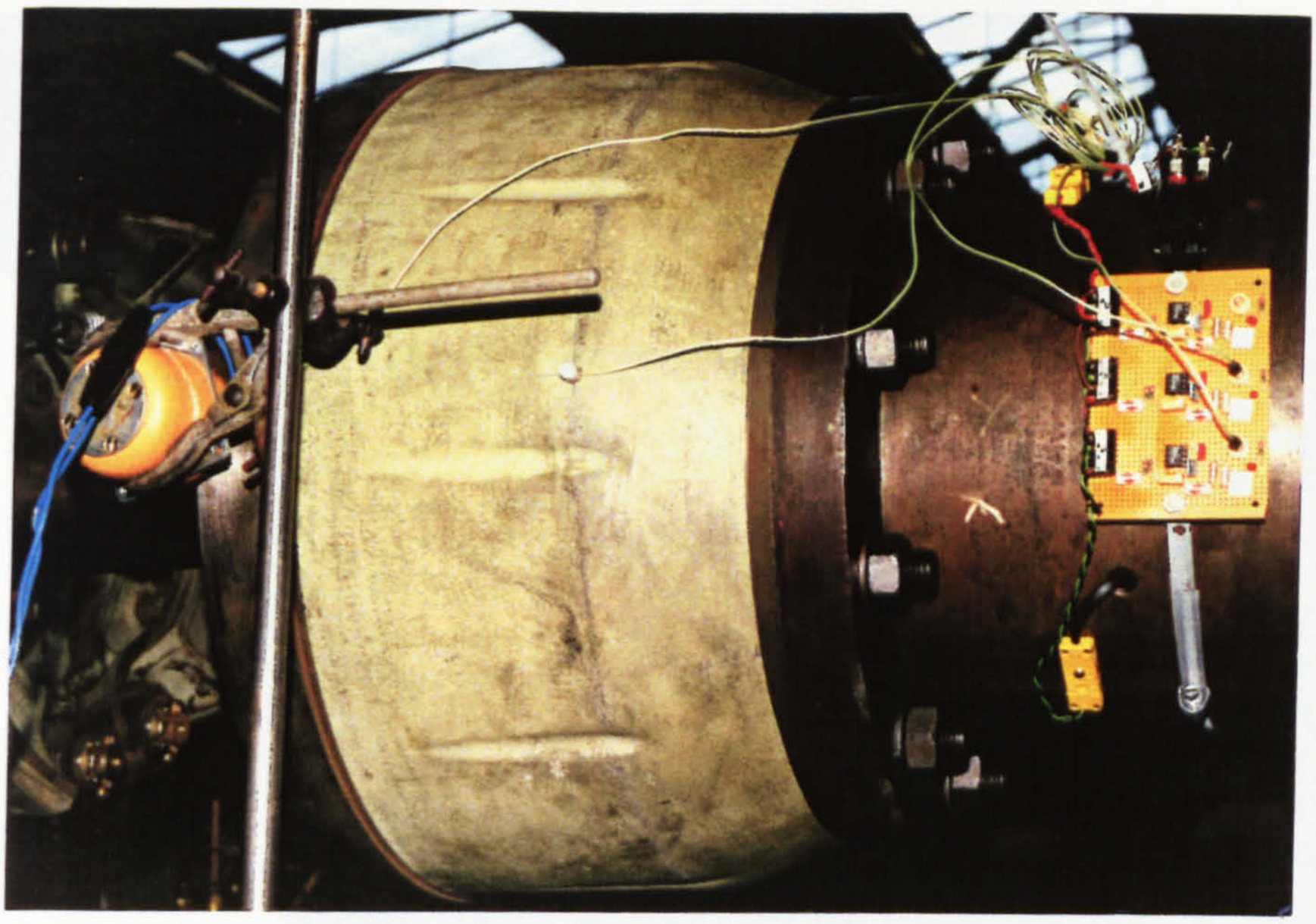

Figure 6.9 **The Steyr 'S'-cam brake, showing the 10 axial grooves which introduce a small frequency 'split' in the n=5,s=0 squeal mode.**

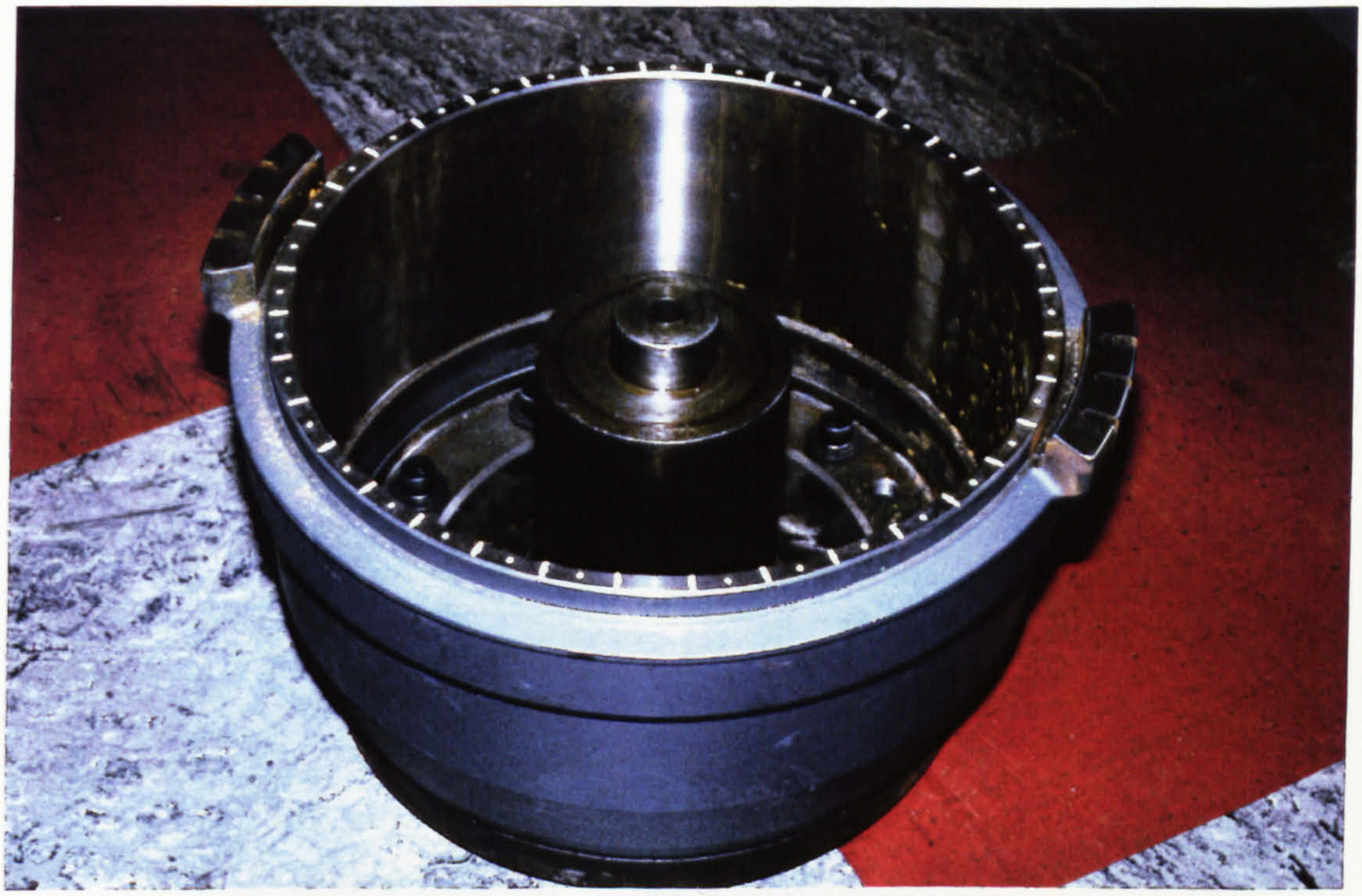

Figure 6.10 **A heavy vehicle 400mm x 200mm drum with added mass cast into the drum mouth. the masses are slotted to reduce the additional stiffness**

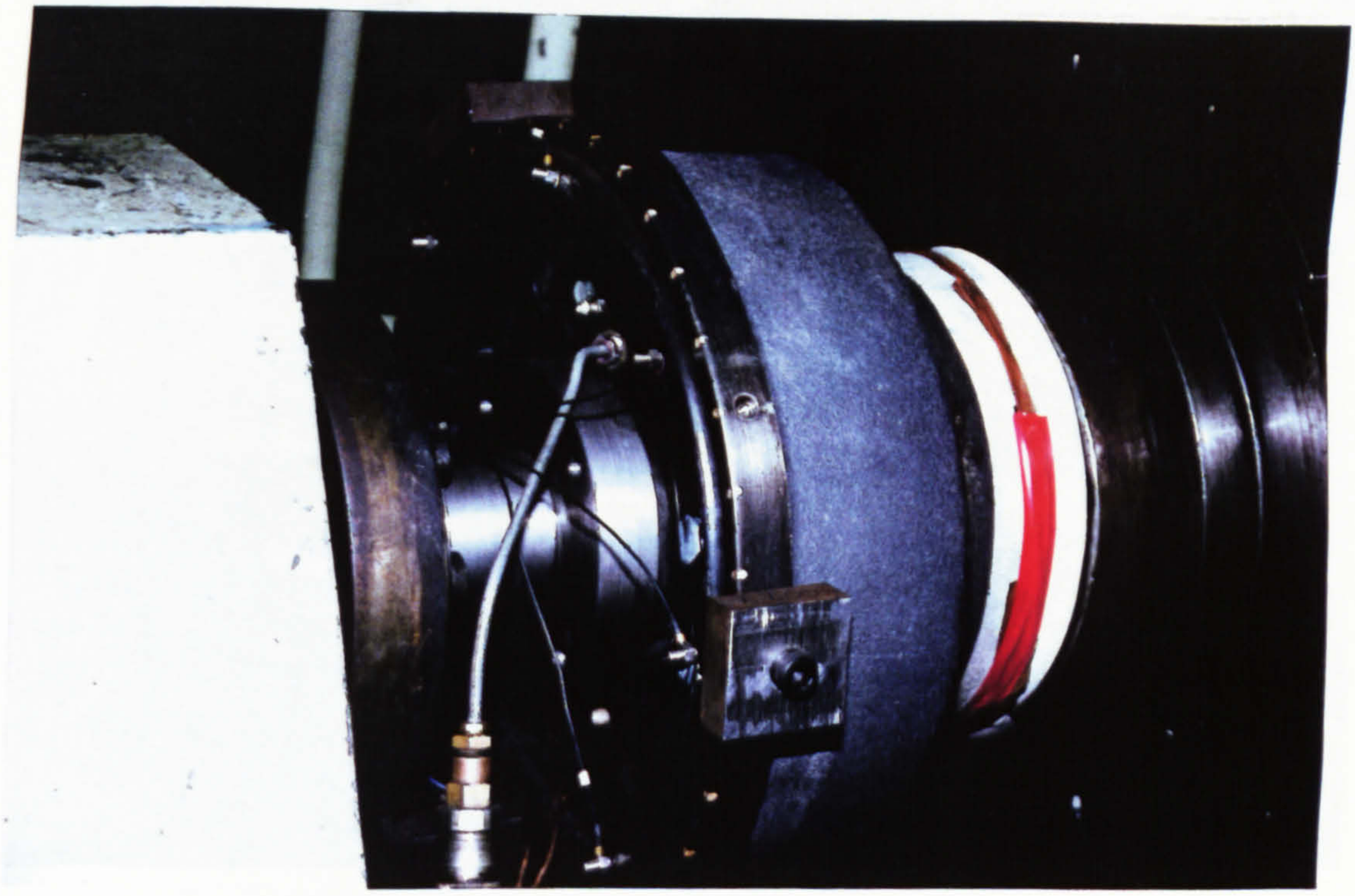

Figure 6.11 The Ford 308mm x 89mm light truck brake with masses attached to the drum periphery for evaluation of symmetry reduction on high frequency squeal

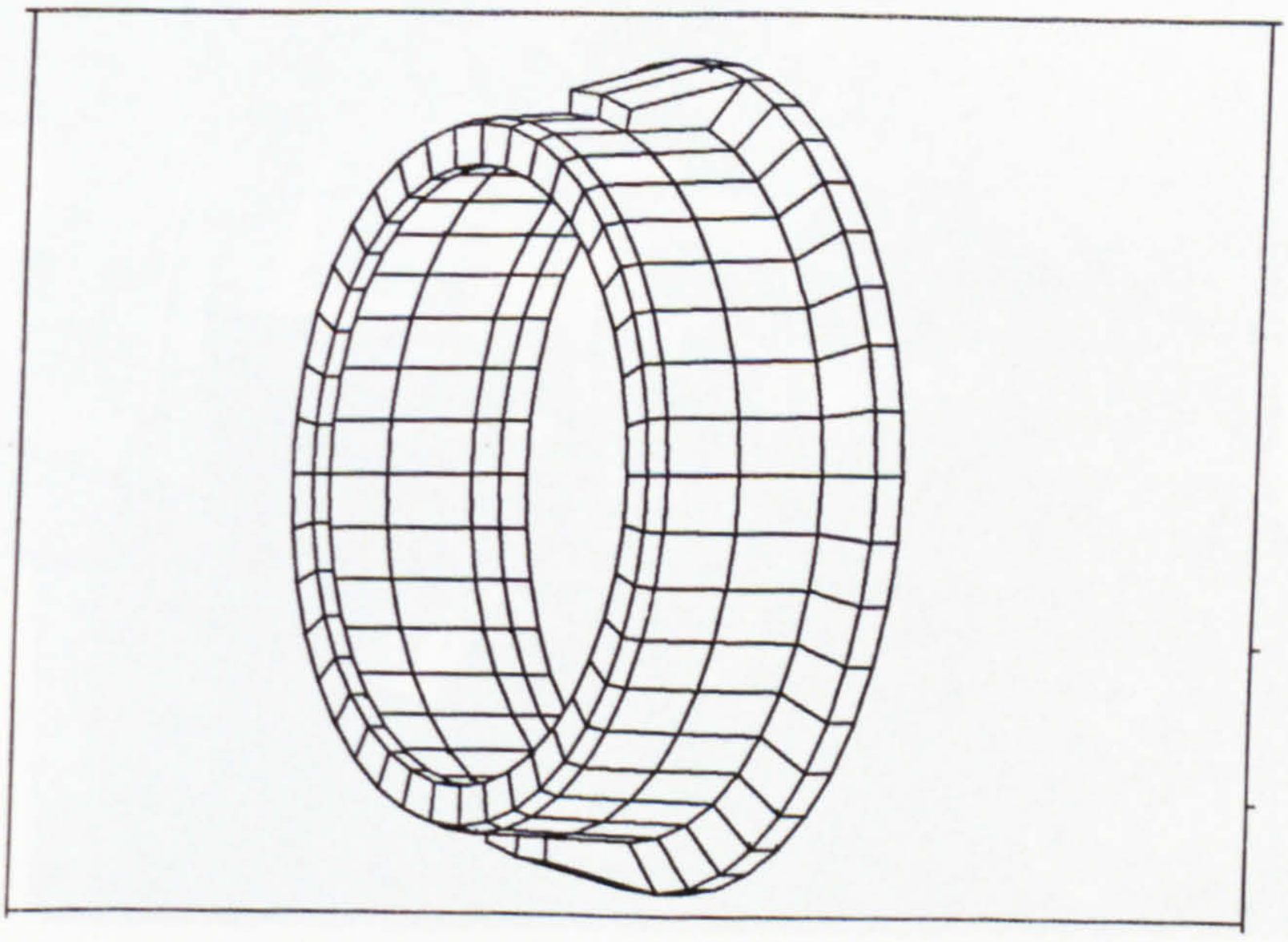

Figure 6.12 Finite element model of the drum in fig 6.11, used to optimise the mass addition

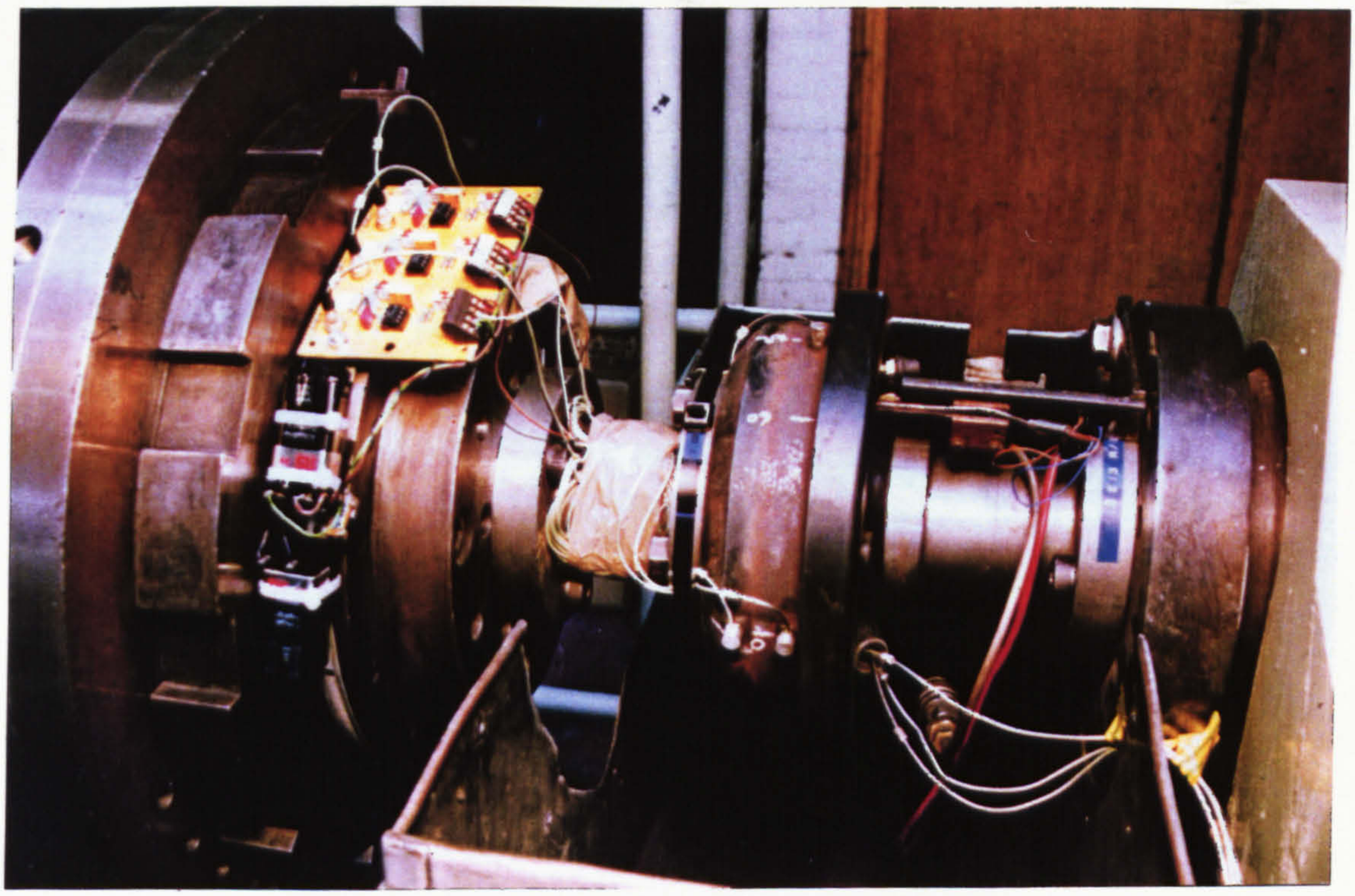

Figure 6.13 Arrangements for modal analysis of a 180mm x 30mm passenger car drum brake using the method described in Chapter 3

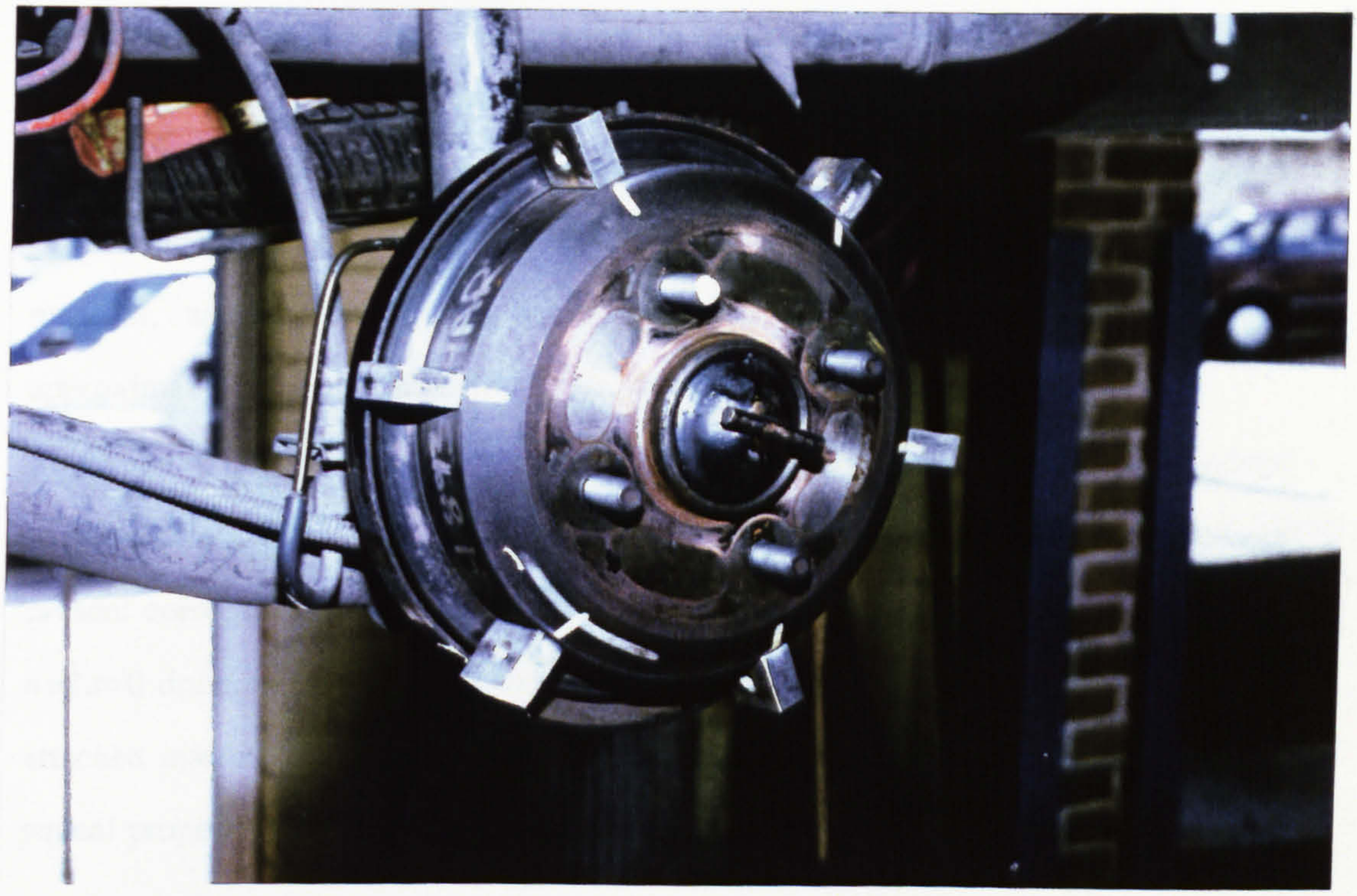

Figure 6.14 Six masses, attached to the passenger car drum using adhesive, which eliminated the 3.3khz squeal.

CHAPTER 7

THE SIGNIFICANCE OF THE NORMAL MODES OF THE ACTUATED BRAKE SYSTEM

7.1 Introduction

In chapter 5, the effect of the rotor modes on stability was considered in some detail, and it was suggested that decoupling rotor modes by reducing rotational symmetry can be stabilising. If the total actuated brake is considered, however, including the brake shoes and friction material, it is clear that this system does not have the inherent rotational symmetry of the drum alone and so would be expected to vibrate in modes which have fixed angular positions, due to the extended, but discontinuous, loading effects of the shoes on the symmetric drum. In such a system the drum mode shape will remain qualitatively similar to that of the drum alone due to the predominance of its mass and the relatively light coupling to the shoes through the low modulus friction material, and so the system modes can be conveniently described by their approximation to drum diametral mode shapes (eg n=2,s=0).

In chapter 4, these system modes were investigated experimentally and it was indeed seen that the modes take up fixed angular positions and that at least two modes are present corresponding to each of the drum flexural modes (ie two modes involving n=2,s=0 drum motion etc), a behaviour qualitatively similar to that of a drum with attached masses. In this chapter, the likely influence of this system asymmetry on squeal propensity will be discussed.

7.2 Static Normal Modes of the Binary Flutter Model

Consider now how these static system modes relate to the simple binary flutter model described in chapter 5. In the model shown in fig 5.10, the static brake system is simulated by removing the frictional forces at the drum/lining interface, and the two natural frequencies of the system are now, clearly,

$$\omega_{st} = \left(\frac{k_d + k_p}{M} \right)^{\frac{1}{2}} \tag{7-1}$$

and

$$\omega_{sr} = \left(\frac{S_d + \frac{1}{3} k_p l^2}{I} \right)^{\frac{1}{2}} \tag{7-2}$$

where subscripts *st* and *sr* indicate the translational and rotational modes of the system respectively.

The condition for instability of the model, equation 5-43, now becomes

$$\frac{4 \mu^2 N h k_p}{MI} > \left(\omega_{st}^2 - \omega_{sr}^2 \right)^2 \tag{7-3}$$

$$\Rightarrow \quad 2\mu \sqrt{\frac{N h k_p}{MI}} > \left| \left(\omega_{st} - \omega_{sr} \right) \left(\omega_{st} + \omega_{sr} \right) \right| \tag{7-4}$$

If $(\omega_{st} + \omega_{sr})/2$ is taken as the mean system natural frequency, ω_s, then, for instability

$$\mu\sqrt{\frac{Nhk_p}{MI}} \quad > \quad |\omega_{st} - \omega_{sr}|\bar{\omega}_s \tag{7-5}$$

and hence stability is increased by increased separation of the static system mode natural frequencies.

Reducing the rotational symmetry of the drum, as described in chapter 5, is one effective means of increasing this static mode separation, which will, however, depend upon the angular position of the masses used and so lead to the cyclic decoupling effects described earlier. However, in the static model, equations 7-1 and 7-2 indicate that other system parameters involving stiffness could also modify the separation of the static system modes. Based on the above analysis S Y Kim (41) has investigated the influence of various parameters on the static mode separation of a 3 - dimensional finite element model of a statically actuated heavy vehicle drum brake, with a view to using this separation as a criterion tor the design of quiet braking systems. The modelling work confirms the positive effect of reduced drum symmetry on static mode separation and, of the parameters assessed, this was found to be the most effective technique. Of the other parameters investigated, the coupling stiffness between shoe and drum (a combination of lining stiffness and 'contact' stiffness between lining and drum) also increased the mode separation, whilst shoe and drum stiffness changes had little effect.

7.3 The Effect of Friction on the System Mode Frequencies

The above 2-degree of freedom analysis, and the FEM modelling work referred to, both assume a non-rotating brake and hence no sliding friction forces. If friction forces are now reintroduced into the binary flutter model, their effect on the system natural frequencies can be assessed, and the significance of the static system mode separation more graphically illustrated.

Referring to the binary flutter model (fig 5.10) the eigenvalue solution is given in equation 5-40 and is repeated below .

$$\lambda = \pm \frac{1}{\sqrt{2}} \left((a+d) \pm \sqrt{(a+d)^2 - 4(ad - bc)} \right)^{\frac{1}{2}} \qquad (7\text{-}6)$$

using $(a+d)^2 - 4(ad-bc) = (a-d)^2 + 4bc$ this becomes:-

$$\lambda = \pm \frac{1}{\sqrt{2}} \left((a+d) \pm \sqrt{(a+d)^2 + 4bc} \right)^{\frac{1}{2}} \qquad (7\text{-}7)$$

Comparing equations 5-30 with equations 7-1 and 7-2, indicates that

$$a = \omega_{st}^2 \quad \text{and} \quad d = \omega_{sr}^2$$

and also that $bc = - \mu^2 N h k_p / MI$

Hence equation 7-7 becomes

$$\lambda = \pm \frac{1}{\sqrt{2}} \left(\omega_{st}^2 + \omega_{sr}^2 \pm \sqrt{\left(\omega_{st}^2 - \omega_{sr}^2\right)^2 - \frac{4\mu^2 N h k_p}{MI}} \right)^{\frac{1}{2}} \qquad (7\text{-}8)$$

and the dynamic system frequencies with friction, λ, can now be related to the static system frequencies, In order to illustrate this relationship, values for N, h, k_p, M and I are required, some of which are, in practice, not readily defined quantitatively, making it difficult to relate these simple model parameters to the much more complex real brake characteristics. If, however, the factor $4Nhk_p / MI$ is taken as a constant, K^2, for the brake, an estimate can be made of its value from a knowledge of the behaviour of the real brake under investigation.

From equation 5-43, the stability boundary occurs when

$$K^2\mu^2 = \left(\omega_{st}^2 - \omega_{sr}^2\right)^2 \qquad (7\text{-}9)$$

or

$$K\mu = \pm\left(\omega_{st}^2 - \omega_{sr}^2\right) \qquad (7\text{-}10)$$

Now the frequencies of the pair of static system modes involving n=2,s=0 drum motion are known, for the brake under investigation, from measurements in chapter 4, and, although these cannot be identified as 'transverse' or 'rotational' modes, this will not be significant to the argument due to the symmetry of equation 7-10. So, from chapter 4, let $\omega_{st} = 578$ Hz and $\omega_{sr} = 608$ Hz and as the nominal friction coefficient of the friction material is, say, $\mu = 0.3$ when squeal occurs, then a value of K can be calculated from equation 7-10. Using this data gives $K = 4.7\text{x}10^6$ s^{-2}.

Substituting this value for K, and the measured values of ω_{st} and ω_{sr} in equation 7-8 allows the system frequencies, λ , to be calculated for a range of values of friction coefficient, μ.

These frequencies are plotted in fig 7.1, and it can be seen that increasing the friction coefficient causes the pair of system natural frequencies to converge until they coincide at $\mu = 0.3$, when the system becomes unstable and squeals. From this point the eigenvalue, λ, becomes complex and the real part of the eigenvalue only is plotted, which represents the squeal frequency (the method of evaluating the squeal frequency is shown in Appendix 3).

The effect of changing the separation of the static system mode frequencies is illustrated in fig 7.2 which shows clearly that increased separation has a stabilising effect on the model in the sense that a higher coefficient of friction is required to

produce squeal. If this relationship was translatable to a real brake, it would provide a practical approach to retrospective 'fixing' of brake squeal by structural or geometric modifications to increase the mode separation.

Not only this static system mode frequency separation influences stability, however, but also the value of K (and, of course, μ). Fig 7.3 illustrates the effect of changing K, showing that increasing K is destabilising as expected from equation 7-5. Here, for a given static frequency separation, increasing K results in more rapid convergence of the mode frequencies with increasing μ. Of course, the static frequency separation and K are not independent parameters of either the model or of a real brake, both having more fundamental parameters, such as M and k_p , in common. This suggests that even static brake system modelling using comprehensive finite element models, such as those developed by Kim, should be used with care, and an awareness maintained of the 'convergence factor', K. This limitation of static system modelling, implied by the simple binary flutter model, serves to reinforce the need for a more comprehensive dynamic (ie including dynamic friction) model of the braking system, and such a model will be discussed in the next chapter.

7.4 Summary

Based on the simple binary flutter model, the separation of the static system mode frequencies (ie with μ=0) is shown to have a positive influence on stability. The analysis suggests, however, that this criterion cannot be used in isolation for design as the rate of convergence of these modes with increasing friction also depends upon design parameters, reinforcing the need for a comprehensive stability model for the operating brake.

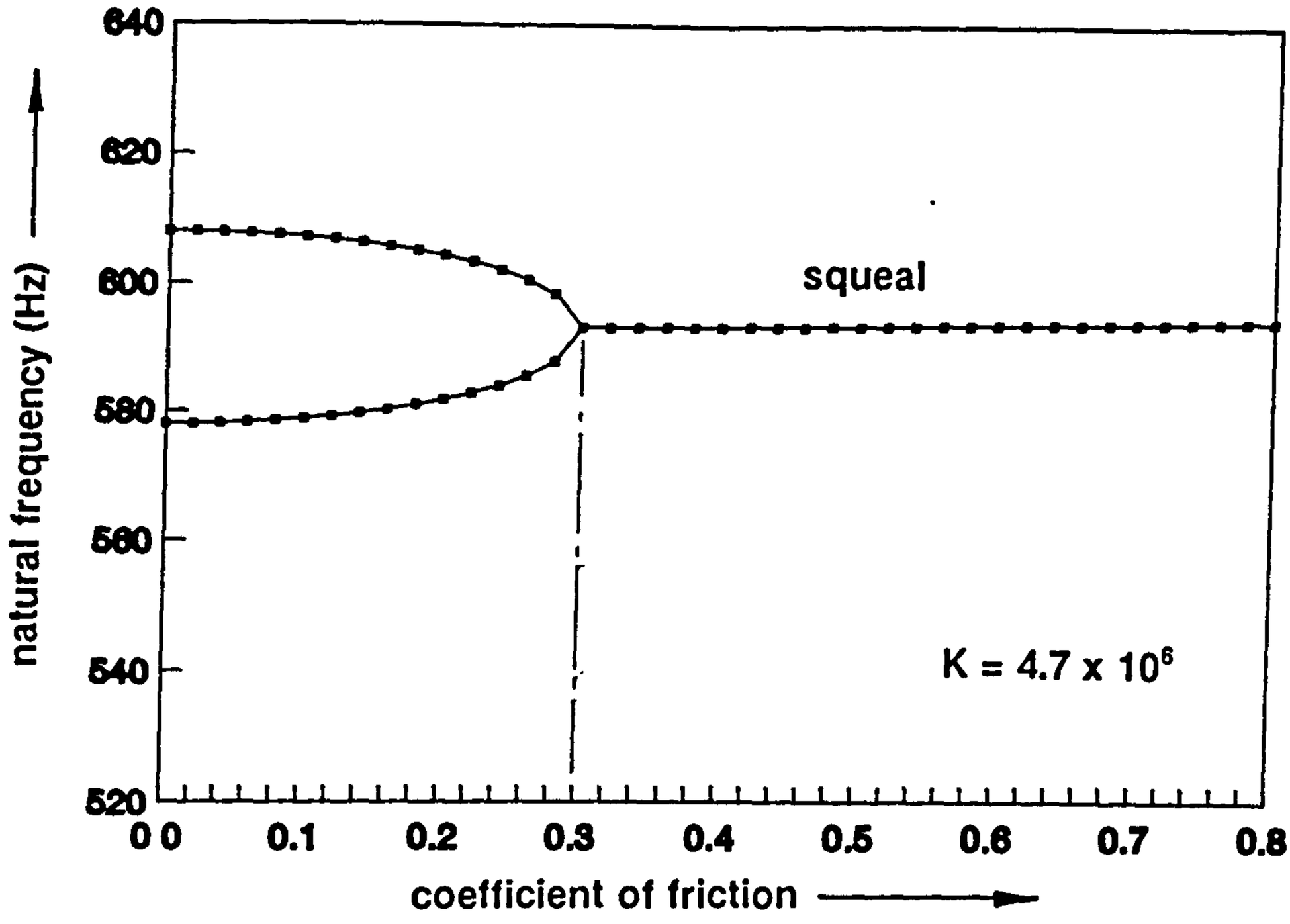

Figure 7.1 The effect of friction coefficient on the 2-dof binary flutter model, showing convergence of modes to produce instability

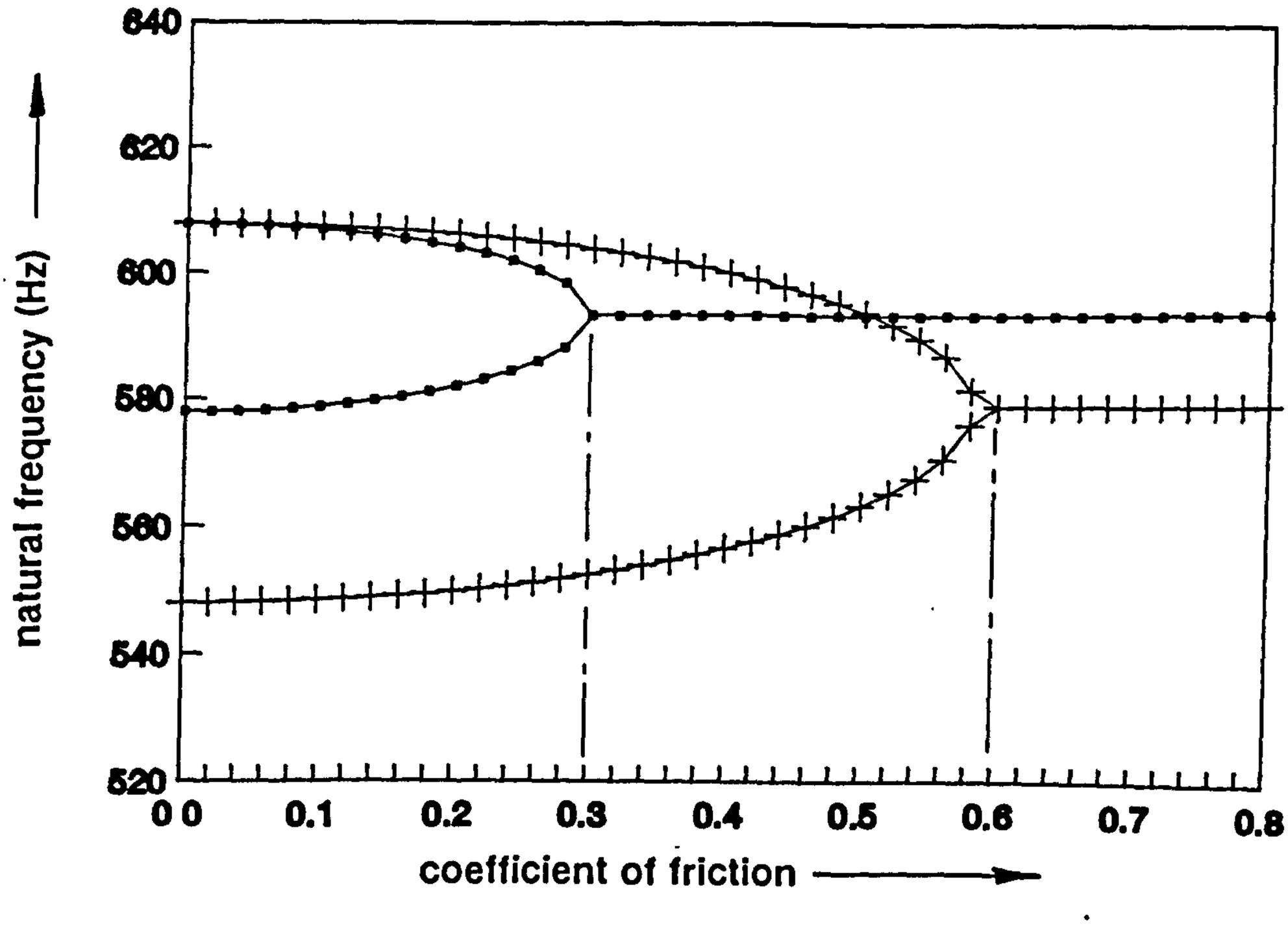

Figure 7.2 Showing how the difference in the natural frequencies of the binary flutter model can influence the μ required for squeal

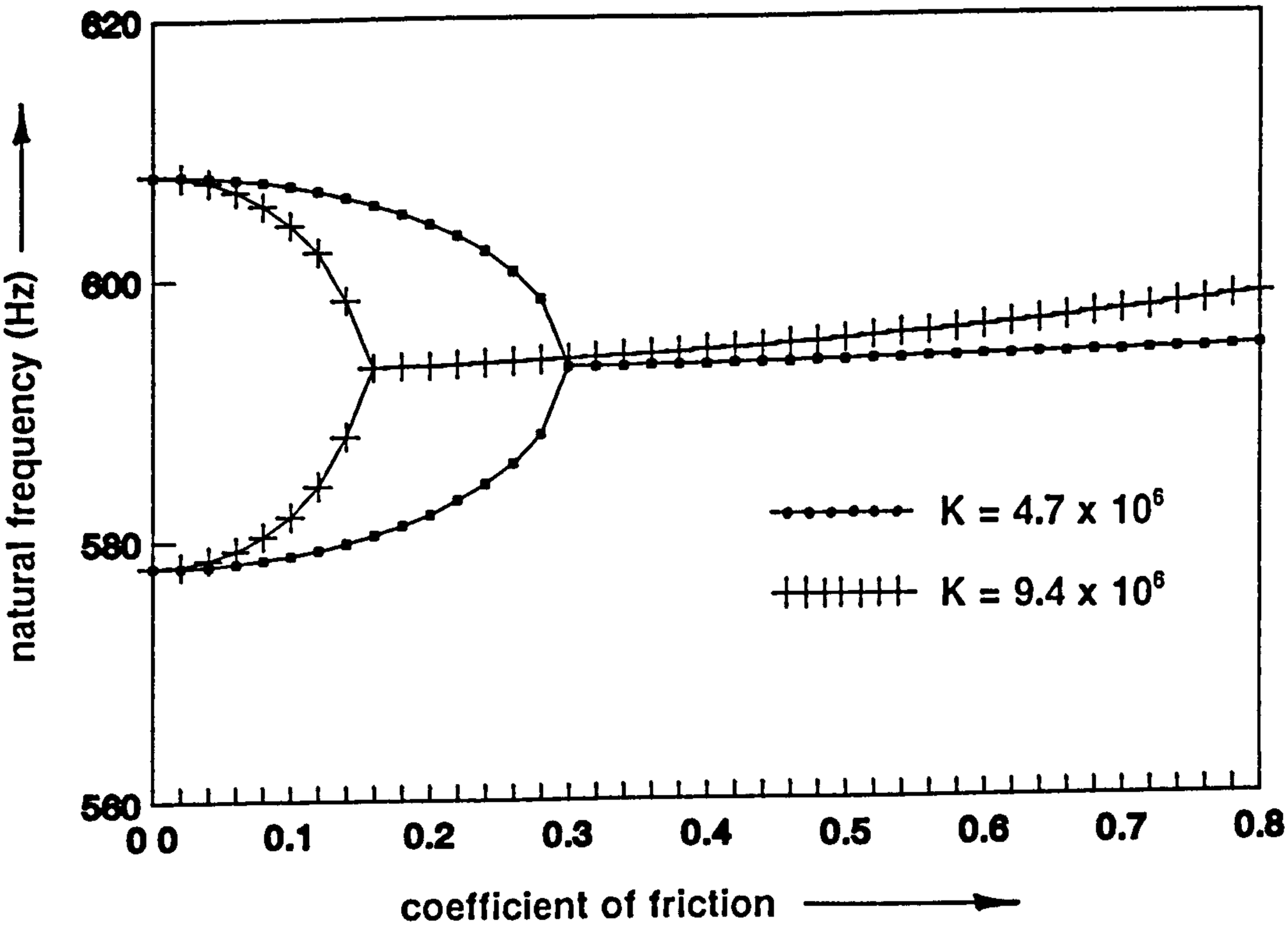

Figure 7.3 Showing how an increase in the 'convergence factor',K, decreases the μ required for instability of the binary flutter model

CHAPTER 8

FINITE ELEMENT MODELLING OF THE OPERATING BRAKE

8.1 Introduction

Throughout the previous chapters, only a simple two degree of freedom lumped parameter model of the dynamic brake has been considered. Although this model is clearly a very limited representation of an actual brake, its consistent use has been justified as follows.

(i) The predicted unstable behaviour of the model rotor segment is in good qualitative agreement with the essential features of any short segment of the experimentally measured modal behaviour of the real brake rotor.

(ii) Although more comprehensive lumped parameter models with more degrees of freedom, based upon the binary flutter mechanism, have been developed (eg refs 21 & 22), these require numerical solution techniques which can 'mask' the conceptual understanding obtainable from the analytical solution processes possible with a simple model.

(iii) Analysis of the model has produced practically useful results in highlighting the significance of rotor symmetry and the separation of the frequencies of modes of the static brake system.

Such a model is, however, of very limited application as a brake design tool, as are most lumped parameter models, particularly when applied to drum brakes with their distributed coupling between shoes and drum and the complex flexural behaviour of their components.

Finite element modelling can address the problem of ensuring the required structural complexity of the brake, but, as argued at the end of chapter 7, purely structural models representing the stationary brake are also limited to predicting the effect of brake parameters on the separation of the frequencies of modes of the static system, which, although thought to influence squeal, cannot be considered in isolation from other factors. A comprehensive squeal design tool would combine the sophisticated structural simulation of a finite element model with the ability to represent the dynamic frictional coupling at the lining/drum interface, as in the simple binary flutter model. This simulation of friction coupling in dynamic models, together with the associated complex eigenvalue analysis capability, are not standard features of most commercial finite element software packages. One package, ANSYS, does, however, have complex eigenvalue analysis capability, together with user definable stiffness elements which can be defined to have non-symmetric matrices. It will be shown that this latter feature can allow suitable friction forces to be simulated at the lining/drum interface.

As part of a collaborative project between Mintex Don in the UK and Saab Scania in Sweden (who had the ANSYS software available) the concept of using stiffness elements having non-symmetric matrices (based on the binary flutter stiffness matrix) was implemented on a very detailed 3-dimensional ANSYS model of the brake used for the experimental work detailed earlier. The work is described by Lundström (42) and in internal Saab-Scania/Mintex Don collaborative project reports. This model

predicted squeal at a frequency close to that of the actual brake tested and at a friction coefficient typical of the brake lining used, but the cpu time required to run the model (typically 6 hours) severely restricted its use for parametric studies. As a result of this initial success of the FEM/flutter approach, ANSYS was purchased and installed at Mintex Don, where the work detailed here was carried out, to develop a more efficient model to explain the squeal behaviour of the brake.

The approach taken here is to produce undamped dynamic models of the individual brake components using standard finite element techniques, but then to couple all corresponding nodes across the interface between the drum and the friction material using specially designed elements which introduce frictional forces proportional to the normal forces at the interface. The design of these interface elements is discussed below.

8.2 Frictional Interface Elements

The equations of motion of the 2 - degree of freedom binary flutter model, equations 5-28 and 5-29, expressed in matrix form are

$$\begin{bmatrix} M & 0 \\ 0 & I \end{bmatrix} \begin{pmatrix} \ddot{y} \\ \ddot{\theta} \end{pmatrix} + \begin{bmatrix} k_d + k_p & \mu N \\ -\mu h k_p & S_d + k_p \frac{l^2}{3} \end{bmatrix} \begin{pmatrix} y \\ \theta \end{pmatrix} = 0 \qquad (8\text{-}1)$$

The stiffness matrix is non-symmetric, due to the representation of dynamic friction forces in the model, leading to the possibility of complex eigenvalues and unstable oscillation. If $\mu = 0$, the stiffness matrix is symmetric and unstable oscillation is not possible. If this potential instability mechanism is to be incorporated into a finite

element model, a means of introducing dynamic friction forces is therefore required as outlined along the lines indicated above.

Consider the modified version of the 2 degree of freedom binary flutter model shown in fig 8.1. The combination of compression and torsional springs representing the friction material has been replaced by two compression springs spaced apart by a distance $2l/\sqrt{3}$, which can be shown to produce equivalent forces and moments on the drum section. Each of these springs applies both normal and friction forces to the drum surface, and so can be depicted as shown below.

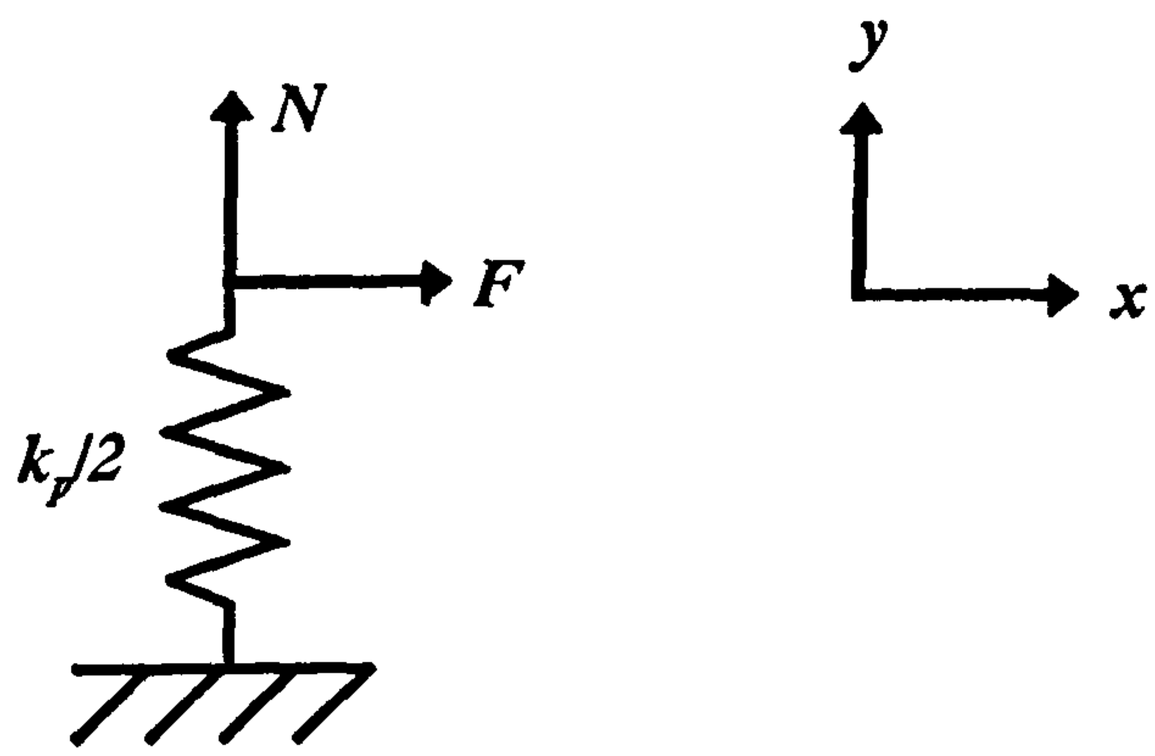

The forces on the drum are independent of the tangential displacement x as the spring has stiffness only in the direction normal to the interface. Hence

$$N = \frac{k_p}{2} y \qquad , \qquad F = \mu \frac{k_p}{2} y \tag{8-2}$$

or

$$\begin{pmatrix} N \\ F \end{pmatrix} = \begin{bmatrix} \frac{k_p}{2} & 0 \\ \mu \frac{k_p}{2} & 0 \end{bmatrix} \begin{pmatrix} y \\ x \end{pmatrix} \tag{8-3}$$

The above stiffness matrix can be expressed as

$$\begin{bmatrix} \frac{k_p}{2} & 0 \\ \mu\frac{k_p}{2} & 0 \end{bmatrix} = \begin{bmatrix} \frac{k_p}{2} & 0 \\ 0 & \frac{k_p}{2} \end{bmatrix} \begin{bmatrix} 1 & 0 \\ \mu & 0 \end{bmatrix} \qquad (8\text{-}4)$$

ie a symmetric stiffness matrix multiplied by a non-symmetric 'friction' matrix.

In principle, this type of linear spring representation of the friction material could be used in a finite element model to connect the shoe and drum, but in practice, this would limit the accuracy of the structural effects of the friction material, a shortcoming which is overcome by considering a further representation of the 'friction material' spring below.

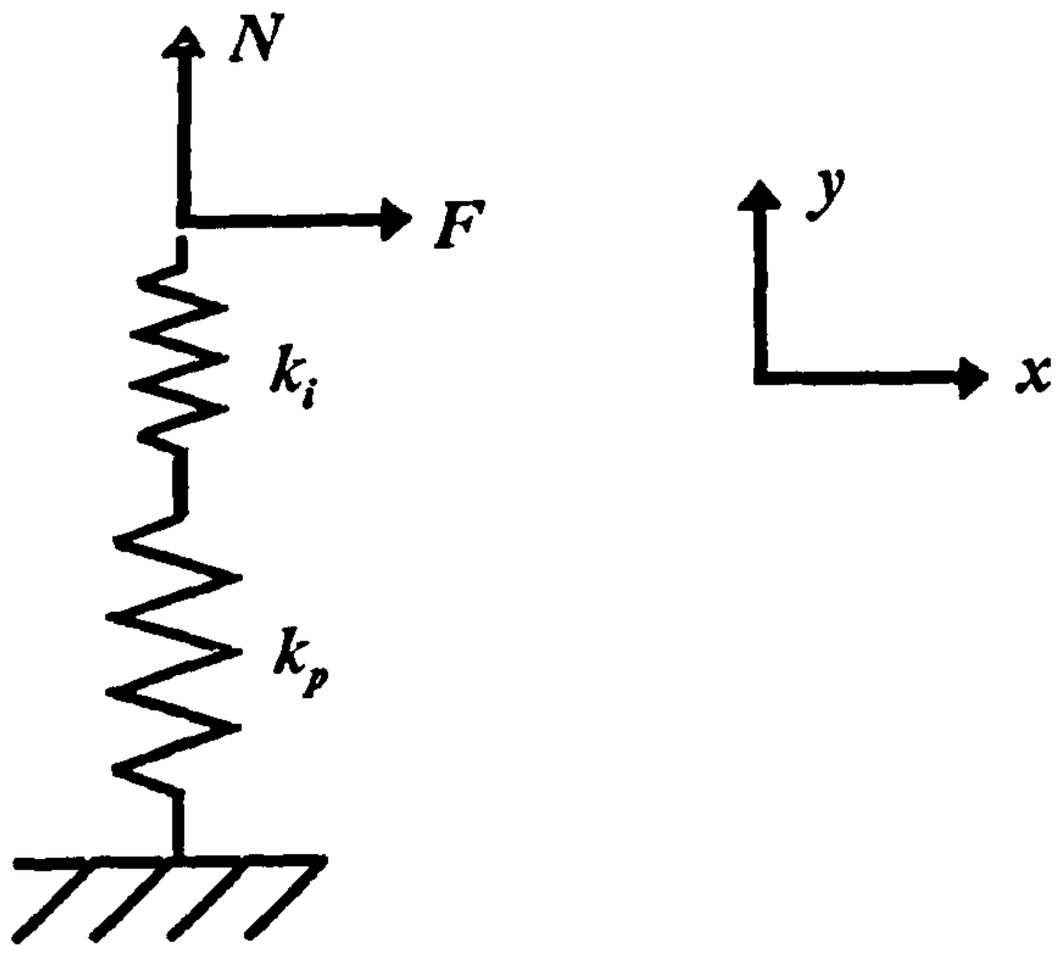

(note here that $k_p/2$ has been replaced by k_p for simplicity)

Here an 'interface stiffness', k_i , has been introduced between the friction material and the drum.

The total stiffness of this system, k , consisting of two springs in series is given by the equation

$$k = \frac{k_p k_i}{k_p + k_i} \tag{8-5}$$

Now, if $k_i >> k_p$, the total stiffness $k \approx k_p$, and the addition of k_i has little effect on the model behaviour. The arrangement does, however, provide a means of applying friction forces to the interface without restricting the friction material to being a purely compressive spring-like element.

Taking the interface spring element now in isolation,

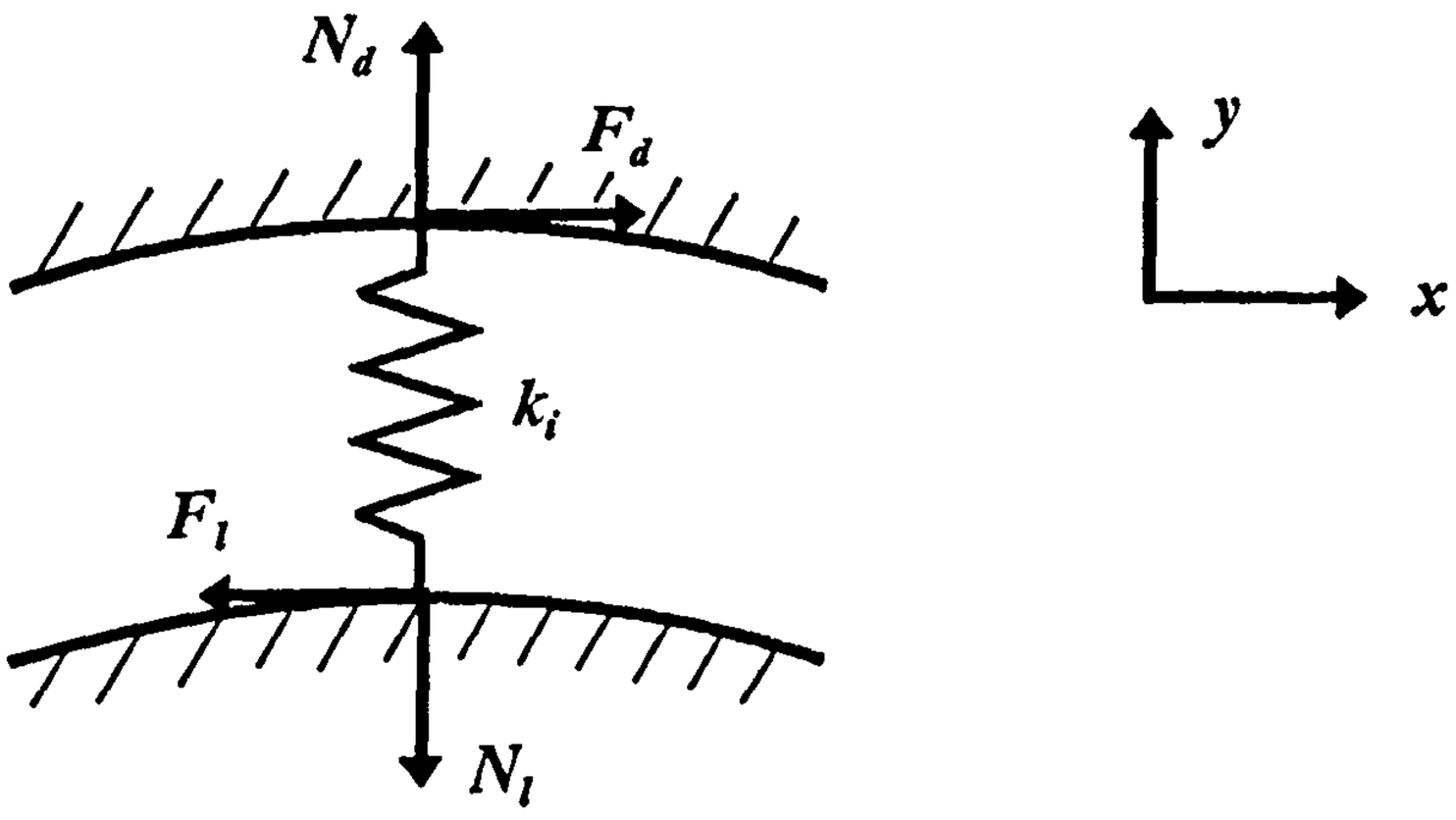

gives the force equation

$$\begin{aligned} N_d &= -N_l = k_i (y_d - y_l) \\ F_d &= -F_l = \mu k_i (y_d - y_l) \end{aligned} \tag{8-6}$$

and so

$$\begin{pmatrix} N_d \\ F_d \\ N_l \\ F_l \end{pmatrix} = \begin{bmatrix} k_i & 0 & -k_i & 0 \\ \mu k_i & 0 & -\mu k_i & 0 \\ -k_i & 0 & k_i & 0 \\ -\mu k_i & 0 & \mu k_i & 0 \end{bmatrix} \begin{pmatrix} y_d \\ x_d \\ y_l \\ x_l \end{pmatrix} \tag{8-7}$$

In ANSYS, spring elements can be defined to have the above stiffness matrix by using the STIF27 user-defined element described in the ANSYS manual (43). The actual stiffness matrix used in the model is somewhat larger due to the rotational degrees of freedom at the nodes (which are taken to have no influence on the frictional forces). The matrix used is

$$K = k_i \begin{bmatrix} 1 & 0 & 0 & -1 & 0 & 0 \\ \mu & 0 & 0 & -\mu & 0 & 0 \\ 0 & 0 & 0 & 0 & 0 & 0 \\ -1 & 0 & 0 & 1 & 0 & 0 \\ -\mu & 0 & 0 & \mu & 0 & 0 \\ 0 & 0 & 0 & 0 & 0 & 0 \end{bmatrix} \tag{8-8}$$

(In practice, even in a 2-D analysis, ANSYS requires a full 12x12 matrix to include all 3-D degrees of freedom)

As maintained earlier, if the role of the interface element is to provide friction forces only, then k_i should be much greater than k_p, and in practice, the value of k_i was chosen to be $k_i > 100k_p$, where in this case, k_p represents the compressive stiffness of the small section of friction material associated with each interface element. Trials with a range of values of k_i showed that results were sensibly independent of k_i above this value.

8.3 Modelling the Brake 2-Dimensionally

It was remarked earlier that the detailed 3-dimensional finite element model of the brake produced by Saab Scania, using the above friction interface elements, required excessive cpu time and so could not be readily used for parametric studies and hence as a design tool. The experimental modal analysis work carried out on the squealing brake in chapters 3 and 4 suggests, however, that the modal behaviour of both the brake drum and shoes is essentially two-dimensional in nature. The drum vibrates in modes having axial nodal lines only with no phase shift across the rubbing path - only an increase in amplitude from the mounted side to the mouth of the drum. Similarly, the shoes are seen to exhibit essentially bending motion with no significant torsional component - again showing only an increase in amplitude across the platform approximately matching that of the drum. Further modal analysis of other squealing brakes at various frequencies has shown qualitatively similar results, suggesting that this 2-dimensional behaviour is a common feature of squeal. This suggests that for modelling purposes, the brake could be represented by a 2-dimensional idealisation without significant loss of essential dynamic similarity to the real brake, provided that the individual component models behave dynamically similarly to the actual components in the relevant modes.

8.4 2-Dimensional Representation of the Shoe

This condition is relatively easily achieved for the shoes as they are composed of essentially two parts, the platform and the web, each of which can be considered as having a uniform section in the axial direction. The platform approximates to a uniform curved plate having a depth in the axial direction equal to the drum rubbing path width, whilst the two webs can be represented by a single curved beam, as shown

in fig 8.2. In the finite element model the 3-dimensional features of the shoe can thus be accommodated by variations in the axial thickness of an essentially 2-dimensional model.

The shoes are cast from malleable iron having the following properties,

Young's modulus = 1.75×10^{11} Nm^{-2}

Density = 7300 kgm^{-3}

Poisson's ratio = 0.17

and using these values, this simple representation of the shoe exhibited a free fundamental bending natural frequency of 1930 Hz, much higher than the measured 1075 Hz. Adding point masses to represent the cam rollers (0.7kg), the shoe platform support webs (0.11kg at each end of platform) and thickening of the web at the anchor pin position (0.56kg), reduced this frequency to 1033 Hz, which was considered an acceptable match to the real shoe.

8.5 2-Dimensional Representation of the Drum

2-dimensional idealisation of the drum is not so clearly achievable, due to the influence of the mounting flange and its attachment to the hub, which modifies the dynamic behaviour of the rubbing path annulus in an axially non-symmetric manner, unlike the symmetric effect of the shoe web on the platform. In this case it is necessary to design an annular ring to represent the drum which has similar dynamic characteristics to, say, that of the mid point of the drum rubbing path. Thus, the annular ring should have the same natural frequency in the mode(s) of interest, and the same single degree of freedom equivalent mass (M) in that mode referred to the mid rubbing path position on the drum. These two conditions will then ensure that the stiffness of the ring is also equivalent at the reference position.

A further proposed requirement is that the ring should have a similar radial thickness to that of the rubbing path portion of the drum, in order to maintain the torsional effect of the friction forces on the drum elements - the equivalent of the parameter h in the 2 degree of freedom flutter model.

The required values of ω_n and M for the n=2,s=0 mode of the drum were obtained by modal analysis of the drum mounted to its dynamometer adaptor, using the impact excitation technique described earlier. The equivalent mass, M, was measured by attaching small masses of mass m, to the drum at an antinode 25mm from the drum mouth, and recording the resultant reductions in natural frequency, $\Delta\omega$.

It can be shown that for small m (ie $m << M$),

$$M \approx \frac{m\,\omega_n}{2\,\Delta\omega} \qquad (8\text{-}12)$$

The experimental results for the n=2,s=0 mode of the drum (for which ω_n = 405.6 Hz) are given below.

Table 5 Measurement of the Effective Mass of the n=2,s=0 Drum Mode

m (kg)	Δω (Hz)	M (kg)
0.32	3.28	19.6
0.47	5.15	18.3
0.60	7.03	17.0
0.75	8.28	18.0

Some scatter in the above values is observed which is thought to be due to some angular deviation of the antinodal position from the added mass position during the

test due to some inherent rotational asymmetry in the drum structure. This deviation will change with the magnitude of the added mass, thus changing the equivalent mass at the measurement point. An average value of M = 18.2kg was chosen, and referring this to the rubbing path centre, where the amplitude is typically 0.75 times that at the position of mass addition, gives a value of M = 32kg, which was used for the model design.

The average thickness of the drum rubbing path region was estimated as 28mm, and the resulting drum model geometry is shown fig 8.3, the angular size of the elements being chosen as 9° for convenience in coupling to the brake lining elements.

The properties of the drum cast iron are:-

Young's modulus	$= 1.25\times10^{11}\ Nm^{-2}$
Density	$= 7100\ kgm^{-3}$
Poisson's ratio	$= 0.25$

and using these, the basic annulus model of the drum exhibited a n=2 mode frequency of 302 Hz, much lower than the measured 410 Hz, as would be expected due to the lack of representation of the drum mounting stiffness. To increase this frequency and provide some restraint on rigid body motion, radial springs were attached between each external node and 'earthed' nodes. The stiffness of these springs was adjusted to bring the n=2 mode frequency to 407 Hz (for which each spring had stiffness $5x10^6\ Nm^{-1}$) and under this condition, the generalised mass was shown to be 34.9 kg, a reasonable match to the required value, without resorting to the adjustment to the material density which had been anticipated.

8.6 Shoe Boundary Conditions

It can be seen from fig 8.4 that the shoes are attached to the torque plate by fixed anchor pins about which they are free to rotate; and that braking expansion force is applied to their free ends, through rollers by rotation of the 'S' cam. A first approximation to the boundary conditions at the shoe ends was therefore based on the assumption that the anchor pins and cam shaft were rigidly fixed, so allowing only rotation of the anchor pin shoe nodes and radial sliding of the cam roller shoe nodes. Using these boundary conditions, however, no instability could be achieved.

To determine whether these assumed boundary conditions were realistic further modal analysis was carried out on the anchor pins and cam during squeal of the brake. The results, summarized in Appendix 4, clearly indicated significant tangential motion in both the camshaft and anchor pins, the latter moving together as may be expected due to the connecting link between their ends.

Based on these observations, the anchor pin and cam roller nodal restraints were released and these points were connected to earth through springs, in both the radial and tangential directions for the anchor pins and the tangential direction only for the cam rollers, as shown in fig 8.5. The spring constants used were estimated values, 10^7 Nm^{-1} for the anchor pins and 3×10^7 Nm^{-1} for the cam rollers (the cam shaft support structure being significantly stiffer than that of the anchor pins). The anchor pin nodes were coupled to move identically, reflecting their physical coupling, and the cam roller nodes connected by a rigid link to represent the fixed separation imposed by the cam itself.

The complete model geometry is summarised in a fig 8.6.

8.7 Friction Material Properties

It was noted earlier that friction material generally has anisotropic elastic properties and the Don D7115 material used in this work is no exception. Its dynamic modulus was measured in two directions, by measuring the response of small samples of the material to a non-resonant compressive cyclic force in a 'Metravib' viscoanalyser. A typical result for the radial direction, that is through the thickness of the lining, is illustrated in fig 8.7, which shows the dynamic elastic modulus (E') and the ratio of loss modulus to elastic modulus (tan delta), for a range of excitation frequencies up to 900 Hz and at temperatures from -100°C to 200°C. The elastic modulus is seen to be relatively insensitive to frequency but decreases with temperature over most of the brake working temperature range. The elastic modulus in the tangential direction that is along the lining length, was typically 2 x this value, this being the direction of the preferred orientation of the fibrous content of the liner. For the purpose of the finite element model, the friction material was assumed to be isotropic, and the modulus value chosen was that measured radially as this would have the greater influence on the modal coupling effect in the flutter mechanism. From fig 8.7, it can be seen that the modulus value required at the estimated mean lining temperature of 80°C during squeal, is 2×10^9 Nm^2. The measured density of the Don D7115 material is 2000 kgm^{-3}.

8.8 Model Predictions

A typical model data file is listed in Appendix 5, and this was run on ANSYS version 5.0 using the Lancxos unsymmetric eigenvalue solver. The eigenvalues produced using a coefficient of friction of $\mu = 0.4$ and other friction material properties described earlier are tabulated overleaf.

Table 6 Eigenvalues for $\mu = 0.4$

Mode Number	Eigenvalues	
	Real	Imaginary
1	205.4	0
2	231.8	0
3	312.9	0
4	608.8	-10.5
5	608.8	+10.5
6	644.7	0
7	1157.1	0
8	1368.1	0
9	1512.2	0
10	1945.2	0

Most modes have real eigenvalues indicating that they are normal modes of the system, which, in practice would be damped, but two modes occur as a complex conjugate pair with the same frequency, 609 Hz, one being stable and the other unstable. The magnitude of the imaginary component of the eigenvalue gives a measure of the degree of instability of the mode, or 'squeal propensity' as it has been described by previous workers.

The predicted squeal frequency of 609 Hz is in fairly good agreement with the observed value of 585-600 Hz, and the associated mode shape components, illustrated in fig 8.8, show qualitatively similar characteristics to those measured in chapters 3 and 4. The predicted mode shapes are in the form of real and imaginary components, both involving n=2 drum motion, with an angular shift of ≈45° between the two.

The model was analysed for a range of friction coefficients, from μ=0 to μ=0.5, and the resulting eigenvalues are plotted in fig 8.9, (in this case using a value of $E_f = 1x10^9\ Nm^{-1}$ for the friction material). The region of greatest interest is shown in more detail in fig 8.10, and several features of this eigenvalue - friction coefficient characteristic are noteworthy.

i) When μ=0, three normal mode frequencies occur in the vicinity of the squeal frequency, ie 603Hz, 612Hz and 656Hz, and their associated eigenvectors show that each involves n=2 drum motion. This behaviour is similar to the measured behaviour of the static system summarised in Table 3 of Chapter 4, where five 'n=2' frequencies are found - 528Hz, 548Hz, 578Hz, 608Hz and 663Hz. It must be noted, however, that the conditions are somewhat different, in that sliding of the friction interface probably does not occur in the latter case due to the static friction forces.

11) The influence of friction forces on the frequencies of most modes is small.

iii) Two of the modes involving n=2 drum motion are very close in frequency when μ=0 (only 9Hz apart) and the effect of the friction forces is to cause these frequencies to converge, and, at μ=0.16, to coincide. Above this friction coefficient, the eigenvalue becomes complex, and the magnitude of the imaginary part increases as μ increases, indicating increasing dynamic instability. This behaviour is very similar to that discussed in Chapter 7, for the simple binary flutter model.

8.9 The Effect of Friction Material Modulus Variation

The above model predictions appear to correlate well with the observed behaviour of the actual brake and experience of the generally destabilising effect of increasing friction coefficient. This suggests that this model could be used for predicting the effect of parameter variations on the squeal behaviour of the brake.

It is well known that squeal is a fugitive phenomenon, often depending quite critically on the applied braking pressure and the temperature of the brake, and it is reasonable to suppose that the component whose physical characteristics are most sensitive to these variables is the friction material. Its modulus is somewhat non-linear with applied load, and is very temperature sensitive; its thickness changes as it wears, and its contact to the drum can be nonuniform, decreasing the apparent stiffness between the drum and shoe. All these effects could be considered for modelling purposes as variations in material modulus, and hence the effect of this variation was examined in the model for values of $E_f = 0.5 \times 10^9$ Nm^{-2} to $E_f = 4 \times 10^9$ Nm^{-2}, a range which was considered to cover most service conditions, for the material used in the investigation.

By again carrying out analysis for a range of friction values, the friction coefficient corresponding to the onset of instability was evaluated for each friction material modulus, and the results are plotted in fig 8.11. This characteristic prompts the following observations.

i) No simple monotonic relationship exists between friction material modulus and dynamic stability and so no simple rule could be suggested for friction material design.

ii) The nominal value of modulus for the friction material used produces the greatest potential for instability, but the effect of variations in effective stiffness in service could well explain the fugitive nature of the squeal.

iii) The values of friction coefficient required for instability are below the nominal value for the friction material over a wide range of moduli, suggesting that squeal would always occur. The model does not, however, include damping effects and these would be expected to increase the values of μ required to produce instability.

iv) At a low value of modulus, the pair of modes which couple to produce the instability changes from the 4th+5th modes to the 5th+6th modes.

8.10 The Effect of Reducing Drum Symmetry

It was shown in chapter 5 that a suitable reduction in drum symmetry could have a beneficial effect in reducing or eliminating squeal, and also that this stabilising effect has a cyclic characteristic as the masses used to reduce symmetry rotate around the brake. A useful test of the finite element model would thus be to determine whether this cyclic stabilising effect is reproduced.

As the squeal mode involves n=2 drum motion, four point mass elements were attached to drum model nodes, at positions equally spaced around its periphery. These 2kg masses were moved around the drum with 9° increments (the angular distance between nodes) over a 60° arc length, and an eigenvalue analysis carried out at each

position. In this case, in order to reduce computing time, a single coefficient of friction, μ=0.4, was used, chosen to ensure instability occurred at all mass positions, and the magnitude of the imaginary component of the eigenvalue was used as a measure of the degree of instability. The result is shown in fig 8.12, from which the cyclic nature of the degree of instability is apparent, agreeing qualitatively with the observed squeal behaviour and predictions based on the simple binary flutter model.

The baseline value of the imaginary eigenvalue component, with no mass addition, is also shown in fig 8.12, and it is clear that over part of the cycle instability is increased by the mass addition. The mechanism by which the overall effect during the cycle can be stabilising is, as yet, unclear.

8.11 Summary

It has been shown that the frictional forces at the interface between the friction material and the drum can be represented in a dynamic finite element model by 'spring' elements having non-symmetric stiffness matrices. Under some conditions this results in complex eigenvalues, which predict the presence of unstable squeal modes. A 2-dimensional finite element idealisation of the brake has been justified in terms of the measured experimental mode shapes and computing efficiency, and such a model can predict squeal characteristics in good agreement with those observed in practice, if the dynamic characteristics of the individual component models are carefully simulated.

The model analysed here suggests that dynamic stability, and hence, squeal, is very sensitive to the friction coefficient at the interface and the stiffness of the friction

material, and these results go some way towards explaining the fugitive nature of squeal.

Finally, the decoupling effect of reduced symmetry of the drum predicted from the binary flutter model and observed in its effect on squeal, is reproduced by the finite element model, supporting both the suggested flutter mechanism and the finite element modelling technique used.

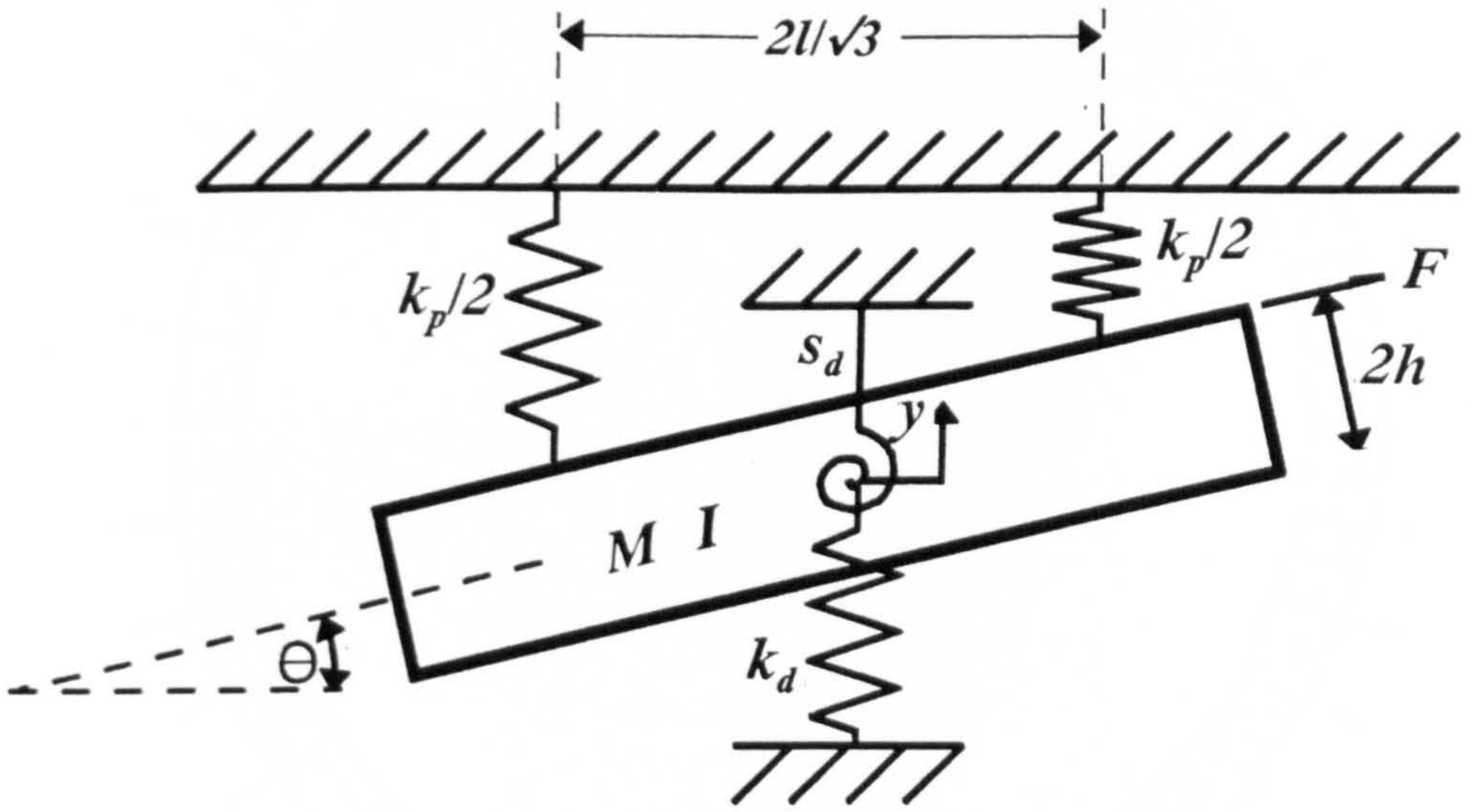

Figure 8.1 Two degree of freedom flutter model modified to represent the friction material by a pair of linear springs

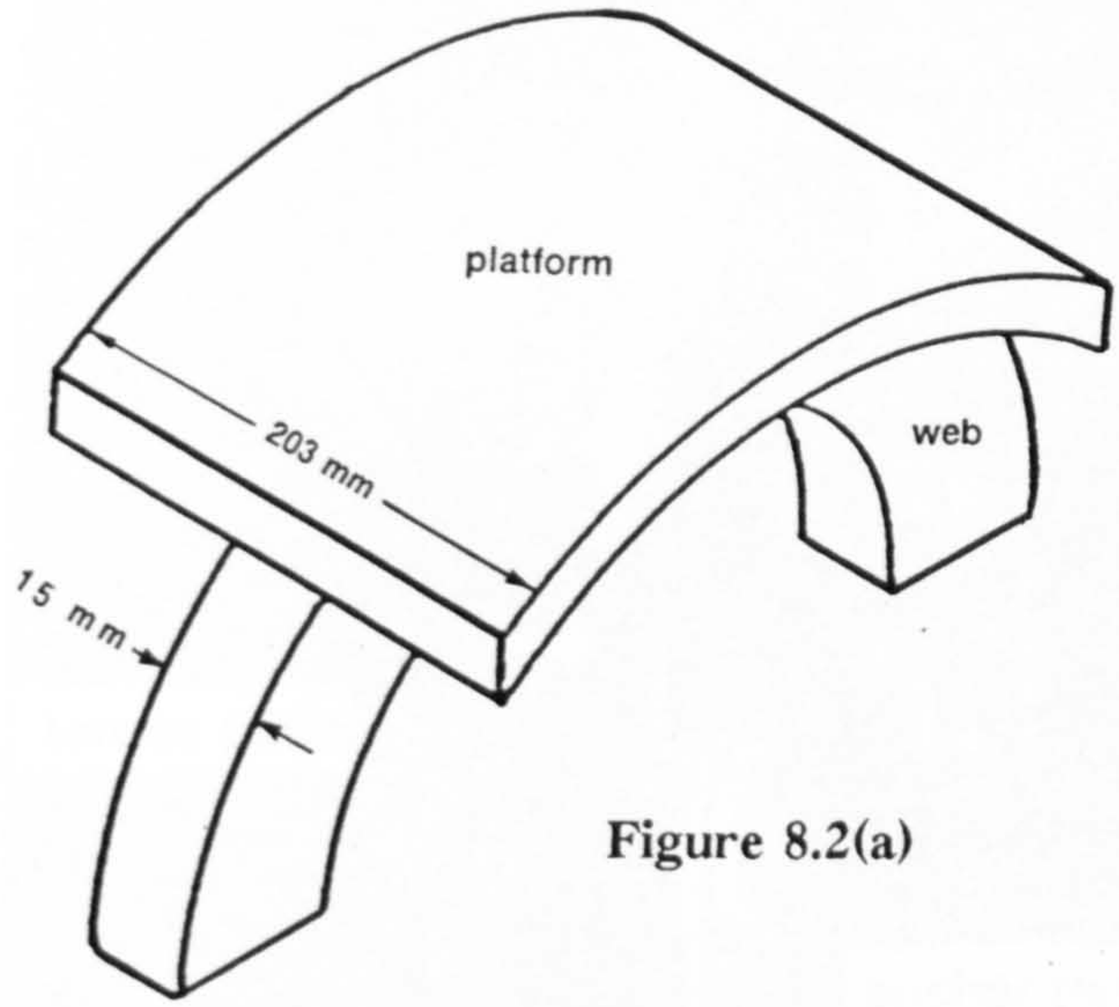

Figure 8.2(a)

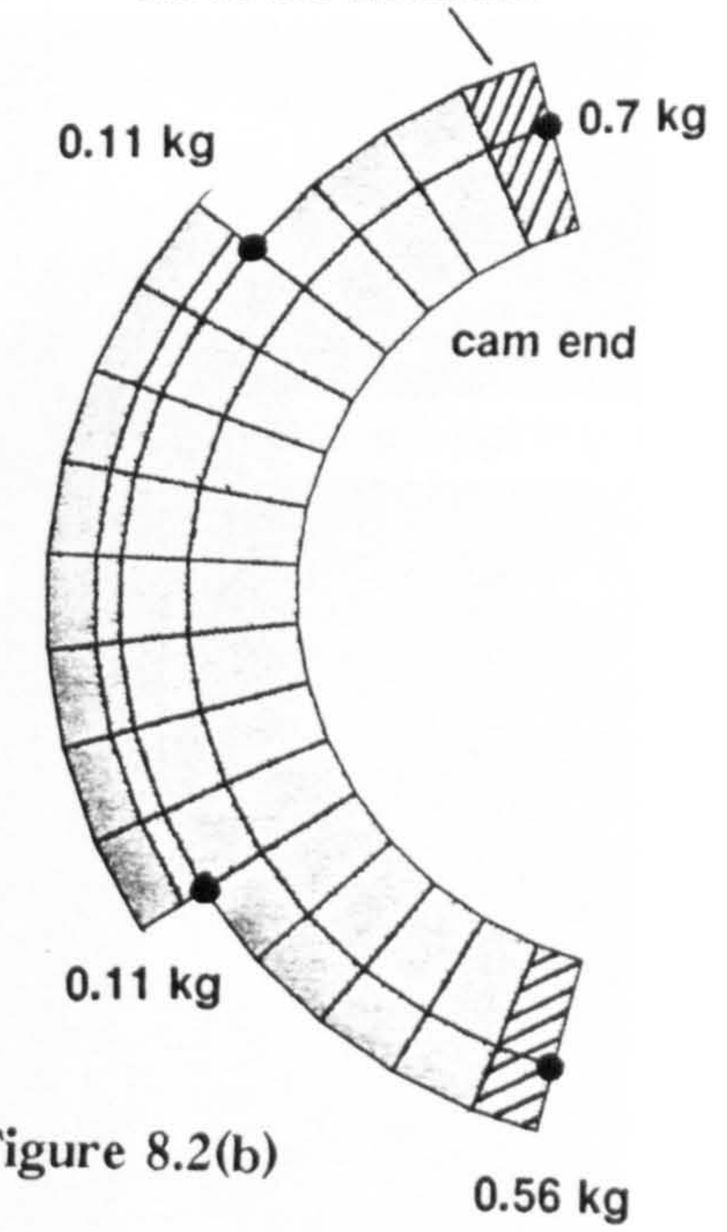

Figure 8.2(b)

Figure 8.2 Idealised brake shoe allowing two-dimensional finite element representation using elements of different thickness for the web and platform. Discrete masses are used to simulate stiffenning webs and reinforcement of the shoe tips

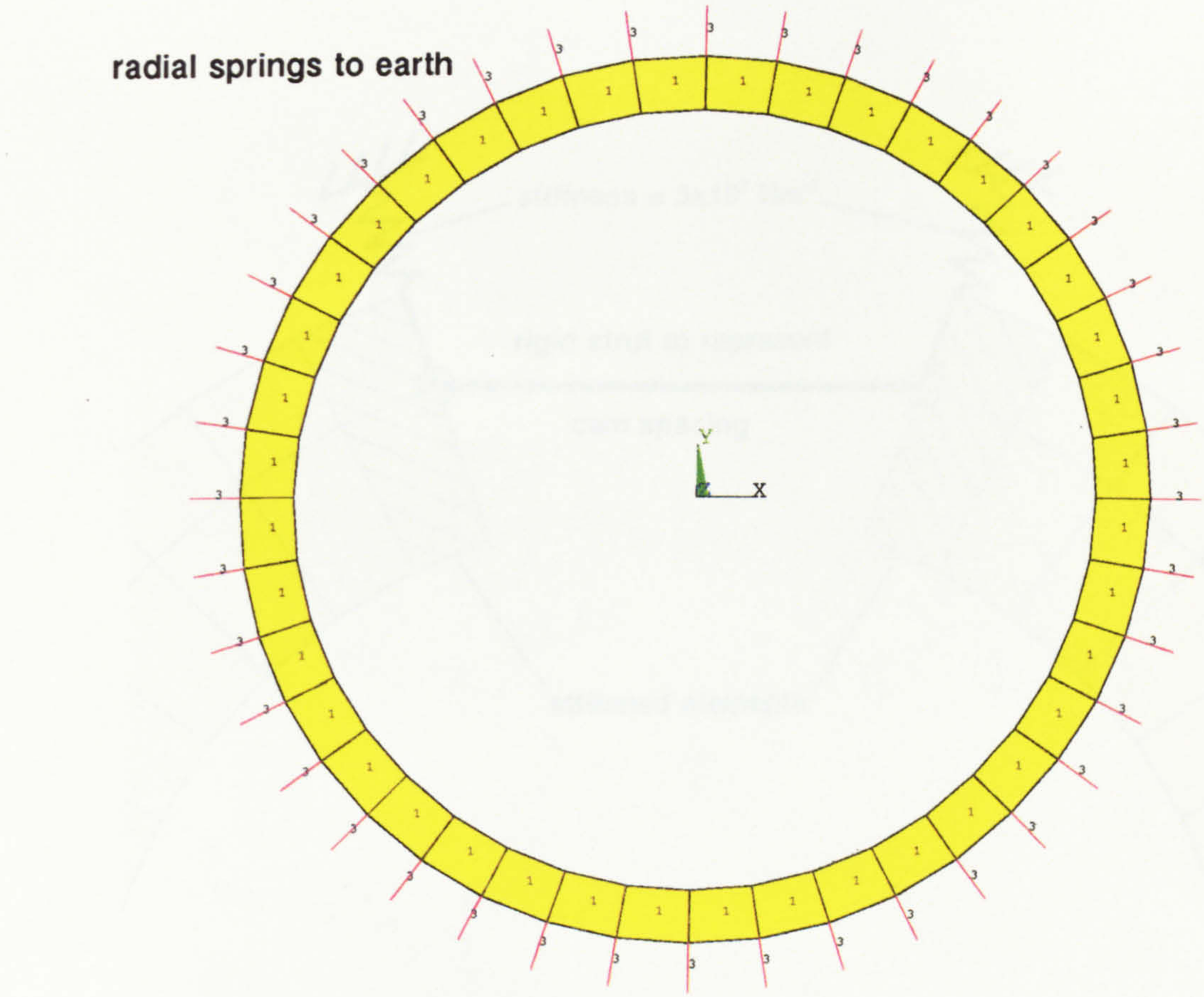

Figure 8.3 Two dimensional idealisation of the brake drum

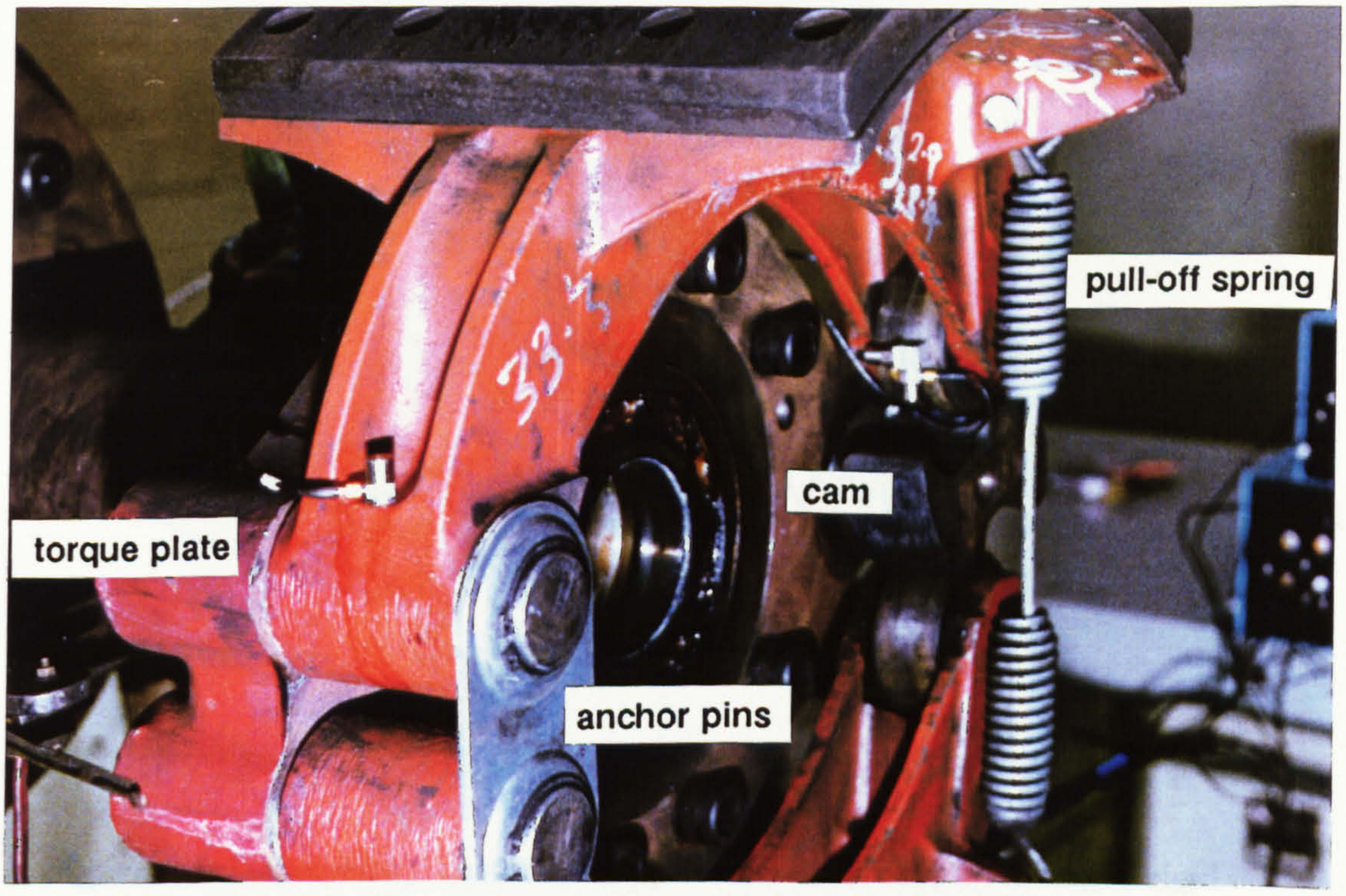

Figure 8.4 The brake shoes mounted on the torque plate showing the anchor pin pivot points and the 'S' cam between the cam rollers

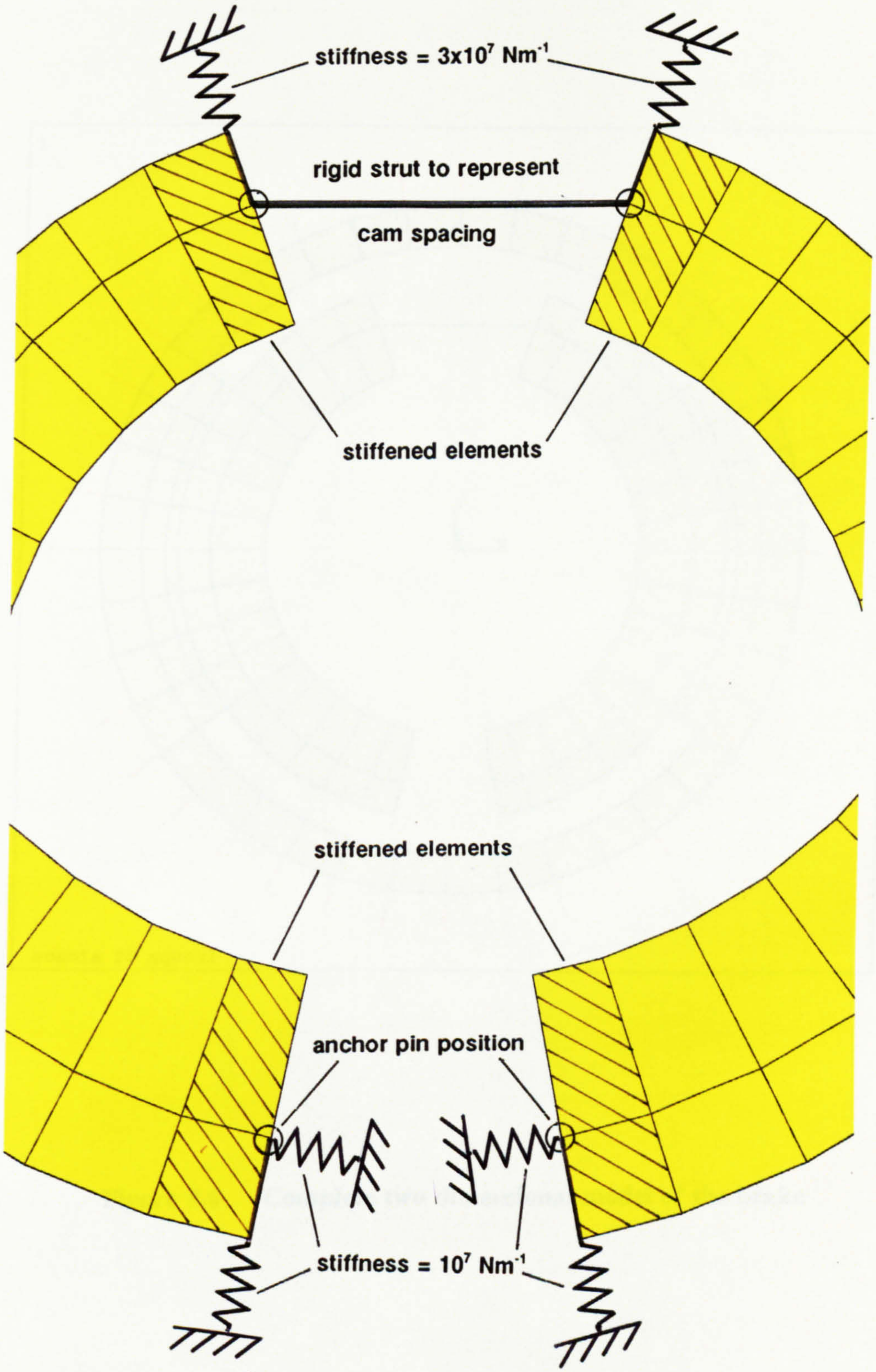

Figure 8.5 **Boundary conditions applied to the shoes, including a rigid strut to couple the motion of this cam ends of the shoes in the tangential direction, representing the effect of the cam. The anchor pins are constrained to move together in the tangential direction as they are linked on the brake**

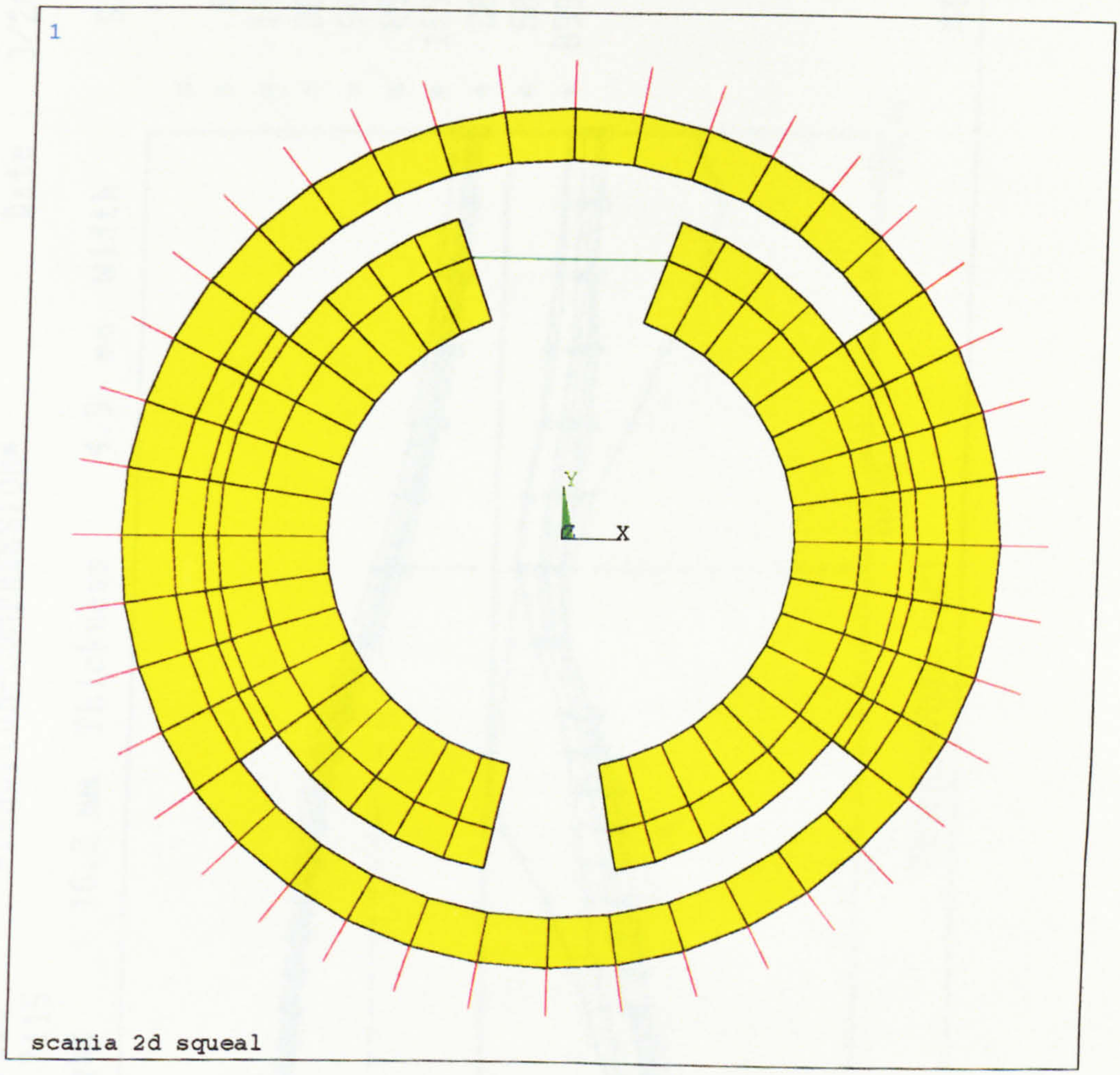

Figure 8.6 Complete two dimensional model of the brake

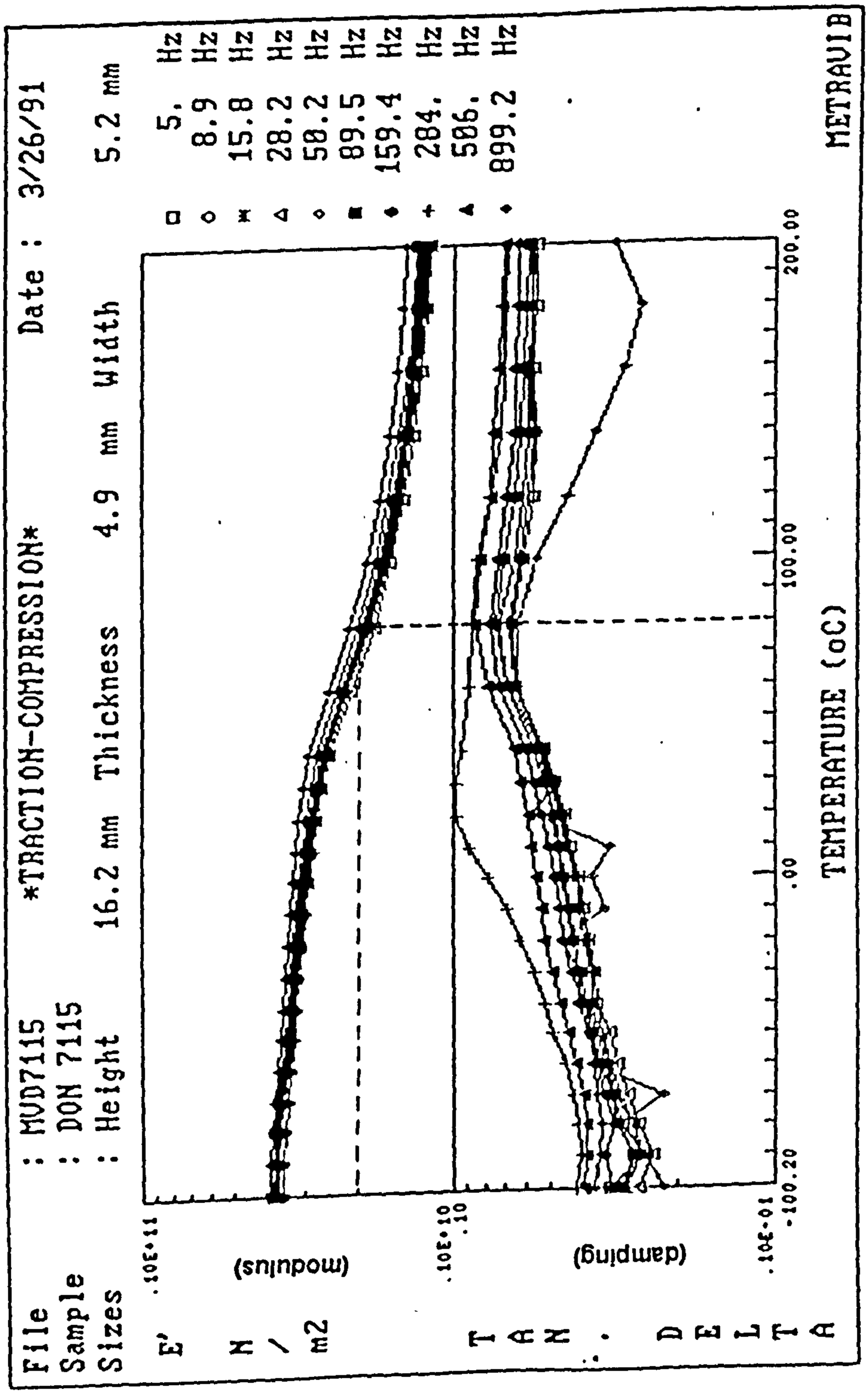

Figure 8.7 **The dynamic elastic modulus characteristic of the friction material (Don 7115), measured in a direction normal to the friction surface using a Metravib viscoanalyser.**

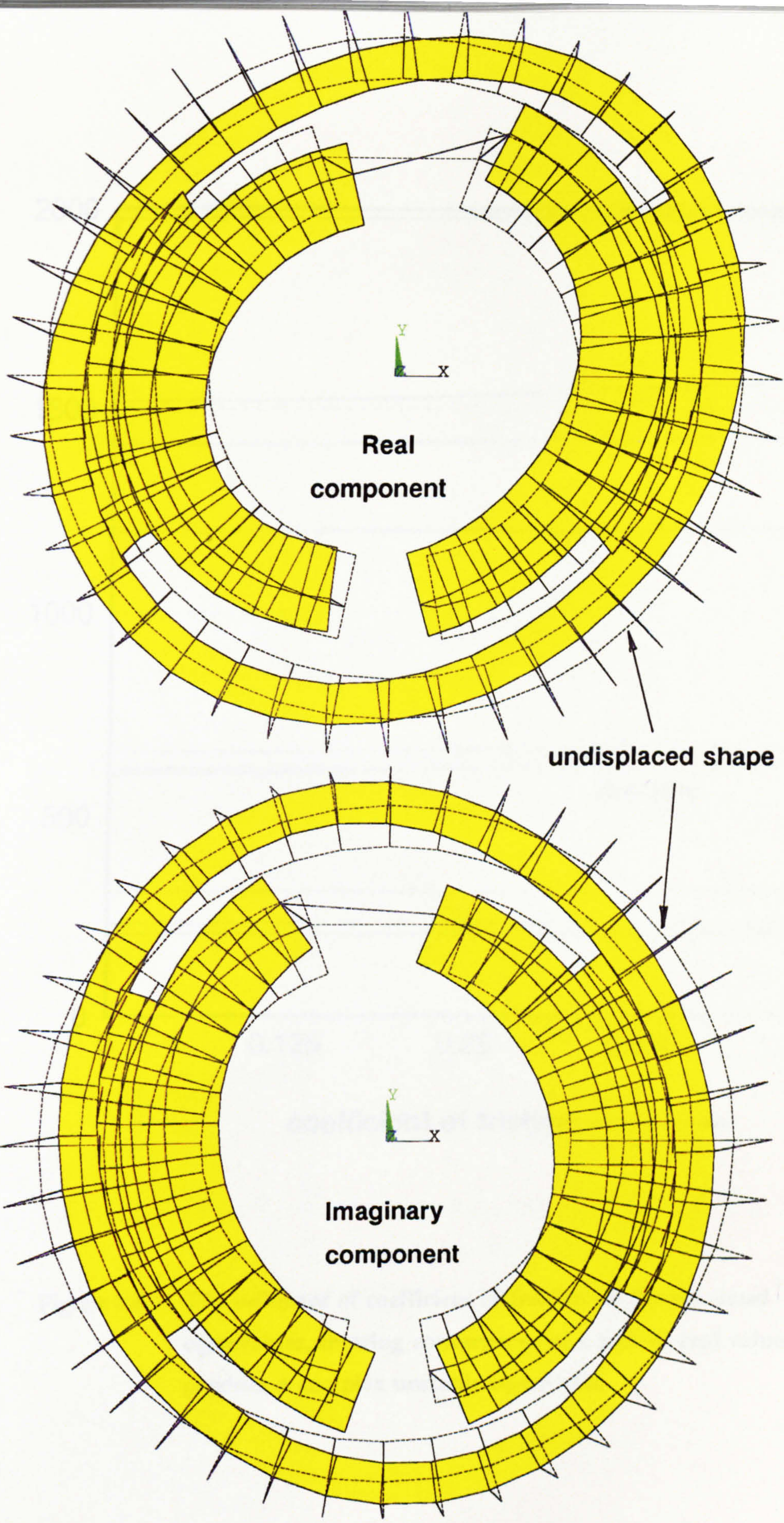

Figure 8.8 **The complex mode shape of the brake associated with the squeal instability at 609Hz**

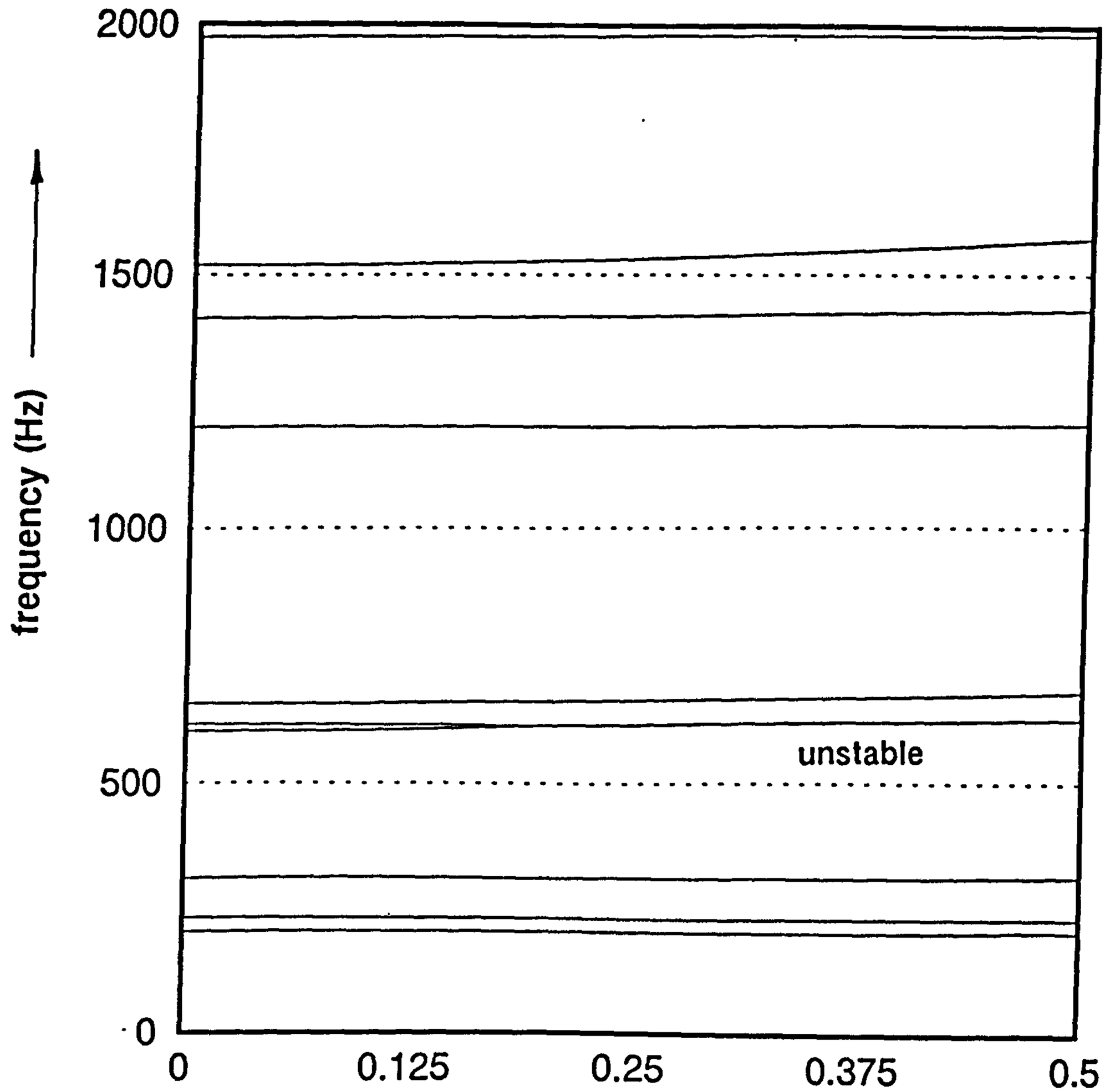

Figure 8.9 **The influence of coefficient of friction on the predicted eigenvalues, showing convergence of a pair of real values to produce a complex unstable eigenvalue.**

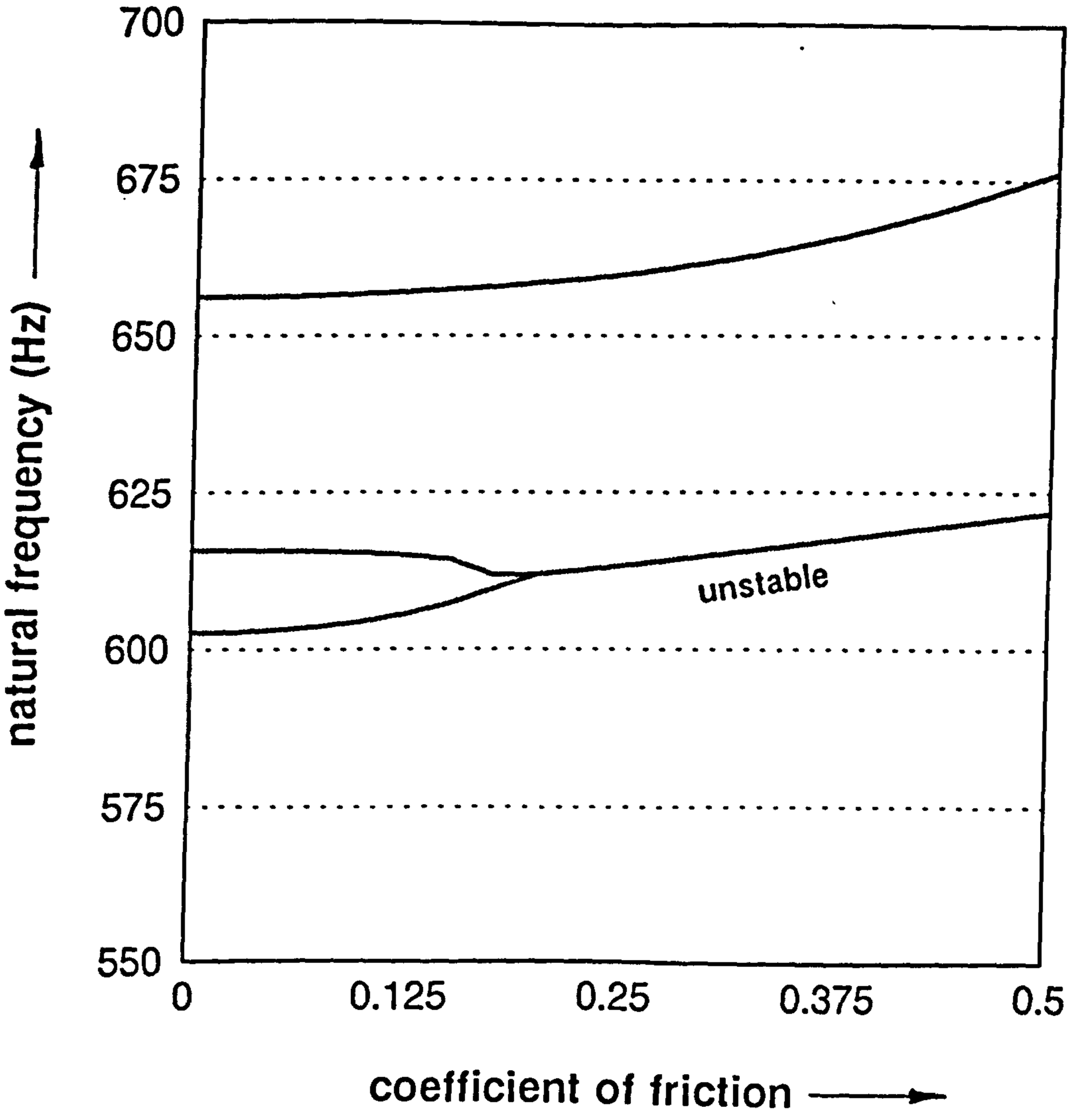

Figure 8.10 **Detail of fig 8.9 in the region of the squeal frequency, showing the convergence of a pair of real eigenvalues to produce a complex unstable eigenvalue**

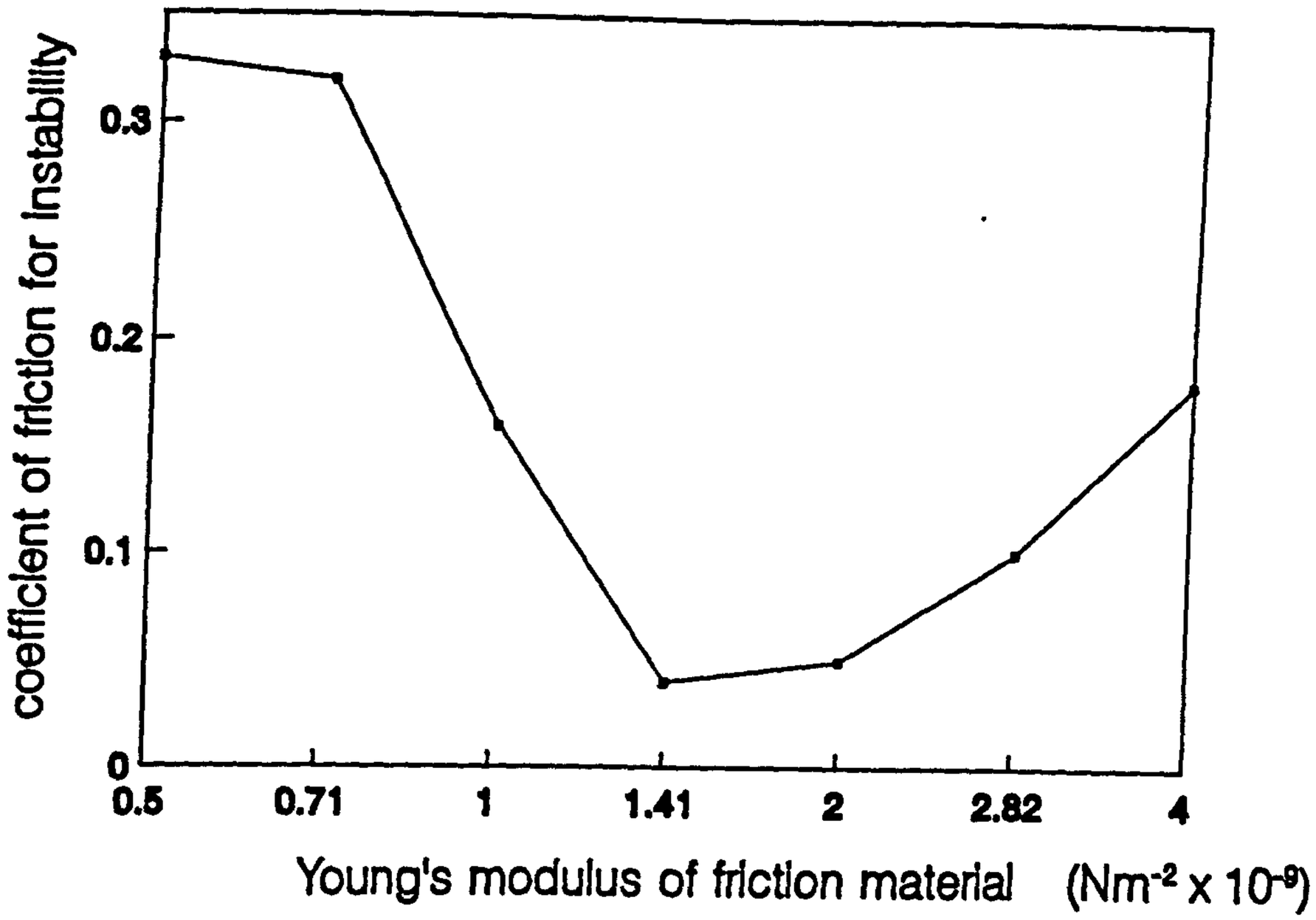

Figure 8.11 **The influence of friction material modulus on the stability of the model. The brake is taken to be more stable if a greater value of friction coefficient is required for instability to occur**

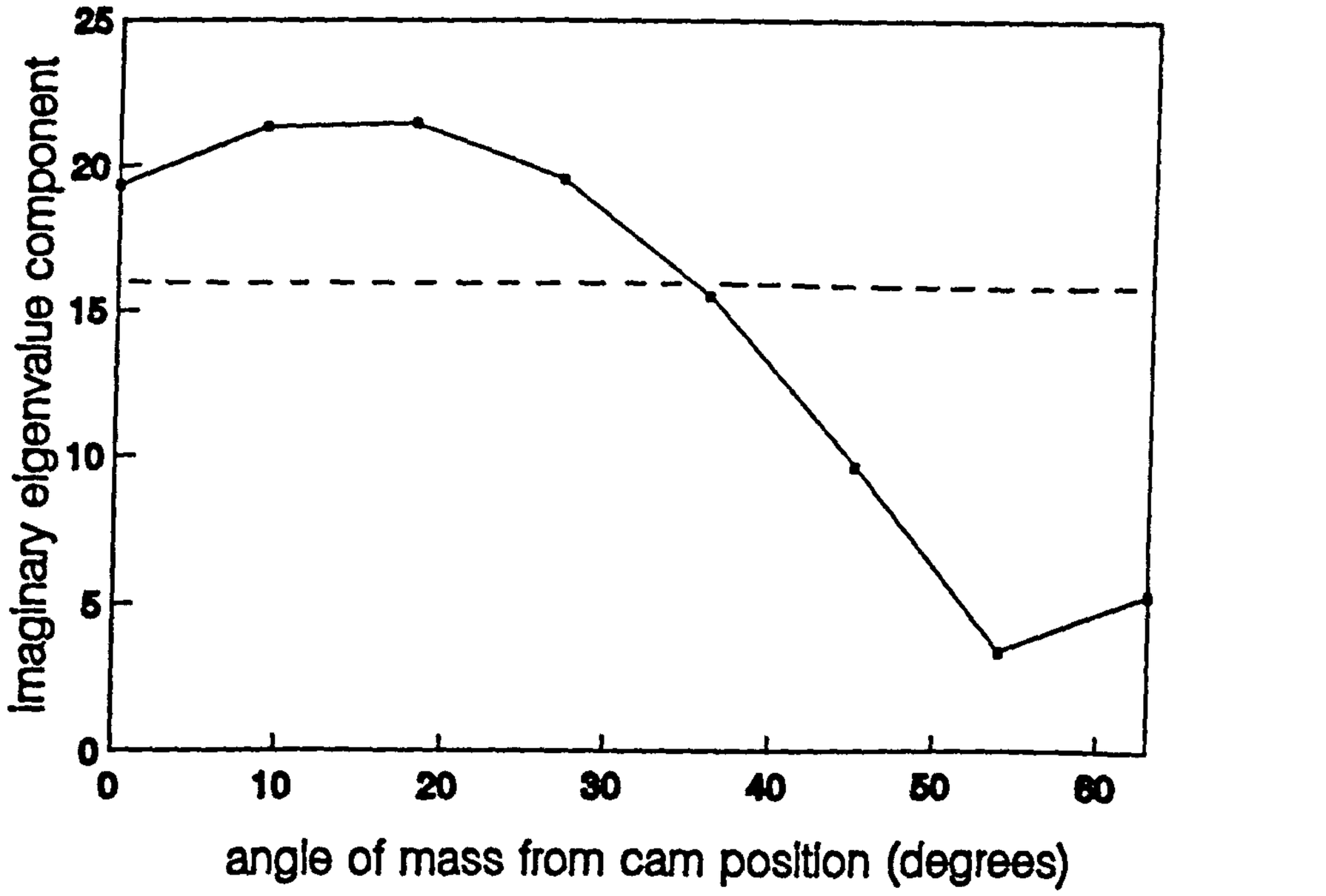

Figure 8.12 **The cyclic effect on stability due to 2x2kg masses attached to the drum and rotating with it ($E_f = 2x10^9$ Nm^{-2})**

CHAPTER 9

SUMMARY, CONCLUSIONS AND RECOMMENDATIONS

9.1 Summary

A survey of the large body of previous work on brake squeal indicated that proposed mechanisms for the phenomenon generally fall into one of three categories:-

i) instabilities due to a decrease in friction coefficient with increasing sliding velocity

ii) pin-disc or kinematic constraint instabilities

iii) binary flutter type instabilities.

and that each type of instability involves distinct types of motion of the brake system components. In particular, binary flutter involves the coupling of two similar brake rotor modes, whereas the pin-disc mechanisms presuppose only a single rotor mode. The μ-velocity mechanism needs no flexural rotor motion for instability, but is clearly relevant to some low frequency brake vibration problems.

The initial aim of this work was to assess the applicability of these proposed mechanism to a typical brake squeal problem by detailed measurement of the vibration characteristics of the drum and shoes during squeal. A large heavy vehicle drum brake was chosen for this purpose because of the increasing significance of noise pollution from these brakes, together with the relative absence of practical palliatives.

The brake chosen for the investigation, a 412mm diameter x 200mm wide air operated 'S' cam drum brake, was found to squeal at a frequency of approximately 600Hz, a squeal frequency region common to many brakes used on heavy vehicles. Testing this brake on a dynamometer braking simulation rig produced squeal with similar characteristics to those on a vehicle, thus allowing subsequent experimental work to be carried out in a controlled environment, with good physical access.

Normal modal analysis of the brake shoes and drum showed poor correlation with the squeal characteristics and even the statically activated brake system natural frequencies,although closer to the squeal frequency, were not identical with it. These observations reinforced the necessity for carrying out modal analysis whilst the brake was actually squealing. Such an analysis could be carried out on the static parts of the brake using standard modal analysis techniques, but the drum, due to its rotation, required the development of a novel modal analysis technique to provide both amplitude and phase characteristics.

The technique developed used accelerometers rotating with the drum to effectively 'scan' the drum mode shape, the amplitude and phase reference for the mode being taken from a stationary accelerometer on the brake shoe. Transfer function analysis between the rotating and static accelerometer signals was carried out at regular angular intervals defined by an angular position sensor, and amplitude and phase distributions were obtained around the drum.

The drum mode was found to be a complex mode which could be described as either a rotating wave around the drum, or the superposition of two similar normal modes, stationary relative to the shoes, but phase shifted both spatially and in time relative to each other. This latter description correlated well with the rotor motion

characteristics predicted by binary flutter type mechanisms of instability. Similar modal analysis on other brakes suggested that this type of complex mode is a common feature of 'mainstream' brake squeal implying that 'pin-disc' mechanisms, which do not require such complex rotor modes for instability, are unrepresentative of the behaviour of actual brake assemblies.

The observed stationary nature of the component modes of the drum, together with constant squeal frequency, implies that the rotational symmetry of the drum plays an important part in the squeal mechanism. A less rotationally symmetric drum would either cause the mode to rotate with it or produce a cyclic frequency change in the noise. Using a simple 2 degree of freedom flutter model, it was shown that reducing the symmetry of the rotor decoupled the flutter modes and potentially increased dynamic stability. Further analysis showed that, in practice, decoupling could be achieved by attaching discrete equispaced masses around the drum periphery, so long as the number of masses is an integral divisor of the numbers of axial modal lines across the drum. The stabilising effect of this decoupling was confirmed by experiment, reducing or eliminating squeal on not only 'S' cam brakes but also a variety of other types and sizes of drum brake installation. Practical aspects of modifying drum rotational symmetry in the design of the drum have been examined using finite element modelling. The simple binary flutter model was now used to show that the influence of rotor symmetry on squeal is part of a more general symmetry effect in the brake system as a whole. Due to the loading of the shoes on the drum, the brake system exhibits pairs of modes corresponding to each type of drum mode shape, and it is shown that frictional forces can cause these modes to converge and coalesce to produce complex squeal modes. The initial separation of these modes and their rate of convergence with friction coefficient have been shown

to depend on brake design parameters, suggesting the potential for the elimination of squeal problems at the brake design stage.

It is clear, however, that brake design to avoid squeal requires much more detailed models of the brake structure than have been considered previously and so the measured squeal modal characteristics and the flutter mechanism have been combined to produce a 2-dimensional ANSYS finite element model of the brake, incorporating many of the brake design parameters. Frictional interface elements have been designed to reproduce the conditions in the flutter model, and a complex eigenvalue analysis carried out to predict dynamic stability. The model showed convergence and coalescence of pairs of system modes with increase of friction coefficient similar to that obtained with the simple binary flutter model. It also correlated well with the observed behaviour of the squealing brake in terms of frequency, mode shape, and the effect of drum asymmetry, and it is believed that such a model may form the basis for the design of all types of brakes in the future.

9.2 Conclusions and Relationship to Other Current Work

As would be expected, investigation into brake squeal has continued by other workers in parallel with that reported here, both independently and in the form of collaborations born of this work. Where these are related to the subject of this thesis, they will be discussed in the following conclusions, and in recommendations for further work.

9.2.1 No simple relationship exists between the natural frequencies of the brake components and the squeal frequency. This is a significant result as it indicates

that one current approach to obtaining a 'fix' to eliminate squeal based upon identifying and modifying frequency coincidences may have limited success.

9.2.2 During squeal both the drum and shoes hold complex modes, which can be best visualised as the superposition of pairs of similar normal modes phase shifted both spatially and in time relative to each other. The drum complex component modes are stationary relative to the shoes and hence the drum rotates through them. Fieldhouse and Newcomb (33) have inferred, from holographic analysis of a squealing disc brake, that travelling waves consistent with this complex modal behaviour are also present on the brake disc, an observation supported by initial application of the 'scanning' modal analysis technique to a brake disc by Lang and Newcomb (44). Further, Mottershead and Chan (45) have recently produced a simplified finite element model of a brake disc to which they applied 'follower forces' representing the pad interface friction, and complex eigenvalue analysis resulted in complex modes almost identical in form to these measured experimentally here.

9.2.3 The measured complex drum mode is consistent with the binary flutter mechanism of brake squeal, which involves 2 degree of freedom rotor motion, as opposed to the pin-disc mechanisms of instability, which require only single degree of freedom rotor motion at the point of contact.

9.2.4 The rotational symmetry of the brake drum is a prerequisite for the presence of stationary mode components with constant frequency, and standard flutter models make use of this symmetry in predicting instability. Reducing this symmetry in a flutter model can increase its stability, and a means of achieving this is by attaching equispaced masses to its periphery. If the number of masses is an integral divisor of the number of axial nodal lines in the drum mode, and the total mass is

large enough to decouple the flutter modes it has been established that squeal is reduced or eliminated entirely. Nishiwaki, Harade, Okamura and Ikeuchi (34) came to a similar conclusion through their concept of forcing rotation of the modes with the disc and thus not allowing the maintenance of constant dynamic conditions at the friction interface, rather than on the basis of decoupling of flutter modes. They achieved significant noise reduction by eliminating six vanes from a ventilated disc.

9.2.5 The measured drum and shoe modes are essentially of a 2-dimensional form, involving no phase shift across the drum rubbing path nor twist of the shoes, suggesting that the instability mechanism is active over the full axial width of the brake rubbing path. This conclusion is particularly important to the modelling of squeal, supporting the basic assumption made by previous workers and justifying the 2-dimensional approach to finite element modelling of squeal in this work.

9.2.6 Pairs of modes of the statically actuated brake involving similar drum mode shapes appear to converge in frequency when frictional forces are introduced at the interface, and can coalesce to produce a single complex mode resulting in squeal. A simple flutter model of the situation suggests that both the static mode frequency separation and the rate of convergence with increasing friction coefficient can influence the occurrence of squeal. Kim (41) has investigated the effect of design parameters on the frequency separation using a finite element model of a heavy vehicle brake similar in size and design to that used in this work. He evaluated the effect of shoe, drum and lining stiffness, of which only the latter influenced the frequency separation significantly, increased stiffness increasing the separation. The decoupling effect of reducing drum symmetry was also confirmed, and had the greatest influence of all the parameters examined.

9.2.7 The frictional coupling forces of the binary flutter mechanism can be included in a finite element model of a brake by incorporating radial spring-like interface elements, having non-symmetric stiffness matrices, between the brake lining and the drum. If these springs are chosen to have a radial stiffness very much greater than the stiffness of the associated area of friction material, the dynamic model results are independent of the actual values chosen.

9.2.8 The essential dynamic features of the squealing brake can be incorporated into a 2-dimensional finite element model on condition that the squeal modes involve only shoe bending and drum diametral modes, as is the case for the brake investigated here. If the 2-dimensional drum and shoe models are adjusted to exhibit similar free natural frequencies and equivalent single degree of freedom masses to those of the real components, and if suitable boundary conditions are imposed, the coupled model is found to predict behaviour similar to that measured from the real brake. In particular, increasing the coefficient of friction causes convergence of certain static system modes to produce a dynamic instability at a fequency approximating to that of the measured brake squeal.

9.2.9 The 2-dimensional finite element model predicts squeal modes having characteristics similar to those measured on the actual brake. The stability of a particular mode can be usefully quantified by either the imaginary part of the eigenvalue, at a fixed friction coefficient, or by the coefficient of friction required for the onset of instability. Using these criteria, reduced symmetry of the drum produced a cyclic modification to the stability, and the tendency to squeal was shown to be significantly influenced by the compressive stiffness of the friction material and the interface. This latter influence, together with that of the friction coefficient, may help to explain the fugitive nature of squeal.

9.3 Recommendations for Further Work

9.3.1 Extension to disc brakes

The work reported in this thesis has been limited, in the main, to large heavy vehicle drum brakes, with some limited results from smaller drum brakes which have also been shown to exhibit similar vibration characteristics. Only cursory examination of disc brake characteristics has been carried out using the rotor modal analysis technique, however (Lang and Newcomb (44)), and whilst this, together with holographic analysis by Fieldhouse and Newcomb (33), suggests that similar types of wavelike complex stationary modes are present on the non-loaded portion of the disc, the loading effect of the pads appears to significantly modify the local disc motion. The resulting non-uniformity of the wavelike modes may well influence the effect of rotor asymmetry as a means of eliminating noise, and it is suggested that detailed modal analyses of squealing disc brakes are carried out if such an approach is to be optimised for this application.

If the measured disc and pad modes show essentially 2-dimensional behaviour, it should, in principle, be possible to construct a 2-dimensional finite element idealisation of a disc brake, by treating the disc as a uniform beam representing a development of the disc rubbing path. The ends of the beam could be effectively joined by the use of nodal coupling in the finite element code, thus simulating the dynamic behaviour of the annular rubbing path. Again, the natural frequency and mass of the required mode could be simulated as described for the 2-dimensional drum model. The result of an initial trial of this technique is shown in fig 9.1, where the normal mode natural frequencies up to 10 kHz were found to be in acceptable agreement with the actual disc modes involving diametral modes only.

9.3.2 3-dimensional finite element modelling

Although the simplified 2-dimensional brake model described here could be used to indicate major design modifications to reduce squeal, it clearly has limitations as a true design tool as the dynamics can only be optimised for a small number of modes at best. If the whole range of potential squeal problems is to be addressed, more detailed 3-dimensional model would be necessary, with the associated computing time penalty. It is possible, however, that the computing time problem may be eased by taking a more structured approach to evaluating the effects of parameter variations, such as the use of sensitivity analysis applied by Brooks et al (46) to a very comprehensive lumped parameter disc brake model.

9.3.3 Improved friction material modelling

The material of the brake lining has been represented in the finite element model as a homogeneous, isotropic material, which it is not, due to the raw materials and manufacturing process used. In particular, the fibrous content, together with the uniaxial compression of a relitively low density mix of the raw materials produces a high degree of orthotropy in the product. Experimental work on the influence of friction materials on squeal by Borchert (47) has suggested that the orthotropic modulus properties of the material can be significant and it is therefore suggested that such properties be incorporated in future stability models as a means of potentially designing friction materials themselves to reduce squeal.

The finite element model is also based on the assumption of having initially perfectly uniform contact between the brake lining and drum. This is not the case in practice

as variable service conditions produce variable lining wear profiles, and, under some conditions, extremely non-uniform circumferential contact such as 'crown' contact (near the centre of the lining) or leading and trailing end contact are thought to be possible. Unfortunately, no direct method of measurement of contact pressure distribution is available, and current finite element models can only predict pressure distributions for short periods after well-defined initial conditions. Even with relatively uniform circumferential contact, local variations in pressure distribution will influence the stiffness of contact to the drum, and it is clear from the modelling in chapter 8 that this stiffness can have a very significant influence on dynamic stability. Such non-uniform contact effects, both geometrical and in terms of contact stiffness, may partly explain the fugitive nature of squeal, and, as such, their evaluation in the finite element model may provide information on desirable wear characteristics for friction materials, to minimise geometry variations and maximise contact stiffness.

9.3.4 Incorporating damping into the model

The proposed finite element modelling technique neglects damping, whereas significant damping is clearly present in the structure and materials (particularly the friction material) of real brakes. North (22) incorporated damping in his lumped parameter flutter model and found that it was generally stabilising, and hence for true quantitative evaluation of squeal propensity, damping should be included. This would be particularly valuable when using a model for retrospective noise 'fixing' when applying optimum damping may be the only practicable method allowable.

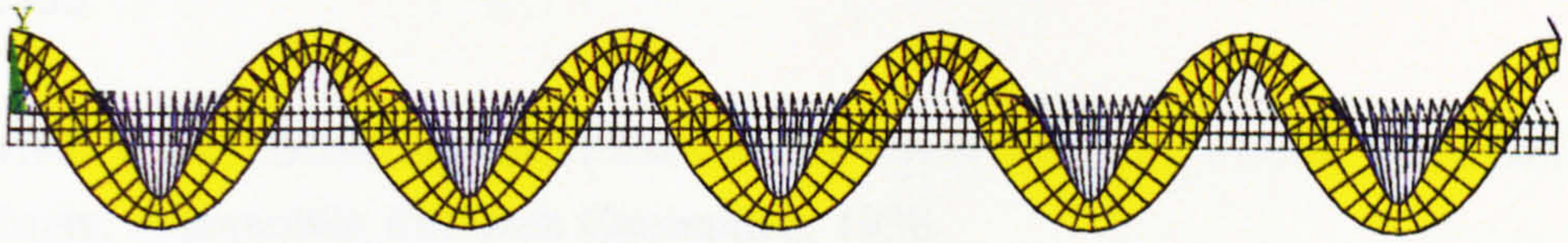

Figure 9.1 A typical mode shape produced from a two-dimensional FE idealisation of a brake disc. The ends of the beam are stiffened locally to avoid distortion of the end element sides, and the ends are then 'joined' by constraining the nodal degrees of freedom to be identical

REFERENCES

(1) **Lamarque P V,** "Brake squeak - the experiences of manufacturers and operators and some preliminary experiments", Inst Auto Engrs, paper 8500B May 1935

(2) **Williams C G,** "Some preliminary experiments on the origin of brake squeak", Report No. 8500B, Inst Auto Engrs, Research and Standardisation Committee, 1935

(3) **Mills H R,** "Brake squeak; First interim report", Report 9000B, Inst Auto Engrs, Automobile Research Committee, 1938

(4) **Fosberry R A C and Holubecki Z,** "An investigation of the cause and nature of brake squeal", MIRA Report No. 1955/2, 1955

(5) **Fosberry R A C and Holubecki Z,** "Interim report on disc brake squeal", MIRA Report No. 1959/4, 1959

(6) **Fosberry R A C and Holubecki Z,** "Disc brake squeal - its mechanism and suppression", MIRA Report No. 1961/2, 1961

(7) **Sinclair D,** "Frictional vibrations", J Appl Mech 1955, pp 207-214

(8) **Basford P R and Twiss S B,** "Properties of friction materials I - Experiments on variables affecting noise", ASME Trans, Vol 80, 1958, pp 402-406

(9) **Basford P R and Twiss S B,** "Properties of friction materials II - Theory of vibration in brakes", ASME Trans, Vol 80, 1958, pp 407-410

(10) **Wagenfuhrer H,** "Bremsgerausche", ATZ, Vol 66, No.8, Aug 1964, pp 217-222 (MIRA Translation No. 15/65)

(11) **Chikamori S,** "Study on brake noise", Journal of Society of Automotive Engineering of Japan, Vol 23, No 2, 1969, pp 120-129

(12) **Spurr R T,** "A theory of brake squeal", I Mech E Auto Div Proc, No.1 1961/64, pp 33-40.

(13) **Spurr R T,** "Brake squeal", Paper C95/71, Symposium on Vibration and Noise in Motor Vehicles, I Mech E and Advanced School of Automobile Engineering, published by I Mech E, July 1971, pp 13-16

(14) **Jarvis R P and Mills B,** "Vibrations induced by dry friction", Proceedings I Mech E, Vol 178, Pt.1, No.32, 1963/64, pp 847-857

(15) **Hales F D,** Communication referring to "Vibrations induced by dry friction" by Jarvis and Mills, Proceedings I Mech E, Vol 178, Pt 1, No 32, 1963-64, pp 860-862

(16) **Crisp J D C,** Communication referring to "Vibrations induced by dry friction" by Jarvis and Mills, Proceedings I Mech E, Vol 178, Pt 1, No 32, 1963-64, pp 857-859

(17) **Earles S W E and Soar G B,** "Squeal noise in disc brakes", Paper C101/71, Joint Symposium on Vibration and Noise in Motor Vehicles, I Mech E and Advanced School of Automobile Engineering, Published by I Mech E, 1971, pp 61-69

(18) **Earles S W E and Lee C K,** "Instabilities arising from the frictional interaction of a pin-disc system resulting in noise generation", Paper No. 75-DET-25. Design Engineering Technical Conference, Washington DC, Sept 1975

(19) **Earles S W E and Badi M N M,** "On the interaction of a two-pin-disc system with reference to the generation of disc brake squeal", SAE Congress and Exposition, Detroit 1978, Ppaper 780331

(20) **Lang A M and Smales H,** "An approach to the solution of disc brake vibration problems", Conference on Braking of Road Vehicles paper C37/83, Proceedings of I Mech E, 1983, pp 223-231

(21) **Gouya M and Nishiwaki M**, "Study on disc brake groan", SAE paper 900007, Congress and Exposition, Detroit, 1990

(22) **North M R**, "Disc brake squeal - a theoretical model", Motor Industries Research Association Research Report No. 1972/5, 1972

(23) **North M R**, "Disc brake squeal", Paper C38/76, I Mech E Conference on Braking of Road Vehicles, 1976, pp 169-176

(24) **Millner N**, "An analysis of disc brake squeal", SAE paper 780332, Detroit, 1978

(25) **Murakami H, Tsunada N and Kitamura T**, "A study concerned with a mechanism of disc brake squeal", SAE paper 841233, 1984

(26) **Millner N**, "A theory of drum brake squeal", I Mech E Conference on Braking of Road Vehicles paper C39/76 1976, pp 177-185

(27) **Millner N**, "A study of the squeal of Drum Brakes", PhD Thesis, University of Leeds, 1976

(28) **Okamara H and Nishiwaki M**, "A study on brake noise (drum brake squeal)", Journal of JSME, Series III, Vol 32, No 2, 1981, pp 206-214

(29) **Susuki V and Ohno H**, "A study on drum brake noise of heavy duty vehicles", SAE Paper 811399, 1981

(30) **Kusano M, Ishidou H, Matsumura S and Washizu S**, "Experimental study on the reduction of drum brake noise", SAE Paper 851465, 1985

(31) **Felske A, Hoppe G and Matthai H**, "Oscillations in squealing disc brakes - analysis of vibration modes by holographic interferometry", SAE paper 780333, Congress and Exposition, Detriot 1978

(32) **Felske A, Hoppe G and Matthai H**, "A study on drum brake noise by holographic vibration analysis", SAE Paper 800221, Detroit, 1980

(33) **Fieldhouse J and Newcomb T P,** "The application of holographic interferometry to the study of disc brake noise", SAE Paper 930805, Congress and Exposition, Detroit, 1993

(34) **Nishiwaki M, Harada H, Okamura H and Ikeuchi T,** "Study on disc brake squeal", SAE paper 890864, Congress and Exposition, Detroit 1989

(35) **Liles G D,** "Analysis of disc brake squeal using finite element method", SAE paper 891150, 1989

(36) **Ghesquiere H,** "Brake squeal noise analysis and prediction", I Mech E, Autotech 1992, paper C389/257

(37) **Rayleigh,** "The Theory of Sound", Second Edition, Vol 1, Revised and Enlarged 1945, Dover Publications, New York, page 360

(38) **Perrin P and Charnley T,** "Group theory and the bell", Journal of Sound and Vibration", 1973, 31(4), pp 411-418

(39) **Newcomb T P and Spurr R T,** "The Braking of Road Vehicles", Chapman and Hall, 1967, page 125

(40) **Schafer D R,** "Ford 350 light truck drum brake noise - Investigation of drum asymmetry by finite element modelling", Mintex Don research report number RES1783, 1993

(41) **Kim S Y,** "A study of the vibration characteristics of an S-cam drum brake using finite element analysis, and its relevance to drum brake noise generating mechanisms and properties", M Phil Thesis, University of Bradford 1993

(42) **Lundström H,** "Analys av bromsskrik med hjälp av finita element metoden", Final degree project report, Technical College of Luleå, Södertälje, Sweden, No.117E, 1990

(43) **Desalvo G J and Gorman R W,** "ANSYS engineering analysis system users manual Revision 4.4", Swanson Analysis Systems Inc, Houston, Pennsylvania, 1989

(44) **Lang A M and Newcomb T P,** "The vibration characteristics of squealing brakes", FISITA 1990, paper 905170

(45) **Mottershead J E and Chan S N,** "Brake squeal - an analysis of symmetry and flutter instability", ASME 1992, DE-Vol 49, pp 87-97

(46) **Brooks P C, Crolla D A and Lang A M,** "Eigenvalue sensitivity analysis applied to disc brake squeal", Conference on Braking of Road Vehicles, paper C444/004/93, Proceedings of I Mech E, 1993, pp 135-143

(47) **Borchert T,** "Comfort optimisation in passenger car disc brake systems", EAEC paper Number 91086, 1991

(48) **Rinsdorf A and Schiffner K,** "Practical evaluation and FEM-Modelling of a squealing disc brake", SAE paper 933071, 11th SAE Brake Colloquium, Florida, 1993

(49) **Matsuzaki M and Izumihara T,** "Brake noise caused by longitudinal vibration of the disc rotor", SAE paper 930804, International Congress and Exposition, Detroit, 1993

(50) **Lang A M and Newcomb T P,** "An experimental investigation into drum brake squeal", Proceedings of EAEC conference on New Developments in Powertrain and Chassis Engineering, Strasbourg, 1989, paper C382/051, pp 431-444

APPENDIX 1

INSTRUMENTATION

1 Accelerometers and signal conditioning

Initial experiments were carried out using low cost type A/04 accelerometers manufactured by D.J.Birchall. These are low mass (2g) adhesive bonded piezo-electric transducers having a relatively low working temperature (170°C) and maximum acceleration, and, due to these limitations, were found to be unreliable in the braking environment, and were therefore replaced by Bruel & Kjaer low mass 'Isoshear' accelerometers having the following specification.

Type	Bruel & Kjaer type 4393
Mass	2.4g
Charge sensitivity	3.1 pC/g +/-2%
Frequency response (to +10dB)	0.1 Hz - 16.5 kHz
Mounted resonant frequency	55 kHz
Maximum temperature	250°C
Attachment	M3 stud

They were attached using B & K UA0867 cement studs and cyanoacrylate adhesive. These are charge generating transducers and the signals were therefore transmitted via low noise coaxial cables to charge amplifiers, having the specification shown overleaf.

Type	D.J.Birchall type CA/04/F
Frequency response	0.03 Hz - 10 kHz +/-3 dB
Gain accuracy	+/- 2%
Output	10mV/g

This combination of accelerometer and charge amplifier was used for all modal analysis work on static components, but measurements from the rotating drum required special consideration.

2 Charge amplifiers for use on the rotating drum

The accelerometers used for the modal analysis are piezo-electric, charge generating devices requiring very high impedance signal conditioning circuitry. The problem of transmitting this charge signal from accelerometers on the rotating drum to stationary instrumentation was first tackled through a pair of capacitor plates on the brake axis, one rotating and one stationary. This proved unsuccessful due to interference from mains radiation in the high impedance circuit. (Such a technique had proved successful in an undergraduate project on rotating disc vibrations, but in a less 'noisy' electrical environment). Slip rings are also generally unsuitable for the very low level, high impedance signals direct from accelerometers, but preamplification and conversion of the signals to low impedance would make slip ring transmission feasible. The standard charge amplifiers used for the other aspects of modal analysis are relatively large and mains powered, and unsuitable for mounting on the rotating drum. As small battery powered amplifiers were not commercially available, these were designed and constructed especially for this application.

A circuit diagram of the charge amplifier is shown in fig A1.1. The circuit consists of a charge to voltage converter followed by a voltage amplifier, both based on low

noise J-FET integrated circuit operational amplifiers. The charge amplifiers were originally designed for use with D.J.Birchall type A/04 accelerometers, having a charge sensitivity of 2.4 pC/g, and thus, for the maximum envisaged acceleration of 100g to produce a 1 volt output, the nominal transfer function required of the charge converter is $4.2x10^{-3}$ V/pC. Due to the very high gain of the operational amplifier, IC1 (106 dB or $2x10^5$), the transfer function of the charge converter, V_1/Q, approximates to the reciprocal of the feedback capacitance (C3), which is thus chosen as 240 pF to give the above transfer function. A second feedback capacitor, C2, can be switched to give $4.2x10^{-4}$ V/pC, allowing for the possibility of accelerations greater than 100g. Resistor R1 is included to introduce a low frequency cut-off of 7 Hz (or 0.7 Hz with C2) to avoid drift due to integration of very low frequency signals.

The voltage amplifier allows the overall sensitivity of the charge amplifier to be increased and adjusted to compensate for variations in accelerometer sensitivity. Its gain is equal to the ratio of the feedback resistance (R2 or R3) to the input resistance (VR1). The three available transfer functions, based on 2.4 pC/g accelerometers, are therefore,

Feedback Capacitor	Feedback Resistor	Transfer Function (g/V)
240 pF	10K	10^{-2}
240 pF	100K	10^{-1}
2400 pF	10K	10^{-3}

To maintain this relationship between switched gains and ensure stability, close tolerance, high stability components were used, ie +/- 1% polystyrene film capacitors and +/- 1% metal film resistors. The calibration was adjusted by setting the gain of the voltage amplifier to suit the quoted sensitivity of the accelerometer being used, and

was confirmed by back to back comparison on a shaker with a second system using a commercial charge amplifier.

3 Signal Recording

The modal analysis technique used on the operating brake required simultaneous recording of several accelerometer and other signals. The recorder used was a magnetic tape recorder employing VHS video tape to allow the simultaneous recording of up to 14 signals, which were recorded in the form of frequency modulated (FM) signals to overcome the inherent frequency response inaccuracies associated with magnetic tape recording. The specification can be summarised briefly as follows:-

Type	TEAC type XR5000
Tape type	VHS video
No of channels	14
Tape Speeds	1.2cms^{-1} to 76cms^{-1}
Frequency response	DC - 625 Hz (1.2cms^{-1})
	DC - 40 kHz (76cms^{-1})

A feature of this type of FM recorder is that the signals can be reproduced at a different playback speed to that used for recording, allowing transient signals, such as those involved in squeal, to be expanded in time by a factor of up to 64 for detailed analysis.

4 Signal Analysis

Both the normal modal analysis and squeal modal analysis techniques require the calculation of the dynamic transfer function between either response and excitation or pairs of spatially separated acceleration measurements, respectively. This transfer

function analysis was carried out using a 2-channel fast fourier transform (FFT) signal analyser briefly specified below.

Type	Scientific Atlanta SD380Z
No. of channels	2
Frequency range (0.5dB)	0 - 40 kHz
Resolution	100/200/400/800 lines
Zoom magnification	up to x256
Dynamic range	>80dB
Real time bandwidth (2ch)	2 kHz
Weighting characteristics	Hanning, flat top, rectangular, force/response, exponential
Averaging	Sum, exponential, peak
Waterfall capacity	200 spectra or transfer functions

An important feature of this analyser in the development of the drum squeal modal analysis technique is the facility for carrying out a type of analysis often referred to as a 'poor man's modal analysis'. In it's usual form in normal modal analysis, the analyser calculates the imaginary component of the transfer function between the response of the structure and an impact excitation force. This is repeated for a range of excitation points around the structure in a well defined sequence eg. at incremental angular positions around a drum, and the imaginary Transfer Function components assembled by the analyser into a waterfall diagram. The analyser can now display a graphical representation of the imaginary components, at the chosen natural frequency, which is a one-dimensional representation of the mode shape of the structure along the line of the sequential impacts. (Note that the imaginary component is used because, for a normal mode, the displacement lags the force by 90° at resonance). If

the path along which the impacts are repeated is simple, the relationship between this one-dimensional representation and the real structural mode shape can be readily interpreted. Fig 3.1 in chapter 3 is an example of such a mode shape.

The same technique can, however, be used for the squeal modal analysis of the drum, with the rotating accelerometer replacing the moving impact point. In this case however, the mode is not normal, but complex and requires both real and imaginary components to define it. The analyser has only a single waterfall file however and so two separate analyses are required for the two components, which can then be superimposed during the graph plotting stage. This clearly requires careful synchronisation of the two analyses to maintain the correct spatial phasing between the two mode components, and this has been achieved by use of an optical angular position encoder as described in chapter 3.

The optical encoder used was a Hohner type 140 absolute position encoder, having an 8-bit binary parallel output, and therefore TTL signals are available ranging from 1 pulse per revolution to 128 pulses per revolution, in binary increments. In practice, for the modal analysis method described in chapter 3, only the 1ppr and 128ppr signals were used, but during earlier development work, before the waterfall triggering facility was available, all channels were used with a digital to analogue converter to produce an analogue voltage proportional to the drum angular position, which could then be used to correct for the drum deceleration.

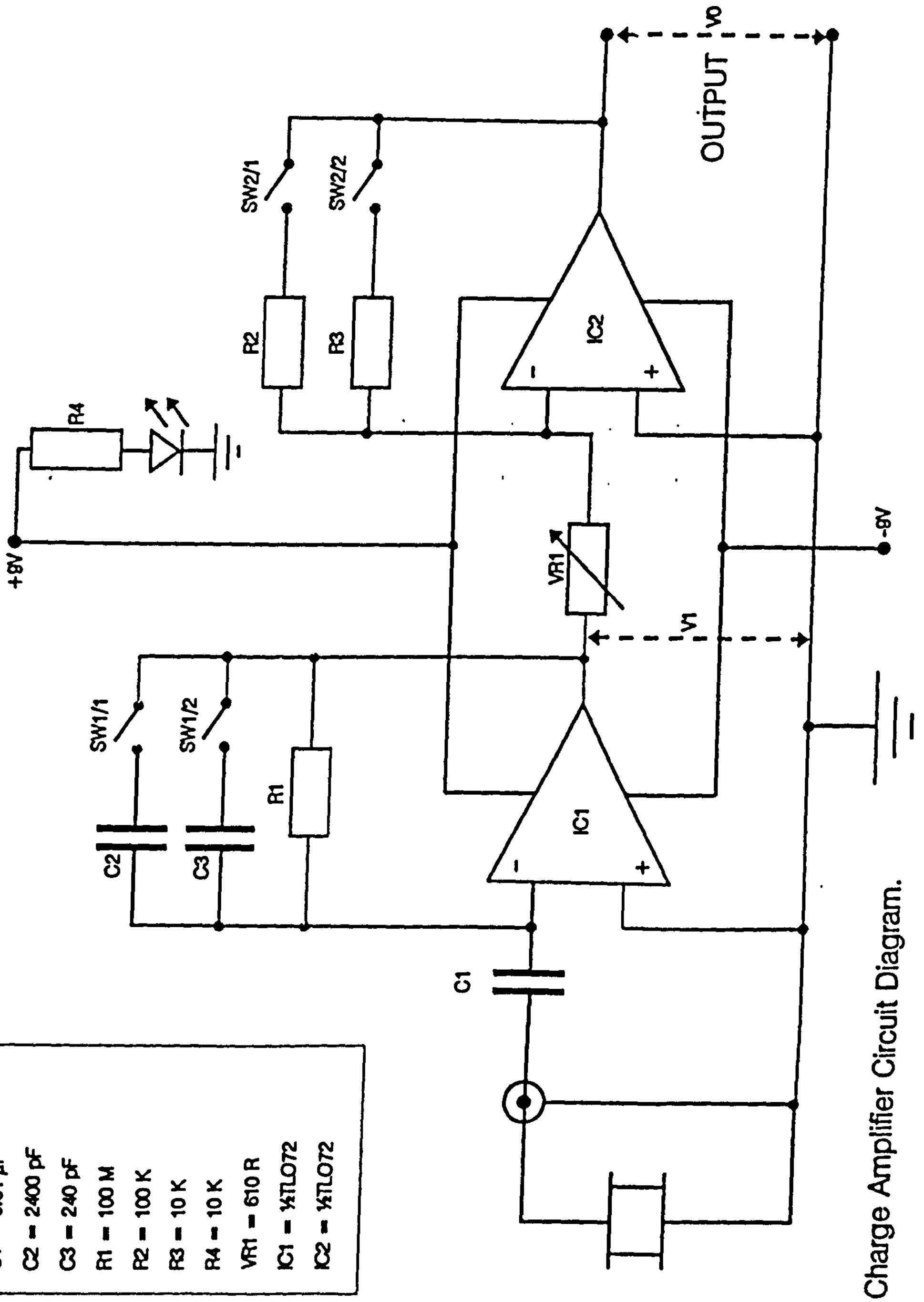

Charge Amplifier Circuit Diagram.

Figure A1.1 Charge amplifier circuit diagram

APPENDIX 2

THE CONDITION FOR INSTABILITY OF THE BINARY FLUTTER MODEL

The eigenvalues from the binary flutter model, discussed in chapter 5, take the following form

$$\lambda = \pm\frac{1}{\sqrt{2}}\left(-(a+d) \pm \sqrt{(a+d)^2 - 4(ad-bc)}\right)^{\frac{1}{2}} \tag{A1-1}$$

substituting

$$u = -(a+d) \tag{A1-2}$$

$$v = (a+d)^2 - 4(ad-bc) \tag{A1-3}$$

then

$$\lambda = \pm\frac{1}{\sqrt{2}}(u \pm \sqrt{v})^{\frac{1}{2}} \tag{A1-4}$$

Considering first the condition $v<0$, which implies that

$$\sqrt{v} = \pm i\sqrt{|v|} \tag{A1-5}$$

and the eigenvalues become

$$\lambda = \pm\frac{1}{\sqrt{2}}(u \pm i\sqrt{|v|})^{\frac{1}{2}} \tag{A1-6}$$

Using DeMoivre's theorem

$$\pm\frac{1}{\sqrt{2}}(u \pm i\sqrt{|v|})^{\frac{1}{2}} = \pm\frac{1}{\sqrt{2}}(r\,(\cos\theta \pm i\sin\theta))^{\frac{1}{2}}$$

$$= \pm\sqrt{\frac{r}{2}}\left(\cos\frac{\theta}{2} \pm i\sin\frac{\theta}{2}\right) \qquad \text{(A1-7)}$$

$$= \pm(p \pm iq)$$

where

$$p = \sqrt{\frac{r}{2}}\cos\frac{\theta}{2} \qquad q = \sqrt{\frac{r}{2}}\sin\frac{\theta}{2} \qquad \text{(A1-8)}$$

The eigenvalues thus take the form of two complex conjugate pairs,

$$\begin{aligned} \lambda_1 &= +p + iq \\ \lambda_2 &= +p - iq \\ \lambda_3 &= -p + iq \\ \lambda_4 &= -p - iq \end{aligned} \qquad \text{(A1-9)}$$

If p is positive, λ_1 and λ_2 have positive real parts and hence describe unstable oscillation, while λ_3 and λ_4 describe damped oscillation. If, however, p is negative, λ_3 and λ_4 describe unstable oscillation so that for only non-zero values of p, unstable modes are present. This confirms that $v<0$ always produces unstable modes.

Consider now the condition $v\geq 0$, which implies that

$$\sqrt{v} = \pm\sqrt{|v|} \qquad \text{(A1-10)}$$

and the eigenvalues become

$$\lambda = \pm \frac{1}{\sqrt{2}} \left(u \pm \sqrt{|v|}\right)^{\frac{1}{2}} \qquad \text{(A1-11)}$$

If $u > \sqrt{|v|}$, the values of λ are real and no oscillation occurs.

If $u < \sqrt{|v|}$, the values of λ are imaginary and stable, constant amplitude oscillation occurs.

Thus for $v \geq 0$ no unstable oscillation occurs.

Hence, the condition for unstable oscillation is that $v < 0$, or

$$4(ad - bc) > (a + d)^2 \qquad \text{(A1-12)}$$

APPENDIX 3

THE SQUEAL FREQUENCY IN THE BINARY FLUTTER MODEL

Equation 7-8 in chapter 7 gives the eigenvalues of the binary flutter model

$$\lambda^2 = \frac{1}{2}\left(\omega_{st}^2 + \omega_{sr}^2 \pm \sqrt{\left(\omega_{st}^2 - \omega_{sr}^2\right)^2 - K^2\mu^2}\right) \qquad \text{(A3-1)}$$

putting

$$\begin{aligned} 2u &= \omega_{st}^2 + \omega_{sr}^2 \\ 2v &= \left(\omega_{st}^2 - \omega_{sr}^2\right)^2 - K^2\mu^2 \end{aligned} \qquad \text{(A3-2)}$$

then

$$\lambda^2 = u \pm \sqrt{v} \qquad \text{(A3-3)}$$

Using DeMoivre's theorem

$$\lambda^2 = r(\cos\theta \pm i\sin\theta) \qquad \text{(A3-4)}$$

$$\rightarrow \quad \lambda = \sqrt{r}\left(\cos\frac{\theta}{2} \pm i\sin\frac{\theta}{2}\right) \qquad \text{(A3-5)}$$

where $r^2 = u^2 + v^2$ and $\theta = \tan^{-1}v/u$

Hence the frequency of unstable oscillation (the squeal frequency) is given by

$\omega = \sqrt{r}\cos\theta/2$, or

$$\omega = \frac{1}{\sqrt{2}}\left[\left(\omega_{st}^2 + \omega_{sr}^2\right)^2 + \left(\left(\omega_{st}^2 - \omega_{sr}^2\right)^2 - K^2\mu^2\right)^2\right]^{\frac{1}{4}} \cos\left[\frac{1}{2}\tan^{-1}\left(\frac{\left(\omega_{st}^2 - \omega_{sr}^2\right)^2 - K^2\omega^2}{\omega_{st}^2 + \omega_{sr}^2}\right)\right]$$

(A3-6)

APPENDIX 4

RESULTS OF CAM AND ANCHOR MOTION ANALYSIS

The following table gives the transfer functions at various positions around the regions of the cam, cam rollers and anchors, relative to the reference point (position 1) used throughout the experimental work. The positions are identified in fig A4.1.

Position	Magnitude	Measured ϕ	Corrected ϕ
5	.113	41	41
6	.105	50	50
7	.227	-144	-144
8	.052	-113	-113
9	.546	2	2
10	.606	167	-13
11	.512	-110	70
12	.359	-48	132
13	.843	-2	2
15	.391	-49	131
16	.765	-173	7
17	.653	178	-2
19	.371	68	-112
20	1.005	17	-163
21	.261	108	108

The phase values are corrected for the direction of measurement, the reference directions being radially towards the centre and tangentially anticlockwise.
Note that positions 14 and 18 are omitted because of suspect measurements.

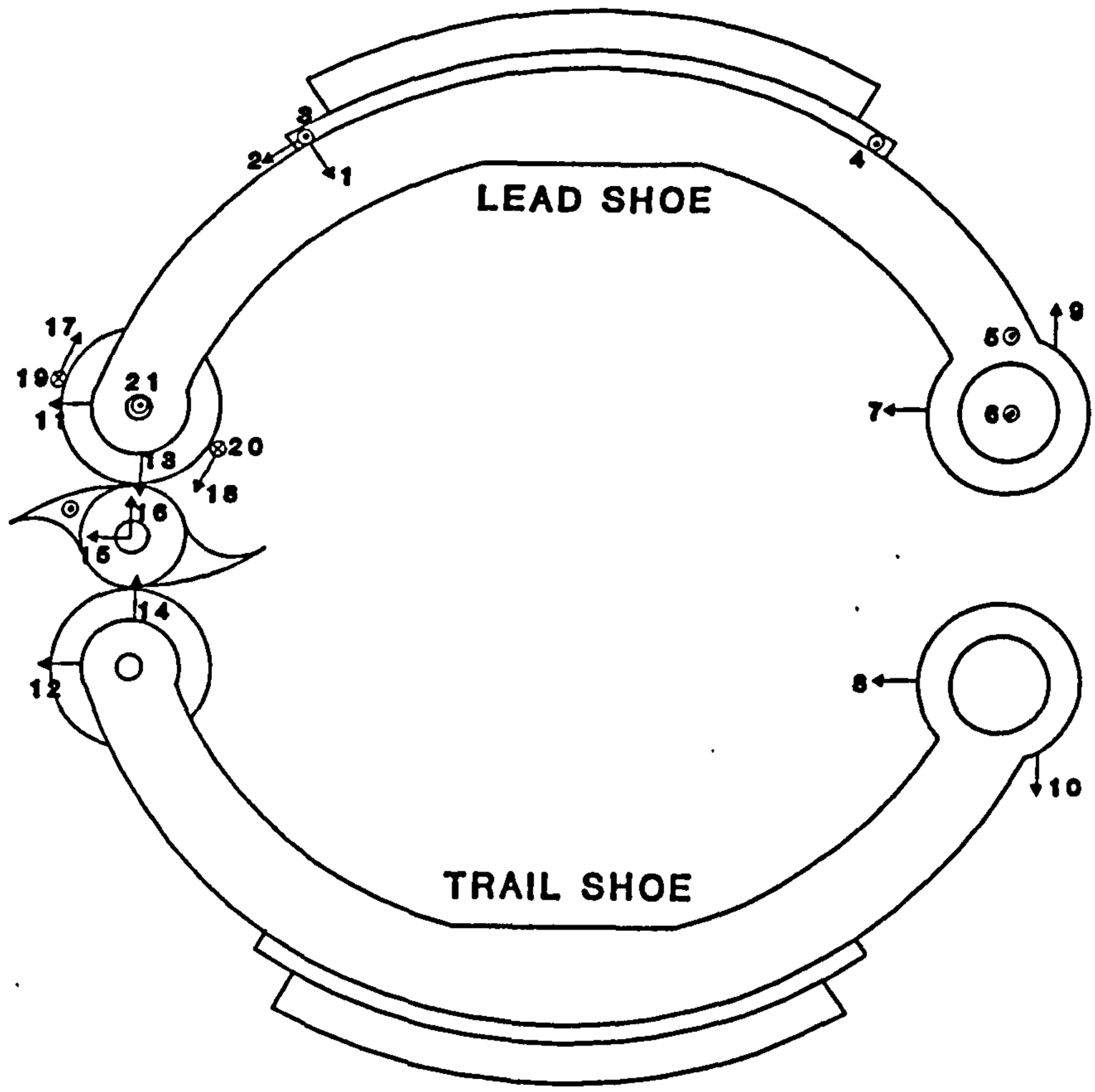

Figure A4.1 **The positions of the accelerometers used to examine the motion of the cam, rollers and anchor pins during squeal**

APPENDIX 5

LISTING OF ANSYS DATA FILE FOR 2-D BRAKE FEM

```
/title, scania 2d squeal model
save
! define element types
et,1,42,0,0,3
et,2,27,0,1,4
et,3,14,0,1
et,4,14,0,2
et,5,21,,,4
et,6,1
et,7,21,,,0
! material properties
! shoe cast iron
mp,ex,1,180e9
mp,nuxy,1,0.17
mp,dens,1,7200
! friction material
mp,ex,2,2e9
mp,nuxy,2,0.45
mp,dens,2,2000
! drum cast iron
mp,ex,3,1.25e11
mp,nuxy,3,0.25
mp,dens,3,6100
! thickened shoe ends
mp,ex,4,700e9
mp,nuxy,4,0.17
mp,dens,4,7300
! element thicknesses
! platform
r,1,0.2
! web
r,2,0.015
! cylindrical coordinate system
csys,0
local,11,1,0,0,0,90,0,0
! define stif27 matrix
! interface stiffness
k=1e12
! friction coefficient
m=0.4
*create,rdef,mac
r,arg1,k,0,0,0,0,0
rmore,-k,0,0,0,0,0
rmore,0,0,0,0,0,-m*k
rmore,0,0,0,0,0,0
rmore,0,0,0,0,0,0
rmore,0,0,0,0,0,0
rmore,0,0,0,0,0,0
rmore,0,0,0,k,0,0
rmore,0,0,0,0,0,0
rmore,0,0,0,0,0,0
rmore,0,0,0,0,0,0
rmore,m*k,0,0,0,0,0
rmore,0,0,0,0,0,0
rmore,0,0,0,-k,0,0
rmore,0,0,0,-m*k,0,0
rmore,0,0,0,0,0,0
rmore;0,0,0,0,0,0
rmore,0,0,0,0,0,0
rmore,0,0,0,0,0,0
rmore,0,0,0,0,0,0
rmore,0,0,0,0,0,0
rmore,0,0,0,0,0,0
*end
rdef,3
! define nodes
! drum
n,10,0.206,0,0
n,50,0.234,0,0
ngen,40,1,10,50,40,0,9,0
! leading block
n,116,0.206,54,0
n,166,0.190,54,0
ngen,9,1,116,166,50,0,9,0
! trailing block
n,136,0.206,234,0
n,186,0.190,234,0
ngen,9,1,136,186,50,0,9,0
! leading shoe
n,213,0.182,27,0
n,263,0.160,27,0
n,313,0.124,27,0
ngen,16,1,213,313,50,0,9,0
n,212,0.182,19,0
n,262,0.160,19,0
n,312,0.124,19,0
n,229,0.182,169,0
n,279,0.160,169,0
n,329,0.124,169,0
! trailing shoe
n,232,0.182,198,0
n,282,0.160,198,0
n,332,0.124,198,0
ngen,16,1,232,332,50,0,9,0
n,231,0.182,191,0
n,281,0.160,191,0
n,331,0.124,191,0
n,248,0.182,341,0
n,298,0.160,341,0
n,348,0.124,341,0
! define elements
! drum
type,1
mat,3
real,1
en,1,11,10,50,51
egen,39,1,1
en,40,10,49,89,50
! drum radial springs
! earth nodes
n,450,0.260,0,0
ngen,40,1,450,,,0,9
! nrotat,all
d,450,all,0,,489
```

```
! spring elements
r,41,3.5e6
type,3
real,41
en,400,50,450
engen,1,40,1,400
! leading block
type,1
mat,2
en,50,167,166,116,117
egen,8,1,50
! trailing block
type,1
mat,2
real,1
en,60,187,186,136,137
egen,8,1,60
! leading platform
type,1
mat,1
real,1
en,70,217,216,166,167
egen,8,1,70
! trailing platform
en,80,237,236,186,187
egen,8,1,80
! leading web
type,1
mat,1
real,2
en,100,263,262,212,213
egen,17,1,100
en,120,313,312,262,263
egen,17,1,120
! trailing web
en,140,282,281,231,232
egen,17,1,140
en,160,332,331,281,282
egen,17,1,160
! friction interface elements
type,2
real,3
en,200,116,16
egen,9,1,200,207,1
en,210,136,36
egen,9,1,210,217,1
! thicken shoe tips
emodif,100,mat,4
emodif,120,mat,4
emodif,116,mat,4
emodif,136,mat,4
emodif,140,mat,4
emodif,160,mat,4
emodif,156,mat,4
emodif,176,mat,4
! add masses to shoes
r,4,0.7
r,5,0.11
r,6,0.56
type,5
real,4
en,300,262
en,301,298
type,5
real,5
en,302,216
en,303,223
en,304,236
en,305,243
type,5
real,6
en,306,279
en,307,281
n,1,0.16,19,0
n,2,0.16,341,0
n,4,0.16,191,0
nrotat,all
! couple anchors
cp,3,uy,279,281
cp,4,ux,279,281
! cam link strut
r,7,1.4e-3
mp,ex,6,1.0e15
mp,nuxy,6,0.25
mp,dens,6,7000
type,6
real,7
mat,6
en,312,262,298
! tangential springs at cams
d,1,ux,0,,,,uy
d,2,ux,0,,,,uy
r,9,3e7
type,4
real,9
en,320,1,262
en,321,2,298
type,3
real,9
en,326,1,262
en,327,2,298
! springs at anchors
d,3,ux,0,,,,uy
d,4,ux,0,,,,uy
r,8,1e7
type,3
real,8
en,322,3,279
real,8
en,323,4,281
type,4
real,8
en,324,3,279
real,8
en,325,4,281
nrotat,all
r,42,1.0
type,7
real,42
en,704,279
en,705,281
```